EXCESS CONDUCTIVITY, MAGNETO-CONDUCTIVITY AND AC SUSCEPTIBILITY STUDIES IN La-Ba-Ca-Cu-O SUPERCONDUCTORS

A Thesis Submitted
in Partial Fulfilment of the Requirements
for the Award of the Degree of
DOCTOR OF PHILOSOPHY

by

Pramoda Kumar Nayak

Department of Physics
Indian Institute of Technology Guwahati,
Guwahati-781 039, INDIA

September, 2006

STATEMENT

The work contained in the thesis entitled **"**Excess Conductivity, Magneto-Conductivity and AC Susceptibility Studies in La-Ba-Ca-Cu-O Superconductors" has been carried out by me under the supervision of Dr. S. Ravi, Associate Professor, Department of Physics, Indian Institute of Technology Guwahati, Guwahati. This work has not been submitted elsewhere for the award of any degree.

23rd September, 2006

(Pramoda Kumar Nayak)

Roll No: 01612102

Department of Physics,

Indian Institute of Technology Guwahati,

Guwahati - 781039

CERTIFICATE

It is certified that the work contained in the thesis entitled "Excess Conductivity, Magneto-Conductivity and AC Susceptibility Studies in La-Ba-Ca-Cu-O Superconductors" by Mr. Pramoda Kumar Nayak, a Ph.D student of the Department of Physics, Indian Institute of Technology Guwahati, Guwahati for the award of the degree of Doctor of Philosophy has been carried out under my supervision. This work has not been submitted elsewhere for the award of any degree.

23rd September, 2006

(Dr. S. Ravi)
Associate Professor
Department of Physics,
Indian Institute of Technology Guwahati,
Guwahati – 781 039

Dedicated

to

my Mother

ACKNOWLEDGEMENTS

I express my sincere thanks to my Ph.D. supervisor Dr. S. Ravi for his inspiring guidance, showing interest in my Ph.D. work, helping me to carryout the experimental works and friendly behaviour throughout my research career at Department of Physics, Indian Institute of Technology Guwahati. I am grateful to him for his encouragement and, introducing me to different subjects, such as experimental techniques, solid state physics, superconductivity, magnetism and many other advanced physics subjects. I am happy to carryout my Ph.D. thesis work under such a kind hearted and intelligent person. I will never forget his company and suggestions throughout my life. I will remain ever grateful to him for his constant encouragement and good cooperation till my thesis submission.

I would like to thank Professor A. Srinivasan, chairman of my doctoral committee and doctoral committee members, Dr. P. S. Robi and Dr. P. K. Giri for valuable discussions and help whenever needed.

I am grateful to the former Heads of the Department of Physics, late Dr. Sasanka Ghosh and, Professor A. Srinivasan and the present Head of the Department of Physics, Professor Alika Khare for extending various facilities during the tenure of my Ph.D programme.

I would like to thank my course coordinators for teaching me the advanced topics in physics during my course work.

I am grateful to my senior, Dr. Manoranjan Kar, who guided me a lot during the design and fabrication of experimental setups in the laboratory. He always guides me in understanding physics properly and also inspires me to work with a positive attitude.

I am grateful to superintendent and technical staff of mechanical workshop, Indian Institute of Technology Guwahati for their help during fabrication of furnace, several sample holder assemblies, etc.

I would like to thank, the Head and the Staff of Central Instruments Facility, Indian Institute of Technology Guwahati for their help in recording SEM micrographs and EDX spectra on some of my samples.

I would like thank Mr. Sandeep Kumar Srivastava, Mr. Purnananda Nandi, Mr. Debabrata Mishra, Mr. Rajendra Kumar Singh, Ms. Veena M. Nair, Ms. Meera V, Ms. Sabita Mohan and other research scholars of Physics Department for their help during my Ph.D tenure.

I will not ever forget sisterly affection from Ms. Poulumi Dey, a research scholar of Dept. of physics, during my Ph.D tenure and her constant help during my thesis writing.

My special thanks go to Ms. Sarmistha Nayak, who provides me constant encouragement and moral support to carry out my research work with patience during my Ph.D period. She always inspires me to go in the right direction. I will always remain grateful to her.

Here I would like to thank Scientific officer, Mr. Sidananda Sarma, all Technical Assistants, Clerk and Laboratory Attendant of Department of Physics, IITG for their co-operation during my Ph.D. tenure.

I would like to thank Mr. T. J. Singh, Executive Engineer, Engineering Section, Indian Institute of Technology Guwahati, for extending his help during the installation of electromagnet and for the related civil infrastructures.

I am happy to be a research scholar in Indian Institute of Technology Guwahati, as I got a very friendly and cordial environment from all faculty members, non-teaching staff, administrative staff, securities and all others staying inside the campus. So, my heartiest thank goes towards them for giving me a healthy environment during my Ph.D. tenure.

I gladly recall the friendship I enjoyed with Dr. Kamlesh M. Alti, Mr. Sankar Moni Borah, Mr. Subash Chandra Martha, Mr. Laxmidhar Rout, Mr. Safique Ahmad, and thank them for encouragement and moral support.

I also recall my childhood friends Mr. Suryakanta Mohanty, Mrs. Preeti Mana Mallick, Mr. Saubhagya Ranjan Palaur and Mr. K. P. S. S. Hembram for their inspiration during my embarrassing moments in the Ph.D tenure.

I am grateful to my late father and, my mother, grand father, brother, sister, relatives and friends for their constant encouragement and moral support. I would like to offer my thanks to them for their affection, tolerance and support for which I could reach the present stage.

I am grateful to Indian Institute of Technology Guwahati for providing me financial support to carry out the present thesis work during my Ph.D. period. The financial support from a DST project for a short duration at the end of tenure of institute fellowship is also acknowledged. I have also used some of the equipments and consumables, etc. from the project fund of Department of Science and Technology, New Delhi and UGC-DAE Consortium for scientific Research, Mumbai, and I am thankful to these agencies.

Pramoda Kumar Nayak

ABSTRACT

The discovery of high transition temperature (T_c) superconductivity in (La-Ba)-Cu-O system with $T_c \approx 30$ K in1986 by Bednorz and Müller triggered the development of several high T_c Cu-O based superconductors. Among them, Y-Ba-Cu-O and Bi-Sr-Ca-Cu-O systems are widely studied in literature. Tl-Ba-Ca-Cu-O and Hg-Ba-Ca-Cu-O systems exhibit superconductivity with large transition temperatures such as 120 and 135 K respectively. However, these two series are toxic in nature. There are several reports on the enhancement of critical current density, J_c by novel preparation techniques including melt processing technique.

The temperature variations of precise electrical resistivity and magneto-resistivity measured on most of the above high T_c superconductors have been studied in terms of thermodynamic fluctuations induced excess conductivity above T_c. As a result of thermodynamic fluctuations in the amplitude of order parameter, there is a finite probability of Cooper pair formation above T_c and this leads to excess conductivity. The temperature and magnetic field variations of ac susceptibility and magnetization of high T_c superconductors are widely analyzed in terms of several critical state models. According to critical state models, the penetrated super current flows with a density equal to critical current density.

The non-superconducting parent compound, $La_3Ba_3Cu_6O_z$ discovered in 1981 is basically identical to $LaBaCu_2O_z$ and $La_2Ba_2Cu_4O_z$ compounds. Superconductivity with T_c up to 80 K was found by an addition of $CaCuO_2$ layer to the above compounds, i.e. with compositions such as $La_3Ba_3CaCu_7O_z$, $LaBaCaCu_3O_z$ or $La_2Ba_2CaCu_5O_z$. The crystal structure of the above compounds is comparable to that of tetragonal $YBa_2Cu_3O_{7-\delta}$. However, $YBa_2Cu_3O_{7-\delta}$ in tetragonal form does not exhibit superconductivity for $\delta > 0.5$. So, it would be interesting to study the physical properties of La-Ba-Ca-Cu-O system which exhibits tetragonal structure and superconductivity and compare with those of superconducting $YBa_2Cu_3O_7$.

In the present thesis work, I have prepared the following series of materials in single phase form.

1. $(La_{1-x}Y_x)_2Ba_2CaCu_5O_z$ $(0 \le x \le 0.50)$
2. $(La_{1-x}Y_x)_2Ba_2CaCu_5O_z$ + 5 wt % Ag $(0 \le x \le 0.50)$
3. Pure and Ag doped $(La_{1-x}Y_x)_2Ba_2Ca_yCu_{4+y}O_z$ (y = 4x, x = 0.15, 0.20)
4. Pure and Ag doped $(La_{1-x}Gd_x)_2Ba_2Ca_yCu_{4+y}O_z$ (y = 4x, x = 0.10, 0.20, 0.25)

The first series was prepared to study the effect of Y doping in the rare earth site, where the ionic size of Y is smaller than that of La. The second series was prepared by adding 5 wt % of Ag to the starting compositions of the above series to improve intergranular coupling between the grains, etc. The last two series are basically underdoped materials, where the level of $CaCuO_2$ doping is not up to the optimum concentration except for x = 0.25. The above samples have been prepared to have a wide range of transition temperatures with same crystal structure.

I have characterized the materials by recording X-ray diffraction (XRD) patterns, Scanning electron micrographs (SEM), Energy-dispersive X-ray (EDAX) spectra, etc. The materials were also characterized by measuring temperature variations of electrical resistivity and low field ac magnetic susceptibility. The temperature variations of electrical resistivity and magneto-resistivity have been analyzed in terms of excess conductivity and fluctuation magneto-conductivity due to thermo-dynamic fluctuations in the amplitude of superconducting order parameter. Temperature and ac field amplitude variations of ac susceptibility have been analyzed in terms of critical state models on selected single phase samples. The above experimental data have been also analyzed in terms of excess conductivity in the paracoherence regime, where the fluctuations in the phase of the order parameter play a role.

The present thesis is divided into five chapters, namely, (1) Introduction, (2) Experimental Techniques and Sample Characterization (3) Excess conductivity and Magneto-conductivity (4) AC susceptibility, and (5) Conclusions.

In chapter 1, I have started with historical overview; where, the discovery of superconductivity followed by many hall mark discoveries in experimental and theoretical superconductivity have been reviewed briefly. The discovery of high temperature superconductors and their physical properties with special emphasis on their crystal structure, electrical transport and magnetic properties have been reviewed in detail. Theoretical background on excess conductivity, fluctuation magneto-conductivity, critical state models and the derivation of magnetization using critical state models are reviewed. The results on excess conductivity and fluctuation magneto-conductivity analysis on various high T_c superconductors reported by several authors are reviewed. The susceptibility and magnetization measurements and analysis carried out on various high T_c superconductors in terms of critical state models are reviewed. The motivation for the present thesis work is also mentioned briefly at the end of the chapter 1.

Chapter 2 describes the experimental techniques and sample characterization. Here the technical details of fabrication and calibration of certain experimental facilities such as high temperature furnace for material preparation, and ac susceptibility set up, would be discussed in detail. The experimental techniques followed for sample preparation, XRD, SEM, EDAX, electrical resistivity and ac susceptibility measurements would be given. The detailed analysis of XRD patterns recorded for different samples and the results of various sample characterization are presented.

In chapter 3, the detailed analysis of thermodynamic fluctuations induced excess conductivity on selected samples of the above series are presented. The excess conductivity has been calculated from the zero field resistivity data in the mean field regime. The calculated excess conductivity data have been analyzed using Aslamazov-Larkin as well as Lawrence–Doniach models. Contribution of Maki-Thompson term to the zero field excess conductivity is also investigated. Dimensionality of order parameter fluctuations and the coherence length along c-direction at 0 K, $\xi_c(0)$ have been estimated. Excess conductivity data have also been calculated and analyzed in the paracoherence region in order to determine the critical exponent corresponding to phase fluctuations in the order parameter.

The magneto-conductivity data have been analyzed using Aslamazov-Larkin and Maki-Thompson models for fluctuation magneto-conductivity by taking both orbital and Zeeman terms into account. The pair breaking time, coherence lengths along 'ab' plane and along 'c'-direction at 0 K have been estimated. The results of the above analysis are discussed in detail.

In chapter 4, the temperature and ac field amplitude variations of ac susceptibility have been discussed. Theoretical expressions for susceptibility have been derived from the expressions for magnetization obtained from Kim critical state model. Ac susceptibility data have been analyzed in terms of Kim critical state model and critical current density as a function of temperature has been estimated and their temperature dependence was studied.

In Chapter 5, the important conclusions drawn from the physical measurements and analysis carried out on the above series of superconducting materials are summarized. A few points are listed below.

(1) The La-Ba-Ca-Cu-O superconductors with tetragonal structure exhibit two dimensional fluctuations of superconducting order parameter in the mean field region. (2) Addition of 5 wt % of Ag to the parent compound enhances the superconducting transition temperature and critical

current density by suppressing the weak links between the grains. (3) The contribution of Maki-Thompson term is found to be insignificant. (4) These materials exhibit cross over from ordered phase fluctuations with the critical exponent comparable to that of pure 3D XY ferromagnet to disordered phase fluctuations with the critical exponent comparable to that of disordered 3D Heisenberg ferromagnetic system. (5) Fluctuation magneto-conductivity study suggests that these materials show strong pair breaking effect. (6) The typical values of $\xi_c(0)$ and $\tau_\phi(100\ K)$ from magneto-conductivity analysis are found to be in the range of 0.30 to 0.80 Å and 10^{-16}s. (7) Field variation of ac susceptibility data could be fitted to Kim critical state model. (8) The effective volume fraction of superconducting grain, f_g has been found to be in the range of 10 to 25 %. (9) The Ag doped materials exhibit relatively large J_c. (10) The temperature variation of J_c estimated from the above analysis has been studied by fitting to standard theoretical expression.

CONTENTS

LIST OF TABLES

Tables **Page No.**

Chapter 1:

Chapter 2:

Chapter 3:

Chapter 4:

LIST OF FIGURES

Figures **Page No.**

Chapter 1:

Chapter 2:

Chapter 3:

Chapter 4:

INTRODUCTION

The discovery of superconductivity by Kamerlingh Onnes was one of the hall marks of the 20th century physics. Kamerlingh Onnes at Leiden laboratory in Holland pursued the production of low temperature in an attempt to reach absolute 0 K. He was successful in liquefying Helium gas, with record low temperature of 4.2 K at atmospheric pressure and 1.7 K under reduced pressure. After this success, he measured electrical resistivity of several materials at low temperatures. In 1911, Kamerlingh Onnes discovered sudden disappearance of electrical resistance of mercury at 4.2 K [1]. He recognized that below 4.2 K, mercury enters into a new state with zero electrical resistivity and it is called as superconducting state. Another important property of superconductor is the Meissner effect with perfect diamagnetism [2]. So superconductivity is known as phenomena of zero electrical resistivity and perfect diamagnetism below a certain temperature called transition temperature, T_c. Following the discovery of superconductivity in Hg, several superconductors were discovered in elements, alloys and compounds. Several theoretical models have been developed to understand the various properties of superconductors and soon superconductivity has become one of the interesting areas of solid state physics. These are briefly reviewed as follows.

1.1. Historical Overview

In this section, discovery of several superconductors, many hall mark experiments on superconducting materials and the theoretical models which contributed to the understanding of superconductivity, which are all now a part of any superconductivity text or monograph are reviewed briefly.

1.1.1 Superconducting Phenomena

Soon after the discovery of superconductivity, the first question which came to the mind of the Physicists is, whether the resistivity is really zero or just below the sensitivity of the measuring instrument. This was probed by setting current to the superconducting closed loop and by measuring the change in magnetic flux if any. It is estimated that resistivity of superconductor is less than 10^{-24} Ω.cm, which can be taken as zero. From the fact of zero electrical resistivity and one of the Maxwell's equations, $Curl E = -\frac{\partial B}{\partial t}$, one would expect that B = constant, inside a superconductor. However in 1933, twenty two years after the discovery of superconductivity,

Meissner and Ochenfeld [2] reported that B = 0 inside a superconductor, irrespective of the history of applied magnetic field, i.e. whether zero field cooled or field cooled through the superconducting transition temperature. This important discovery was made from the measurement of magnetic flux distribution outside the tin and lead superconductors and is known as Meissner effect. Thus, the combination of zero resistivity and Meissner effect is the unique property of superconductors such that presence of superconductivity in any new material is investigated by carrying out the above the two measurements. The discovery of superconductivity raised the hope of generating very large magnetic field but it was realized by Kamerlingh Onnes himself in 1913 that superconductivity (in elements) was destroyed by the application of magnetic field above certain threshold value of the order of 100 mT. This is called the critical field B_c [3]. Similarly there is a threshold current density called critical current density above which material turns into normal state. The critical field is found to decrease with increase in temperature by following the relation, $B_c(T) = B_c(0)\left(1 - (T/T_c)^2\right)$. As early as in 1916, Silsbee and Wash [4] put forward the idea of relation between critical field and critical current density. In thick superconductors, the field generated by the critical current passing through a superconducting wire on its surface is equal to critical field and their relation is [5],

$$B_c = \frac{\mu_0 I_c}{2\pi R} \tag{1.1}$$

In 1930's, Schubnikov and other workers working on superconducting lead-indium alloys found that perfect diamagnetism is lost for a critical field of about 65 mT and the materials continue to exhibit zero resistivity up to a much higher field of about 0.16 T [5]. Thus it was known, there are two type of superconductors namely type-I and type-II, with distinct magnetic properties as shown in Fig.1.1. There are two critical fields namely B_{c1} and B_{c2} in type-II superconductors. The discovery of type-II superconductors fulfilled the hope of application of superconductors in generating high magnetic fields. Materials with B_{c2} as high as about 14T have been discovered.

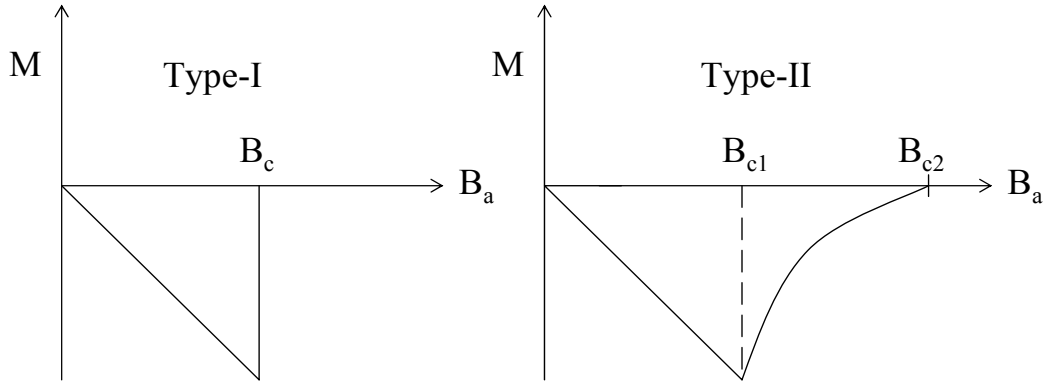

Fig.1.1 Type I and Type II superconductors

In 1950, Maxwell [6] and independently by the group of Reynolds, Serin, Wright and Nesbitt [7] found that the T_c varies with isotopic mass of materials as per the relation, $T_c \propto 1/\sqrt{M}$, even though there is no change in atomic arrangement. This led to the foundation for the understanding of role of lattice vibration or phonons in superconductivity. The temperature variation of specific heat of superconductors exhibit a sharp peak at the transition and at low temperature its electronic contribution varies as exp ($-b/\kappa_B T$) rather than γT, which is generally observed for metallic sample. The exponential dependence implies that there is an energy band gap associated with superconducting electrons. Doll and Näbauer [8] and independently by Deaver and Fairbank [9] measured the magnetic flux trapped inside a hollow superconductor or superconducting ring and found that it is an integral multiple of h/2e, called flux quantum. Such flux quantization was predicted by London as early as in 1950 [10].

In 1957, Glover and Tinkham measured the absorption of electromagnetic radiation in infrared region and it provided for the first time, the most direct evidence for superconducting energy gap [11]. Giaever and his group measured the tunneling current through superconductor-insulator-normal metal (SIN) and superconductor-insulator-superconductor (SIS) junctions [12, 13]. They found that tunneling current appears for the applied voltage, $V = \Delta/e$ in SIN junctions and $V = 2\Delta/e$ in SIS junctions, where Δ is the band gap energy of superconducting electrons. Here, beyond the threshold voltage V, the superconducting electrons (paired electrons) are excited by breaking into normal electrons and tunnel through the junction. Typical I-V characteristics curves are depicted in Fig.1.2 and from that superconducting band gap energy can be measured.

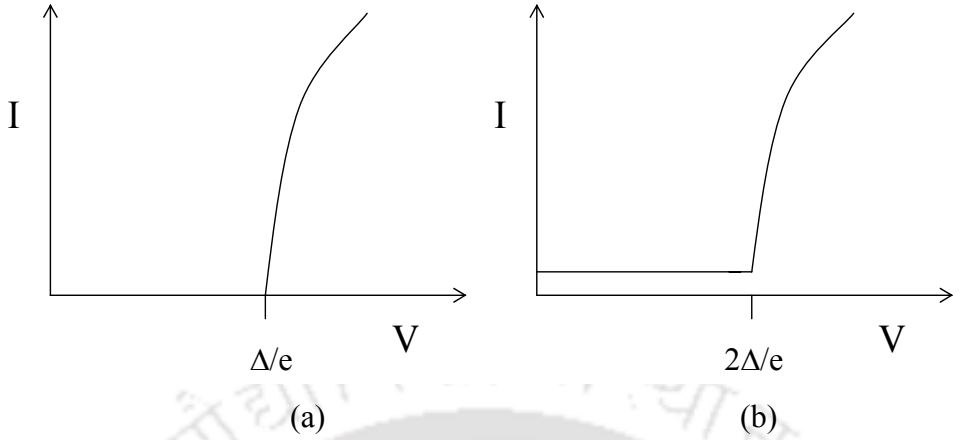

Fig.1.2 I-V Curves for (a) SIN and (b) SIS junctions.

In 1962, Josephson predicted that for small thickness of the insulating layer of the order of 10 Å in SIS junction, there would be a flow of dc current across the junction in the absence of applied voltage and ac current in the presence of applied dc voltage due to the tunneling of superconducting paired electrons [14]. This was demonstrated experimentally by Giaever [15]. These discoveries are so important that these devices could be put into applications, especially magnetic measurements. The combination of flux quantization and Josephson Effect led to the discovery of superconducting Quantum Interference Device, widely called as SQUID. Here current is passed through a superconducting ring with two Josephson weak links opposite to each other as shown in Fig.1.3. The Josephson current passing through the junction is very sensitive to the applied magnetic field as shown in Fig.1.4 and it serves as sensitive magnetometer [16].

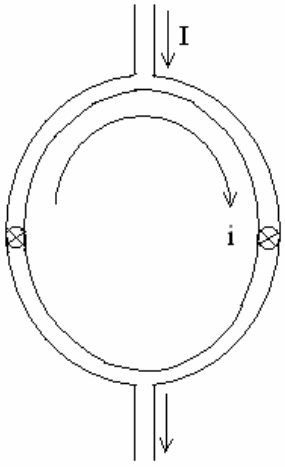

Fig.1.3 SQUID Device

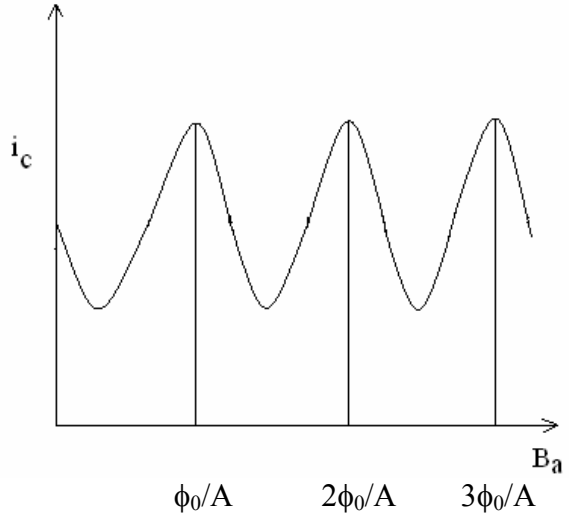

Fig. 1.4 Josephson current versus applied field (ϕ_0-flux quanta)

1.1.2. Classical Superconductors

The pioneering work of Kammerlingh Onnes in low temperature physics and electrical transport studies led to the discovery of superconductivity, a new branch of area in solid state Physics [1]. Soon after the discovery of superconductivity in Hg at 4.2 K, superconductivity in several elements has been identified. The elements which exhibit superconductivity with appreciable T_c values along with their valency are listed in Table 1.1 [ref. 5, 17].

Table 1.1: List of some of element superconductors with their T_c and valency N are given.

Elements	V	Nb	Tc	In	Sn	La (α - hcp)	La (β - fcc)	Ta	Tl	Pb
T_c(K)	5.4	9.2	7.8	3.4	3.7	4.9	6.3	4.5	2.4	7.2
N	5	5	7	3	4	3	3	5	3	4

About half of the element superconductors are the members of transition elements. The noble metals such as Cu, Ag and Au do not show any superconductivity. Most of the superconducting elements have high symmetry crystal structures such as face centered cubic, body centered cubic and hexagonal close packed.

Matthias [18] predicted an empirical rule and according to that materials with average valence electrons 5 or 7 show relatively large transition temperature. Following his empirical rule, several new superconductors in A15 compounds (A_3B type) have been discovered. Some of the A15 compounds and their T_c are given in Table 1.2. We can see that Nb based A15 compounds exhibit comparatively high T_c values [5, 17].

Table 1.2: List of some of the superconducting A15 compounds and their T_c.

A15 compounds	V_3Ga	V_3In	V_3Si	Mo_3Re	Mo_3Os	Ta_3Sn	Ta_3Au	Nb_3Al	Nb_3Ga	Nb_3Si	Nb_3Ge	Nb_3Sn
T_c(K)	16.8	13.9	17.2	15.0	12.7	17.0	16.0	19.0	21.0	19.0	23.2	18.0

The A15 compounds have cubic structure with Pm3n space group. The structure of A15 compounds is shown in Fig.1.5. Here six A atoms are paired on each face of the cubic cell at the positions (0 1/2 1/4); (0 1/2 3/4); (1/2 1/4 0); (1/2 3/4 0); (1/4 0 1/2); (3/4 0 1/2) and two B atoms are situated at the corners and body centered positions, viz. (0 0 0) and (1/2 1/2 1/2).

Laves phases with chemical formula AB_2 exhibit superconducting transitions. The examples for Laves phases are ZrV_2, HfV_2 and $LaOs_2$ with T_c values 9.6, 9.4 and 8.9 K respectively. There is another class of superconductors namely chevrel phases with chemical composition of the form $A_nMo_6X_8$. Here X is S, Se or Te and A is mostly rare earth and transition elements. 'n' takes various values such as n = 1, 1.2, 1.6 and 2.0. Some of the chevrel phases exhibit T_c above 10 K and they are $Cu_2Mo_6S_8$ (T_c = 10.7 K), $La_2Mo_6Se_8$ (T_c = 11.7 K), $PbGd_{0.2}Mo_6S_8$ (T_c = 14.3 K), $PbMo_6S_8$ (T_c = 12.6 K) and $Sn_{1.2}Mo_6S_8$ (T_c = 14.2 K). They exhibit trigonal structure with R3 space group. Some of the oxide materials such as TiO, NbO, $SrTiO_3$ and $BaBi_{0.25}Pb_{0.75}O_3$ are also found to exhibit superconductivity before 1986 with highest transition temperatures 13.0 K [3].

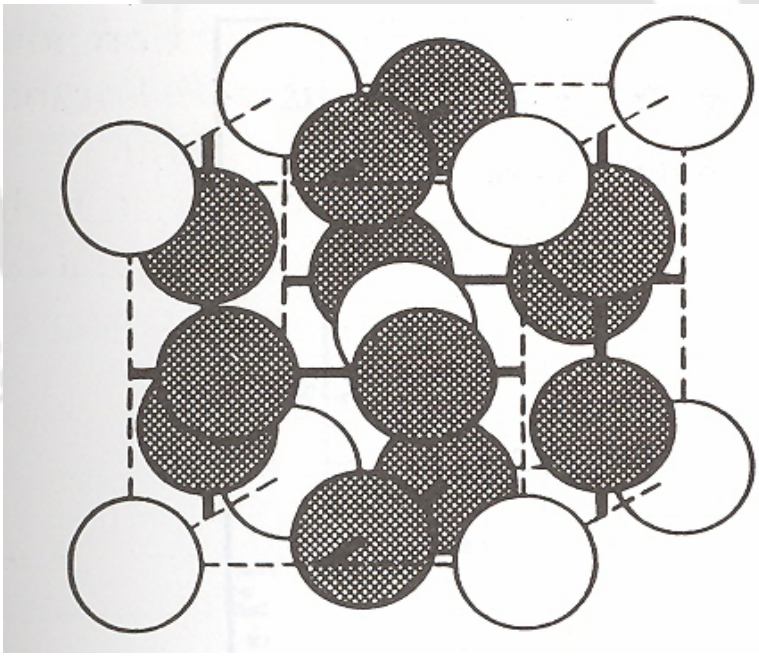

Fig. 1.5 Crystal structure of A15 compound. The B atoms are at the corner and body center positions and A atoms are in pairs on the faces of cubic cell.

1.1.3. Theories of superconductivity

Zero resistivity and, Meissner effect or perfect diamagnetism with magnetic susceptibility $\chi = -1$ are the two fundamental properties of superconductors. In 1935, two years after the discovery of Meissner effect, F. London and H. London [19] derived the electrodynamic equations to explain the above two properties and they are called London's first and second equations as given below,

$$\frac{d\overline{J_s}}{dt} = \frac{1}{\mu_0 \lambda_L^2}\overline{E} \tag{1.2}$$

$$curl\ \overline{J_s} = -\frac{1}{\mu_0 \lambda_L^2}\overline{B} \tag{1.3}$$

Here $\overline{E}$ and $\overline{B}$ are applied electric and magnetic fields, J_s is the current density in superconductors and $\lambda_L = \sqrt{(m/\mu_0 n_s e^2)}$ is the London penetration depth. m, e, n_s are the electron mass, charge and it's density. The first London equation (eqn.1.2) explains the property of zero electrical resistivity of superconductors and second London equation (eqn.1.3) explains Meissner effect, B = 0. The applied magnetic field penetrates over London penetration depth λ_L, beyond which B = 0 as per the relation,

$$B(x) = B(x=0)\exp\left(\frac{-x}{\lambda_L}\right) \tag{1.4}$$

The transition from superconducting to normal state can be considered as a thermodynamic reversible process where the change in Gibb's free energy per unit volume depends only on magnetic energy. So, as described in ref. [16],

$$\Delta g = g_n(T) - g_s(T) = \frac{B_c^2(T)}{2\mu_0} \tag{1.5}$$

where $B_c(T)$ is the critical magnetic field at a given temperature. Using standard thermodynamic functions, the change in entropy and change in specific heat per unit volume can be determined from Δg and they are given as follows,

$$\Delta s = s_n(T) - s_s(T) = -\frac{B_c}{\mu_0}\frac{\partial B_c}{\partial T} \tag{1.6}$$

and $$\Delta c = c_n(T) - c_s(T) = -\frac{T}{\mu_0}\left[\left(\frac{\partial B_c}{\partial T}\right)^2 + B_c\left(\frac{\partial^2 B_c}{\partial T^2}\right)\right] \tag{1.7}$$

The Δs value is positive because $\frac{\partial B_c}{\partial T}$ is negative and it suggests that superconductivity is an ordered state. At T =T_c, B_c = 0, so Δc becomes,

$$\Delta c = -\frac{T_c}{\mu_0}\left(\frac{\partial B_c}{\partial T}\right)^2 \tag{1.8}$$

and it is called Rutgers' formula [20], which explains discontinuity in specific heat at T_c. The sketch of temperature variations of Gibb's free energy, entropy and specific heat are given in Fig. 1.6.

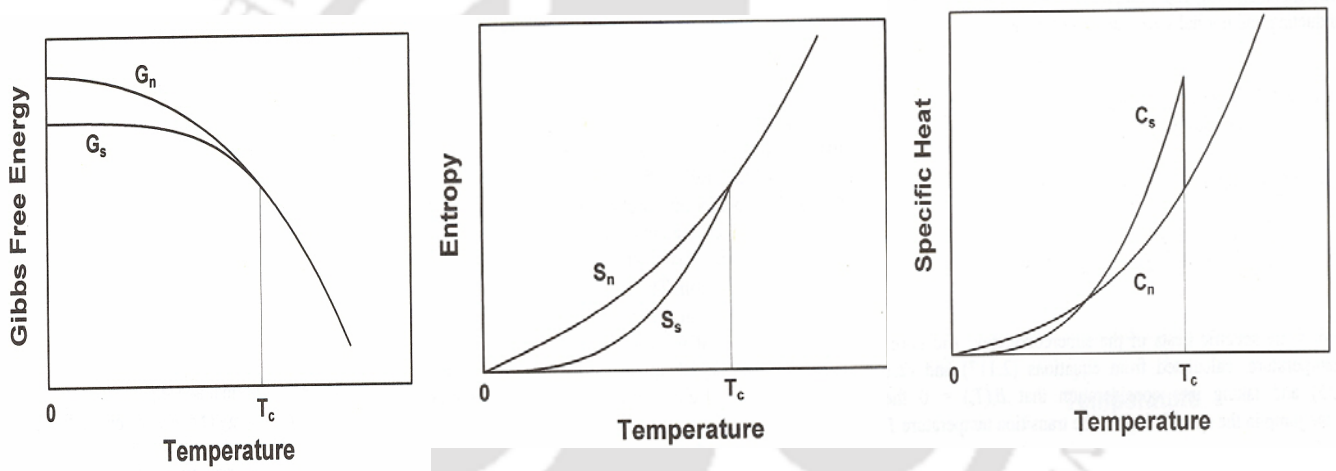

Fig.1.6 (a) Gibb's free energy, (b) entropy and (c) specific heat of superconductors and normal metals versus temperature at zero applied field.

London, predicted that the magnetic flux passing through hole of a hollow superconductor such as superconducting ring is quantized [10]. He took a closed loop inside a superconducting ring, where the magnetic field is zero and using London's equations, he derived that magnetic flux passing through the hole is,

$$\varphi = \frac{h}{e^*}n = n\varphi_0 \tag{1.9}$$

where n is an integer, $\varphi_0 = \frac{h}{e^*}$ is the flux quantum. It was later verified experimentally and the

value of e^*=2e, the charge of the superconducting electron pair was known after the discovery of microscopic theory. The value of φ_0 is 2.07×10^{-15} Tm^2.

Pippard [21] measured the London penetration depth in superconducting alloys and to explain his result, he suggested that London's second equation has to be modified by introducing non-local behavior of current density,

$$J(r) = \int f(r - r')A(r')dr' \tag{1.10}$$

It describes that electrons from different point r/ contribute to the supercurrent at r, J(r). He introduced a new parameter called coherence length, ξ the length over which perturbed forces are appreciable.

Ginzburg-Landau (GL) theory is the most complete and simple phenomenological theory of superconductivity, which explains most of the experimental observations especially at temperatures close to T_c [22]. The importance of the theory was realized only after the discovery of more complete microscopic theory by Bardeen, Cooper and Schrieffer (BCS) [23] and the work of Gor'kov [24], who has showed that GL theory can be obtained from BCS theory under certain limiting cases. By extending the Landau's approach of second order phase transition, Ginzburg and Landau derived the theory of superconductivity. They assumed that the wave function ψ(r) of superconducting electrons as order parameter and the density of super electrons $n_s = |\psi(r)|^2$. The free energy near to superconducting transition, where ψ is small, can be written as power series of ψ as given below,

$$g_s(r) = g_n + \alpha|\psi(r)|^2 + \frac{1}{2}\beta|\psi(r)|^4 + \frac{1}{2m}\left|(-i\hbar\nabla - eA)\psi(r)\right|^2 + \frac{B_a^2}{2\mu_0} \tag{1.11}$$

By expanding the above series and minimizing with respect to ψ or ψ^* and vector potential *A* based on Euler-Lagrange's equation, they arrived at following two GL equations,

$$\frac{1}{2m}(-i\hbar\nabla - eA)^2\psi(r) + \alpha\psi(r) + \beta|\psi(r)|^2\psi(r) = 0 \tag{1.12}$$

and

$$J = -\frac{ie\hbar}{2m}(\psi^*\nabla\psi - \psi\nabla\psi^*) - \frac{e^2A}{m}\psi\psi^* \tag{1.13}$$

where $\alpha = (T - T_c)\alpha_0$ and β = constant. From the above two GL equations, it is possible to obtain London electrodynamic equations and expression for London penetration depth. The temperature dependence of λ and critical field B_c are found to be,

$$\lambda(T) = \lambda(0)\left[1 - \frac{T}{T_c}\right]^{\frac{-1}{2}} \tag{1.14}$$

and

$$B_c(T) = B_c(0)\left[1 - \frac{T}{T_c}\right] \tag{1.15}$$

It can be shown that already known functions of $\lambda(T) \propto \left(1 - (T/T_c)^4\right)^{-1/2}$ and $B_c(T) \propto \left(1 - (T/T_c)^2\right)$ reduce to equations 1.14 and 1.15 at T close to T_c. The properties such as flux quantization and type-II superconductivity can be explained on the basis of GL theory [25].

The complete microscopic theory of superconductivity was derived by Bardeen, Cooper and Schrieffer and called as BCS theory [23]. They have shown that weak attraction between electrons as a result of electron-phonon interaction, leads to pairing of electrons called Cooper pairs. These cooper pairs flow without any resistance leading to zero resistivity. The importance of electron-phonon interaction and possible pairing of electrons were suggested by Frölich way back in 1952 [26]. The BCS theory predicts the superconducting transition temperature as per the following form,

$$T_c = 1.13\frac{\hbar\omega_D}{k_B}\exp\left(\frac{-1}{N(E_F)v}\right) \tag{1.16}$$

where ω_D- Debye temperature, $N(E_F)$-density of states of electrons at Fermi level, k_B-Boltzmann constant and υ is a parameter related to electron-phonon interaction.

In 1957, Abrikosov [27] gave theoretical explanation for the existence of type II superconductors by solving Ginzburg-Landau equations. The mixed state of type II superconductor is shown in Fig.1.7. According to him, the mixed state is characterized by an array of normal cores within the superconductor, which allow magnetic flux to enter into it. Supercurrents encircling the normal cores in the mixed state are called as vertices. The radius of each normal core is the coherence lengthξ. Fig.1.8 shows the variation of Cooper pair density n_c and the magnetic flux density B in the interior of a type II superconductor in the mixed state.

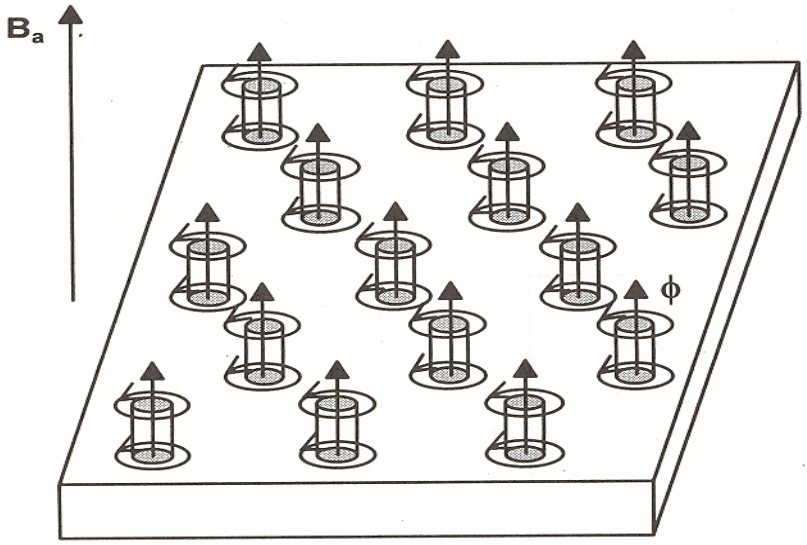

Fig.1.7 Type II superconductor in the mixed state. Each vortex contains just a single fluxoid.

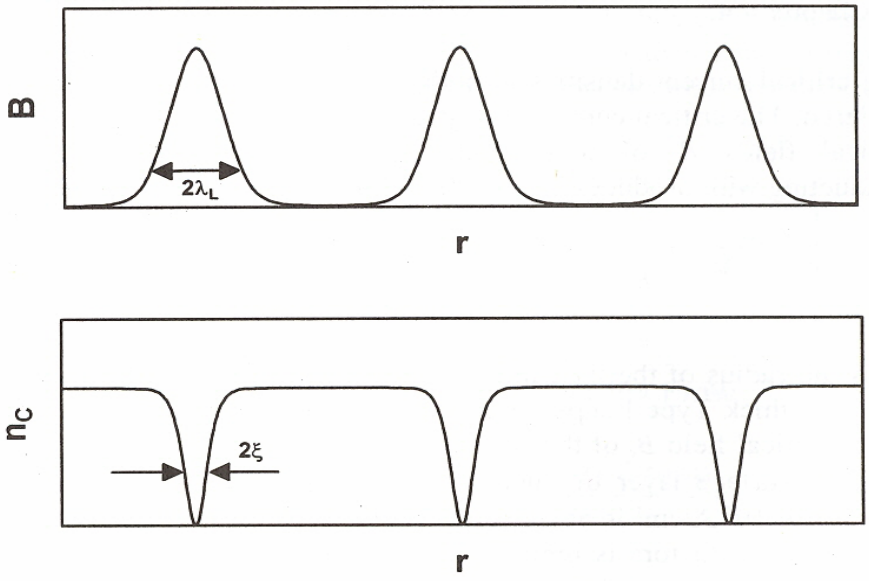

Fig.1.8 Variation of the magnetic flux density B (top) and the Cooper pair density n_c (bottom) in the mixed state of a type II superconductor.

In the advent of the discovery of high T_c superconductivity, there are several theories reported in literature to explain various properties of high T_c superconductors. Its review would be beyond the scope of the introduction of the present thesis.

1.2. High Temperature Superconductors

1.2.1. Materials

Till 1986, the superconductor with highest known T_c was Nb_3Ge with T_c = 23.2 K and it was discovered way back in 1973 [28]. In 1986, Bednorz and Müller [29] made a break through in the history of superconductivity by reporting transition temperature as high as 30 K in a new oxide series namely, (La,Ba)-Cu-O system. The exact composition responsible for superconductivity in the above series was identified as $La_{2-x}Ba_xCuO_{4-y}$ ($0.1< x < 0.2$) by Uchida et al. [30] and Takagi et al. [31]. The general formula of this type of compound is $La_{2-x}A_xCuO_4$ (A = Ca, Ba, Sr). The $La_{2-x}Sr_xCuO_4$ compounds are found to be superconducting with a $T_c(0)$ of ≃ 36.0 K [32, 33]. According to Chu et al. [34], the transition temperature (T_c) of these materials can be increased up to 52.5 K by the application of pressure. These compounds have quasi-two dimensional structure of K_2NiF_4 type with Cu-O_2 layers. To throw light on the mechanism of superconductivity, effects of several substitutions have been studied in $La_{2-x}A_xCuO_4$ system. Replacement of Cu partly by Ni or Zn drastically lowers the T_c [35, 36]. The rapid fall in T_c suggests that superconductivity is confined to the Cu-O_2 plane. Superconductivity in the above series was mainly obtained by Bednorz and Müller by hole doping in the parent compound La_2CuO_4, which induces mixed valency of Cu. The parent compound, La_2CuO_4 is basically an antiferromagnetic insulator with orthorhombic crystal structure at room temperature.

Soon after the discovery of superconductivity in (La,Ba)-Cu-O system at 30 K, there were intense activity of the superconductivity research, which led to the discovery of many new Cu-O based high T_c superconductors, which are reviewed as below. Wu et al. [37] was the first one to report superconductivity above the boiling point of liquid nitrogen (77 K), that is on Y-Ba-Cu-O system with T_c around 90 K. The composition responsible for superconductivity at 91 K was identified as $YBa_2Cu_3O_7$ by Cava et al. [38], Hazen et al. [39], Grant et al. [40] and others [41, 42]. The above discovery culminated the spread of experimental research work on superconductivity in large number of research laboratories across the globe irrespective of their range of funding. The dependency of high cost liquid helium is reduced and replaced with economically cheaper liquid nitrogen.

When "Y" is replaced by most of the rare earth elements (except Pr, Ce and Tb) there is no significant change in the T_c values. The structure of all the compounds are orthorhombic

(except for Pr) at room temperature [43-49]. The superconducting properties of $YBa_2Cu_3O_{7-\delta}$ are very sensitive to its oxygen content [50, 51]. The transition temperature (T_c) can be varied from 91 K to 45 K by increasing the δ value from 0 to 0.5. The compounds with $\delta > 0.5$ were non-superconducting [52, 53]. Two more superconducting phases with compositions $YBa_2Cu_4O_y$ [54-58] and $Y_2Ba_4Cu_7O_y$ [59] have been identified in Y-Ba-Cu-O system with T_c values 80 K and 40 K respectively.

Michel et al. [60] reported superconductivity in a rare-earth free Cu-O system namely Bi-Sr-Cu-O with T_c around 10 K. Maeda et al.[61] reported a large jump in T_c by substituting Ca in the above series, i.e. Bi-Sr-Ca-Cu-O system. They have observed bulk superconductivity with T_c = 85 K and indication for superconductivity even above 100 K. In this system, three superconducting phases have been identified with compositions $Bi_2Sr_2CuO_y$ (2201), $Bi_2Sr_2CaCu_2O_y$ (2212) and $Bi_2Sr_2Ca_2Cu_3O_y$ (2223) with T_c's respectively 10 K, 85 K, and 110 K [62-68]. Cava et al. [69] and Takano [70] reported that partial Pb substitution in place of Bi promotes the formation of 110 K phase. Several authors have suggested different starting compositions for the preparation of 110 K phase in single phase form [71, 72].

Sheng et al. [73, 74], reported superconductivity with T_c up to 90 K in a mixed phase of Tl-Ba-Cu-O system. Same group found that T_c could be enhanced up to 120 K by adding Ca in the above system [75]. The phases responsible for superconductivity in the above series have been identified as $Tl_2Ba_2CuO_y$ with T_c = 0 to 20 K, $Tl_2Ba_2CaCu_2O_y$ with T_c = 95 to 108 K and $Tl_2Ba_2Ca_2Cu_3O_y$ with T_c = 118 to 130 K by Hazen et al. [76] and several other groups [77-79]. It is commonly called as $Tl_2Ba_2Ca_{n-1}Cu_nO_y$ series. Parkin et al.[80] and Herview et al.[81] reported one more Tl-based series with single Tl-O layer and with general formula $TlBa_2Ca_{n-1}Cu_nO_y$ with superconducting T_c= 65 – 85 K for n = 2 and T_c= 100 – 110 K for n = 3. The n = 1 compound in the Tl-monolayer series is not superconducting. So there are six compounds in Tl series with general formula $Tl_mBa_2Ca_{n-1}Cu_nO_y$ with m = 1 & 2, and, n = 1, 2 &3.

Superconductivity with T_c up to 135 K has been observed in Hg-Ba-Ca-Cu-O system [82, 83]. The superconductivity in Cu-Ba-Ca-Cu-O series with T_c up to 126 K has been reported by Ihara group [84-86] and according to them these materials exhibit low anisotropy. However, the main draw back is that this series can be prepared only under high pressure.

Superconductivity in $RuSr_2RCu_2O_8$ (R = rare earth) and $RuSr_2(R,Ce)_2Cu_2O_{10}$ series with T_c around 35 K was first reported by Bauernfeind et al. [87, 88] from electrical resistivity

measurements. The subsequent works in the above series highlighted the interesting properties of coexistence of superconductivity with T_c 15 to 45 K and magnetism with magnetic ordering at around 130 to 180 K [89-93]. Its crystal structure is similar to that of $YBa_2Cu_3O_7$ (YBCO). In view of this structural similarity, it is believed that superconductivity in this compound also originates in the CuO_2 planes, where as ferromagnetism is ascribed to ordering of Ru moments in the RuO_2 planes. The superconducting properties of this compound are highly dependent on the details of sample preparation. The superconductivity in the above series can be obtained mostly by annealing under high oxygen pressure.

In addition to the above high T_c superconductors, the last two decades witnessed the discovery of several new superconductors and T_c of some of them are found to be even less than 30 K. They are briefly mentioned as follows.

Tokura et al. [94] found a new class of superconductor $Nd_{2-x}Ce_xCuO_4$ with T_c onset at around 25 K. The significance of this compound is that electrons are responsible for charge transport rather than holes as observed in other oxide superconductors. Following this discovery, several other electron doped superconductors with general formula, $R_{2-x}M_xCuO_4$ (R = La, Nd, Pr, Sm, Eu, M = Ce, Th) have been discovered [95-100].

Another family of compounds called borocarbide superconductors, with the general formula RT_2B_2C (R = Y, Rare Earth, T = transition element), exhibit superconductivity with T_c up to round 16 K [101-106]. In addition to superconductivity, some of these compounds especially for R = Dy, Ho, Er & Tm exhibit antiferomagnetism. Superconductivity with T_c up to 40 K has been reported in Magnesium Boride (MgB_2) [107].

1.2.2. Crystal Structure

The discovery of various high T_c superconductors with most of them based on Cu-O system has been reviewed in the previous section. In this section, the crystal structure of a few representative Cu-O based superconducting series reported in literature would be briefly reviewed.

The crystal structure parameters of $La_{2-x}Ba_xCuO_4$ was first refined by Jorgensen et al. [108] by recording neutron diffraction patterns and by following K_2NiF_4 type structure predicted by Takagi et al. [109]. The crystal structure of $(La_{2-x}A_x)CuO_4$ (A = Ca, Ba, Sr) superconductors is shown in Fig. 1.6. It has I4/mmm space group in tetragonal structure with two formula units per unit cell. The typical lattice parameters are a = b = 3.787 Å and c = 13.288 Å for A = Ba. The atomic position of each element is given in Table 1.3.

The CuO_2 planes are situated at z = 0, 0.5 & 1.0. Cu-O_2 planes are separated by two La-O planes. Each Cu ion is bonded with four O1 ions in a square planer arrangement at a distance of 1.894 Å and two O2 ions at apical positions at a distance of 2.428 Å. Thus Cu is at the centre of oxygen octahedron elongated along z direction. The crystal structure of the parent compound, La_2CuO_4 is orthorhombic (space group Cmca) with lattice parameters a = 5.356 Å, b = 5.399Å and c = 13.167Å.

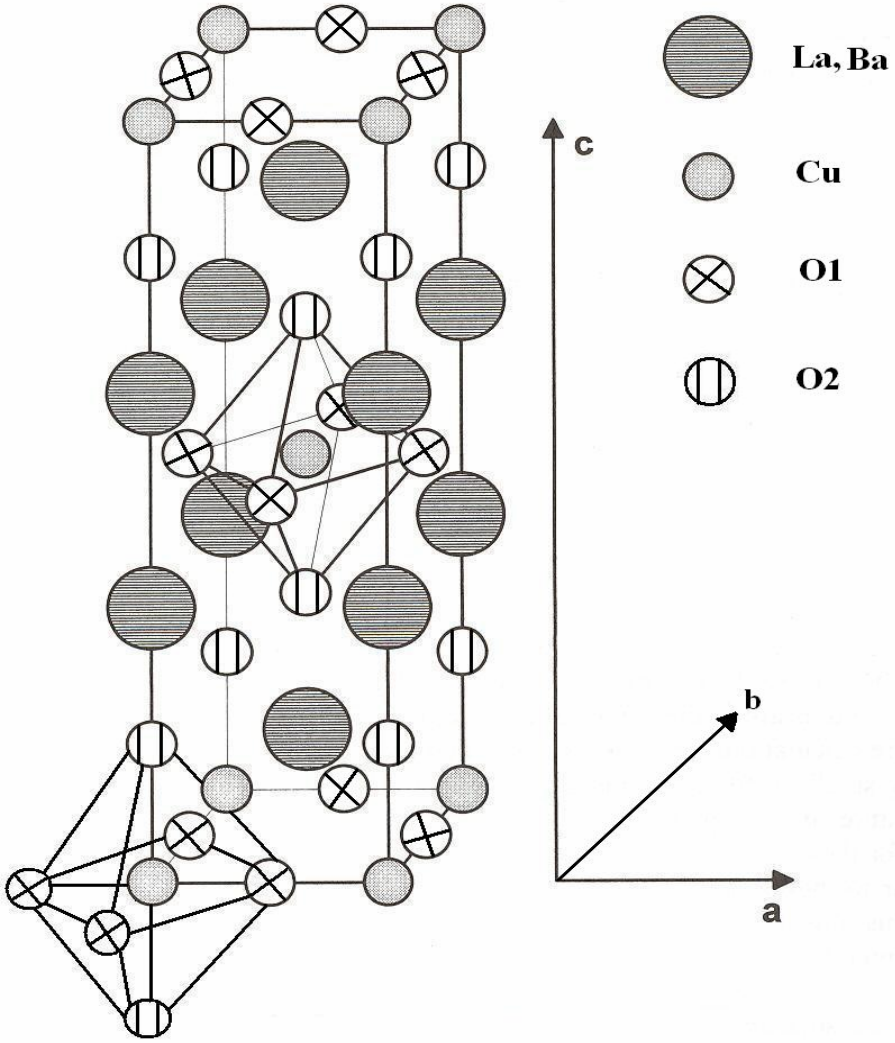

Fig. 1.9. Lattice structure of La_{2-x} Ba_xCuO_4.

Table1.3. Normalized atomic positions in the tetragonal unit cell of $(La_{1.85}Ba_{0.15})CuO_4$.

Atoms	X	Y	Z
La or Ba	0	0	0.36
Cu	0	0	0
O1	0	0.5	0
O2	0	0	0.18

Several groups [38-41,110] reported the crystal structure of $YBa_2Cu_3O_{7-\delta}$ superconductor immediately after its discovery as reviewed in ref. [111]. It has an ideal triple perovskite cube stacked along z direction with 1×1×3 dimension. An ideal triple cell perovskite has 9 oxygen, but in $YBa_2Cu_3O_{7-\delta}$ there are 6 or 7 oxygen per unit cell. Depending on the number of oxygen, it exhibit tetragonal or orthorhombic symmetry. Only after the neutron diffraction experiments by Beno et al. [42] and others [112-115], the oxygen positions and their occupancy were resolved clearly.

Figs.1.10 & 1.11 show the tetragonal and orthorhombic structure of $YBa_2Cu_3O_{7-\delta}$. In both the structures, the Y is in body centered position with Cu-O_2 and Ba-O layer in the form of $BaO/CuO_2/Y/CuO_2/BaO$. The main difference is occupancy of oxygen in (0 1/2 0) and (1/2 0 0) positions. The tetragonal structure has P4/mmm space group. The atomic positions are given in Table 1.4. The occupancy of oxygen O1 (1/2 0 0) is very small and depends on the value of δ. The O3 (1/2 0 .38) positions are slightly displaced towards Y leading to buckling of Cu2 –O3 layers. The Cu2-O3-Cu2 bond angle in tetragonal cell is around 167^o. The lattice parameters are of the order of a = b = 3.86 Å and c =11.82 Å.

The orthorhombic structure in $YBa_2Cu_3O_{7-\delta}$ has Pmmm space group. Here oxygen preferentially occupies in O1B (0 1/2 0) position rather than O1A (1/2 0 0) making the structure orthorhombic with slightly large 'b' axis compared to 'a' axis. The typical lattice parameters are a = 3.83, b = 3.88 and c = 11.65 Å. The atomic positions are given in Table 1.5. The O3 in orthorhombic cell is split into O3A (1/2 0 0.38) and O3B (0 1/2 0.38). Atomic positions of other elements are comparable to tetragonal cell. Y is eight co-ordinated by O3A and O3B oxygens with average Y-O bond length of 2.4 Å. The average Cu2-O3A-Cu2 and Cu2-O3B-Cu2 angles are 165°.

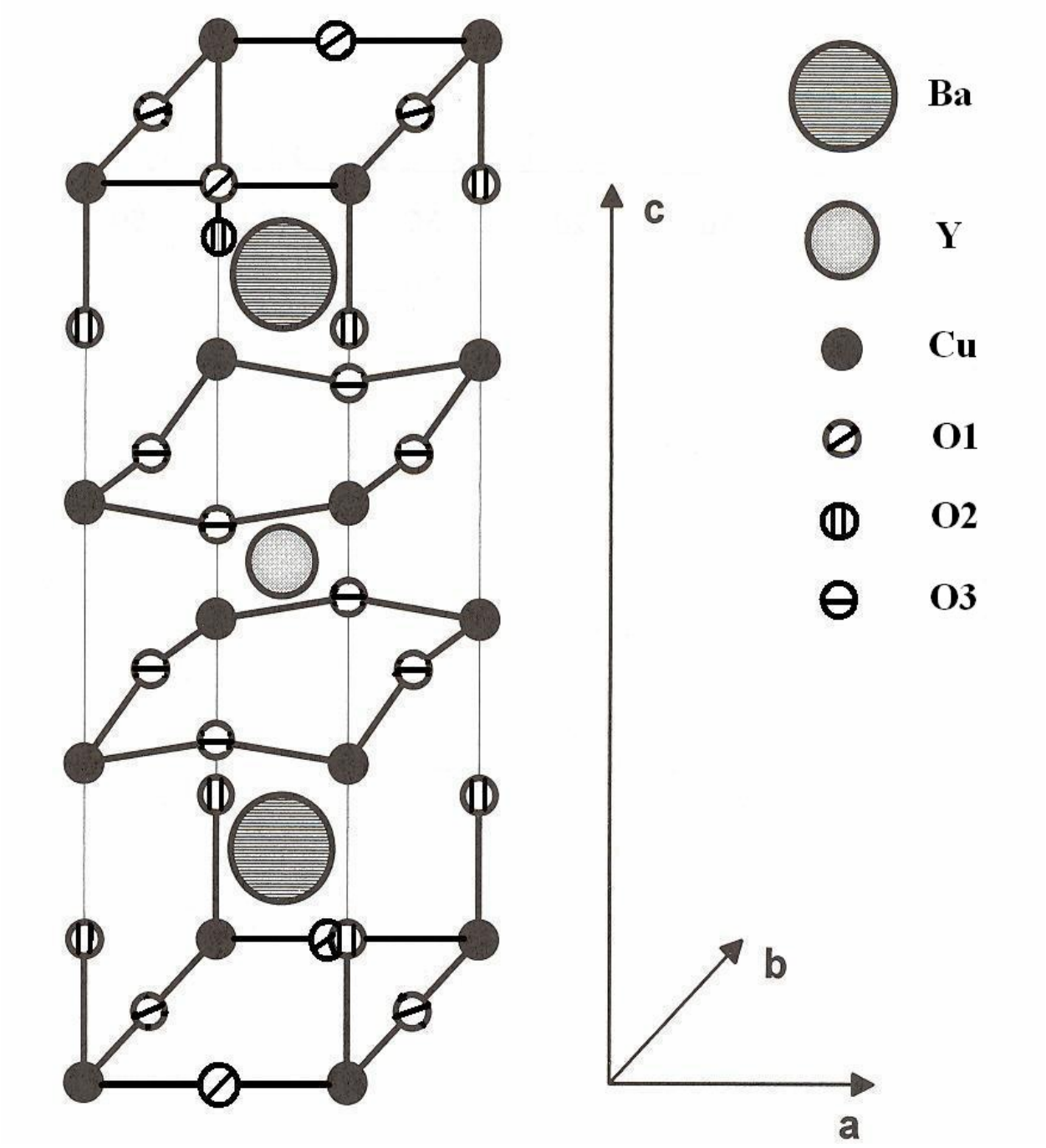

Fig. 1.10. Tetragonal unit cell of $YBa_2Cu_3O_{7-\delta}$ with lattice parameters a = b = 3.86 Å and c = 11.82 Å.

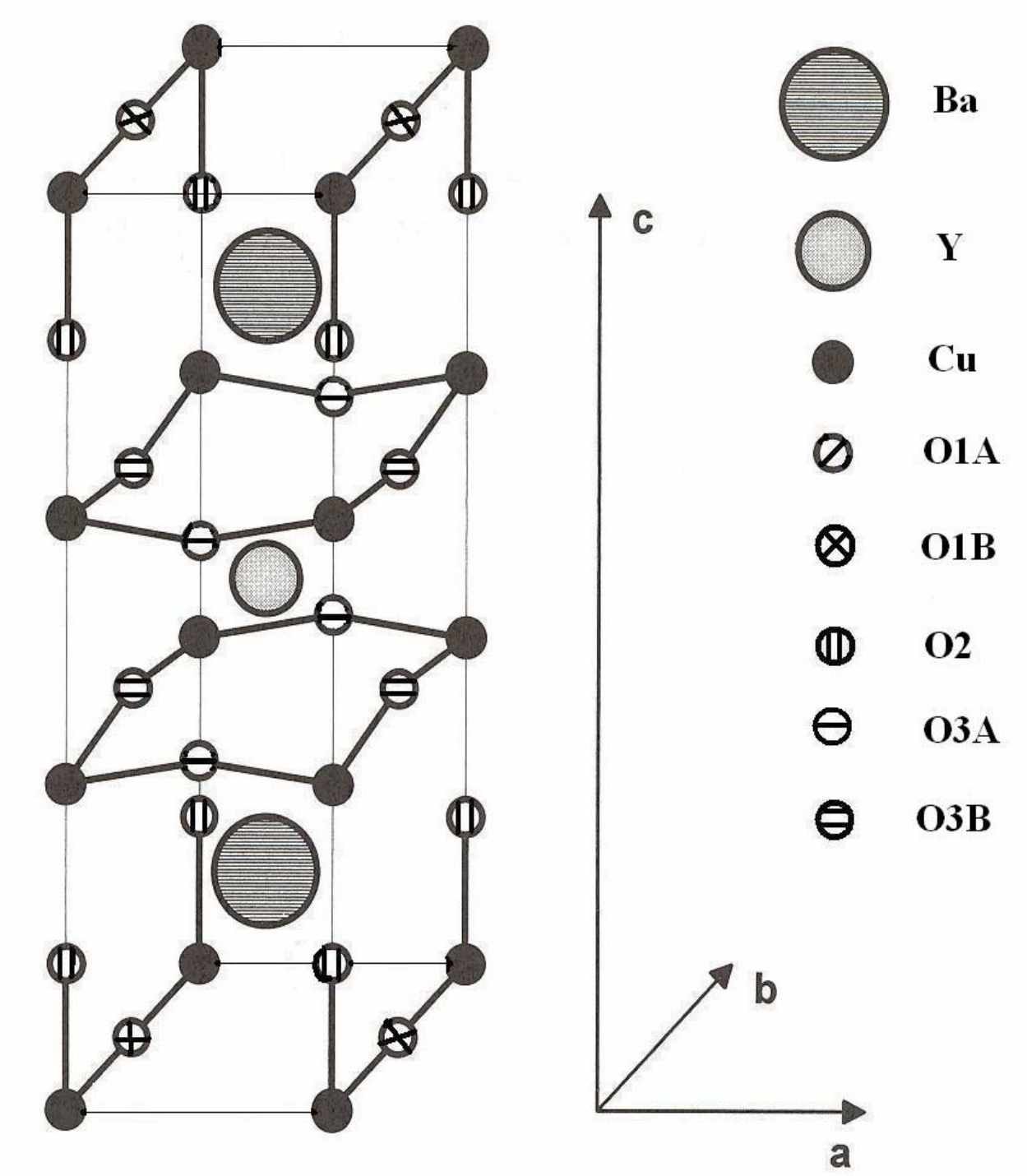

Fig. 1.11. Orthorhombic unit cell of $YBa_2Cu_3O_{7-\delta}$ with lattice parameters a = 3.83 Å, b = 3.88 Å and c = 11.65 Å.

Table 1.4. Normalized atomic positions of tetragonal unit cell of $YBa_2Cu_3O_{7-\delta}$ (P4/mmm).

Atoms	Positions		
	(x	y	z)
Y	0.5	0.5	0.5
Ba	0.5	0.5	0.19
Cu1	0	0	0
Cu2	0	0	0.36
O1	0.5	0	0
O2	0	0	0.15
O3	0.5	0	0.38

Table 1.5. Normalized atomic positions of orthorhombic unit cell of $YBa_2Cu_3O_{7-\delta}$(Pmmm).

Atoms	Positions		
	(x	y	z)
Y	0.5	0.5	0.5
Ba	0.5	0.5	0.18
Cu1	0	0	0
Cu2	0	0	0.35
O1A	0.5	0	0 (zero occupancy)
O1B	0	0.5	0
O2	0	0	0.16
O3A	0.5	0	0.38
O3B	0	0.5	0.38

The crystal structures of Bi-Sr-Ca-Cu-O superconductors are very complicated because of stacking faults, superstructural modulations and, oxygen and cation disorder. Tarascon et al. [67] and Sunshine et al.[68] reported the pseudo tetragonal symmetry with I4/mmm space group for 2201, 2212 and 2223 structures with lattice parameters a = b = 3.8 Å. and c values are respectively 24.6, 30.6 and 37.1 Å. Typical crystal structure of $Bi_2Sr_2CaCu_2O_y$ is shown in Fig. 1.12. They contain the layers of $BiO/SrO_2/CuO_2/Ca/CuO_2/SrO_2/BiO$.The difference between above three phases in Bi-Sr-Ca-Cu-O system is mainly the number of Ca-CuO_2 layers. Unlike

octahedral co-ordination observed in $(La,Ba)_2CuO_4$ system, here Cu has only the nearest neighbour oxygen in square pyramidal form. The crystal structure in Bi-Sr-Ca-Cu-O was also studied by several other groups [115-118].

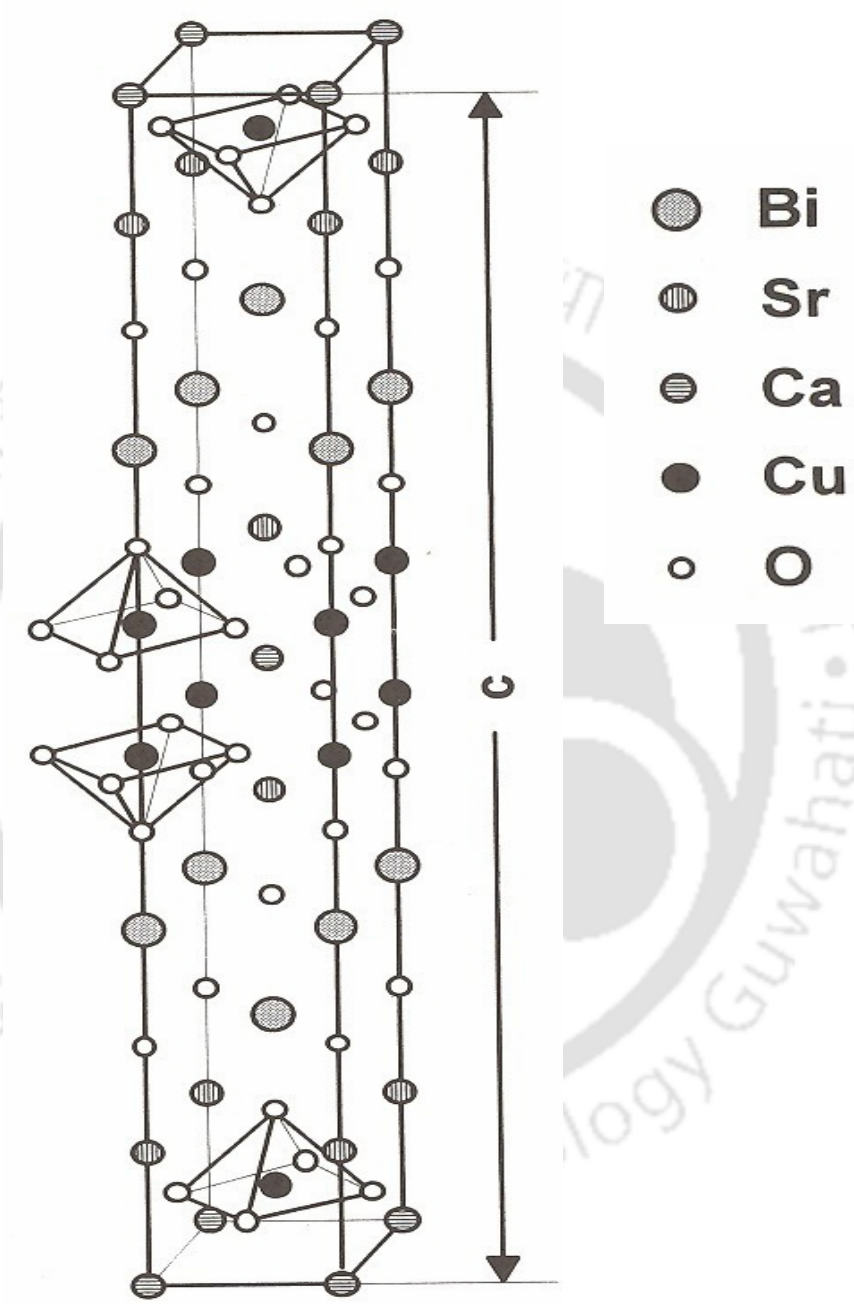

Fig.1.12 Tetragonal Unit cell of $Bi_2Sr_2CaCu_2O_y$ (Bi-2212)

The crystal structure of Tl-Ba-Ca-Cu-O system are strikingly similar to that of Bi-Sr-Ca-Cu-O system. However, the phases are close to ideal tetragonal I4/mmm symmetry without any

structural modulations. It was studied in detail by Hazen et al. [76], Subramanian et al. [77], Torardi et al. [78] and Parkin et al. [79]. The lattice parameters are found to be a = b =3.9 Å. and c = 23.2, 29.4 and 36.0 Å respectively for n = 1, 2 and 3 in $Tl_2Ba_2Ca_{n-1}Cu_nO_y$ series. On the other hand, in $TlBa_2Ca_{n-1}Cu_nO_y$ series, single TlO layers are inserted between neighbouring Cu-O_2 blocks. As a consequence, the c lattice parameters are smaller than those of Tl double layer series. Thus high T_c superconductor based on Cu-O_2 mostly exhibit perovskite layered structure with either elongated octahedral or square pyramidal co-ordination of Cu-O networks.

1.3. La-Ba-Ca-Cu-O Superconductors

The synthesis and crystal structure of non-superconducting parent compound $La_3Ba_3Cu_6O_z$ was studied by Er-Rakho et al. [119] even before the discovery of high T_c superconductors. The above compound is identical to $LaBaCu_2O_z$ and $La_2Ba_2Cu_4O_z$ compounds. Engelsberg [120] demonstrated that superconductivity could be introduced in $La_3Ba_3Cu_6O_z$ series by an addition of $CaCuO_2$ layer, i.e. with the composition $La_3Ba_3CaCu_7O_z$. Similarly superconductivity was reported in other two series with the compositions $LaBaCaCu_3O_z$ [121-123] (La-1113) and $La_2Ba_2CaCu_5O_z$ [124]. David et al. [125] showed that the crystal structure of the above compounds is similar to that of tetragonal $YBa_2Cu_3O_{7-\delta}$. The superconducting $LaBaCaCu_3O_z$ compound can also be compared with $YBa_2Cu_3O_{7-\delta}$, where Y is replaced by Ca and one Ba is replaced by La [121]. Following the discovery of superconductivity in $LaBaCaCu_3O_z$ compound, there are several reports on the substitution of La by other rare earths [126-129]. Unlike $YBa_2Cu_3O_7$, considerable variation of T_c has been observed by the substitution of other rare earth elements in place of La in $LaBaCaCu_3O_z$ superconductor. La could be completely replaced by using Nd or Pr. In Nd substitution, T_c varies from 69 to 33 K and on the other hand, the superconductivity is destroyed for about 60 % of Pr doping. Dy and Sm could be doped up to around 50 % and 75 % respectively without phase segregation [127]. Kuberkar et al. [124] studied the simultaneous substitution at rare earth site and addition of $CaCuO_2$ layers in the $(La_{2-x}R_x)Ba_2Ca_yCu_{4+y}O_z$ (y = 2x) series. In the above series, it has been found that there is an intermixing of Ca at La site and, Ca & La in Ba site [127].

To our knowledge, there is no detailed work on fluctuations induced excess conductivity, magneto-conductivity and, study of intergranular behaviour and critical current density using magnetic measurements. In the present work, we have prepared three series namely $(La_{1-x}Y_x)_2Ba_2CaCu_5O_z$, $(La_{1-x}Y_x)_2Ba_2Ca_{4x}Cu_{4+4x}O_z$ and $(La_{1-x}Gd_x)_2Ba_2Ca_{4x}Cu_{4+4x}O_z$. In each series,

we have prepared the material in pure and by adding 5 wt % Ag to enhance the intergranular coupling and critical current density. First series is to study the effect of Y doping in the La-Ba-Ca-Cu-O series. The second and third series are basically underdoped materials. They have been chosen to have a wide range of T_c and to study the evaluation of superconductivity.

1.4. Excess Conductivity and Magneto-Conductivity

The problem of superconducting fluctuations has been studied for almost four decades. It has attracted considerable interest since it addresses fundamental issues regarding the superconducting phase transition. To treat the problem of fluctuations theoretically, one can either start from a microscopic picture using Green function techniques or use a time dependent Ginzburg Landau (GL) theory. The GL formalism is probably more intuitive and can be used since both the approaches give the same results, at least close to T_c. Fluctuations are included in GL theory by allowing the order parameter to vary about its mean value. Since GL theory assumes that the order parameter takes the value associated with minimum free energy, it will break down when the fluctuations become large, i.e. very close to T_c. The usual criterion of this breakdown, known as the Ginzburg criterion [130], is that the magnitude of the fluctuations is comparable to the order parameter itself. For conventional superconductors like Nb_3Sn, this corresponds to a temperature interval of about 10 μK around T_c. The idea to observe fluctuations in superconductors was not readily accepted since theoretical estimates indicated that they should be extremely small. In the late 1960's, fluctuation effects were observed in thin films [131,132]. These effects are enhanced by the reduced dimensionality. By fortune, the first studied systems [133,134] could be well described by simple theories, which gave the subject a good start. Later development showed interesting anomalies which led to further theoretical investigations. These early measurements often focused on the excess conductivity above T_c associated with the fluctuations.

1.4.1. Theory of Excess Conductivity

The rounding effects on the electrical resistivity of homogeneous superconductors near the transition temperature can be explained as a result of excess conductivity arising from the thermodynamic fluctuations in the amplitude of superconducting order parameter. As a result of thermal fluctuations, there is a finite probability of cooper pair formation above the transition temperature T_c and that gives rise to excess conductivity at $T > T_c$. This phenomenon is understood on the basis of GL theory, which describes the free energy of the superconducting

state in terms of the order parameter. As the temperature is lowered towards T_c, there would be fluctuations in the amplitude of order parameter and their magnitude is initially small. The above region is called mean field regime. If the temperature is further lowered much closer towards T_c, the magnitude of the order parameter fluctuations become high enough to be comparable to the amplitude of order parameter itself. This region is called the critical region. Superconducting fluctuations which occur over the volume ξ^3(ξ-coherence length) cost an energy $(B_c^2(T)/2\mu_0)\xi^3$; where $(B_c^2(T)/2\mu_0)$ is the condensation energy per unit volume with thermo-dynamical critical field $B_c(T)$. The critical region around T_c at which, the mean field theory breaks down can be estimated, from the condition that this energy become comparable to the thermal energy.

$$\frac{B_c^{\,2}(T)}{2\mu_0}\xi^3(T) \approx \kappa_B T \tag{1.17}$$

The mean field temperature dependence of $\xi(T)$ is given by,

$$\xi(T) = \xi(0)\left[\left|T - T_c\right|/T_c\right]^{-1/2}. \tag{1.18}$$

By substituting eqns.(1.15) and (1.18) in eqn. (1.17), the condition for the break down of mean field treatment and entering into the critical region is given by,

$$\left|T - T_c\right|/T_c = \left[\frac{2\mu_0\kappa_B T_c}{B_c^{\,2}(0)\xi^3(0)}\right]^2; \tag{1.19}$$

where $B_c(0)$ and $\xi(0)$ are the thermodynamic critical field and the coherence length at zero Kelvin; κ_B is the Boltzmann constant. For conventional superconductors, T_c is in the range of 1 to 10 K, $B_c(0)$ is in the range of 10 mT to 100 mT and $\xi(0)$ is in the range of 100 to 1000 Å. So, the reduced temperature $|T\text{-}T_c|/T_c$ at which, the fluctuations enter into the critical region, is estimated to be in the range of 10^{-6} to 10^{-8}. Such a low value does not permit an easy experimental access. To observe the fluctuations effect in the conventional superconductors; it is convenient to study systems with reduced dimensionality. When one or more dimensions of the specimen are smaller, compared to the GL coherence length, the fluctuating volume becomes size limited for those directions. In such cases, the fluctuations effect is more easily observable. The reduction of dimensionality can be either geometrical; as in the cases of thin films, thin wires and fine particles, or structural; as in the cases of layered materials and materials with chain-like structures.

In high T_c superconductors, the T_c is around 100 K, $B_c(0)$ is around 10 Tesla and $\xi(0)$ is around 10 Å. So, from eqn.(1.19), the reduced temperature at which, fluctuations enter into critical region is estimated to be of the order of 10^{-2}. Hence in the high T_c superconductors, the cross-over from mean field to critical field regime can be observed.

The Direct (Aslamazov-Larkin) Contribution

Aslamazov and Larkin [135] derived expressions for the excess conductivity by attributing it to, the direct acceleration of the short lived superconducting pairs, created by fluctuations above T_c and is given as follows. The normal DC conductivity without such fluctuations is given by;

$$\sigma_n = \frac{ne^2\tau_{tr}}{m}, \tag{1.20}$$

where, τ_{tr} is the mean scattering time of the normal electrons in transport properties and n is their number density. Similarly, we can write an additional term contributed by superconducting fluctuations; by replacing n, e, m, and τ_{tr} by $n_s/2$, e*, m* and τ_k respectively, i.e.

$$\Delta\sigma = \frac{e^{*2}}{m^*}\sum_k \left\langle |\psi_k|^2 \right\rangle \tau_k / 2 \tag{1.21}$$

where, $n_s = \sum_k \left\langle |\psi_k|^2 \right\rangle$ is the number density of superconducting electrons, e* and m* are charge and mass of superconducting electrons. τ_k is a measure of relaxation time of superconducting fluctuations.

The thermodynamic average of $|\psi_k|^2$ can be worked out by following the statistical mechanical approach using the Boltzmann factor exp $(-F/\kappa_B T)$. Here F is the free energy, which can be obtained from Ginzburg-Landau theory.

$$\left\langle |\psi_k|^2 \right\rangle = (2m^*\kappa_B T)/\hbar^2(k^2 + 1/\xi^2) \tag{1.22}$$

The relaxation time τ_k can be written as [136]

$$\tau_k = \frac{\tau_0}{1 + k^2\xi^2} \tag{1.23}$$

where τ_0 is a constant. By substituting eqns. (1.22) and (1.23) in eqn. (1.21) and converting the summation into appropriate integration depending on the dimensionality of the sample, the $\Delta\sigma$ can be calculated. The summation can be replaced by following type of integrations depending on the nature of dimensionality,

$$\int \frac{d^3k}{(2\pi)^3} \qquad \text{for three dimension(3D)}$$

$$\frac{1}{d}\int \frac{d^2k}{(2\pi)^2} \qquad \text{for two dimension (2D)}$$

$$\frac{1}{S}\int \frac{dk}{2\pi} \qquad \text{for one dimension (1D)}$$

and the expressions for the excess conductivity are as follows:

$$\Delta\sigma_{3D}^{AL} = \frac{e^2}{32\hbar\xi(0)}\varepsilon^{-1/2} \tag{1.24}$$

$$\Delta\sigma_{2D}^{AL} = \frac{e^2}{16\hbar d}\varepsilon^{-1} \tag{1.25}$$

$$\Delta\sigma_{1D}^{AL} = \frac{\pi}{16}\frac{e^2\xi(0)}{\hbar S}\varepsilon^{-3/2}. \tag{1.26}$$

Here $\xi(0)$ is the average coherence length at zero Kelvin; $\varepsilon = (T-T_c)/T_c$ is the reduced temperature; d is the two dimensional characteristic length and S is the cross-sectional area ($S << \xi^2$) of the sample. Skocpol and Tinkham [137] have reviewed the excess conductivity analysis in the conventional superconductors. The theoretical aspects of excess conductivity were reviewed by Hohenberg [138] and Iye [139]. Equations 1.24 to 1.26 are basically referred as Aslamazov-Larkin (AL) theory for excess conductivity in the mean field region.

The initial excess conductivity results on amorphous bismuth films; studied by Glover [131] and, Naugle and Glover [132] were found to follow the AL theory. Experiments carried out on dirty Aluminium films [133] and dirty Lead films [134] were also found to agree with the above Aslamazov-Larkin theory.

The Lawrence-Doniach Model

According to Lawrence and Doniach (LD) [140], the material is built up of superconducting sheets with Josephson coupling between them. They modified the AL term for the layered superconductors, by taking the Josephson coupling between adjacent layers. The LD expression for excess conductivity is as follows;

$$\Delta\sigma_{LD} = \left(\frac{e^2}{16\hbar d}\right)\varepsilon^{-1}\left[1+2\alpha\right]^{-1/2} \tag{1.27}$$

where $\alpha = \alpha_0/\varepsilon = (2\xi_c(0)^2/d^{2)}/\varepsilon$. The advantage of LD expression is that it reduces to AL-2D for large ε values; where the coupling constant, $J = (\xi_c(T)/d)^2$ is quite small ($\xi_c(T) \propto \varepsilon^{-1/2}$) and to AL-3D for small values of ε, where in some cases, the coupling constant J would be quite strong. The cross over from 2D to 3D fluctuations occur at the temperature,

$$T_0 = T_c \exp\left(2\xi_c(0)/d\right)^2. \tag{1.28}$$

Lobb [141] has reported that when the temperature is within 0.1 K above T_c, the Ginzburg-Landau theory breaks down and the fluctuations enter into the critical regime. In the critical regime, Δσ data vary as $\varepsilon^{-0.67}$. If the temperature is further lowered towards T_c, the fluctuations enter into the dynamic critical region, where $\Delta\sigma \sim \varepsilon^{-0.33}$.

The Indirect (Maki-Thompson) Contribution

The magnitudes of excess conductivity observed for cleaner lead and aluminum films were found to be larger than the values expected from AL theory and, their temperature dependences were anomalous [142-145]. The origin of this additional conductivity has been understood, as an indirect effect of the fluctuations on the quasiparticle conductivity. The fluctuating cooper pairs decay into pairs of quasiparticles of nearly opposite momenta. By time-reversal symmetry, the quasiparticles remain in a state of small total momentum, even after scattering from an impurity potential, and continue to be accelerated much as they were before. The quasiparticle lifetime is limited. Maki [146] and Thompson [147] calculated this indirect contribution to fluctuations induced excess conductivity and, it is given as follows;

$$\Delta\sigma_{3D}^{MT} = \frac{4e^2}{32\hbar\xi(0)}\varepsilon^{-1/2} \tag{1.29}$$

$$\Delta\sigma_{2D}^{MT} = \frac{e^2}{8\hbar d}\frac{1}{(\varepsilon - \delta')}\ln\frac{\varepsilon}{\delta'} \tag{1.30}$$

where δ' is the fractional depression of T_c due to pair breaking interactions. The Maki-Thompson (MT) term for three dimensional fluctuations is four times higher than the AL-3D term. The ratio of $\Delta\sigma_{2D}^{MT}/\Delta\sigma_{2D}^{AL}$ goes to 0 at T_c (ε = 0), 2 at $\varepsilon = \delta'$ and, diverges logarithmically for $\varepsilon >> \delta'$. In this picture, the total excess conductivity is given by the sum of, the AL term (1.25) and MT term (1.30). Crow et al. [148] demonstrated that the combined AL & MT theory could fit the experimental data of aluminum and lead films.

The Maki-Thompson term for layered superconductors was derived by Hikami and Larkin [149] and independently, by Maki and Thompson [150] and is given as follows in the absence of applied magnetic field;

$$\Delta\sigma_{MT} = \frac{e^2}{8\hbar d(\varepsilon - \alpha\varepsilon/\delta)} \ln\left[\frac{\delta\left(1+\alpha+\sqrt{1+2\alpha}\right)}{\alpha\left(1+\delta+\sqrt{1+2\delta}\right)}\right]. \tag{1.31}$$

Here $\delta = \left(16\xi_c(0)^2 \kappa_B T \tau_\phi / (\pi d^2 \hbar)\right)$ is the pair breaking parameter; κ_B is the Boltzman constant and τ_ϕ is the phase breaking time. This modified MT term gets reduced to the known 2D or 3D MT expression in the limiting cases.

Corrections and Other Contributions

Besides these direct contribution and indirect contribution to excess conductivity, Dorin et al. [151] proposed that the fluctuation conductivity of layered superconductors can be analyzed, by taking into account, the fluctuations in density of states (DOS) of the quasiparticles due to the formation of the cooper pairs. According to them, the fluctuation induced excess conductivity is the sum of four different contributions: AL, DOS and, regular and anomalous terms of MT, i.e. $\Delta\sigma = \Delta\sigma_{AL} + \Delta\sigma_{DOS} + \Delta\sigma_{MT}^{reg} + \Delta\sigma_{MT}^{an}$ .The contribution of $\Delta\sigma_{DOS}$ and $\Delta\sigma_{MT}^{reg}$ are in negative sign.

To explain the excess conductivity data at high reduced temperature region, the momentum cut off [152-157] and energy cut off [157-161] have been proposed in some of the theoretical papers. According to Viña et al.[161], the expression for excess conductivity based on Gaussian-Ginzburg-Landau (GGL) approach by introducing momentum or total energy cut-off can be written as;

$$\Delta\sigma_{ab}(\varepsilon) = \frac{Ne^2}{16\hbar d}\left[\frac{1}{\varepsilon}\left(1+\frac{N^2 B_{LD}}{\varepsilon}\right)^{-1/2} + f(\varepsilon)\right] \tag{1.32}$$

where N is the number of superconducting layers with length periodicity d. Here $B_{LD} = (2\xi_c(0)/d)^2$ is the Lawrence-Doniach parameter. $f(\varepsilon)$ is a parameter based on GGL approach; $f(\varepsilon) = 0$ for no cut off, $f(\varepsilon) = -\delta - \delta^3 c\,(\varepsilon + c + N^2 B_{LD}/2)$ for momentum cut off and $f(\varepsilon) = c^{-2}(\varepsilon - 2c + N^2 B_{LD}/2)$ for total energy cut off. Here the parameter $\delta = [(\varepsilon + c)(\varepsilon + c + N^2 B_{LD})]^{-1/2}$. Lang [162] discussed that the paraconductivity and magneto-conductivity in high T_c superconductors can be analyzed by taking into account the distribution of transition temperature. He has

demonstrated that by taking into account the Gaussian distribution of T_c, the magneto-conductivity could be fitted well.

1.4.2. Theory on Magneto-Conductivity

Fluctuations induced excess conductivity in the mean field region can also be studied in the presence of magnetic field. The main advantage of magneto-conductivity analysis, over zero field excess conductivity is that, the uncertainty in the estimation of normal state conductivity is eliminated. So, the relevant physical parameters can be estimated without much uncertainty.

The conductivity in the absence and presence of magnetic field can be written as $\sigma(0) = \sigma_n(0) + \Delta\sigma(0)$, and $\sigma(H) = \sigma_n(H) + \Delta\sigma(H)$ respectively. In both the cases, the conductivity is the sum of normal state (σ_n) and excess conductivity ($\Delta\sigma$). The magneto-conductivity, $\Delta\sigma_H = \sigma(H) - \sigma(0) = \Delta\sigma(H) - \Delta\sigma(0)$. In the normal state, the applied magnetic field has negligible effect on its conductivity. The fluctuation magneto-conductivity, $\Delta\sigma_H$ for layered superconductors was theoretically studied by Hikami and Larkin[149], and independently by Maki and Thompson[150]. Their work was based on the pair breaking effect of the magnetic field, which leads to the suppression of T_c in mean-field theory and decreases the fluctuation conductivity. Hence a positive magneto-resistivity results, which is expressed in terms of a negative magneto-conductivity.

They have worked out the AL and MT contributions in the dirty limit. The AL terms correspond to direct contribution to $\Delta\sigma_H$ and MT terms correspond to indirect contribution to $\Delta\sigma_H$. They have carried out the derivation by considering the interactions of magnetic field with orbital motion of charge carriers and they are represented as $\Delta\sigma_{ALO}$ and $\Delta\sigma_{MTO}$. ALO and MTO refer Aslamazov-Larkin-Orbital and Maki-Thompson-Orbital contribution respectively and are given as follows;

$$\Delta\sigma_{ALO} = \frac{-e^2}{64\hbar d\varepsilon^3}\frac{2+4\alpha+3\alpha^2}{(1+2\alpha)^{5/2}}h^2 \tag{1.33}$$

and

$$\Delta\sigma_{MTO} = \frac{-e^2}{48\hbar d(1-\alpha/\delta)\varepsilon^3}\left[\frac{\delta^2}{\alpha^2}\frac{1+\delta}{(1+2\delta)^{3/2}} - \frac{1+\alpha}{(1+2\alpha)^{3/2}}\right]h^2 \tag{1.34}$$

In the above equation, $h^2 = H_{eff}{}^2 (2e\xi_{ab}(0)^2 / \hbar)^2$, where H_{eff} is the effective magnetic field along the c-direction of unit cell. According to Matsuda et al. [163], $H_{eff}{}^2 = H^2 \langle \cos^2\theta \rangle = H^2/3$, and it is to take into account the angular average of superconducting planes in polycrystalline samples. Here H is the applied magnetic field and $\xi_{ab}(0)$ is the coherence length along ab plane at 0 K.

Arnov, Hikami and Larkin [164] derived the expression for $\Delta\sigma_H$ by considering the interaction of magnetic field with spin moments of the charge carriers, i.e. Zeeman splitting and it was later modified by Thompson [165]. According to them, the contribution of Zeeman effect on direct ($\Delta\sigma_{ALZ}$) and indirect ($\Delta\sigma_{MTZ}$) fluctuation conductivity can be written as,

$$\Delta\sigma_{ALZ} = -0.526 \frac{e^2}{\hbar d \varepsilon^2} \frac{1+\alpha}{(1+2\alpha)^{3/2}} \left[\frac{\omega_s}{4\pi\kappa_B T_c} \right]^2 \tag{1.35}$$

and

$$\Delta\sigma_{MTZ} = \frac{-e^2}{16\hbar d\varepsilon} \left[\frac{1+\delta}{(1+2\delta)^{3/2}} - \frac{1+\delta+\delta/\alpha}{[(1+\delta/\alpha)(1+2\delta+\delta/\alpha)]^{3/2}} \right] \left[\frac{\omega_s \tau_\phi}{\hbar} \right]^2 \tag{1.36}$$

Here $\omega_s = g\mu_B H$ is the Zeeman energy; g is the Lande's g factor and μ_B is the Bohr magneton.

Bieri and Maki [166] argued that high T_c superconductors are mostly in clean limit and accordingly derived the expressions for fluctuation magneto-conductivity, where the only difference is that the expression for δ is replaced with a new one as follows,

$$\delta_{clean} = 1.203 \frac{1}{\xi_{ab}} \delta_{dirty}$$

1.4.3. Experimental Works on Excess Conductivity and Magneto-Conductivity

There are different procedures suggested and followed in literature to estimate excess conductivity and to find the dimensionality of the order parameter fluctuations and other material dependent parameters. Brief review of different techniques for Δσ calculation and analysis are given below.

The experimental excess conductivity (Δσ) can be estimated by subtracting the extrapolated normal state conductivity ($1/\rho_n$) from the measured conductivity ($1/\rho$) [167,168]. The normal state resistivity $\rho_n(T)$ is generally obtained by fitting the measured resistivity data to the equation,

$$\rho_n = a + bT \tag{1.37}$$

from $2T_c$ to 300 K. The dimensionality of order parameter fluctuation is obtained by fitting the data of $\ln\Delta\sigma$ versus $\ln\varepsilon$ to the linear equation as per AL model ($\Delta\sigma = C\varepsilon^{\lambda}$).

For the above calculations, an accurate determination of mean field transition temperature T_c is needed. It is taken as a temperature at which, the plot of $d\rho/dT$ versus T exhibits a single peak [168] or the temperature at which the measured resistivity is half of the extrapolated normal state resistivity [169]. The other techniques followed to determine T_c are by extrapolating the plot of $1/\Delta\sigma$ versus T to zero [170] or by assuming it as a free parameter of the fit [171].

For the estimation of normal state resistivity, apart from the linear equation, Anderson-Zou functional form has also been used in literature. According to Anderson and Zou [172], the normal state resistivity can be written as $\rho_n(T) = \frac{C_1}{T} + C_2 T$, where C_1 and C_2 are positive constants. Veira et al. [173] described the normal state resistivity as a combination of resistivity arising from the intergranular weak links and the grains and, is given by $\rho_n(T) = \rho_0 + \frac{1}{p}\rho_{gn}(T)$, where ρ_0 is the resistivity arising from the weak links and the impurities, ρ_{gn} is the grain resistivity and p is to account for the effective reduction in the cross sectional area of the sample due to the orientation mismatch of the ab-planes in the polycrystalline samples.

Hazen et al. [171] argued that the calculation of $\Delta\sigma$ by subtracting the background conductivity from the measured conductivity will lead to an underestimation of $\Delta\sigma$. This is because at high temperatures, both the $\Delta\sigma$ (if 2D) and σ_n vary as 1/T, the estimation of ρ_n (T) as above will give rise to an overestimation of its value. They have fitted the measured conductivity to the sum of excess and normal state conductivities,

$$\sigma(T) = \Delta\sigma(T) + \sigma_n(T) \tag{1.38}$$

Testardi et al. [174] developed a procedure to study the dimensionality of fluctuations without having to know the T_c value. According to them, the AL expression ($\Delta\sigma = c\varepsilon^{\lambda}$) can be written in the form of,

$$\frac{(\rho_n - \rho)}{\rho} = \rho_n c \varepsilon^{-\lambda} \tag{1.39}$$

where c is AL constant and, λ is either 1 or 0.5 depending upon whether 2D or 3D fluctuations. Taking temperature derivative of equation (1.39) on both sides and rearranging; we get

$$\frac{1}{\rho^2}\frac{d\rho}{dT}-\frac{1}{\rho_n{}^2}\frac{d\rho_n}{dT}=\frac{\lambda}{T_c}(c)^{(-1/\lambda)}\left[\frac{\rho_n-\rho}{\rho\rho_n}\right]^{1+(1/\lambda)} \tag{1.40}$$

The exponent λ can be obtained from the slope of log-log plot of the left hand side of eqn. (1.50) versus $\Delta\sigma=\left[(\rho_n-\rho)/(\rho\rho_n)\right]$. The value of transition temperature is not required for this analysis. The slope will be 2 for 2D fluctuations (λ = 1) and 3 for 3D fluctuations (λ = 0.5).

The choice of mean field transition temperature, T_c plays a crucial role on the determination of critical exponents in the mean field region. To independently determine the dimensionality of order parameter fluctuations without the influence of choice of T_c, Kovel and Fisher [175] proposed the technique, mainly to study the critical exponent of ferromagnetic materials and the same technique can be extended for excess conductivity analysis. According to them, the temperature derivative of excess conductivity can be written in the following form,

$$Z(T)=\left\{\frac{d}{dT}\left[\ln\left(\Delta\sigma/\sigma_0\right)^{-1}\right]\right\}^{-1}=\left(T-T_c\right)/\lambda \tag{1.41}$$

Thus the plot of Z (T) versus T gives a straight line in the mean field region with a slope (1/λ) and intercept in the temperature axis (Z →0) at T = T_c. The above method facilitates the determination of critical exponent λ and the mean field transition temperature T_c simultaneously. The above technique has been used by Pureur et al. [176] and Jurelo et al. [177] to study the fluctuations phenomena of $YBa_2Cu_3O_7$ superconductors.

The fluctuation induced excess conductivity data in $YBa_2Cu_3O_7$ superconductors have been studied extensively in polycrystalline [167,169,178-186], single crystal [187-190] and thin film samples [191-194]. In most of the reports, 2D to 3D cross over has been reported in the mean field region. However, a few groups have reported only 3D fluctuations in the mean field region. In some of the reports, the data were analyzed even down to critical regions with critical exponents comparable to that predicted by Lobb [141]. The contribution of Maki-Thompson term to zero field excess conductivity has been studied by a few groups and the estimated value of phase breaking time, τ_ϕ (100 K) is found to be in the order of 10^{-13} to 10^{-14}s; indicating moderate pair breaking effect [195-200]. The coherence length along c-direction at 0 K, (ξ_c) is found to be in the range of 1.0 to 3.0 Å.

The fluctuation magneto-conductivity in polycrystalline$YBa_2Cu_3O_7$ was studied by Matsuda et al. [163] and they have analyzed the data in terms of ALO and MTO terms. They have also carried out the analysis of $\Delta\sigma_H$ measured on single crystal thin film samples of $YBa_2Cu_3O_7$, by applying magnetic field both parallel and perpendicular to ab plane [197]. Here, they have considered the contributions of both orbital and Zeeman effect on AL and MT terms and, the estimated values of ξ_c (0), ξ_{ab} (0) and τ_ϕ(100 K) are found to be 1.5 Å, 11.5 Å and 10^{-13}s respectively. Following Matsuda's reports, there are several papers reported on the $\Delta\sigma_H$ analysis in polycrystalline [201], single crystals [198, 202-208] and thin film [197, 209-213] samples of $YBa_2Cu_3O_7$. In most of the reports, the orbital and Zeeman contributions of AL and MT terms have been taken into account. The values of ξ_c (0), ξ_{ab} (0) and τ_ϕ(100 K) are found to be in the range of 1 to 3 Å, 11 to 15 Å and 10^{-13} to 10^{-14}s respectively. In $NdBa_2Cu_3O_7$ thin film, significant contributions of both orbital and Zeeman terms of MT model have been reported [214]. The value of ξ_c (0), ξ_{ab} (0) and τ_ϕ(100 K) are found to be 2.4 Å, 21.0 Å and 4.5×10^{-13}s respectively.

Vidal et al. [215] and a few other groups [216,217] reported 2D fluctuations in the 85 K phase of Bi-Sr-Ca-Cu-O system. Balestrino et al. [218] and a few other groups [219,220] reported 2D fluctuations on multiphase compound of Bi-Sr-Ca-Cu-O system with 110K phase as major phase. Ravi and Seshu Bai [221,222] studied the excess conductivity on single phase samples of 85 K and 110 K phase superconductors and reported 2D fluctuations in the mean field region. There are also similar conclusions on single crystal and thin film samples of Bi-Sr-Ca-Cu-O system [223-227]. Ravi and Seshu Bai [228] fitted the excess conductivity data of Bi system to the sum of the LD and MT terms. The estimated values of τ_ϕ(100 K) are 3.7×10^{-16}s and 11.3×10^{-16}s respectively for the 85 K and 110 K phases of the system. The contribution of MT term is reported to be negligible in the magneto-conductivity of $Bi_2Sr_2Ca_2Cu_3O_z$ [229]. The fluctuation induced excess conductivity in Bi-Sr-Ca-Cu-O system have been also analyzed by considering fluctuations in density of states, anomalous and regular contributions of MT term [230]. To explain the excess conductivity in high reduced temperature, total energy cut-off has been applied [231].

The excess conductivity in Tl-Ba-Ca-Cu-O system has been studied by several groups and most of them reported 2D fluctuations in the mean field region [232-236]. The excess conductivity and fluctuation magneto-conductivity in the above system have been also analyzed

by taking MT contributions into account and the value of phase breaking time, τ_ϕ (100 K) is found to be in the order of 10^{-13} to 10^{-15}s [237-239]. The excess conductivity in Tl-Ba-Cu-Ca-O system was also analyzed by taking into account fluctuations in quasiparticle density of states (DOS) and by imposing momentum and total energy cut off [230,231,238,239].

In addition to excess conductivity studies on the above high T_c superconductors, there are a few reports on Hg-Ba-Ca-Cu-O [240,241] and MgB2 [242] superconductors. In Hg-Ba-Ca-Cu-O system, 2D fluctuations are observed in the mean field regime and moderate pair breaking effect has been observed with τ_ϕ (100 K) $\approx 2.3\times10^{-13}$s and $\xi_{ab}(0) = 7$ Å. In MgB_2 superconductors, 3D fluctuations have been reported.

In (La, Sr)-Cu-O system, 3D fluctuations was observed in the mean field region [243,244]. In $CaLaBaCu_3O_y$ and $CaSmBaCu_3O_y$, Krishnan et al. [245] fitted the measured conductivity to the sum of Veira's normal state conductivity and LD excess conductivity expressions.

1.4.4. Excess Conductivity in Paracoherence Regime

So far we reviewed about the excess conductivity arising out of the fluctuations in the magnitude of order parameter (ψ) in the mean field region. Similarly in the paracoherence region, i.e. from zero resistivity transition temperature (T_{c0}) to transition mid-point (T_c), there would be fluctuations in the phase of the order parameter and that also gives rise to excess conductivity. At the transition mid point, T_c, even though all the individual grains become superconducting, the phase of the order parameter is still different from grain to grain. The phase coherence of all the superconducting grains starts at the temperature T_{c0}, at which the electrical resistivity of the material becomes zero.

According to Rosenblatt et al.[246, 247], the conditions under which such transitions can be observed are, (1) the grain size is larger than a critical size, a_0 and (2) the Josephson coupling strength J, between adjacent grains is smaller than the superconducting condensation energy of the grains.

In the temperature range T_c to T_{c0}, the magnitude of the order parameter assumes an identical non-zero value in each grain. But however, the phase ϕ of the order parameter fluctuates from grain to grain. The fluctuations in the phase of the order parameter give rise to excess conductivity in the above temperature range, and is given by [248],

$$\Delta\sigma' = \frac{1}{\rho(T)} - \frac{1}{\rho(T_c)} \tag{1.42}$$

where $\rho(T_c)$ is the measured resistivity at T_c. The $\Delta\sigma'$ varies as,

$$\Delta\sigma' \propto \left(\frac{T - T_{c0}}{T_{c0}}\right)^{-\gamma} \tag{1.43}$$

where γ is the critical exponent of excess conductivity.

The paracoherence to coherence transition in granular superconductors is analogous to paramagnetic to ferromagnetic transition in three dimensional (3D) XY ferromagnets [249]. So, the excess conductivity critical exponent 'γ' of superconductors can be compared to the ac susceptibility critical exponent of ferromagnets. Le Guillou and Zinn-Justin [250] predicted the value of 'γ' to be 1.32 for the pure 3D XY ferromagnetic system. Rushbrooke et al. [251] from the high temperature series expansion of the random site diluted Heisenberg model found that the 'γ' value increases from its pure value of nearly 1.36 to values higher than 2.36 when the concentration goes above the percolation threshold. However, by applying the high temperature series method to the random bond diluted Heisenberg model, Brown et al. [252] found that 'γ' retains its pure value for concentrations close to the percolation threshold.

Rosenblatt et al.[246,247] and Raboutou et al. [249] measured the temperature variations of penetration depth and dynamic resistance on Nb and Ta bulk superconducting grains pressed with epoxy resin and, on sintered $YBa_2Cu_3O_7$. They have found the critical exponents $\beta > 0.7$ and $\gamma = 2.6 \pm 0.2$. These are twice the value predicted for 3DXY ferromagnet and they have explained the discrepancy in terms of disorder in the coupling energy. In $YBa_2Cu_3O_{7-\delta}$, superconductors, Krishnan et al. [248] reported the 'γ' values close to 1.33. According to Marhas et al. [253], the 'γ' value changes from 1.99 to 1.62 on thin film of $YBa_2Cu_3O_{7-\delta}$ upon irradiation. In $NdBa_2Cu_3O_7$ thin film, ordered phase fluctuations ($\gamma \approx 1.33$) have been reported in the absence of applied magnetic field, however in the presence of magnetic field, cross-over from ordered to disordered (≈ 2.7) phase fluctuations has been observed [254]. In polycrystalline sample of $YBa_2Cu_3O_{7-\delta}$, Sharma et al. [255] reported that $\gamma = 1.33$.

In 85 K and 110 K phases of Bi-Sr-Ca-Cu-O system, Isaac Samuel et al. [256] reported a critical exponent close to 2.7 and it is comparable to that of disordered 3D Heisenberg ferromagnet system. γ value was found to be 1.33 in polycrystalline $Bi_{1.6}Pb_{0.4}Sr_2Ca_2Cu_3O_y$ sample [255]. In $Tl_2Ba_2CaCu_2O_8$ compound, γ value was reported to be 1.33 by Krishnan et al.

[248]. In $(La_{1.8}Sr_{0.2})CuO_4$ compound, the γ value was reported to be 1.33 and 2 by Sharma et al. [255] and Levy et al. [257] respectively. In $CaLaBaCu_3O_{7-\delta}$ compound, Krishnan et al. [248] reported the γ values close to 1.33.

1.5. **AC Susceptibility**

AC susceptibility is one of the important tools among the magnetic measurements for the characterization of high T_c superconductors. It not only facilitates an unambiguous determination of macroscopic parameters like T_c onset of different phases, critical current density, etc. but also allows us to learn about the nature of coupling between the grains [258-262]. The complex ac susceptibility χ is the sum of real part χ' and imaginary part χ'', i.e. $\chi = \chi' + i\chi''$. The real part of susceptibility (χ') normally shows a sharp drop below T_c as a result of diamagnetic shielding of superconducting grains, and approaches -1 depending on the temperature and field amplitude. The imaginary part of susceptibility (χ'') measured in polycrystalline materials exhibits peaks below T_c, which are as a result of losses incurred due to flux motions in the grains and/or at the grain boundaries [263].

The measurement of ac susceptibility as a function of temperature, ac field amplitude and superimposed dc field allows us to learn about the coupling between the grains, estimate the effective volume fraction of the superconducting grains and determine the critical current densities [264-266].

AC susceptibility can also be studied using frequency variation. From the χ'' data measured at different frequencies, the shift in the χ'' peak temperature with frequency can be analyzed based on Anderson's flux creep model [259, 267]. The shift in the intergrain peak temperature gives the activation energy for flux creep at the grain boundaries, which is a measure of the bulk pinning strength. Very weak frequency dependence of χ'' peak temperature was observed in high T_c superconductors [259, 268-271] in the range 10 Hz to 10 kHz. So, the flux vortex is almost stable in high T_c superconductors at low frequency.

AC susceptibility measured at low frequencies can be analyzed in terms of critical state models. These models give information about the distribution of current inside the superconducting specimen with respect to applied external magnetic field. According to these models, the penetrated super current flows with a density equal to the critical current density J_c

(H_i), where H_i is the local internal field. According to Ampere's law, the penetrated supercurrent is a function of field gradient as given below,

$$\frac{dH_i(r)}{dr} = \pm J_c(H_i) \tag{1.44}$$

where the ± sign determines, whether the super current is trying to screen out the magnetic flux line from entering the sample when the applied field is being increased or it is trying to confine the magnetic flux lines which have already entered the sample from exiting as the applied field is being reduced.

For simplicity, Bean [272] assumed that J_c is independent of H_i. According to the critical state model, the J_c at χ'' peak temperature (T_m) can be written as,

$$J_c(T_m) = \frac{H_m}{a} \tag{1.45}$$

where H_m is the amplitude of the applied magnetic field at the surface of a sample and a is the radius of the cylindrical sample or the half thickness of parallelepiped shaped sample. Here the field is applied along the length of the sample. When the applied field reaches a particular value (H_p) at the surface of the cylinder, the field just completely penetrates to the center of the superconducting sample. At this condition, the applied field, $H_m = H_p$ is compensated by the field produced by the supercurrent ($J_c a$).

Subsequent to Bean's field-independent critical state model, several models for the field dependence of J_c (H_i) have been proposed in the literature [273-278]. According to Kim model [273],

$$J_c(H_i) = \frac{k}{H_0 + |H_i|} \tag{1.46}$$

where k and H_0 are positive constants. Watson [274] reported a simple linear function

$$J_c(H_i) = A - C|H_i|, \tag{1.47}$$

where A and C are positive constants. Irie et al. [275] and Green et al. [276] proposed a power-law model

$$J_c(H_i) = K_1|H_i|^{-q}, \tag{1.48}$$

where K_1 and q are positive constants. Fietz et al. [277] and Karasik et al. [278] proposed an exponential law model

$$J_c(H_i) = A_1 \exp\frac{-|H_i|}{C_1}, \tag{1.49}$$

where A_1 and C_1 are positive constants. Out of all the models mentioned above, Kim model is the more generalized. It reduces to the linear model when $H_0 >> H_i$, to Bean model when k and H_0 become infinite in such a way that k/H_0 is a constant and to the power law model for q = 1 if $H_0 = 0$.

By employing Bean model, Clem [279] has derived expressions to estimate intergranular and intragranular $J_c(T)$ from the measured susceptibility. Clem has assumed that the superconducting grains are in cylindrical shape with their long axes parallel to the applied field. According to Murphy et al. [265] Clem's expressions can be written as

$$\chi'(T) = -1 + \frac{J_c(T_m)}{J_c(T)}\left[1 - \frac{5J_c(T_m)}{16J_c(T)}\right] \quad \text{for } T < T_m \tag{1.50}$$

$$\chi'(T) = \frac{-5J_c(T)}{16J_c(T_m)} \quad \text{for } T > T_m \tag{1.51}$$

where χ' (T) is the real part of susceptibility as a function of temperature and $J_c(T_m)$ is the J_c at χ'' peak temperature (T_m). Müller [280] has calculated ac susceptibility for a sample of slab geometry using critical state model, by taking J_c (H_i) function very close to that of Kim model. The local intergranular and intragranular current densities have been assumed to be $J_{cj} \sim \alpha_j / (H_{0j} + |H_i|)$ and $J_{cg} \sim \alpha_g / (H_{0g} + |H_i|)$, where H_{0j} and H_{0g} are positive constants. α_j and α_g are respectively the pinning force densities for intergranular Josephson vortices and intragranular Abrikosov vortices, and they are assumed to be independent of field. To calculate the temperature dependences of χ' and χ'', Müller has taken the temperature dependences of α_j and α_g as α_j (T) $\sim(1-(T/T_c))^2$ and α_g (T) $\sim[1-(T/T_c)^2]^2$ and shown that his theoretical model could fit the experimental susceptibility data of Goldfarb et al. [258].

Ji et al. [281] derived expressions for magnetization using a simplified version of Kim model with J_c (H_i) = k/H_i, for a slab geometry sample. Ishida et al. [282] found that the harmonic susceptibility measured on polycrystalline $YBa_2Cu_3O_7$ could be explained well using the expressions derived by Ji et al. Xu et al. [283] derived the expression for initial and descending branch of M-H loop by using an extended Kim critical state model, where an additional parameter β is introduced, i.e. J_c (H_i, T) = J_c (T)/ $[1+ (H_i/H_0 (T))]^{\beta}$. Lam et al. [284] have derived

expressions for susceptibility using a modified critical state model in which steeper field dependence of J_c (H_i) was taken (J_c (H_i) ~$H_i^{-1.8}$) compared to Kim model. Ravi Kumar and Chaddah [285] discussed a numerical method for the calculation of magnetization and critical current density based on exponential critical state model.

Chen et al.[286], have derived detailed analytical expressions for magnetization as a function of applied field at low, medium and high fields for an orthorhombic sample geometry with a cross section 2a × 2b, using Kim model (eqn.1.46) for $J_c(H_i)$. At low fields, the amplitude of applied field (H_m) is less than the full penetration field (H_p). The full penetration field, H_p is the field at which applied field just reaches the center of the sample. For $H_m > H_p$, there are two cases namely medium field & high field. In high field case, the reverse super current completely penetrates to the center of the sample before the applied field, H has decreased to 0. This corresponds to $H_m > H_m^* = (H_0^2+4ka)^{1/2}-H_0$. In the medium field case, the reverse super current does not completely penetrate to the sample even when H has reduced to zero. If H is the applied field and M_i is the local magnetization, i.e. the field produced by bulk super currents, we have

$$M_i = H_i - H \qquad (1.52)$$

The total magnetization M is the average of M_i over the sample cross section. The expression for total magnetization is obtained as follows.

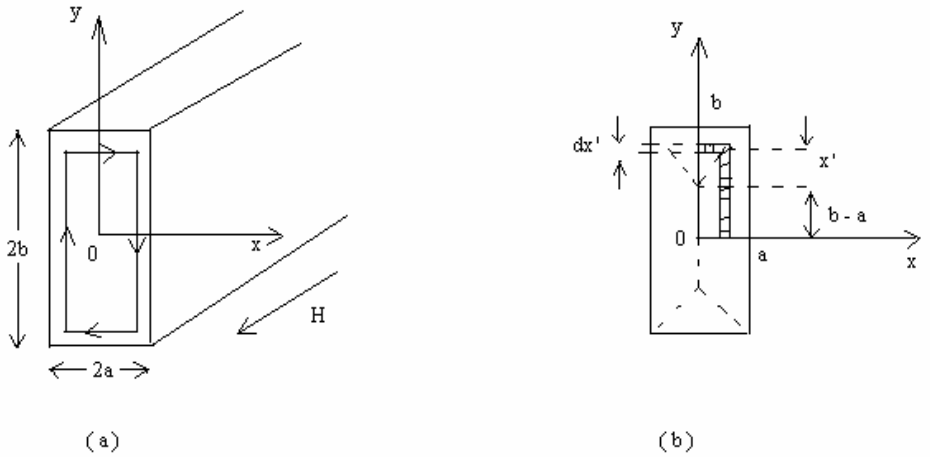

Fig.1.13 (a) Sample configuration. (b) Supercurrent path.

Let's consider an infinitely long orthorhombic sample with cross section 2a × 2b (b ≥ a). An external field H is applied along the z-axis. By application of this magnetic field, the induced

super currents have the x and y components and the path is the rectangular circuit as shown in Fig.1.13 (a). For an infinitely long sample, the super current density J, H_i and M_i are written as functions of x: J(x), $H_i(x)$ and $M_i(x)$. By integrating $M_i(x)$ over the cross-sectional area, we get the total magnetization M given by,

$$M = \frac{1}{ab}\int_0^a (2x' + b - a)M_i(x')dx' \tag{1.53}$$

In this case the area is ab, and the differential area element is $(2x' + b - a)dx'$ as shown in Fig. 1.13(b).

For low field case, the schematic variation of super current density and local internal field as a function of distance with in the sample are shown in Fig.1.14. Figs.1.14 (a) and 1.14(b) show the starting point with $H = H_m$ ($< H_p$) and a negative super current penetrates up to a distance of x_m. When H decreases from H_m, the induced positive super current penetrate from sample surface to $x = x_1$, and the corresponding J(x) and $H_i(x)$ are shown in Figs. 1.14(c) and 1.14(d). At this point, J(x) is $J_m(x)$ from $x_m < x < x_1$ and $J_1(x)$ from $x_1 < x < a$. This arrangement is maintained until H = 0 as shown in Figs.1.14 (e) and 1.14(f). Up to this point it is taken as stage-I ($H_m > H > 0$). The stage-II begins when the applied field decreases towards the negative value and it complicates the situation. The expression for J(x) has to be divided into three parts $J_m(x)$, $J_2(x)$ and $J_3(x)$ and the corresponding H_i changes sign at $x = x_3$ as shown in Figs.1.14 (g) and 1.14(h). This situation stays until $H = -H_m$, when both J_m and J_2 no longer exist. Figs.1.14 (i) and 1.14(j) show J(x) and $H_i(x)$ for $H = -H_m$. They are opposite to the case shown in Figs.1.14 (a) and 1.14(b).

From the figures given below, the expressions for local field H_i can be derived in terms of applied field and super current densities. From the value of H_i and using the equation (1.52), the local magnetization and the average magnetization over the cross section of the sample can be calculated. The magnetization for the stage-I and stage-II are given as follows.

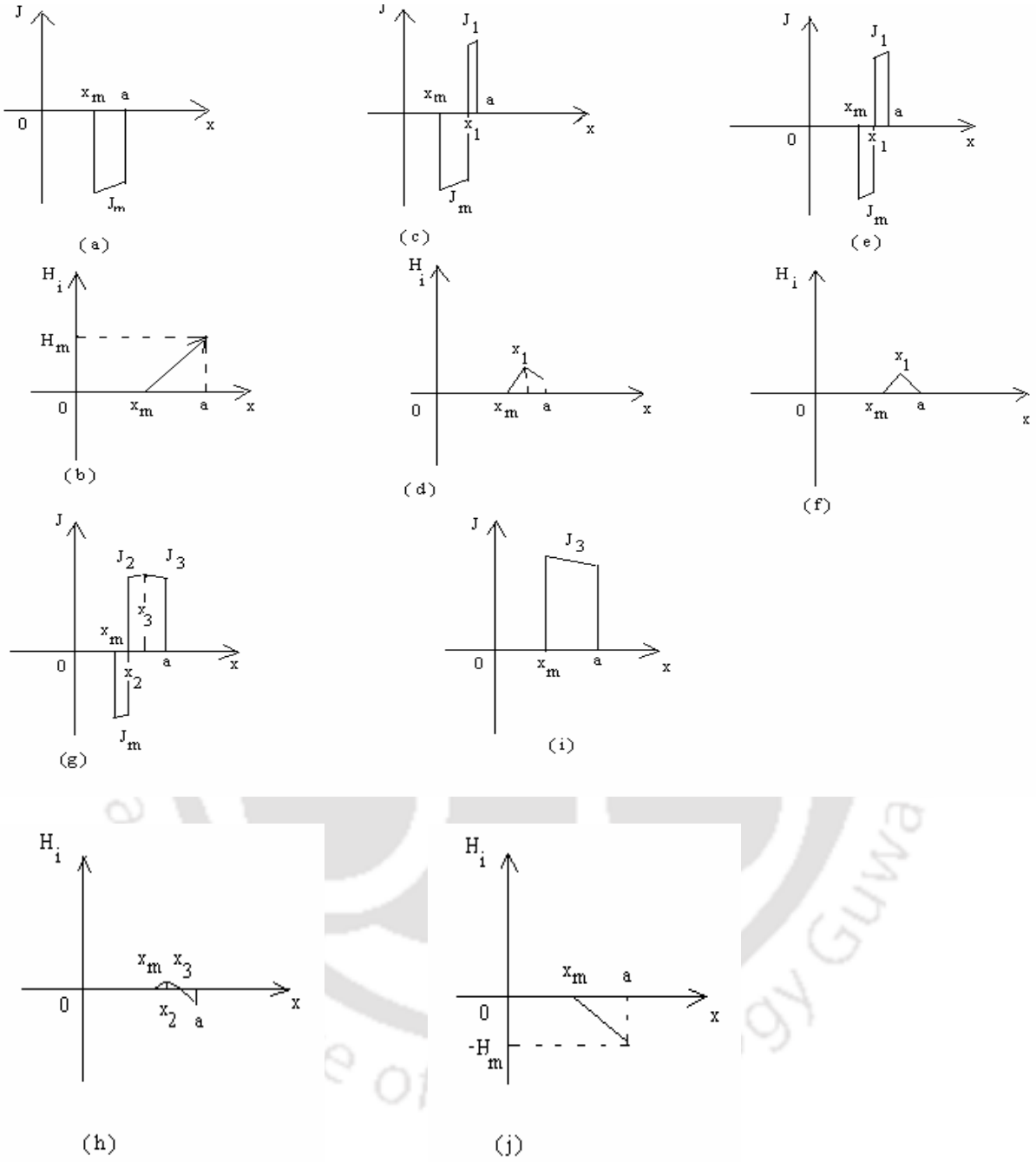

Fig. 1.14 Schematic diagram of super current density (J) and local internal field (H_i) as a function of x for the reverse magnetizing process in the low field ($H_m < H_p$) case.

Stage-I ($0 < H < H_m$)

$$M(H) = -Hx_m(b - a + x_m)/ab - S_1[ab + (a - b)x_m - x_m^2]/ab$$
$$-(S_1^3 - R_2^3)Q_2 + (R_2^3 - H_0^3)Q_3$$
$$+ 2[(x_1 - a)R_2^3 + (x_1 - x_m)H_0^3]/5kab \quad (1.54)$$

Stage-II ($-H_m < H < 0$)

$$M(H) = -Hx_m(b - a + x_m)/ab + S_3(a - x_3)(b + x_3)/ab$$
$$-S_1(x_3 - x_2)[2(b - a + x_2) + x_3 + x_m]/ab$$
$$-(S_3^3 - H_0^3)Q_4 + (R_3^3 - H_0^3)(Q_5 + Q_6)$$
$$+ 2[(x_3 - a)H_0^3 - (x_3 - x_2)(R_3^3 - H_0^3)]/5kab \quad (1.55)$$

where,

$$S_1 = H_0 + H$$

$$S_3 = H_0 - H$$

$$x_m = a - [S_2^2 - H_0^2]/2k$$

$$x_1 = a - [S_2^2 - S_1^2]/4k$$

$$x_2 = a - [S_3^2 + S_2^2 - 2H_0^2]/4k$$

$$x_3 = a - [S_3^2 - H_0^2]/2k$$

$$R_2 = [S_1^2 + 2k(a - x_1)]^{1/2}$$

$$R_3 = [H_0^2 + 2k(x_3 - x_2)]^{1/2}$$

$$Q_2 = [5k(a + b) + 2S_1^2]/15k^2ab$$

$$Q_3 = [10k(a + b) + 3S_1^2 - 7S_2^2]/30k^2ab$$

$$Q_4 = [5k\,(a + b) - 2S_3^2]/15k^2ab$$

$$Q_5 = [5k\,(a + b) - 5S_3^2 + 7H_0^2]/15k^2ab$$

$$Q_6 = [10k\,(a + b) - 3S_3^2 - 7S_2^2 + 6H_0^2]/30k^2ab \qquad (1.56)$$

The J(x) and $H_i(x)$ for the high H_m case are shown in Fig.1.15. Figs.1.15 (a) and 1.15(b) correspond to the starting point when $H = H_m$ ($> H_m$*) and the sample is completely penetrated by negative current with density $J_m(x)$. When the field decreases from H_m to H, a positive super current with a density $J_1(x)$ is induced and it penetrates up to $x = x_1$ which is shown in Fig.1.15(c) and Fig.1.15 (d). At $H = H_{prh}$ the full reverse penetration field for high-H_m, the positive super current completely penetrates to the center of the superconducting sample and up to this it is taken as Stage I.

Stage II starts when $x_1 = 0$ as shown in Figs.1.15 (e) and 1.15(f) and ends when H = 0 as shown in Figs.1.15 (g) and 1.15(h). Then stage III comes, in which local fields at the center and surface of the sample have different signs corresponding to different functions of $J_2(x)$ and $J_3(x)$, with a boundary at $x = x_3$, where $H_i = 0$. This situation is shown in Figs.1.15 (i) and 1.15(j). Further decreasing of H results in the situation shown in the Figs.1.15 (k) and 1.15(l), where the whole sample has negative H_i and the magnetization process enters the stage IV. In stage IV, J(x) keeps the form of $J_3(x)$ until $H = -H_m$, and the final J(x) and $H_i(x)$ are shown in Figs.1.15 (m) and 1.15(n).

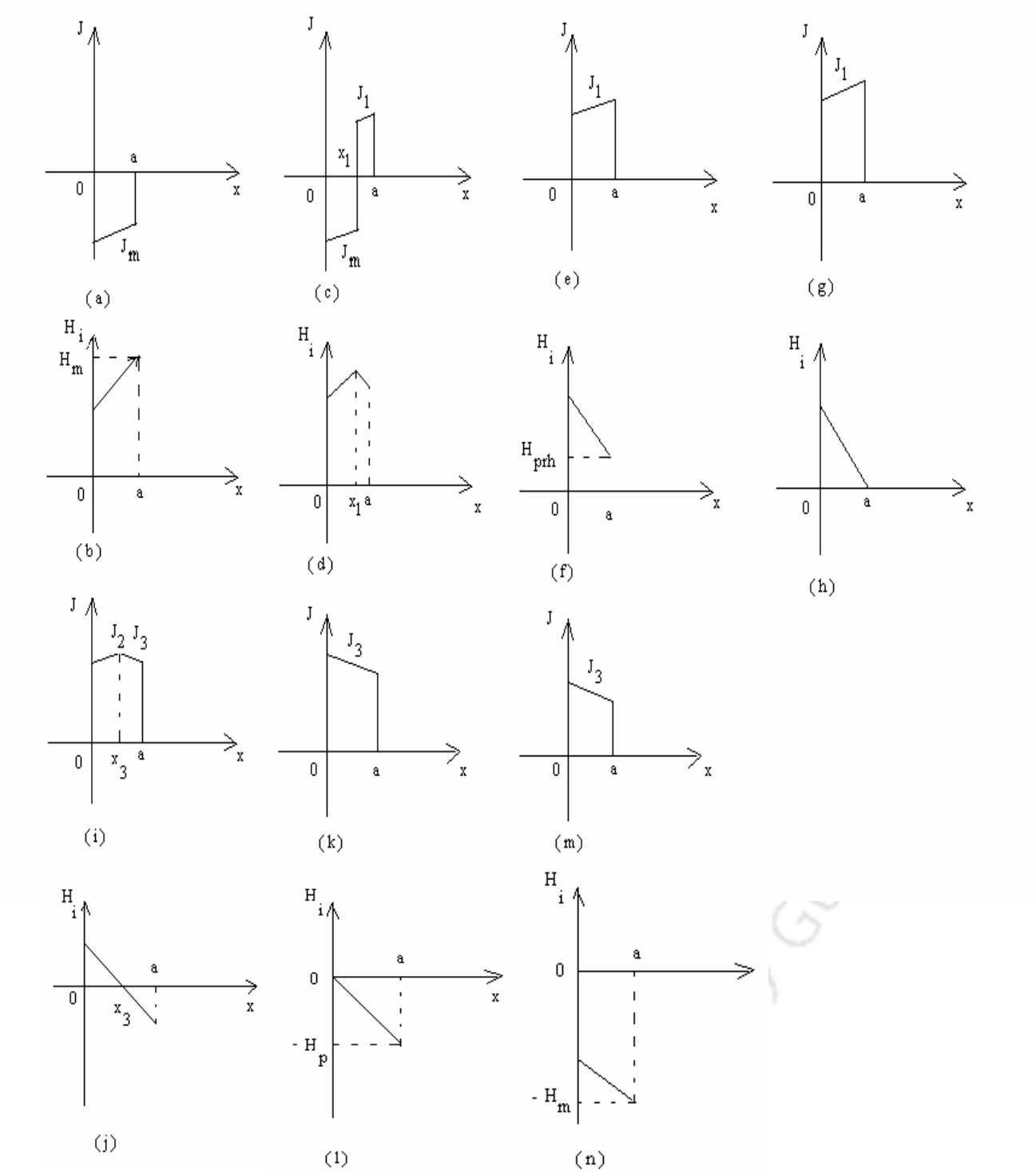

Fig. 1.15 Super current density (J) and local internal field (H_i) as a function of distance (x) from the center of the sample, for the high field ($H_m > H_m^*$) case.

Using the above mentioned procedure the expressions for magnetization at high fields have been calculated at different stages as follows:

Stage-1

$$M(H) = -S_1 - (S_1^3 - R_2^3)\,Q_2 + (R_2^3 - R_4^3)\,Q_3 + 2[(x_1 - a)\,R_2^3 + x_1 R_4^3]/5kab$$

$$(H_{prh} < H < H_m) \qquad (1.57)$$

Stage-II

$$M(H) = -S_1 - (S_1^3 - R_5^3)\,Q_2 - 2R_5^3/5kb$$

$$(0 < H < H_{prh}) \qquad (1.58)$$

Stage-III

$$M(H) = S_3\,(a - x_3)\,(b + x_3)/ab - S_1 x_3\,(b - a + x_3)/ab - (S_3^3 - H_0^3)\,Q_4 - (H_0^3 - R_6^3)\,Q_5$$

$$-2[(a - x_3)\,H_0^3 + x_3 R_6^3]/5kab$$

$$(-H_p < H < 0) \qquad (1.59)$$

Stage-IV

$$M(H) = S_3 - (S_3^3 - R_7^3)\,Q_4 - (2R_7^3)/5kb$$

$$(-H_m < H < -H_p) \qquad (1.60)$$

where, H_{prh} is the reverse full-penetration field for high H_m case and it is calculated to be,

$$H_{prh} = [(H_0 + H_m)^2 - 4ka]^{1/2} - H_0 \qquad (1.61)$$

In the eqns. (1.57) to (1.60), the parameters R_4, R_5, R_6 and R_7 have the following definitions:

$$R_4 = (S_2^2 - 2ka)^{1/2}$$

$$R_5 = (S_1^2 + 2ka)^{1/2}$$

$$R_6 = (H_0^2 + 2kx_3)^{1/2}$$

$$R_7 = (S_3^2 - 2ka)^{1/2} \qquad (1.62)$$

For medium field case, the schematic diagram for the local internal field $H_i(x)$ and penetrated super current J(x) are shown in Fig.1.16. The difference between the medium field case and the high field case is only in stage II. At the end of stage I (Figs. 1.16(e) and 1.16(f)), H = 0, but x_1 is still greater than 0. Therefore in stage II, when H < 0, J(x) has to be divided into three parts: $J_m(x)$, $J_2(x)$ and $J_3(x)$ as shown in Figs.1.16 (g) and 1.16(h). The next stage starts from the point where $x_2 = 0$ as shown in Figs. 1.16(i) and 1.16(j) and the expressions for J(x) are the same as in the high H_m case.

The expressions for magnetization for different stages in the medium field case are as follows:

Stage-I

In this stage M (H) has the same expression as in the high field case except that the concerned field interval is ($H_m < H < 0$).

Stage-II ($H_{prm} < H < 0$)

$$M(H) = S_3 (a - x_3) (b + x_3)/ab - S_1[x_3^2 + (b - a) x_3]/ab - (S_3^3 - H_0^3) Q_4 - (H_0^3 - R_3^3) Q_5$$

$$+ (R_3^3 - R_4^3) Q_6 - 2[(a - x_3) H_0^3 + (x_3 - x_2) R_3^3 - x_2 R_4^3]/5kab \qquad (1.63)$$

where H_{prm}, the reverse full penetration field in the medium field is given by

$$H_{prm} = H_0 - [4ka + 2H_0^2 - (H_0 + H_m)^2]^{1/2} \qquad (1.64)$$

The expression for M in stage-III is same as in the high field case except for the field interval, which is from H_{prm} to $-H_p$. The stage-IV is same as in the high field case.

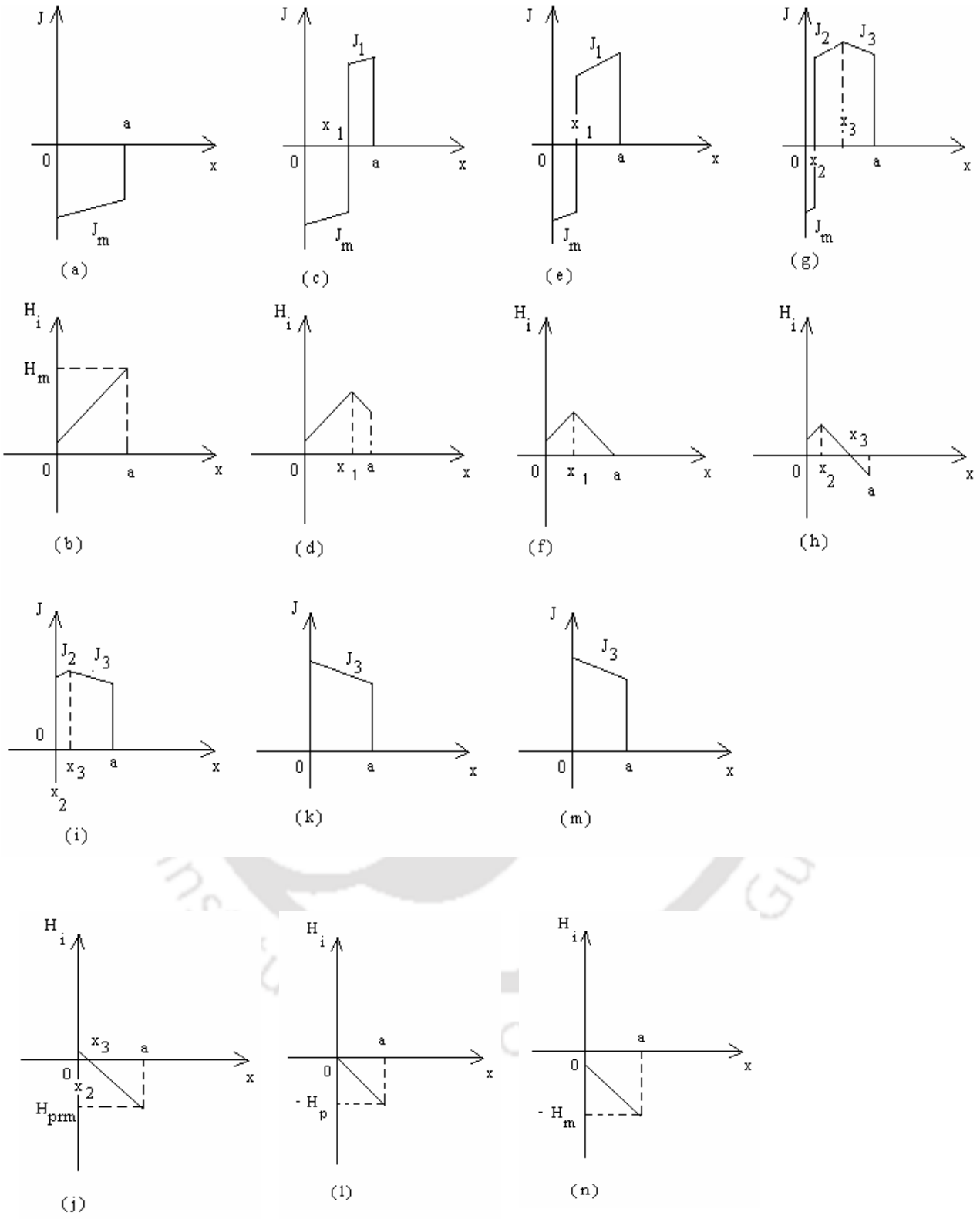

Fig. 1.16 Super current density and local internal field as a function of x for the medium field ($H_p \leq H_m \leq H_m^*$) case.

Following the above works, there are several reports on the derivation of expressions for magnetization as a function of magnetic field using several critical state models such as Kim model [287], exponential model [288, 289], and by taking various other extended critical current density functions [290-292].

Chen et al. [293] reported a numerical technique for the calculation of internal field and hence the average magnetization. The advantage of this method is arbitrary J_c (H_i) function can be taken for the analysis. According to this model, the internal field is calculated by dividing the rectangular cross section 2a×2b (a ≤ b) of the sample into N≅200 rectangular tubes with thickness Δx = a/N. The internal field for a maximum applied field, H_m in a given loop can be written as,

$$H_i(k) = H_i(k-1) - J_c[H_i(k-1)]\,\Delta x, \text{ for } k=2 \text{ to } k_p \qquad (1.65)$$

For k = 1, H_i is taken as H_m. k_p = N for high field case, and k_p< N for low field case, where the field penetration is incomplete. For applied field H < H_m, in the descending loop, the internal field can be calculated as follows,

$$H_i(k) = H_i(k-1) + J_c[H_i(k-1)]\,\Delta x, \text{ for } k = 2 \text{ to } k_b \qquad (1.66)$$

$$H_i(k) = H_i(k-1) - J_c[H_i(k-1)]\,\Delta x, \text{ for } k = k_{b+1} \text{ to } N \qquad (1.67)$$

For k = 1 in eqn. (1.66), H_i is taken as the applied field H. For k > k_b, the penetrated super current changes sign and eqn. (1.67) has to be taken for H_i (k). For low field case, N is replaced by k_p. Theoretical magnetization can be calculated using the relation,

$$M = \left[\sum_{k=1}^{N} (2x_k + b - a)\, H_i(k)\,\Delta x/(ab)\right] - H \qquad (1.68)$$

where x_k = a – (k – 0.5) Δx, k=1 to N.

The above numerical technique would be useful in analyzing the magnetization data. The extension of above model for susceptibility calculation requires an additional numerical technique for Fourier analysis.

Ravi et al. [294] have reported the study of (M-H) loops on a polycrystalline sample of YNi_2B_2C. They fitted their experimental data to eqns. (1.65) to (1.68) by taking $J_c(H_i)$ function from Bean, Kim, exponential and power law models. Their experimental data could be fitted

well to Kim and exponential models. From the fit, they have calculated the field variation of J_c. The field dependence of DC magnetization on Bi (2212) sample with a maximum applied field of 160 kA/m were analyzed in terms of Kim critical state model [295].

The expressions for magnetization loops have been also derived by several groups by taking into account equilibrium magnetization, M_{eq} and surface barrier effects in addition to critical state models [277, 296-303]. The equilibrium magnetization, M_{eq} is associated with the flow of surface current over the thickness of the order of London penetration depth [304]. The surface barrier arises due to the pinning of vortices at the sample surface and as a result, the flux lines enter the sample for an applied field $H > H_{c1}$ and exit at $H < H_{c1}$ [304,305]. In order words, there is a barrier at surface for the entry and exit of flux lines. However, these effects are dominant only on intra-grain magnetization. The M-H loops recorded at high magnetic fields on high T_c superconductors, i.e. M-H loops due to intra-grain superconductors could only be fitted to the expressions for magnetization, where the surface barrier modified equilibrium magnetization has been taken into account [295, 306, 307].

In polycrystalline cylindrical $YBa_2Cu_3O_7$ samples, Gömöry et al. [264] estimated shielding current density J_c (T) from their temperature dependence of ac susceptibility measured at different applied ac field amplitudes using equation (1.45). Murphy et al. [265] from their χ' (T) and χ'' (T) measurements on polycrystalline $YBa_2Cu_3O_7$ samples found that the values of $\chi'(T_m)$ and $\chi''(T_m)$ closely follow Bean's theoretical values of -0.33 and 0.21 respectively. They have estimated J_c (T) using equation (1.45) and also using Clem's expressions (equations (1.50) and (1.51)) close to T_m. In thin films of $YBa_2Cu_3O_7$, Lam et al. [308] have measured the complex susceptibility as a function of the applied field. They observed only intragranular peak at around 95 Oe and they could fit their complex ac susceptibility data to Bean's model. Using Kim field dependent model, Chen et al. [266] have estimated J_c (T), f_g etc. for the polycrystalline $YBa_2Cu_3O_7$ samples from the χ' (T) and χ'' (T) data and by analyzing the data using Kim model. Similar work was carried out by Kumaraswamy et al. [309] on $ErBa_2Cu_3O_7$.

Lam et al. [284, 310] have measured complex susceptibility on $YBa_2Cu_3O_7$ pellet, as a function of the ac field amplitude in the range of 0.05 to 500 Oe. They have fitted their data using a modified critical state model, where a steeper field dependence of J_c (H_i) has been taken

(J_c (H_i) ~ $H_i^{-1.8}$) compared to Kim model. Although, the intergranular susceptibility agrees with their model, the intragranular susceptibility shows a considerable deviation from their theoretical values. The complex susceptibility as a function of ac field amplitude and superimposed dc field have been measured on cylindrical samples of polycrystalline $YBa_2Cu_3O_7$ by Angurel et al. [311]. They have fitted their experimental data to a quadratic model (J_c (H_i) ~ ($H_0^2 + |H_i|^2)^{-1}$), Kim model and an exponential model. They found that all the above models fit equally well to the experimental data.

Shatz et al. [312] derived the expressions for harmonic susceptibility using a universal parameter δ for an ac field superimposed on a large dc field, where the flux profile inside the superconductor is assumed to be linear. They have tested their model on harmonic susceptibility measured on $YBa_2Cu_3O_7$ superconductors. Hari Babu et al. [313] demonstrated the applicability of above model on fundamental susceptibility of (Bi-Pb)-Sr-Ca-Cu-O system. Ravi [314] has obtained the expression for susceptibility in terms of universal parameter δ by using Bean model, where the flux profile is linear in the absence of large dc field and the model could be fitted to one of the Bi-Sr-Ca-Cu-O superconductors. Sedky et al. [315] estimated $J_c(T)$ of R: 123 compounds (R = Er, Gd, Nd) by using Ravi expressions.

Chen et al. [316] estimated J_c (T) using Kim model in a multiphase sample of Bi-Sr-Ca-Cu-O system with the nominal composition $Bi_{1.8}Pb_{0.2}Sr_2Ca_2Cu_3O_y$. For the above calculation they compared the theoretical intergranular matrix susceptibility ($\chi_m^{//}$ (H_m/H_p)) as a function of H_m/H_p to the temperature dependence of experimental intergranular matrix susceptibility $\chi_m^{//}$ (T). In 85 K and 110 K phases of Bi-Sr-Ca-Cu-O system, the intergranular critical current density (J_c) and effective volume fractions of superconducting grains have been estimated [317, 318] using Bean's and Kim critical state models. Similarly by using various critical state models, the J_c (T) and related parameters have been reported by several authors on Bi-Sr-Ca-Cu-O system [319-322] and Tl-Ba-Ca-Cu-O system [323]. Similar analysis has been carried out in other systems such as Hg-Ba-Ca-Cu-O [324,325] and Cu-Ba-Ca-Cu-O [326] systems.

Schilling et al. [327] and Ravi [328] estimated distribution in the inter-grain critical current density of Tl-Ba-Ca-Cu-O and Bi-Sr-Ca-Cu-O superconductors respectively by

analyzing the ac susceptibility data using extended Bean critical state model. Here, the susceptibility expression has been modified by introducing appropriate distribution function.

It is well known that the polycrystalline superconductors are arrays of weak links, which behave like Josephson junctions. The temperature dependence of the critical current density that flows through the Josephson junctions can be written in the form,

$$J_c \sim \left(1 - \frac{T}{T_c}\right)^n \tag{1.69}$$

where T_c is the superconducting transition temperature and n is a positive constant. The value of n is 2 for superconductor-normal metal-superconductor (SNS) type junctions [329], and 1 for superconductor-insulator-superconductor (SIS) junctions [330]. The values of n in between 1 and 2 indicate the formation of superconductor-insulator-normal metal-superconductor (SINS) junctions [331].

1.6. Motivation of the Present Work.

As reviewed in section 1.3, even though the La-Ba-Ca-Cu-O superconductors with tetragonal structure is known for about two decades, to our knowledge there is no detailed work on fluctuations induced excess conductivity, fluctuation magneto-conductivity and magnetic studies in terms of critical state models. The above compounds are widely reported with several different type of starting compositions such as $La_3Ba_3CaCu_7O_z$, $La_2Ba_2CaCu_5O_z$, and $LaBaCaCu_3O_z$ with T_c ranging from 66 to close to 80 K. Even though there are several reports on the partial replacement of La by several rare earths such as Pr, Nd, Gd, Dy, there is no report of Y doping to our knowledge except on underdoped materials. The interesting feature of the above compounds is that they exhibit tetragonal structure similar to that of tetragonal $YBa_2Cu_3O_{7-\delta}$ with comparable lattice parameters. However, $YBa_2Cu_3O_{7-\delta}$ in tetragonal form does not exhibit superconductivity for $\delta > 0.5$. So, it would be interesting to study this series of compounds, which exhibit tetragonal structure and superconductivity and compare with those of superconducting $YBa_2Cu_3O_7$.

So, I have chosen following three series of superconductors namely $(La_{1-x}Y_x)_2Ba_2CaCu_5O_z$, $(La_{1-x}Y_x)_2Ba_2Ca_{4x}Cu_{4+4x}O_z$ and $(La_{1-x}Gd_x)_2Ba_2Ca_{4x}Cu_{4+4x}O_z$ and in each

series, with and without Ag doping. First series has been chosen to study the effect of Y doping in the La-Ba-Ca-Cu-O. The second and third series are basically underdoped materials. They have been chosen to have a wide range of T_c with same crystal structure, so that the fluctuations phenomena and ac susceptibility can be studied in detail.

2.1. EXPERIMENTAL TECHNIQUES

In this section, the experimental techniques followed for; materials preparation, various physical measurements, cryostat design, calibration, etc. are described in detail. I started my research work, by setting up required facilities for preparing the proposed superconducting materials by solid state and nitrate route. The first step was fabrication of a high temperature furnace. The details about the design and fabrication of the furnace are discussed in this chapter. In addition to that, I have used a commercial furnace and its detail would be given. The prepared materials were characterized by using: X-ray diffraction (XRD) to check their phase purity and study their crystal structure; scanning electron micrographs (SEM) to study the microstructure and, energy dispersive X-ray analysis (EDAX) for determining sample composition. The sample holder assemblies fabricated for electrical resistivity and magneto-resistivity measurements will be described in detail. Temperature variations of dc electrical resistivity and magneto-resistivity measurements have been carried out for studying the fluctuations induced excess conductivity and fluctuation magneto-conductivity. Low field ac susceptibility set-up was designed and fabricated by employing mutual induction bridge method and calibrated against standard samples. Temperature and ac field amplitude variations of complex susceptibility was measured and analyzed, using critical state models to estimate critical current density, etc. The above techniques are discussed at length as given below.

2.1.1. Sample Preparation

In the present thesis work, three series of superconductors namely $(La_{1-x}Y_x)_2Ba_2CaCu_5O_z$, $(La_{1-x}Y_x)_2Ba_2Ca_yCu_{4+y}O_z$ and $(La_{1-x}Gd_x)_2Ba_2Ca_yCu_{4+y}O_z$ were chosen to carryout detailed analysis of fluctuations induced excess conductivity and, fluctuation magneto-conductivity and, ac susceptibility studies using critical state models. In each series, pure and 5 wt % Ag doped samples have been prepared. The complete list of prepared samples along with assigned names are given below.

1. $(La_{1-x}Y_x)_2Ba_2CaCu_5O_z$ $(0 \le x \le 0.5)$
   (i) $La_2Ba_2CaCu_5O_z$ (Sample A)
   (ii) $La_{1.8}Y_{0.2}Ba_2CaCu_5O_z$ (Sample B)
   (iii) $La_{1.6}Y_{0.4}Ba_2CaCu_5O_z$ (Sample C)
   (iv) $La_{1.5}Y_{0.5}Ba_2CaCu_5O_z$ (Sample D)
   (v) $La_{1.2}Y_{0.8}Ba_2CaCu_5O_z$ (Sample E)

(vi)$LaYBa_2CaCu_5O_z$ (Sample F)

2. $(La_{1-x}Y_x)_2Ba_2CaCu_5O_z$ + 5 wt % Ag $(0 \leq x \leq 0.5)$
   (i) $La_2Ba_2CaCu_5O_z$ + 5 wt % of Ag (Sample A1)
   (ii) $La_{1.8}Y_{0.2}Ba_2CaCu_5O_z$ + 5 wt % of Ag (Sample B1)
   (iii) $La_{1.6}Y_{0.4}Ba_2CaCu_5O_z$ + 5 wt % of Ag (Sample C1)
   (iv) $La_{1.5}Y_{0.5}Ba_2CaCu_5O_z$ + 5 wt % of Ag (Sample D1)
   (v) $La_{1.2}Y_{0.8}Ba_2CaCu_5O_z$ + 5 wt % of Ag (Sample E1)
   (vi) $LaYBa_2CaCu_5O_z$ + 5 wt % of Ag (Sample F1)
3. Pure and Ag doped $(La_{1-x}Y_x)_2Ba_2Ca_yCu_{4+y}O_z$ (y = 4x, x = 0.15,0.20)
   (i) $La_{1.7}Y_{0.3}Ba_2Ca_{0.6}Cu_{4.6}O_z$ (Sample G)
   (ii) $La_{1.6}Y_{0.4}Ba_2Ca_{0.8}Cu_{4.8}O_z$ (Sample H)
   (iii) $La_{1.7}Y_{0.3}Ba_2Ca_{0.6}Cu_{4.6}O_z$ + 5 wt % of Ag (Sample G1)
   (iv) $La_{1.6}Y_{0.4}Ba_2Ca_{0.8}Cu_{4.8}O_z$ + 5 wt % of Ag (Sample H1)
4. Pure and Ag doped $(La_{1-x}Gd_x)_2Ba_2Ca_yCu_{4+y}O_z$ (y = 4x, x = 0.10, 0.20, 0.25)
   (i) $La_{1.8}Gd_{0.2}Ba_2Ca_{0.4}Cu_{4.4}O_z$ (Sample I)
   (ii) $La_{1.6}Gd_{0.4}Ba_2Ca_{0.8}Cu_{4.8}O_z$ (Sample J)
   (iii) $La_{1.5}Gd_{0.5}Ba_2CaCu_5O_z$ (Sample K)
   (iv) $La_{1.8}Gd_{0.2}Ba_2Ca_{0.4}Cu_{4.4}O_z$ + 5 wt % of Ag (Sample I1)
   (v) $La_{1.6}Gd_{0.4}Ba_2Ca_{0.8}Cu_{4.8}O_z$ + 5 wt % of Ag (Sample J1)
   (vi) $La_{1.5}Gd_{0.5}Ba_2CaCu_5O_z$ + 5 wt % of Ag (Sample K1)

The first series was chosen to study the effect of Y doping in the rare earth site, where the ionic size of Y is smaller than that of La. The second series was prepared by adding 5 wt % of Ag to the starting compositions of the above series to enhance the superconducting transition temperature and intergranular critical current density by suppressing the intergranular weak links between the grains. The last two series have been prepared to study the evolution of superconductivity in the under doped $CaCuO_2$ layers. The above samples have also been chosen to have a wide range of transition temperatures with same crystal structure.

The above samples were prepared from the following starting compounds and elements, such as, Lanthanum Oxide (La_2O_3, 99.9%), Yttrium Oxide (Y_2O_3, 99.9%), Gadolinium Oxide (Gd_2O_3, 99.9 %), Barium Carbonate ($BaCO_3$, 99%), Calcium Carbonate ($CaCO_3$, 99.5%), Silver

Nitrate ($AgNO_3$, 99.9%), Copper Acetate ($(CH_3COO)_2Cu.H_2O$, 99%), Copper Oxide (CuO, 99%) and Copper metal (Cu, 99%).

The stoichiometric ratio of starting compounds and/or elements were weighed using an electronic balance supplied by Mettler Toledo model no. AG135 with an accuracy of ± 0.01mg. The weighed compounds were ground under the medium of acetone (99%) using an agate mortar and pestle. The homogeneous mixture of starting compounds was transferred into an alumina crucible and was presintered in the temperature range 850 to 900^0C for over 48h with a few intermediate grindings at room temperature. The presintered powder was pressed into cylindrical shape pellets by using a 13mm die and a hydraulic press supplied by Techno Search instruments with a maximum load capacity of 6 Ton/cm^2. The final sintering in pellet form was carried out at 950°C in O_2 atmosphere for 24 h followed by slow cooling, at the rate of 50°C/h to room temperature. To oxygenate the samples, the pellets were annealed at 500°C for about 24 h in oxygen atmosphere followed by slow cooling to room temperature. The Ag doped samples were prepared by adding 5 wt % of Ag to the stoichiometric ratio of above starting compounds and by following the same heat treatments mentioned above.

In nitrate route, the stoichiometric ratio of starting materials were weighed and transferred into separate 250ml Borosil beakers. The starting compounds in the form of oxides, carbonates and metals were dissolved in nitric acid (HNO_3) and required quantity of distilled water was also added to completely dissolve the nitrates. The starting compounds in the form of nitrates & acetates were dissolved in distilled water. The nitrate solutions of all compounds were mixed together in a single beaker so that one can get a homogeneous mixture. The mixed solution was heated by using a hot plate to evaporate the excess acid and distilled water to get a dry precursor. This dry precursor was heated at 200^0C for 4 h using a rectangular muffle furnace. Then the temperature was raised to 400^0C and kept for about 4 h, so that dry precursor decomposed into a black powder. The resultant powder was ground and presintered at about 850 to 900^0C for over 48 h with a few intermediate grindings at room temperature. The remaining heat treatments were similar to that of solid state route.

2.1.2. High Temperature Furnace

A high temperature furnace was designed and fabricated; which can go up to the maximum operating temperature of 1200^0C. Other than this, one home made furnace with maximum

temperature of 1000^0C and a commercial high temperature furnace with maximum operating temperature of 1400^0C were used for sintering the samples.

The commercial furnace was supplied by N. R. Enterprises, Kolkata. It is powered by a thyristor unit of 30A rating. The temperature was controlled using; West, UK make, PID programmable temperature controller (model no. 6400) with 16 segment programming feature. The platinum versus platinum-rhodium (Platinum + 10 % Rh) thermocouple was used for sensing the temperature. The heating elements are based on Si-Carbide rods. The temperature was controlled to an accuracy of $\pm 1^0$C. The furnace could be operated up to 1400^0C.

The home made furnace (1200^0C) was fabricated using a cylindrical alumina muffle with an inner diameter of 5.8cm and 50cm length. Six silicon carbide rods of 45 cm length each are used as heating element. The muffle loaded with heating elements is housed in a cylindrical container made up of galvanized aluminum sheet with dimensions 50 cm diameter and 50 cm length. High temperature ceramic bricks and ceramic wools are used as thermal insulation. The Chromel-Alumel (Cr-Al) thermocouple and a commercial on/off type temperature controller are used for temperature measurements and controlling. The input power to the furnace was regulated using a variac (dimmerstat) of 15A capacity. An external on/off relay (15A capacity) was used for controlling the power supply to the heater wire. The relay was triggered using the temperature controller. The block diagram of the furnace is shown in Fig. 2.1. The furnace could be operated up to a maximum temperature of 1200^0C. The temperature could be controlled with an accuracy of $\pm 5^0$C.

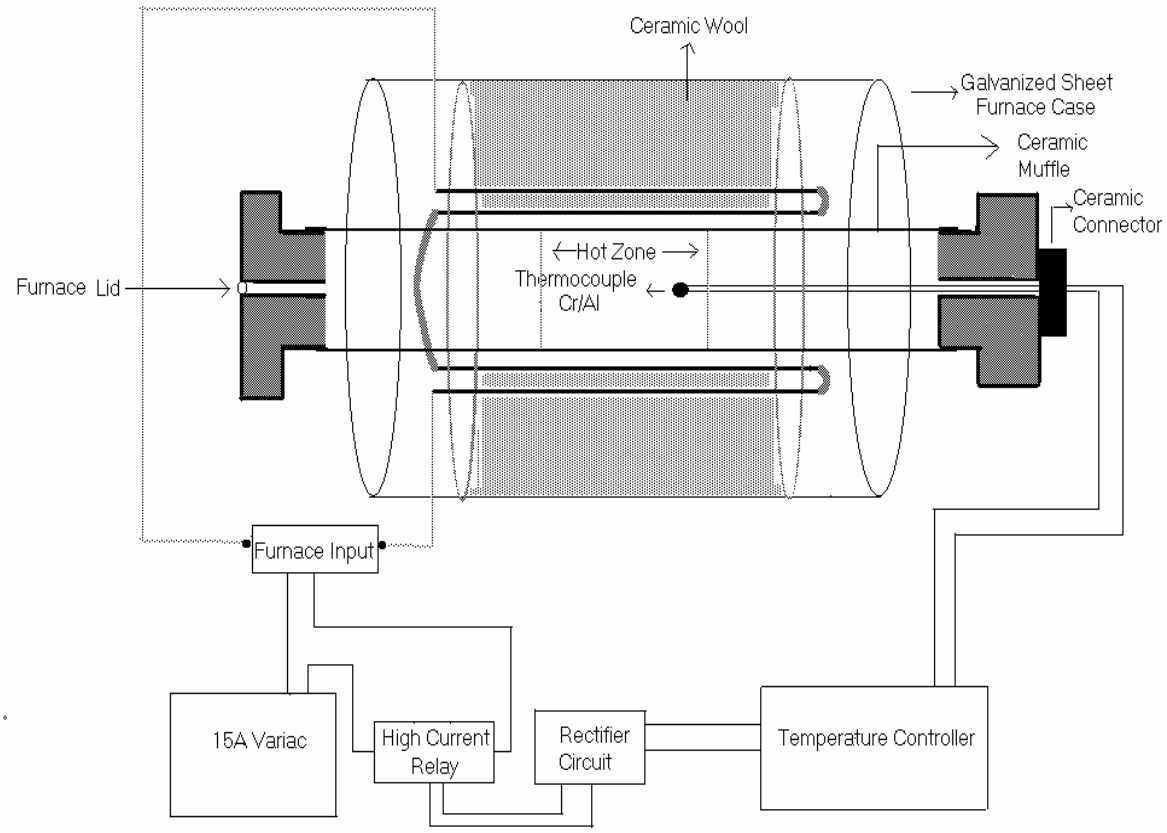

Fig. 2.1: Block diagram of the furnace with maximum operating temperature of 1200^0C.

2.1.3. X-ray Diffraction

The X- ray diffraction technique has been used to study the phase purity and crystal structure of the prepared compounds. Powder X-ray diffraction (XRD) measurements were carried out at room temperature using a commercial X-ray diffractometer supplied by Seifert (model no. 3003TT) by employing CuK_α radiation (1.5418Å). In the present investigation, all the XRD data were collected with the setting of 30mA current and 40kV voltage for X-ray generator. The instrument is based on the Bragg-Brentano geometry as shown in Fig. 2.2. In this geometry, the source to sample distance and the sample to detector distance are kept equal. A perspex sheet with rectangular groove was used for mounting the sample, where the powder sample was filled uniformly in the groove. The data were collected in a usual θ-θ scan with an angular speed of 1-2^0/minute and a step size of 0.01-0.05^0. The phase purity of the samples was examined by comparing the XRD patterns with that reported in literature for similar compounds. The XRD patterns of single phase samples were analyzed by employing rietveld refinement technique

[332] and by using the Fullprof program. The background signal was fitted to a polynomial. The profile shape was fitted to Pseudo-Voigt function. The fitting was carried out by refining atomic positions, isotropic temperature parameters and occupancy values of different elements. The global parameters such as, scaling factor, zero error, a, b, c parameters etc were also varied during the fit. From the refined values of atomic positions, the bond length and bond angles were determined using the technique described below.

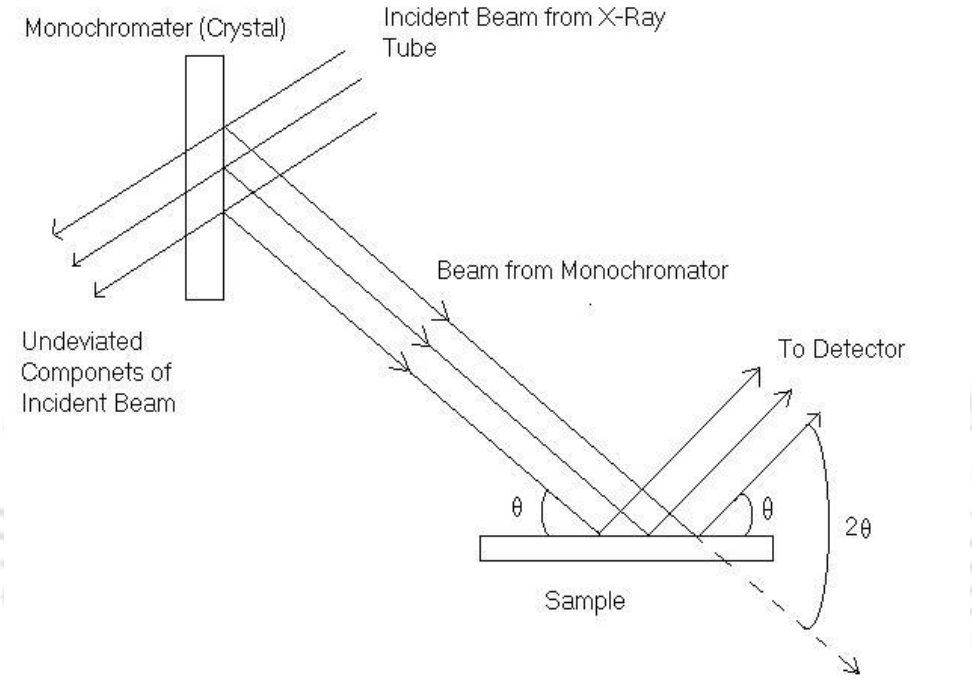

Fig. 2.2: Ray diagram of X- ray diffractometer.

Inter atomic distances (bond length) and bond angles were calculated using the refined fractional coordinates and lattice parameters as follows. Let us consider two position vectors $\overline{A}$ (x_1,y_1,z_1) and $\overline{B}$ (x_2,y_2,z_2), referred to the same base system consisting of three non-coplanar vectors r_1, r_2 and r_3, and they can be written as,

$$\overline{A}\cdot\overline{B} = \left(x_1 r_1 + y_1 r_2 + z_1 r_3\right)\cdot\left(x_2 r_1 + y_2 r_2 + z_2 r_3\right) \quad \text{---------} \quad (2.1)$$

Equation 2.1 can be written as,

$$\overline{A}\cdot\overline{B} = \begin{bmatrix} x_1 & y_1 & z_1 \end{bmatrix}\begin{bmatrix} r_1\cdot r_1 & r_1\cdot r_2 & r_1\cdot r_3 \\ r_2\cdot r_1 & r_2\cdot r_2 & r_2\cdot r_3 \\ r_3\cdot r_1 & r_3\cdot r_2 & r_3\cdot r_3 \end{bmatrix}\begin{bmatrix} x_2 \\ y_2 \\ z_2 \end{bmatrix} \quad \text{---------} \quad (2.2)$$

The above equation can be written in simple form as,

$$\overline{A} \cdot \overline{B} = A' G B \qquad \text{----------} \qquad (2.3)$$

Here A$^{/}$ is a transpose matrix of A, and G is a matrix tensor. The elements $g_{ij} = r_i \cdot r_j$ are the scalar product of the base vectors. Let us assume that $\overline{A} = \overline{B}$, so that the equation 2.3 will be,

$$\overline{A} \cdot \overline{A} = |A| \cdot |A| = A' G A \qquad \text{----------} \qquad (2.4)$$

$$\Rightarrow |A| = \sqrt{A' G A} \qquad \text{----------} \qquad (2.5)$$

The scalar product of two vectors can be written as,

$$\overline{A} \cdot \overline{B} = |A||B|\cos(\theta) \qquad \text{----------} \qquad (2.6)$$

where, θ is the angle between the vectors A and B. Using eqns. 2.5 and 2.6, we can get,

$$\cos(\theta) = \frac{A' G B}{\sqrt{A' G A} \cdot \sqrt{B' G B}} \qquad \text{----------} \qquad (2.7)$$

Eqns. 2.5 and 2.7 are generally used to obtain the vector lengths and the angles between the vectors. In crystallography, the vectors r_1, r_2, r_3 can be replaced by lattice parameters a, b & c (translation vectors). The inter atomic bond length, 'd' can be obtained using the following matrix product,

$$d^2 = \begin{bmatrix} \Delta x & \Delta y & \Delta z \end{bmatrix} \begin{bmatrix} a \cdot a & a \cdot b & a \cdot c \\ b \cdot a & b \cdot b & b \cdot c \\ c \cdot a & c \cdot b & c \cdot c \end{bmatrix} \begin{bmatrix} \Delta x \\ \Delta y \\ \Delta z \end{bmatrix} \qquad \text{----------} \qquad (2.8)$$

Here x, y, z and x+Δx, y+Δy and z+Δz are the positions of two atoms forming the bonds in fractional coordinates. For an orthorhombic system (a ≠ b ≠ c and α = β = γ = π/2), the bond length is found to be,

$$d = \sqrt{a^2 \Delta x^2 + b^2 \Delta y^2 + c^2 \Delta z^2} \qquad \text{----------} \qquad (2.9)$$

Similarly for a tetragonal system (a = b ≠ c, α = β = γ = π/2),

$$d = \sqrt{2a^2 \Delta x^2 + c^2 \Delta z^2} \qquad \text{----------} \qquad (2.10)$$

2.1.4. Scanning Electron Microscope (SEM)

The composition of bulk samples could be analyzed using Scanning Electron Microscope (SEM) with Energy Dispersive X-ray analysis (EDAX) accessory. EDAX analysis of the composition of the sample is based on the following principle. When an electron beam strikes a solid surface, electrons and X-rays are emitted from the surface (Fig. 2.3). The X-ray photon may be absorbed by an atom resulting in the ejection of one of the bound electrons of that atom. The energy distribution of emitted X-rays and electrons are shown in Fig. 2.3 (a) and 2.3 (b) respectively.

Compositional analysis was carried out on a few samples using a commercial SEM-EDAX instrument (LEO 1430VP) at Central Instrumental Facility (CIF), IIT Guwahati. Both spot and overall analysis were performed on the samples. The SEM-EDAX was operated with energy range of (1-20kV).

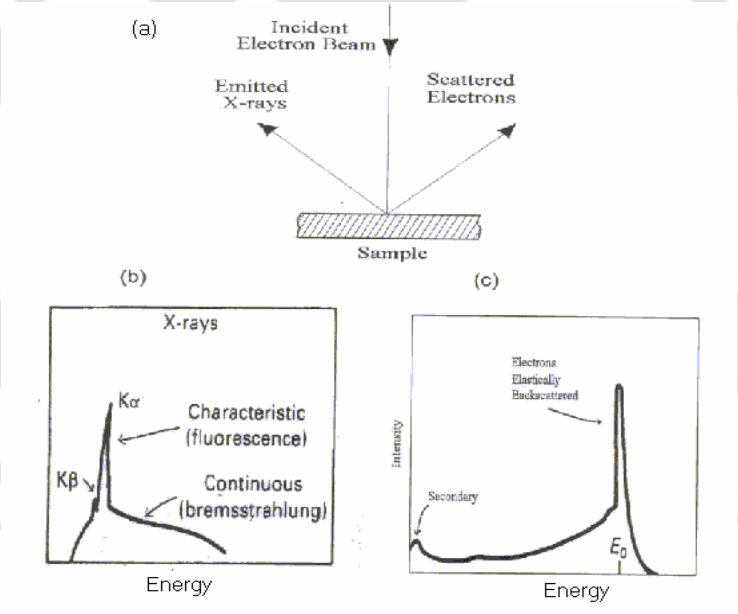

Fig. 2.3: (a) The scattering process of an electron beam in a SEM. The energy distribution of (b) X-rays and (c) electrons, after emission from the sample surface.

2.1.5. Sample Characterization using Resistivity Measurements

Temperature variation of dc electrical resistivity measurements down to 20K were carried out to study the electrical transport properties of superconducting samples. The temperature variation was achieved using a commercially supplied APD make Closed Cycle Helium refrigerator cryostat equipped with a temperature controller. The schematic diagram of the cryostat is shown in the Fig. 2.4. A copper sample holder $(27\times22\times6)mm^3$ was fabricated. It was mounted on the cold tip of the cryostat to load the sample. The temperature variation was achieved by using a heater wire wound in the vicinity of the cold tip.

The top view of sample holder is shown in Fig. 2.5. The sample holder was made up of copper block of dimension $(27\times22\times6)mm^3$. A groove of 10mm length and 3mm diameter was made in the copper block to mount the calibrated Pt-100 sensor for measuring the sample temperature. A calibrated Si-diode sensor was used as controlling sensor and it was mounted at the cold tip, where the heater wire of 37 Ω resistance was also installed. To electrically insulate the sample from the copper sample holder, a thin mica sheet was used. Electrical contacts on the sample were made with the help of silver paint and/or Indium soldering. A printed circuit board (PCB) with four copper strips was mounted on the sample holder. The copper wires of 32SWG (0.2743mm) were used for electrical connection between PCB and sample. Standard linear four probe technique was used to eliminate the contribution of contact resistance and lead resistance coming into picture. Current through the sample was passed using outer two leads and a programmable Keithley constant current source, model no. 224. The voltage drop across the sample was measured using Keithley nanovoltmeter, model no. 2182. To eliminate the thermo-emf generated across the voltage leads, measurements were carried out for both positive and negative current. The experimental data were collected using a personal computer equipped with GPIB board. The block diagram of the resistivity set-up is shown in Fig. 2.6. The necessary software in quick Basic language was developed for temperature controlling and data acquisition using a personal computer.

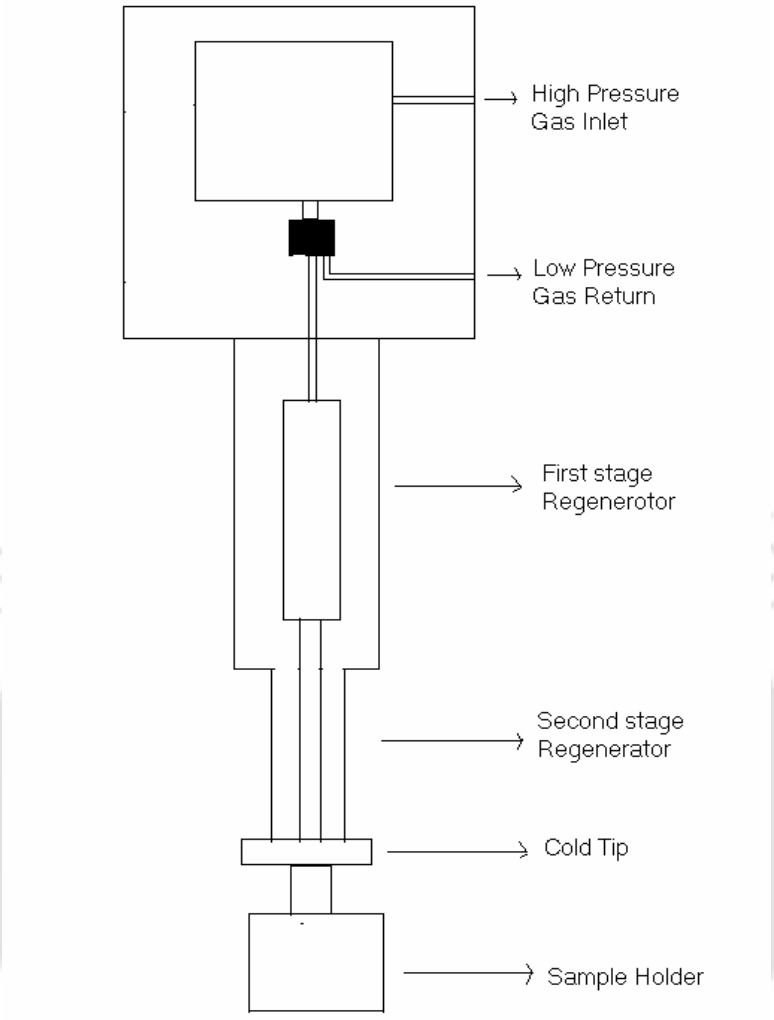

Fig. 2.4: Block diagram of APD Cryostat.

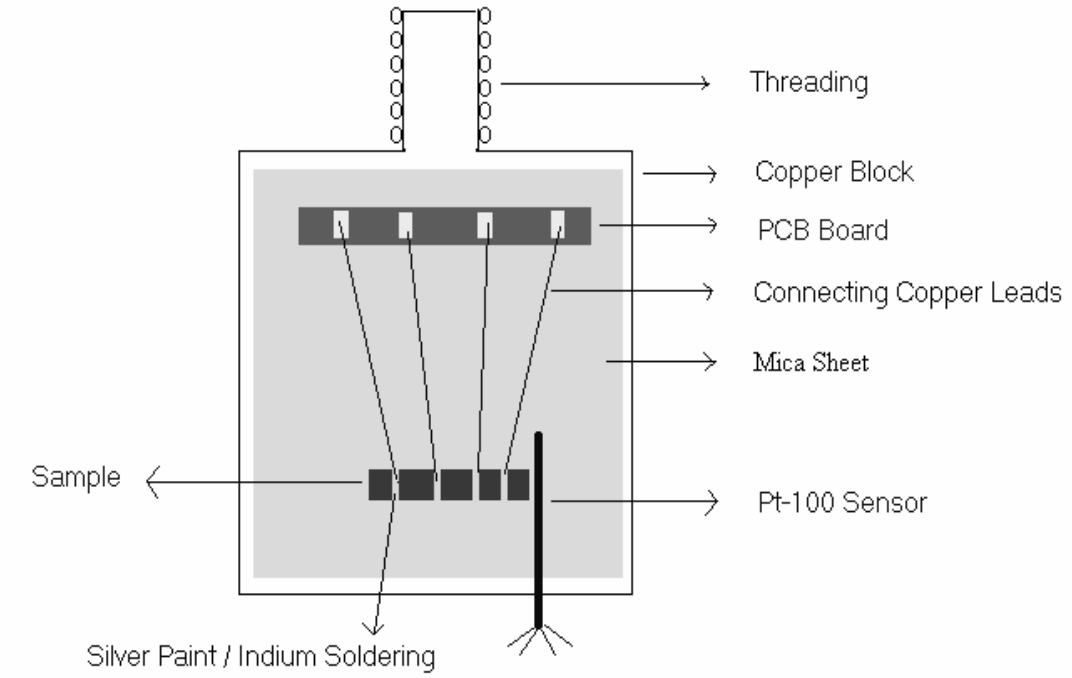

Fig. 2.5: Top view of sample holder for resistivity measurement.

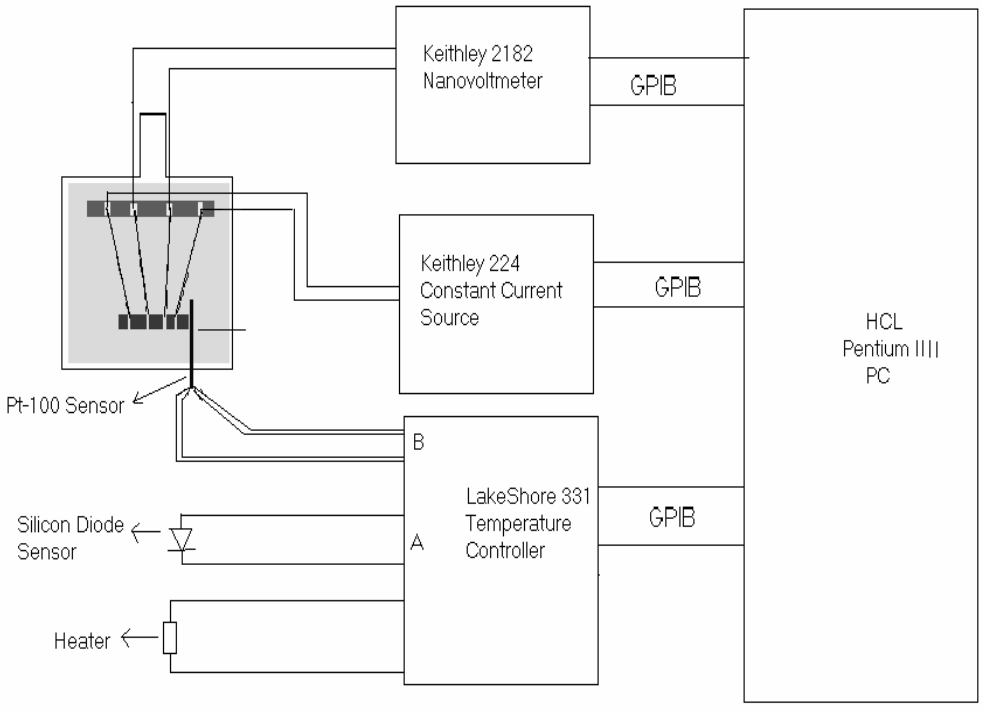

Fig. 2.6: Block diagram of electrical resistivity measurement set-up.

2.1.6. Electrical Resistivity and Magneto-Resistivity Measurements

The experimental data of temperature variations of electrical resistivity and magneto-resistivity for the analysis of excess conductivity and fluctuations magneto-conductivity have been measured by controlling the temperature precisely and by collecting the data at an interval of 0.1 K in the vicinity of transition temperature. For carrying out the above measurements, a top loading helium exchange gas cooled type closed cycle helium refrigerator cryostat fabricated by; Cryo Industries of America, USA using a CTI make compressor and cold head motor has been used. The temperature was controlled using a Lakeshore temperature controller, Model no.331 and a Lakeshore Calibrated Si-diode sensor mounted on the cold head. To facilitate the temperature variation, a heater wire of 50 W capacity mounted on the cold tip was used. The display resolution of temperature controller was 1 mK and 10 mK respectively for below and above 100 K.

A sample insert assembly has been designed and fabricated for quick loading & unloading of the samples. The schematic diagram of the sample holder is shown in Fig. 2.7. Separately the sample holder is shown in Fig. 2.8. A LakeShore calibrated GaAlAs diode sensor was used for measuring the sample temperature. The sensor is mounted at the rear side of the sample holder and at the same height from the bottom, where the sample is mounted. For each measurement, the sample chamber is evacuated followed by purging the helium gas and the sample is kept under the helium gas environment for uniform temperature. The temperature was measured with an accuracy of better than ± 50 mK. To facilitate the magneto-resistivity measurements, the CCR cryostat is placed in between the pole pieces of an electromagnet supplied by Walker Scientific Instruments, model no. HV-10H. The sample can be positioned at the centre of pole face using the Wilson nut arrangement. The pole pieces of $10^{//}$ diameter are tapered to$3^{//}$ diameter. The magneto-resistivity measurements have been carried out by applying a magnetic field strength of 10 kOe (1 T).

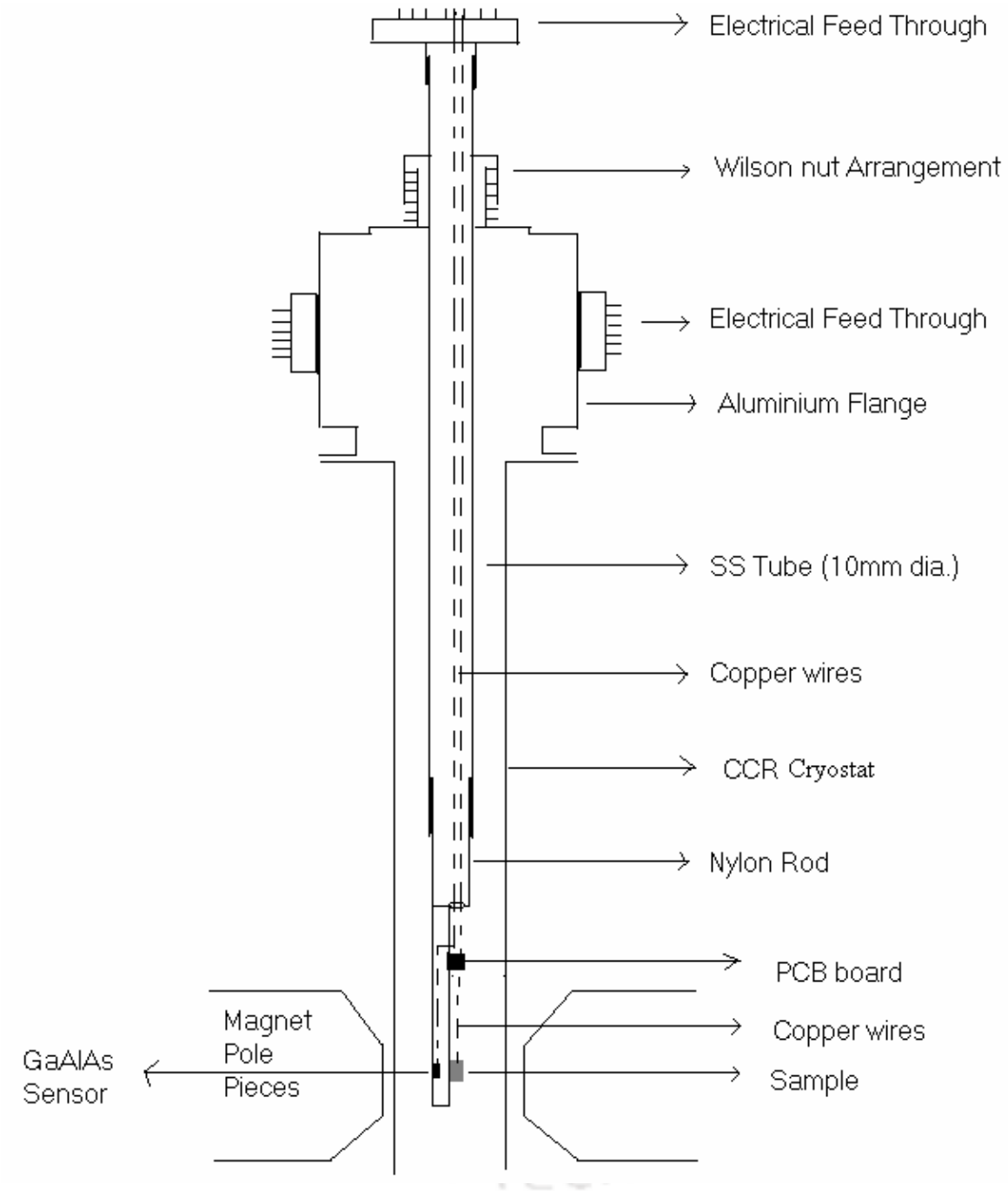

Fig. 2.7. Fabricated sample holder attached to the CCR cryostat for resistivity and Magneto-resistivity measurements.

Parallelepiped shaped samples with uniform cross-sectional area have been taken for the above measurements. Four probe contacts were made with the help of silver paint/indium soldering to eliminate contact and lead resistances. As mentioned earlier, constant current source

and nano-voltmeter have been used. Data were collected for forward and reverse currents to eliminate thermo-emf contribution.

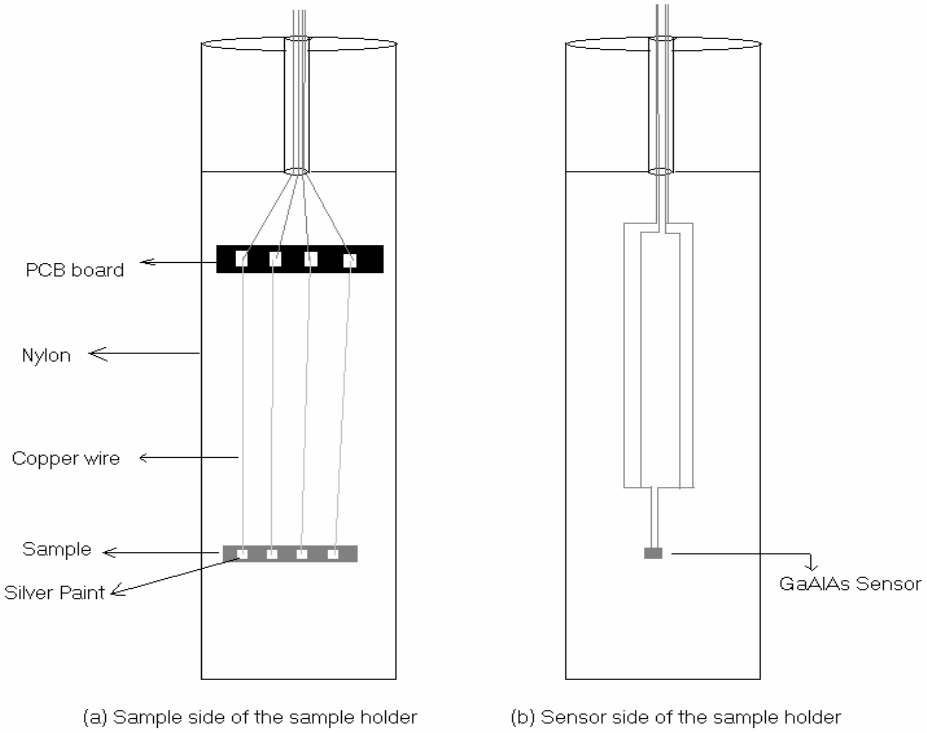

Fig. 2.8: Expanded view of magneto-resistivity sample holder. (a) Sample side of the sample holder and (b) Sensor side of the sample holder.

2.1.7. AC Susceptibility Measurement

AC susceptibility technique is one of the important tools for studying the magnetic properties of the high T_c superconductors. It has the advantage over other techniques in terms of cost and one can get additional information, such as loss components, which is very essential for studying the granular nature of superconductors. The ac susceptometer with temperature variation down to 20K has been designed and developed by me and, the details are given as follows. It is basically designed by employing mutual inductance bridge method [333]. It consists of a primary coil and coaxially wound two identical secondary coils as shown in Fig. 2.9. One secondary coil is used for mounting the sample and is called sample secondary and, the other one is reference secondary. The primary coil is energized using a sinusoidal signal of desired frequency and voltage, $E = E_0 e^{i\omega t}$. Magnetic field, $H = H_0 e^{i\omega t}$ is generated along the axis of the solenoid

(primary coil) corresponding to applied voltage in the primary. In the absence of sample, the induced voltage in each secondary coil would be almost equal and its differential output would be close to zero. When sample is inserted into the sample secondary coil, the net induced emf, '*e*' across the secondary coils is a measure of susceptibility of the material, as given in the following expression,

$$e = (\alpha n_s V_s \omega \mu_0 H_0)\chi \qquad \text{----------} \qquad (2.11)$$

where, n_s is the number of turns per unit length in the secondary coil; ω is the angular frequency of input signal to primary coil and V_s is the volume of the sample. The filling factor coefficient, α depends on the geometry and dimension of the sample and secondary coils. χ is the susceptibility of the material.

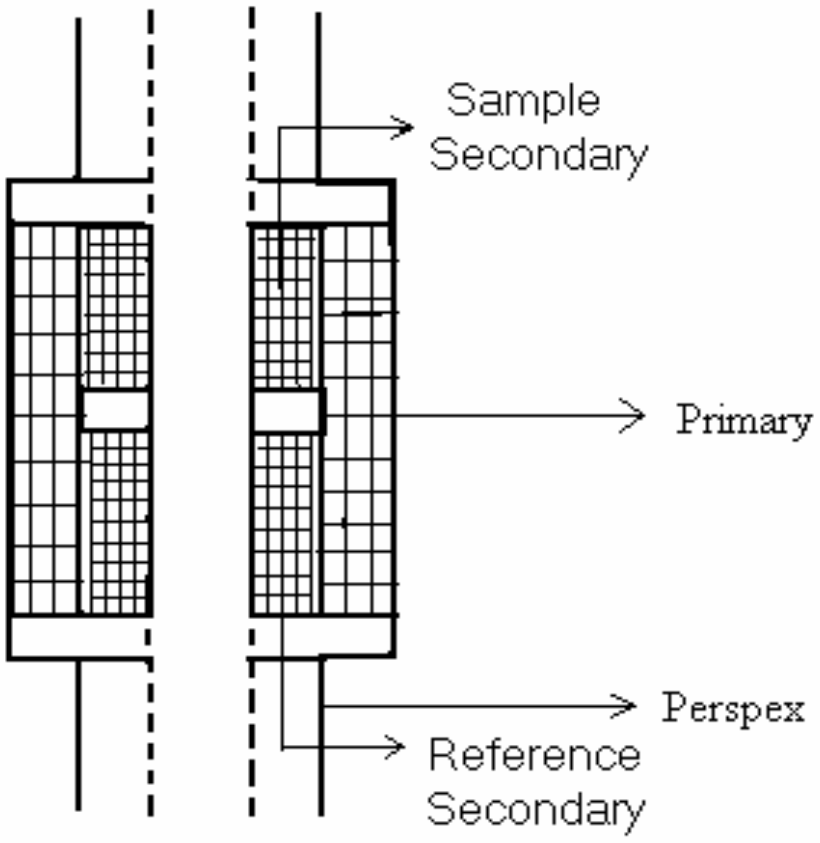

Fig. 2.9: Block diagram of Mutual Inductance Coil assembly.

The outline of the mutual inductance coil assembly is shown in Fig. 2.9. Two identical secondary coils of length 15mm each were wound with 39SWG (diameter 0.1312mm) insulated

copper wire on a perspex tube of outer diameter 12mm and inner diameter 6mm.They are separated by a distance of 3mm along the length of the coil. The primary coil with same SWG was wound over the secondary coils with inner diameter 18mm and outer diameter 23mm. The number of turns in each secondary coil was 1370 and that of primary coil was 2689.

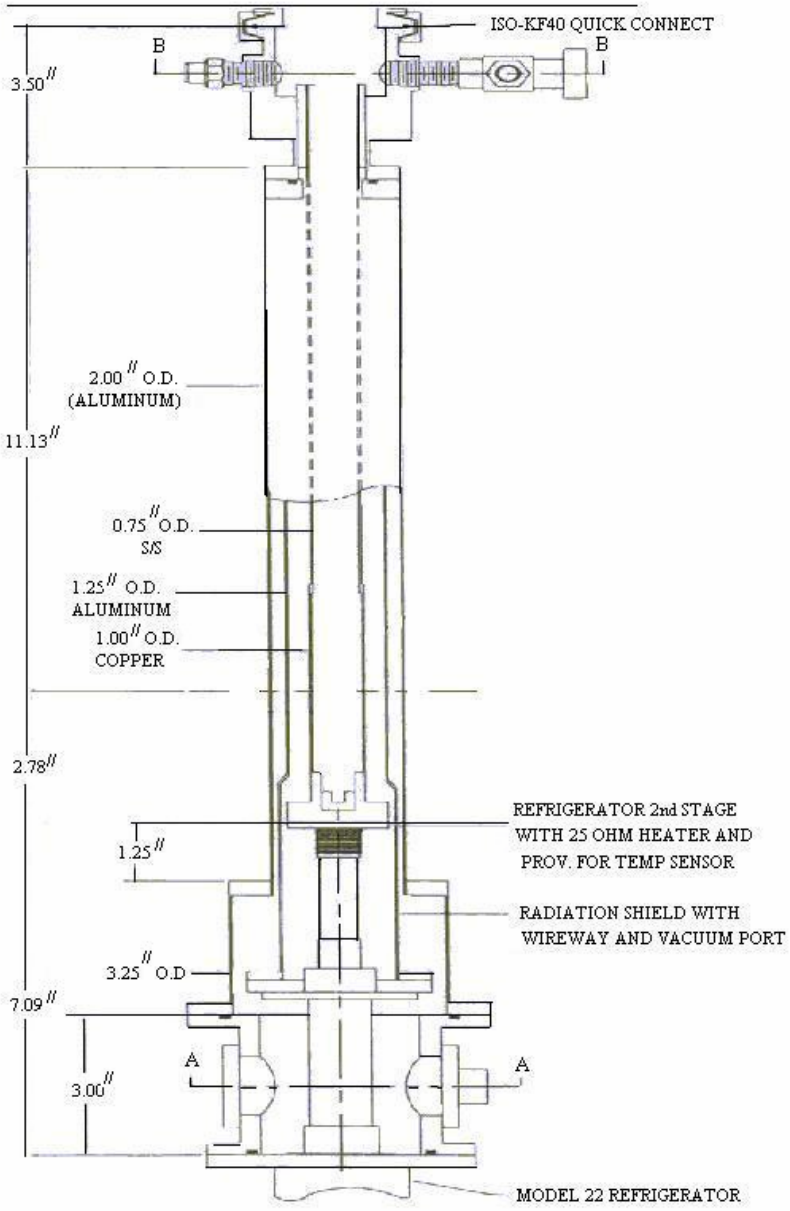

Fig. 2.10: Block diagram of CCR cryostat.

The temperature variation down to 20 K was achieved using the closed cycle Helium refrigerator cryostat along with the temperature controller as described in the section 2.1.6. However, a separate sample insert assembly was fabricated for ac susceptibility measurements. The schematic diagram of the CCR cryostat is shown in Fig. 2.10. The sample chamber of 1"

diameter is covered by non-magnetic radiation shield and vacuum shroud as shown in Fig.2.10. The sample chamber is cooled with the help of helium exchange gas.

A sample insert assembly attached with a sample holder has been designed and fabricated for quick loading & unloading of samples. The schematic diagram of the sample insert assembly along with Coil housing assembly for mutual inductance bridge is shown in Fig. 2.11. The non magnetic thin walled stainless steel (SS) tube with outer diameter 10mm and length 550mm is coupled to the sample holder made up of Perspex rod of length 100mm. The bottom part of Perspex rod was made into a flat surface to load the sample and temperature sensor. The other end of the SS tube passing through the Wilson nut is fitted with an electrical feed through and it is used for connecting the sensor leads mounted nearby sample area. Electrical feed through adapter attached to aluminum flange was used for connecting the primary and secondary Coil leads. The position of sample holder can be adjusted with the help of Wilson nut arrangement. A Lakeshore supplied Si diode sensor, which follows a standard curve was mounted in the vicinity of sample position as shown in the Fig. 2.11.

The block diagram of the ac susceptibility set-up is shown in Fig. 2.12. The primary coil is connected to the output of a Function Generator supplied by Stanford Research Systems, model no. DS360. The maximum oscillator output of Function Generator is 14V (rms). The magnetic field was calculated using the standard relation of the solenoid,

$$H = \frac{NI}{L} \text{ (A/m)} \qquad \text{----------} \qquad (2.12)$$

or,

$$H = \frac{NI}{L} 4\pi \times 10^{-3} \text{ (Oe)} \qquad \text{----------} \qquad (2.13)$$

Here, N is the total number of turns in the primary coil; I is the amplitude of current flowing through the primary in Ampere and L is the length of primary in meter. The maximum amplitude of magnetic field in the present set-up was found to be around 19 Oe. The output of both the secondary coils are connected to the differential input (A-B) of the lock-in amplifier, which can measure the in-phase and out of phase components of ac susceptibility signal simultaneously. For controlling the temperature, Lakeshore supplied silicon diode sensor (model no. DT-470) has been used. This sensor was mounted at the cold tip of the CCR, where a heater wire of 50Ω

resistance was also installed. Four leads of the controlling sensor are connected to the A-channel input of the temperature controller. The sample temperature is measured using another silicon diode sensor (model no. DT-670) which is connected to the B-channel input of the temperature controller. The temperature controller, lock-in amplifier and function generator were connected to a personal computer equipped with a GPIB board for data acquisition. The necessary software in the language of Quick Basic was developed for the acquisition of temperature variation of ac susceptibility data. The temperature was measured with an accuracy of better than ± 0.2 K.

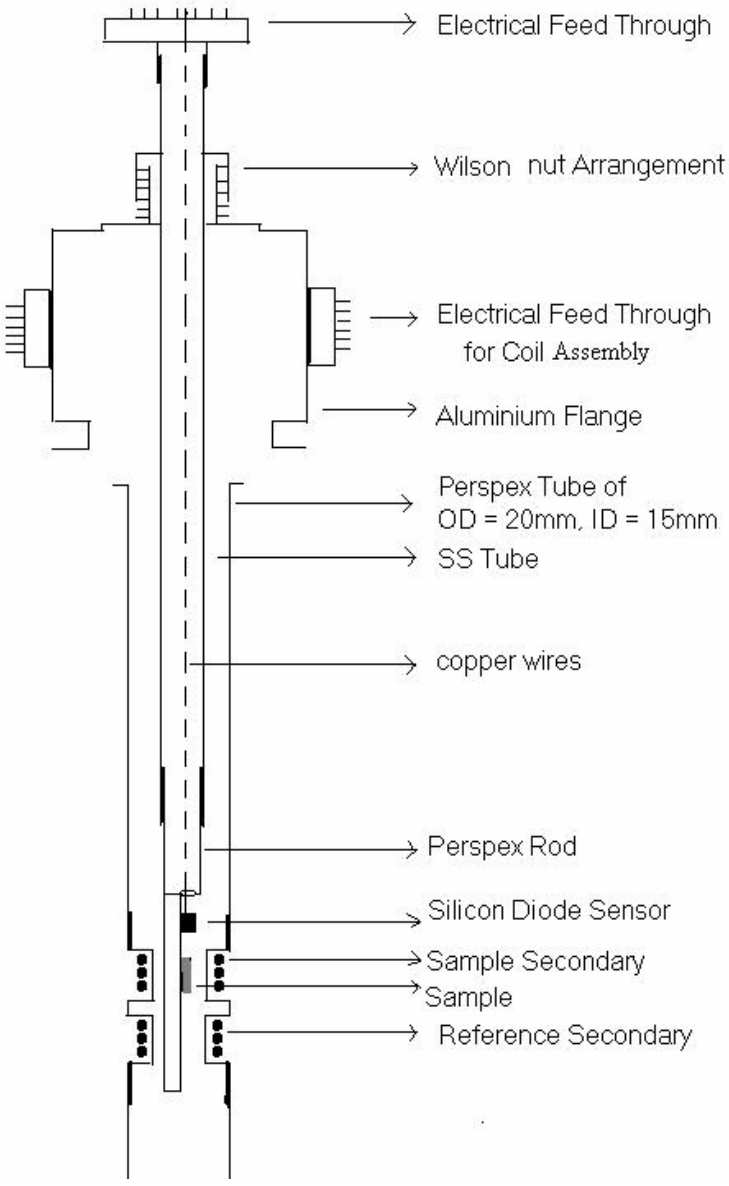

Fig. 2.11: Sample insert and Coil housing assembly

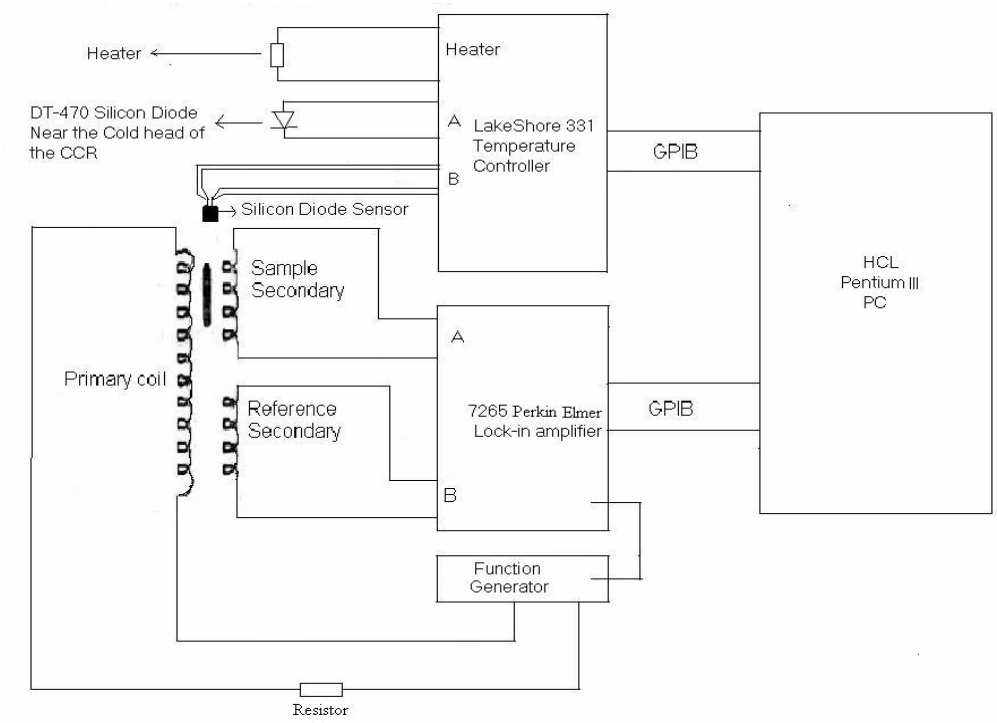

Fig. 2.12: Block diagram of ac susceptibility set-up.

To completely separate the real and imaginary components of ac susceptibility, appropriate reference phase angle needs to be set, in the lock-in amplifier. The phase angle ϕ was obtained by adjusting the reference phase in the lock-in amplifier such that the signal of the out of phase (loss/imaginary component) component is zero at very low temperature, i.e. in completely diamagnetic region. One can also numerically separate the real and imaginary components, by measuring the susceptibility in zero phase and using the following expressions [334],

$$\chi' = \chi_0' \cos\phi + \chi_0'' \sin\phi \text{ ----------} \quad (2.14)$$

$$\chi'' = \chi_0'' \cos\phi - \chi_0' \sin\phi \text{ ----------} \quad (2.15)$$

Where χ_0' and χ_0'' are the measured susceptibilities before phase adjustment (at zero phase).

The applied magnetic field and ac susceptibility have been corrected for demagnetization by following ref. [334, 335] as given below. The expression for intrinsic magnetic field (H_{in}) is given as follows,

$$H_{in} = H_{exp} - NM \quad (2.16)$$

Here N is the demagnetizing factor ($0 < N < 1$); M is the magnetization of the material and H_{exp} is the external applied field. The demagnetization factor is a geometric effect.

In ac susceptometer, by the application of external magnetic field H_{exp}, the measured experimental susceptibility is χ_{exp} and the intrinsic susceptibility which is the characteristic of the material is χ_{in}. The two susceptibilities are related by,

$$\chi_{in} = M / H_{in} = \chi_{exp} / (1 - N\chi_{exp}) \tag{2.17}$$

and

$$\chi_{exp} = M / H_{exp} = \chi_{in} / (1 + N\chi_{in}) \tag{2.18}$$

The complex susceptibility can be written as, $\chi_{in} = \chi_{in}^{/} + i\,\chi_{in}^{//}$. Similarly the experimental complex susceptibility can be written as, $\chi_{exp} = \chi_{exp}^{/} + i\,\chi_{exp}^{//}$. The in phase and out of phase components of intrinsic susceptibility $\chi_{in}^{/}$ and $\chi_{in}^{//}$ are separated from the measured susceptibility $\chi_{exp}^{/}$ and $\chi_{exp}^{//}$ using the relations,

$$\chi_{in}^{/} = \frac{\left[\chi_{exp}^{/} - N\left(\chi_{exp}^{/2} + \chi_{exp}^{//2}\right)\right]}{\left[N^2\left(\chi_{exp}^{/2} + \chi_{exp}^{//2}\right) - 2N\chi_{exp}^{/} + 1\right]} \tag{2.19}$$

$$\chi_{in}^{//} = \frac{\chi_{exp}^{//}}{\left[N^2\left(\chi_{exp}^{/2} + \chi_{exp}^{//2}\right) - 2N\chi_{exp}^{/} + 1\right]} \tag{2.20}$$

The expression for H_{in} can be written as,

$$H_{in} = H_{exp}\left[\frac{\left(\chi_{exp}^{/2} + \chi_{exp}^{//2}\right)}{\left(\chi_{in}^{/2} + \chi_{in}^{//2}\right)}\right] \tag{2.21}$$

Similar technique has been followed by Youssif et al. [336]. The demagnetization factor for orthorhombic sample geometry is calculated as follows. Let's consider an orthorhombic sample with thickness '*l*' as shown in Fig. 2.13. The breadth (along y) and length (along z axis) of the orthorhombic sample is expressed in terms of the thickness of the sample using multiplication constants n_1 and n_2.

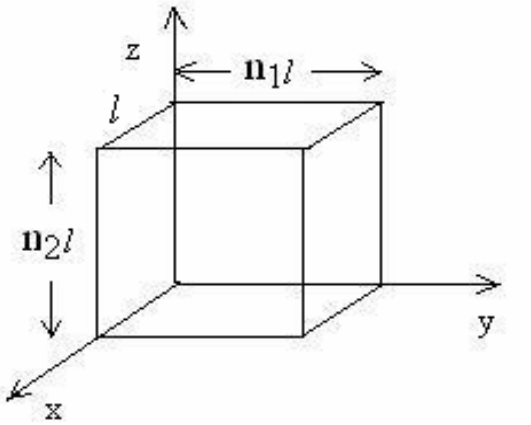

Fig. 2.13. Orthorhombic sample with thickness *l*.

According to Sato et al. [337], the relation between demagnetization factor along x, y and z directions, i.e. N_x, N_y and N_z can be written as,

$$N_x + N_y + N_z = 1 \tag{2.22}$$

The demagnetization factors are generally inversely proportional to the dimension of the sample along the particular direction. So, N_x, N_y and N_z can be written as,

$$N_x = \frac{c}{l}$$

$$N_y = \frac{c}{n_1 l} \tag{2.23}$$

$$N_z = \frac{c}{n_2 l}$$

where c is proportionality constant. By substituting these values in eqn.2.22, we get

$c = n_l n_2 l/(n_1+n_2+n_1 n_2)$. So the demagnetization factor N_z can be written as

$$N_z = \frac{c}{n_2 l} = \frac{n_1}{n_1 + n_2 + n_1 n_2} \tag{2.24}$$

where, n_1 = breadth/thickness, n_2 = length/thickness and can be obtained from sample dimension.

Calibration of the ac susceptometer was carried out by using the standard paramagnetic salts [338]. Here Gd_2O_3 was taken as the standard and its temperature dependent gram susceptibility is given as, [339]

$$\chi = \frac{45684}{T+18} \times 10^{-6} \text{ c.g.s} \qquad \text{----------} \qquad (2.25)$$

Here, T is in Kelvin. The Gd_2O_3 powder was pressed into a cylindrical pellet of ≈ 13mm diameter and 4-5mm thickness. A parallelepiped shaped sample with dimension $(4\times2\times12)mm^3$ was cut from the pressed pellet. The above piece was used for calibration. The ac loss for above paramagnetic salt was found to be zero. The temperature variation of in-phase signal, $e^{/}$ was measured and was converted into the unit of μV/gmOe and, it is shown in Fig. 2.14. The experimental data could be fitted to Curie-Weiss law, [340]

$$\chi = \frac{C}{T-\theta} \qquad \text{----------} \qquad (2.26)$$

where, 'C' is the Curie constant and 'θ' is the Curie temperature and the fit is shown in the inset of the Fig. 2.14 as solid line. The fitted parameters are $-\theta/C = -(7.15 \pm 0.53)\times10^{-3}$ gm.Oe/μV and $1/C = (4.80 \pm 0.04) \times10^{-4}$ gm.Oe.K/μV.

By comparing the above experimental data with the standard value (calculated using the eqn. 2.25), the calibration constant is determined and it is found to be $1\mu V/gmOe = (1.06 \pm 0.06)\times10^{-5}$ emu/gmOe.

The above calibration constant is used for calculating the susceptibility in terms of emu/gmOe from the measured signal in the unit of μV/gmOe. To confirm the validity of the above calibration constant, another standard paramagnetic salt namely Mohr salt $(Fe(NH_4)_2(SO_4)_2.6H_2O)$ was measured and the absolute susceptibility was determined using the above calibration constant. The temperature variations of standard susceptibility for Mohr salt is known as [341],

$$\chi = \frac{9500}{1+T} \times 10^{-6} \text{ c.g.s.} \qquad \text{----------} \qquad (2.27)$$

The experimental data of temperature variations of $1/\chi^{/}$ for Mohr Salt is shown as circles in Fig. 2.15. The solid line represents the standard values. As can be seen from the Fig. 2.15 that the experimental susceptibility closely follows the literature value.

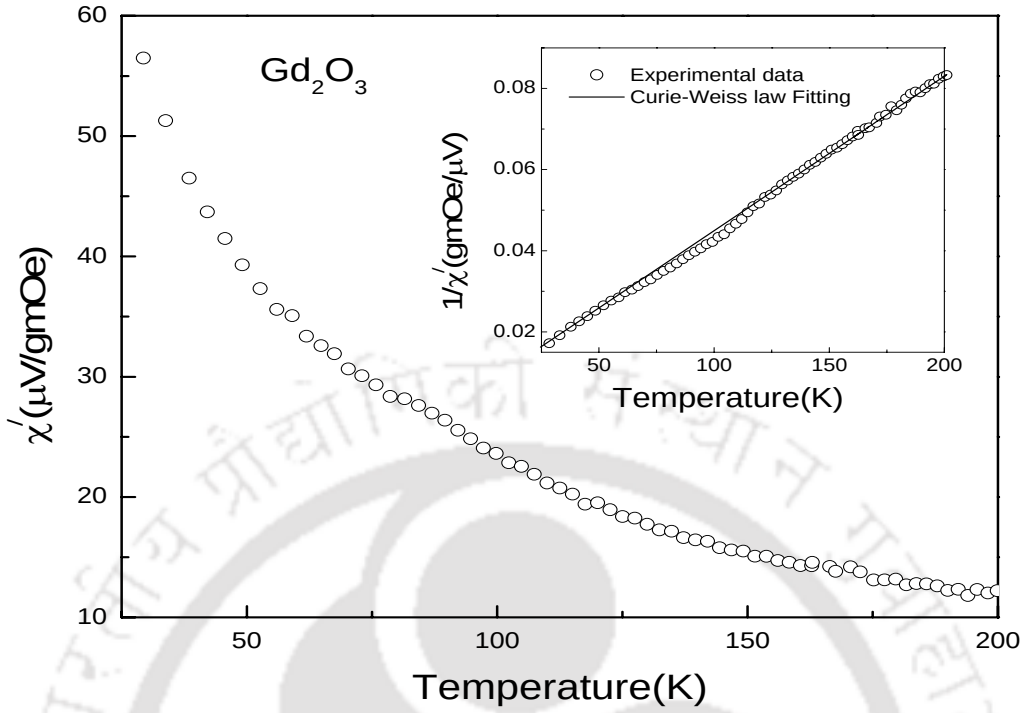

Fig. 2.14: Temperature variation of ac susceptibility (χ') in μV/gmOe for Gd_2O_3. Inset shows the $1/\chi'$ vs. Temperature plot. Circles represent the experimental data and solid line represents the fit to Curie-Weiss law.

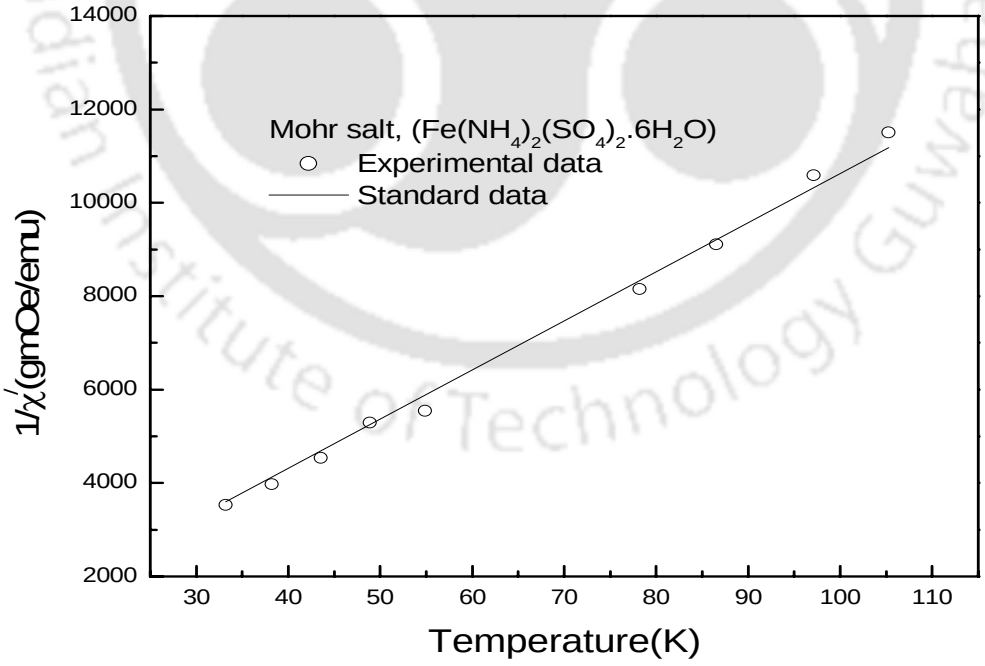

Fig. 2.15: $1/\chi'$ (gmOe/emu) versus temperature for Mohr Salt. The solid line represents the standard literature value.

2.2. SAMPLE CHARACTERIZATION

2.2.1. $(La_{1-x}Y_x)_2Ba_2CaCu_5O_z$ $(0 \leq x \leq 0.5)$

In this section, the characterization of Y doped $(La_{1-x}Y_x)_2Ba_2CaCu_5O_z$ samples by using X-ray diffraction, scanning electron microscope, electrical resistivity and ac susceptibility techniques are given.

(a) Crystal Structure

The X-ray diffraction patterns recorded for $(La_{1-x}Y_x)_2Ba_2CaCu_5O_z$ compounds for x = 0 to 0.50 are shown in Fig.2.16. We can see that all samples are essentially in single phase form. The XRD patterns were analyzed with the help of fullprof program by employing rietveld refinement technique [332]. All the patterns could be refined by using P4/mmm space group in tetragonal cell. The typical XRD patterns along with rietveld refinement are shown in Fig.2.17 for (a) x = 0.10 (Sample B), (b) x = 0.20 (Sample C), (c) x = 0.25 (Sample D) and (d) x = 0.50 (Sample F). The solid circles represent experimental data and the solid line represents Rietveld refined data. The dotted lines show the difference between experimental and refined data. The allowed Bragg positions are marked in each figure. In Table 2.1, the refined parameters such as atomic positions, occupancies and isotropic temperature factors, reliability parameters for the above four samples are mentioned. About 51 to 55% of Ca is found to occupy the La(Y) site and the remaining Ca occupies the Ba site. The Ba site is also occupied by about 44 to 55 % of La/Y. The intermixing of La and Ca in Ba site and Ca in La site are widely reported in La-1113 type of compounds [123,128-129]. The occupancy values of oxygen were kept fixed in the above refinement. We can see that the doped Y also occupies both La and Ba site. Some vacancy in the Cu site has been observed.

The lattice parameters, unit cell volume, bond length, bond angles and total occupancy of each element are given in Table 2.2 for the samples in $(La_{1-x}Y_x)_2Ba_2CaCu_5O_z$ series. The lattice parameters of x = 0 sample is comparable to those reported in literature [127, 128]. The lattice parameters mostly decrease with increase in doping concentration and it can be understood as a result of smaller ionic size of Y compared to La. The occupancy values of Y are comparable to the doped concentration. From the occupancy of various elements, we can see that the composition leads to close to the La-1113 form. The Cu2-O3-Cu2 bond angle is found to be mostly in the range of 162 to 164^o. The above bond angle is about 3 to 5^o less than that reported

for tetragonal $YBa_2Cu_3O_{7-\delta}$ [342] and this deviation could be mainly due to the partial occupation of Ca in La site. Even though there are a few reports on the structural study of undoped materials, the bond length and bond angles are not tabulated in details in literature.

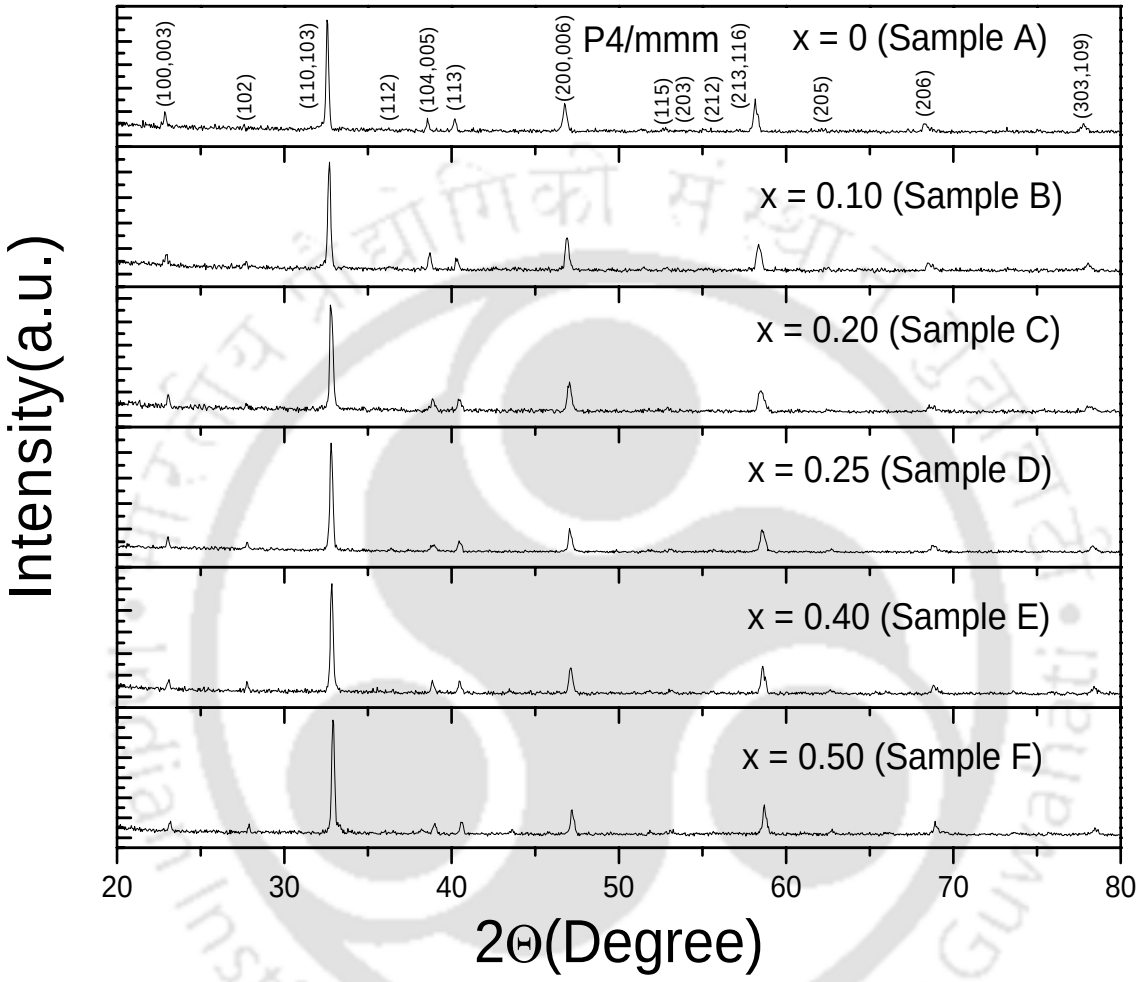

Fig. 2.16. XRD patterns of $(La_{1-x}Y_x)_2Ba_2CaCu_5O_z$ compounds for x = 0, 0.10, 0.20, 0.25, 0.40 and 0.50.

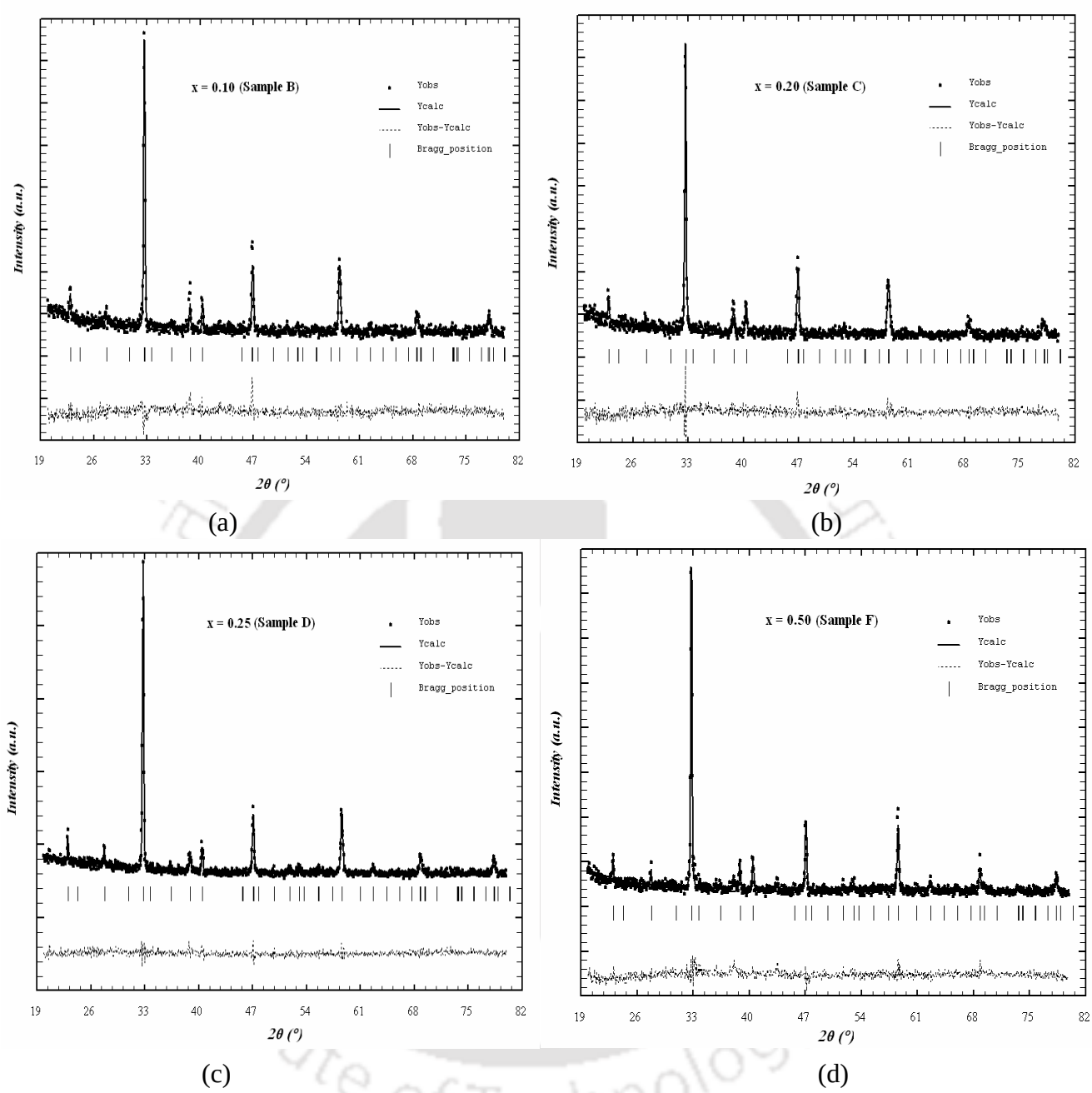

Fig. 2.17. XRD patterns for the samples (a) x = 0.10, (b) x = 0.20, (c) x = 0.25 and (d) x = 0.50 of $(La_{1-x}Y_x)_2Ba_2CaCu_5O_z$ compounds. The solid circles represent experimental data and the solid line represents Rietveld refined data. The dotted lines show the difference between experimental and refined data. The possible Bragg positions are marked at the bottom of each pattern.

Table 2.1.Parameters such as atomic positions, isotropic temperature factors and occupancies obtained from Rietveld analysis for samples x = 0.10, 0.20, 0.25 and 0.5 in $(La_{1-x}Y_x)_2Ba_2CaCu_5O_z$ series. R_p, R_B, R_F and χ^2 are the reliability factors.

x = 0.10 (Sample B)				x = 0.20 (Sample C)			
Atoms	Site(x, y, z)	Biso (Å^2)	Occupancy	Atoms	Site(x, y, z)	Biso (Å^2)	Occupancy
La Y Ca	(0.5, 0.5, 0.5)	1.47	0.393 0.038 0.529	La Y Ca	(0.5, 0.5, 0.5)	2.75	0.413 0.067 0.445
Ba La Y Ca	(0.5, 0.5, 0.1862)	1.87	0.988 0.404 0.032 0.437	Ba La Y Ca	(0.5 ,0.5, 0.1869)	1.27	0.898 0.309 0.072 0.434
Cu(1)	(0, 0, 0)	4.03	0.868	Cu(1)	(0, 0, 0)	1.20	0.804
Cu(2)	(0, 0, 0.3544)	2.03	1.932	Cu(2)	(0, 0, 0.3496)	3.31	1.734
O(1)	(0.5, 0, 0)	4.68	1.000	O(1)	(0.5, 0, 0)	2.20	1.000
O(2)	(0, 0, 0.1550)	1.22	2.000	O(2)	(0, 0, 0.1587)	0.85	2.000
O(3)	(0.5, 0, 0.3773)	0.43	4.000	O(3)	(0.5, 0, 0.3751)	0.93	4.000
R_p=18.6, R_B=14.5, R_F=14.4, χ^2=1.39				R_p=17.5, R_B=14.1, R_F=14.7, χ^2=1.31			
x = 0.25 (Sample D)				x = 0.50 (Sample F)			
Atoms	Site(x, y, z)	Biso (Å^2)	Occupancy	Atoms	Site(x, y, z)	Biso (Å^2)	Occupancy
La Y Ca	(0.5, 0.5, 0.5)	0.66	0.315 0.109 0.521	La Y Ca	(0.5, 0.5, 0.5)	2.92	0.230 0.245 0.506
Ba La Y Ca	(0.5, 0.5, 0.1824)	1.57	0.975 0.398 0.111 0.456	Ba La Y Ca	(0.5 ,0.5, 0.1869)	1.80	0.995 0.201 0.239 0.441
Cu(1)	(0, 0, 0)	1.53	0.972	Cu(1)	(0, 0, 0)	4.87	0.851
Cu(2)	(0, 0, 0.3575)	2.03	1.792	Cu(2)	(0, 0, 0.3528)	4.69	1.890
O(1)	(0.5, 0, 0)	2.26	1.000	O(1)	(0.5, 0, 0)	0.82	1.000
O(2)	(0, 0, 0.1546)	1.45	2.000	O(2)	(0, 0, 0.1487)	1.64	2.000
O(3)	(0.5, 0, 0.3870)	4.05	4.000	O(3)	(0.5, 0, 0.3791)	1.02	4.000
R_p=14.7, R_B=10.1, R_F=13.9, χ^2=1.40				R_p=17.0, R_B=15.6, R_F=13.8, χ^2=1.38			

Table 2.2. Parameters obtained from XRD pattern refinement of $(La_{1-x}Y_x)_2Ba_2CaCu_5O_z$ compounds. a and c are the lattice parameters. La (G), Y (G), Ba (G), Ca (G) and Cu (G) are the refined cation occupancies. ⟨Cu-O⟩ are the bond lengths and ∠Cu-O-Cu is the bond angle.

Sl. No	Parameters	Compositions					
		x = 0 Sample A	x = 0.10 Sample B	x = 0.20 Sample C	x = 0.25 Sample D	x = 0.40 Sample E	x = 0.50 Sample F
1	a = b (Å) c (Å)	3.879 11.646	3.869 11.627	3.870 11.600	3.859 11.561	3.857 11.589	3.856 11.576
2	Volume (Å^3)	175.2	174.0	173.8	172.1	172.3	172.2
3	⟨La-O3⟩ (Å)	2.425	2.403	2.418	2.330	2.374	2.383
4	⟨Cu1-O1⟩ (Å)	1.939	1.935	1.935	1.929	1.928	1.928
5	⟨Cu1-O2⟩ (Å)	1.806	1.808	1.841	1.787	1.930	1.721
6	⟨Cu2-O3⟩ (Å)	1.959	1.953	1.958	1.959	1.947	1.952
7	∠Cu2-O3-Cu2 (deg.)	163.7	164.3	162.6	160.0	164.1	162.0
8	La (G) Y (G)	0.999 --	0.797 0.070	0.722 0.140	0.713 0.220	0.522 0.381	0.431 0.484
9	Ba (G)	0.999	0.988	0.898	0.975	0.999	0.995
10	Ca (G)	0.960	0.966	0.879	0.977	0.955	0.947
11	Cu(1) (G)	0.863	0.868	0.804	0.972	0.891	0.851
12	Cu(2) (G)	1.866	1.932	1.734	1.792	1.813	1.890

(b) Microstructure

The SEM photographs have been taken for this series of compounds to see the morphology and to find out the average particle size. The typical SEM photographs for x = 0.40 and 0.50 samples are given in Fig. 2.18 and 2.19 respectively. The average grain size values are found to be 1.4 and 1.5 μm for x = 0.40 and 0.50 samples respectively. The EDAX Patterns were taken for these samples to carry out the compositional analysis. For x = 0.40 sample, the nominal starting composition is $(La_{1.2}Y_{0.8})Ba_2Ca_1Cu_5O_{11}$. The composition as per EDAX analysis is found to be $(La_{1.34}Y_{0.74})Ba_{2.26}Ca_{0.85}Cu_5O_{11\pm\delta}$ and it is comparable to the nominal starting compositions. By converting this 2215 form of this compound to 1113 form, the nominal starting composition can be written as $(La_{0.60}Y_{0.40})BaCaCu_3O_7$. The composition as per EDAX analysis is $(La_{0.64}Y_{0.35})Ba_{1.08}Ca_{0.81}Cu_3O_{7\pm\delta}$. Similarly for x = 0.50, the composition is found to be $(La_{1.09}Y_{0.85})Ba_{2.20}Ca_{0.72}Cu_5O_{11\pm\delta}$ or in alternate form, $[(La_{0.53}Y_{0.42})Ba_{1.18}Ca_{0.71}Cu_3O_{7\pm\delta}]$ against the nominal starting compositions of $(La_1Y_1)Ba_2Ca_1Cu_5O_{11}$ (in alternate form, $La_{0.50}Y_{0.50})BaCaCu_3O_7$). So from the EDAX analysis, it is confirmed that the final compositions are comparable to the starting compositions. The average grain size values for different samples are given in Table 2.5. We can see that the grain size reduces uniformly with increase in doping.

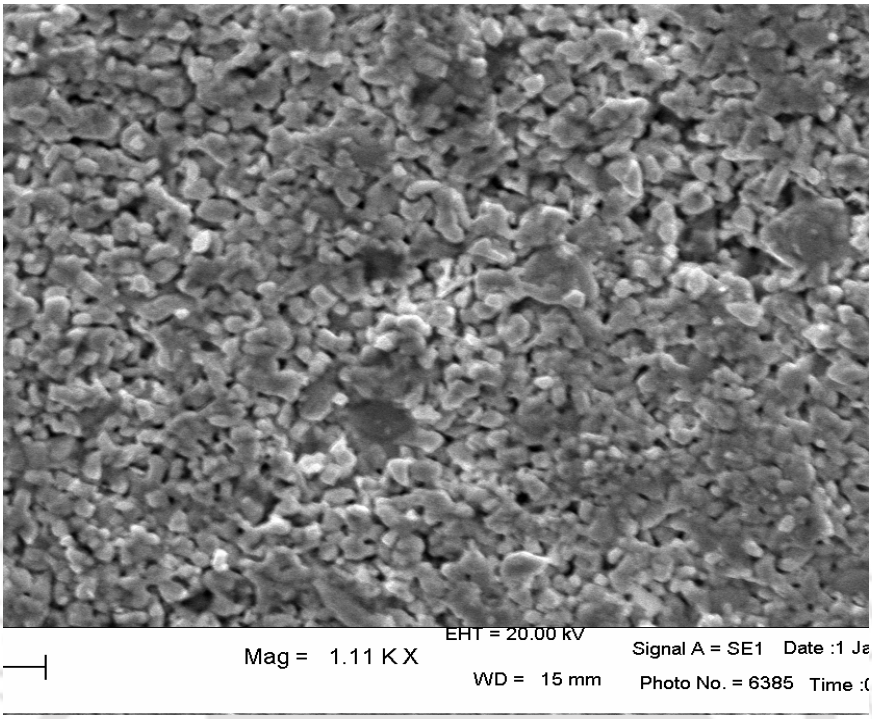

Fig. 2.18: SEM photograph for x = 0.40 (Sample E). The magnification is 1110. The average particle size is 1.4μm.

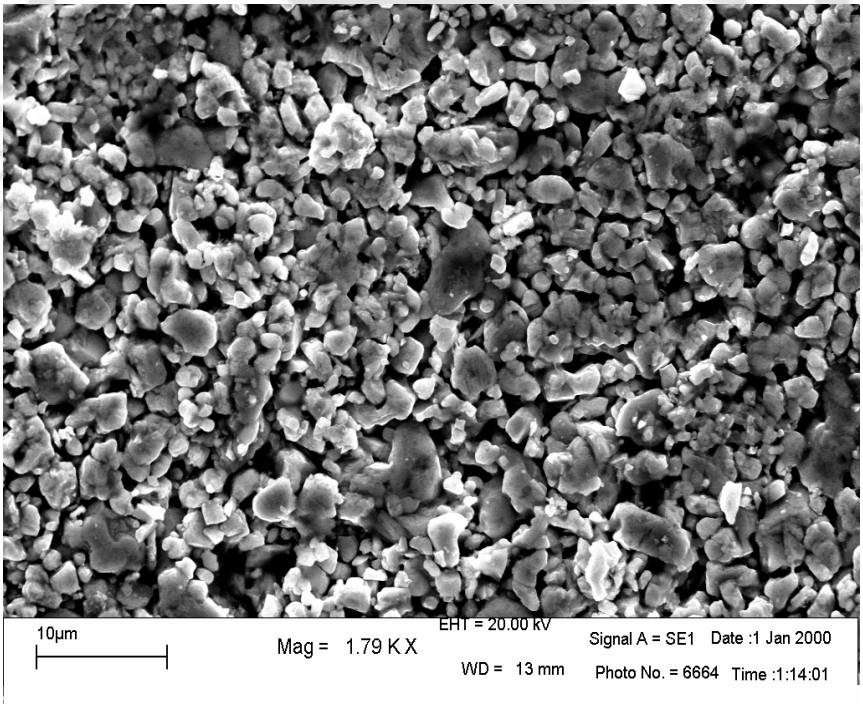

Fig. 2.19: SEM photograph for x = 0.50 (Sample F). The magnification is 1790. The average particle size is 1.5μm.

(c) DC Electrical Resistivity

The temperature variation of electrical resistivity was measured on the above samples as shown in Fig.2.20. They exhibit superconducting transition with zero resistivity. The transition temperature varies from 60 to 74 K. The superconducting transition temperature mostly decreases with Yttrium (Y) doping baring an anomaly for x = 0.25. The transition midpoint, T_c is determined by plotting the derivative of resistivity as a function of temperature. The transition width is taken from the full width at half maximum of dρ/dT versus T plots.

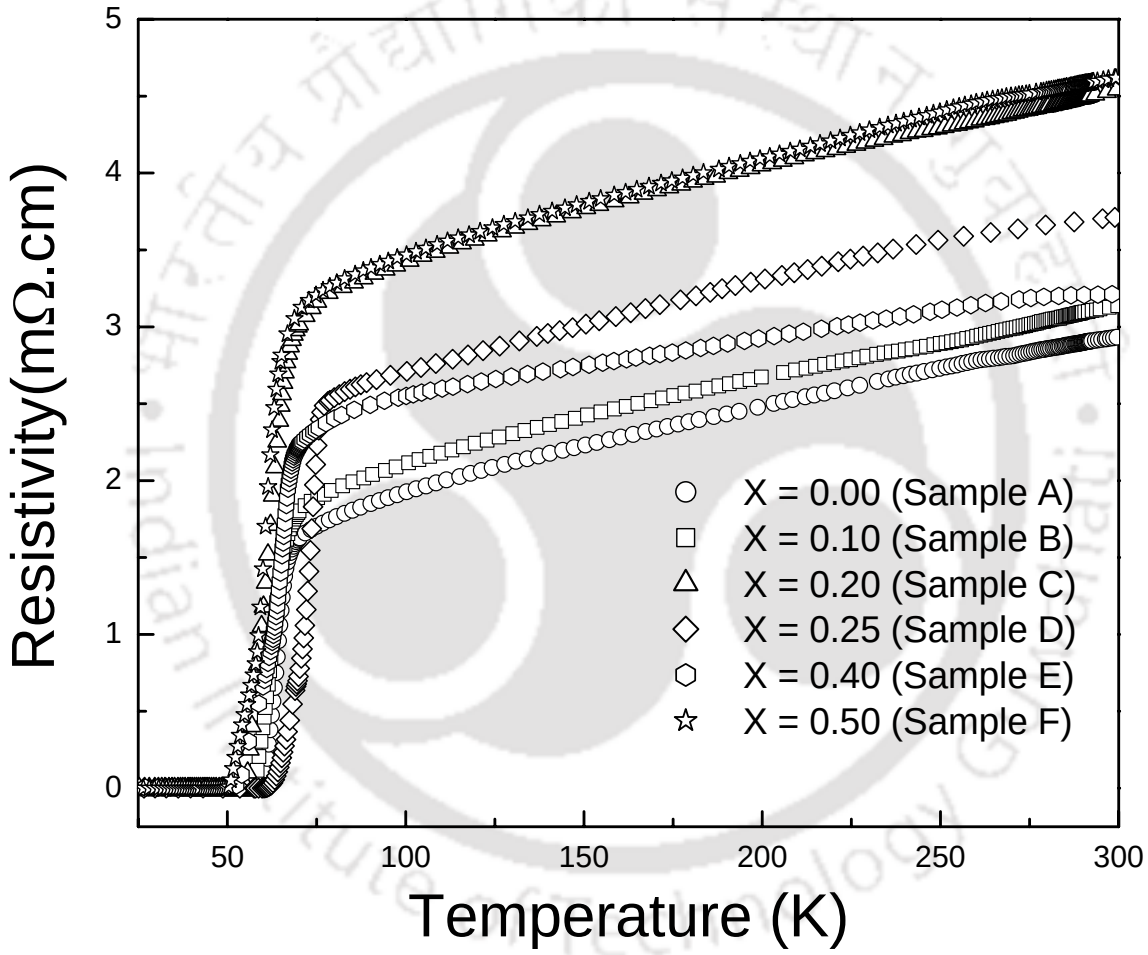

Fig. 2.20. Plots of temperature versus resistivity for $(La_{1-x}Y_x)_2Ba_2CaCu_5O_z$ series.

The values of $T_c(0)$, T_c, ΔT_c and ρ(300 K) are given in Table-2.5. The ΔT_c values are found to be mostly in the range of 4 to 5 K and is reasonably a small width. This type of materials generally show large transition width due to intermixing of site occupancy. The ρ(300 K) values are found to be 3.0 to 4.8 mΩ.cm. The T_c of present series of samples is comparable to the pure and Dy doped samples reported by Singh et al. [127]. The ionic size of Dy is comparable to that of Y ion. In most of the reports, electrical resistance is given rather than resistivity, so it is difficult to compare with literature. Peng et al. [123] reported room temperature resistivity of 57.0 mΩ.cm and the present materials show very low value.

(d) AC Susceptibility

Temperature variations of ac susceptibility have been measured for this series of compounds at an ac field amplitude of 23 A/m. For each run, the samples are cooled through superconducting transition in the absence of applied field. These data are shown in Fig.2.21. All the samples exhibit superconducting transition. The diamagnetic transition temperature varies from 62 to 70 K. Maximum T_c is observed for x = 0.25 sample. Most of the samples exhibit a small high temperature diamagnetic transition followed by large fall in susceptibility at lower temperature. These are the feature of presence of intra and inter-granular nature of superconducting samples. At low temperature, the χ' values approach -1. The diamagnetic transition shifts towards low temperature with increase in doping up to x = 0.20 and then increases with doping. Maximum T_c was obtained for x = 0.25 sample. The χ'' plots show peaks corresponding to the transition of bulk intergranular material.

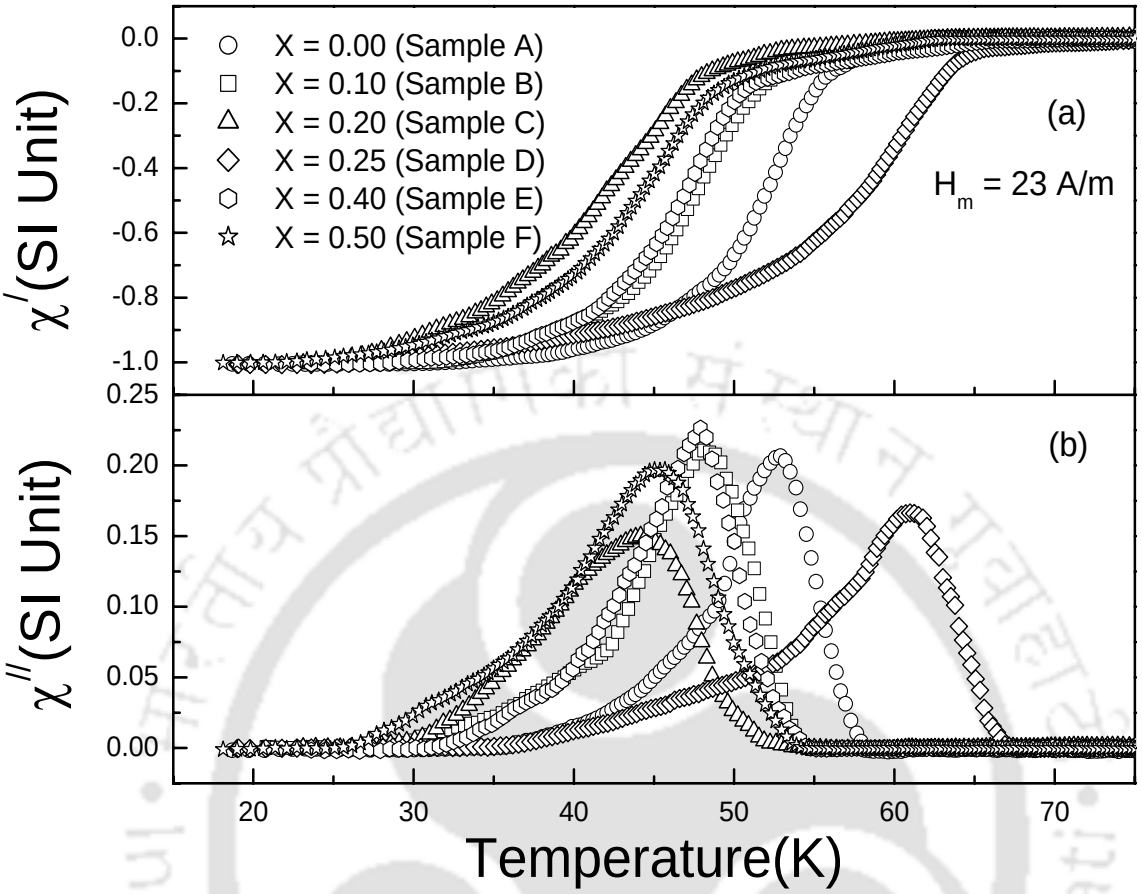

Fig. 2.21. Plots of temperature versus (a) in phase ac susceptibility $\chi^{/}$ and (b) out of phase ac susceptibility $\chi^{//}$ of $(La_{1-x}Y_x)_2Ba_2CaCu_5O_z$ series at an ac field amplitude of 23 A/m.

2.2.2. $(La_{1-x}Y_x)_2Ba_2CaCu_5O_z$ + 5 wt % Ag $(0 \leq x \leq 0.5)$

This series is similar to that of previous series but it was prepared by adding 5 wt % of Ag. They are prepared mainly to enhance the bulk property of the materials, such as improved connectivity between the grains by reducing the porosity, etc. at intergranular region, so that they can exhibit improved critical current density.

(a) Crystal Structure

Fig.2.22 shows the X-ray diffraction patterns recorded for 5 wt% of Ag doped $(La_{1-x}Y_x)_2Ba_2CaCu_5O_z$ compounds for x = 0 to 0.50. All samples are essentially in single phase form and the XRD patterns could be refined using P4/mmm space group. These XRD patterns are basically comparable to those of pure samples given in Fig.2.16. Typical XRD patterns along with rietveld refinement are shown in Fig.2.23 for (a) x = 0.10 (Sample B1), (b) x = 0.20 (Sample C1), (c) x = 0.25 (Sample D1) and (d) x = 0.50 (Sample F1). The solid circles represent

experimental data and the solid line represents Rietveld refined data. The dotted lines show the difference between experimental and refined data. The possible Bragg positions are marked in each figure.

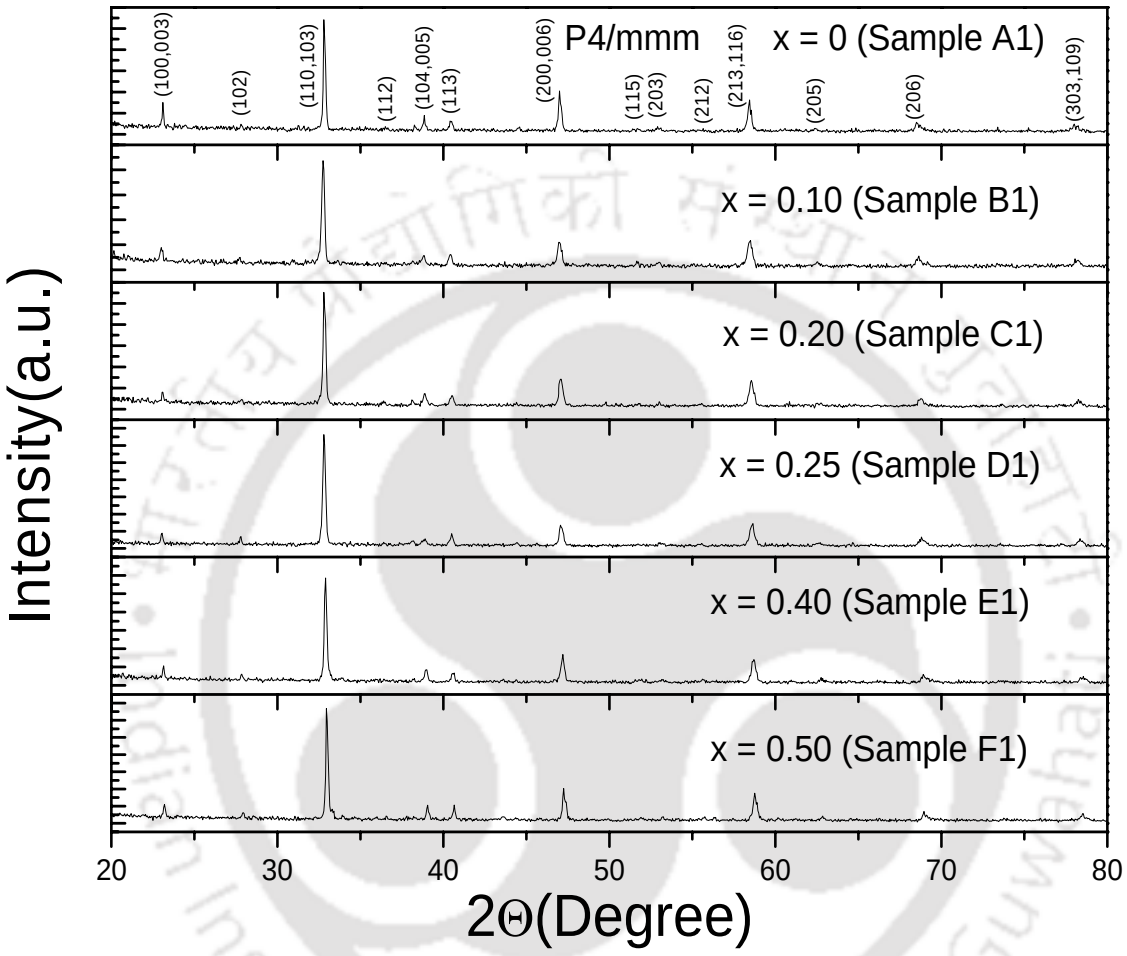

Fig. 2.22. XRD patterns of Ag doped $(La_{1-x}Y_x)_2Ba_2CaCu_5O_z$ for x = 0, 0.10, 0.20, 0.25, 0.40 and 0.50.

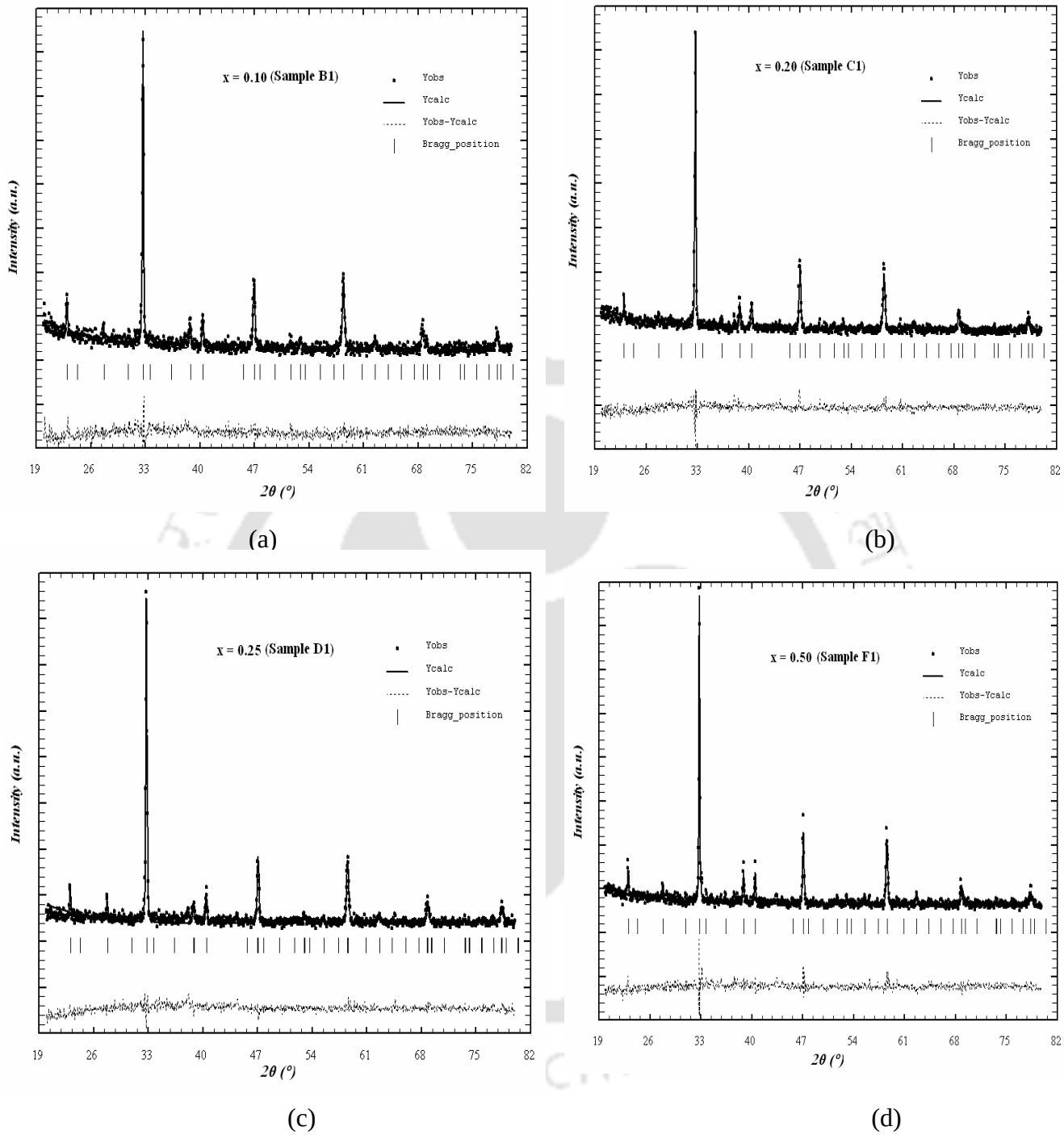

Fig. 2.23. XRD pattern for the samples (a) x = 0.10, (b) x = 0.20, (c) x = 0.25 and (d) x = 0.50 of Ag doped $(La_{1-x}Y_x)_2Ba_2CaCu_5O_z$ compounds. The solid circles represent experimental data and the solid line represents Rietveld refined data. The dotted lines show the difference between experimental and refined data. The possible Bragg positions are shown in each figure.

In Table 2.3, the refined parameters such as atomic positions, occupancies and isotropic temperature factors, reliability parameters for four samples namely x = 0.10, 0.20, 0.25 and 0.50 in Ag doped $(La_{1-x}Y_x)_2Ba_2CaCu_5O_z$ series are mentioned. The lattice parameters, unit cell volume, bond length, bond angles and total occupancy of each element are given in Table 2.4. For this series of compounds, Ca at La(Y) site is found to vary from 52 to 56 % and the La(Y) at Ba site is found to be around 48 to 59 %. The lattice parameters systematically decrease with increase in doping and it is on the expected line because the ionic size of Y is less than that of both La and Ba. The occupancy ratio of La and Y are comparable to the nominal composition to some extent and some vacancy in 'La' has been observed. The occupancy values of Cu ions are comparable to those obtained on pure samples. The Cu2-O3-Cu2 bond angle varies from 161 to 164^o.

Table 2.3. Parameters such as atomic positions, isotropic temperature factors and occupancies obtained from Rietveld analysis for samples x = 0.10, 0.20, 0.25 and 0.50 in Ag doped $(La_{1-x}Y_x)_2Ba_2CaCu_5O_z$ series. R_p, R_B, R_F and χ^2 are the reliability factors.

x = 0.10 (Sample B1)				x = 0.20 (Sample C1)			
Atoms	Site(x, y, z)	Biso (Å^2)	Occupancy	Atoms	Site(x, y, z)	Biso (Å^2)	Occupancy
La Y Ca	(0.5, 0.5, 0.5)	2.22	0.392 0.042 0.536	La Y Ca	(0.5, 0.5, 0.5)	1.32	0.343 0.109 0.547
Ba La Y Ca	(0.5, 0.5, 0.1836)	1.80	0.978 0.420 0.033 0.444	Ba La Y Ca	(0.5 ,0.5, 0.1873)	1.38	0.977 0.328 0.081 0.442
Cu(1)	(0, 0, 0)	2.55	0.865	Cu(1)	(0, 0, 0)	3.80	0.822
Cu(2)	(0, 0, 0.3573)	2.96	1.772	Cu(2)	(0, 0, 0.3512)	2.14	1.790
O(1)	(0.5, 0, 0)	3.14	1.000	O(1)	(0.5, 0, 0)	0.90	1.000
O(2)	(0, 0, 0.1557)	0.47	2.000	O(2)	(0, 0, 0.1570)	1.17	2.000
O(3)	(0.5, 0, 0.3822)	0.05	4.000	O(3)	(0.5, 0, 0.3788)	0.26	4.000
R_p=17.5, R_B=13.9, R_F=17.1, χ^2=1.33				R_p=17.0, R_B=12.7, R_F=12.8, χ^2=1.23			
x = 0.25 (Sample D1)				x = 0.50 (Sample F1)			
Atoms	Site(x, y, z)	Biso (Å^2)	Occupancy	Atoms	Site(x, y, z)	Biso (Å^2)	Occupancy
La Y Ca	(0.5, 0.5, 0.5)	0.80	0.315 0.067 0.517	La Y Ca	(0.5, 0.5, 0.5)	3.56	0.231 0.240 0.497
Ba La Y Ca	(0.5, 0.5, 0.1868)	2.02	0.959 0.337 0.217 0.456	Ba La Y Ca	(0.5 ,0.5, 0.1865)	2.73	0.975 0.323 0.246 0.455
Cu(1)	(0, 0, 0)	3.13	0.992	Cu(1)	(0, 0, 0)	3.95	0.920
Cu(2)	(0, 0, 0.3499)	4.05	1.862	Cu(2)	(0, 0, 0.3576)	4.10	1.728
O(1)	(0.5, 0, 0)	0.40	1.000	O(1)	(0.5, 0, 0)	3.96	1.000
O(2)	(0, 0, 0.1680)	0.29	2.000	O(2)	(0, 0, 0.1604)	1.57	2.000
O(3)	(0.5, 0, 0.3768)	0.05	4.000	O(3)	(0.5, 0, 0.3842)	0.04	4.000
R_p=17.5, R_B=12.1, R_F=11.2, χ^2=1.49				R_p=18.0, R_B=11.9, R_F=11.9, χ^2=1.47			

Table 2.4. Parameters obtained from XRD pattern refinement of Ag doped $(La_{1-x}Y_x)_2Ba_2CaCu_5O_y$ compounds. a and c are the lattice parameters. La(G), Y(G), Ba(G), Ca(G) and Cu(G) are the refined cation occupancies. ⟨Cu-O⟩ are the bond lengths and ∠Cu-O-Cu is the bond angle.

Sl. No	Parameters	Compositions					
		x = 0 Sample A1	x = 0.10 Sample B1	x = 0.20 Sample C1	x = 0.25 Sample D1	x = 0.40 Sample E1	x=0.50 Sample F1
1	a = b (Å) c (Å)	3.878 11.645	3.867 11.600	3.864 11.592	3.857 11.585	3.856 11.576	3.856 11.575
2	Volume ($Å^3$)	175.20	173.4	173.1	172.3	172.1	172.2
3	⟨La-O3⟩ (Å)	2.408	2.399	2.388	2.399	2.322	2.348
4	⟨Cu1-O1⟩ (Å)	1.939	1.933	1.932	1.928	1.928	1.928
5	⟨Cu1-O2⟩ (Å)	1.868	1.806	1.820	1.946	1.801	1.856
6	⟨Cu2-O3⟩ (Å)	1.959	1.955	1.958	1.953	1.9407	1.953
7	∠Cu2-O3-Cu2 (deg.)	164.1	163.0	161.2	161.6	161.6	161.8
8	La (G) Y (G)	0.997	0.812 0.075	0.672 0.190	0.652 0.284	0.559 0.387	0.554 0.486
9	Ba (G) Ca (G)	0.975 0.975	0.978 0.980	0.977 0.989	0.959 0.973	0.989 0.979	0.975 0.952
10	Cu(1) (G) Cu(2) (G)	0.864 1.670	0.865 1.772	0.821 1.790	0.992 1.862	0.881 1.876	0.920 1.728

(b) Microstructure

Typical SEM photographs for two Ag doped samples such as x = 0.40 and 0.50 are shown in Fig. 2.24 and 2.25 respectively. The average grain size was found to be 1.2 and 1.3 μm respectively. The EDAX Patterns were taken for these samples to carry out the compositional analysis. The compositions of x = 0.40 sample as per EDAX analysis are found to be $(La_{1.16}Y_{0.66})Ba_{2.01}Ca_{0.94}Cu_5O_{11\pm\delta}$ and it is comparable to the starting composition. The corresponding composition in La-1113 form is $(La_{0.59}Y_{0.34})Ba_{1.02}Ca_{0.95}Cu_3O_{7\pm\delta}$. Similarly, the compositions of x = 0.50 sample as per EDAX analysis are found to be $(La_{0.99}Y_{0.84})Ba_{2.21}Ca_{0.81}Cu_5O_{11\pm\delta}$ or $(La_{0.52}Y_{0.45})Ba_{1.17}Ca_{0.86}Cu_3O_{7\pm\delta}$. The above compositions are comparable to the nominal starting compositions. The amount of Ag present in the above two compounds are found to be 1.33 wt % and 1.77 wt% respectively. The average grain size for different samples is given in Table 2.5 and they are marginally smaller than that observed for pure samples.

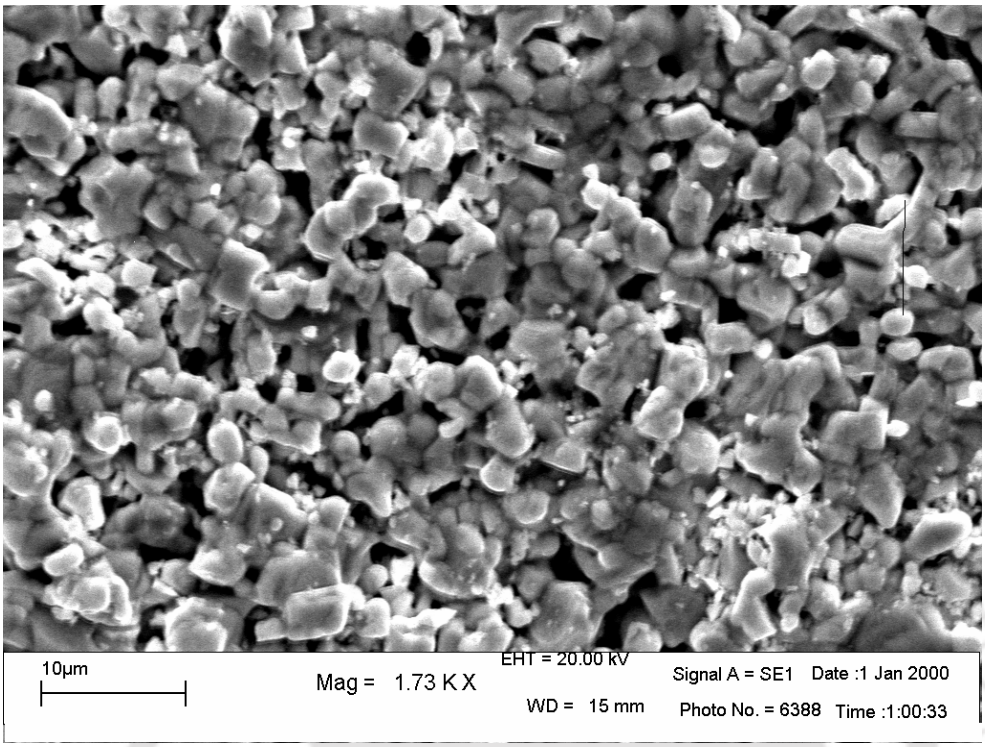

Fig. 2.24: SEM photograph for the x = 0.40 sample in Ag doped $(La_{1-x}Y_x)_2Ba_2CaCu_5O_z$ series. The magnification is 1730. The average particle size is 1.2µm.

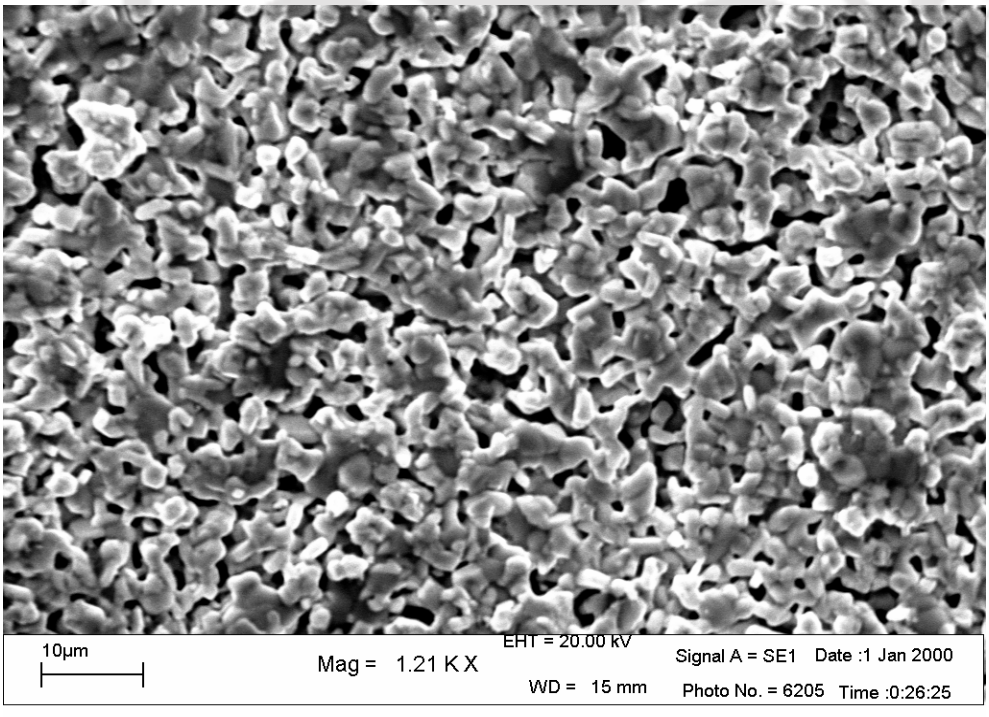

Fig. 2.25: SEM photograph for the x = 0.50 sample in Ag doped $(La_{1-x}Y_x)_2Ba_2CaCu_5O_z$ series. The magnification is 1210. The average particle size is 1.3µm.

(c) DC Electrical Resistivity

The temperature variations of electrical resistivity were measured on above samples and are shown in Fig.2.26. They exhibit superconducting transition with transition temperature varying from 64 to 75 K. The values of $T_c(0)$, T_c, ΔT_c and ρ(300 K) are given in Table-2.5. We can see the improvement in T_c and reduction of ρ(300 K) compared to pure sample of same composition. The marginal reduction in ρ(300 K) explains that Ag doping improves the intergranular coupling between the grains by reducing porosity etc. Similar to pure samples, the x = 0.25 sample exhibits maximum T_c with small transition width.

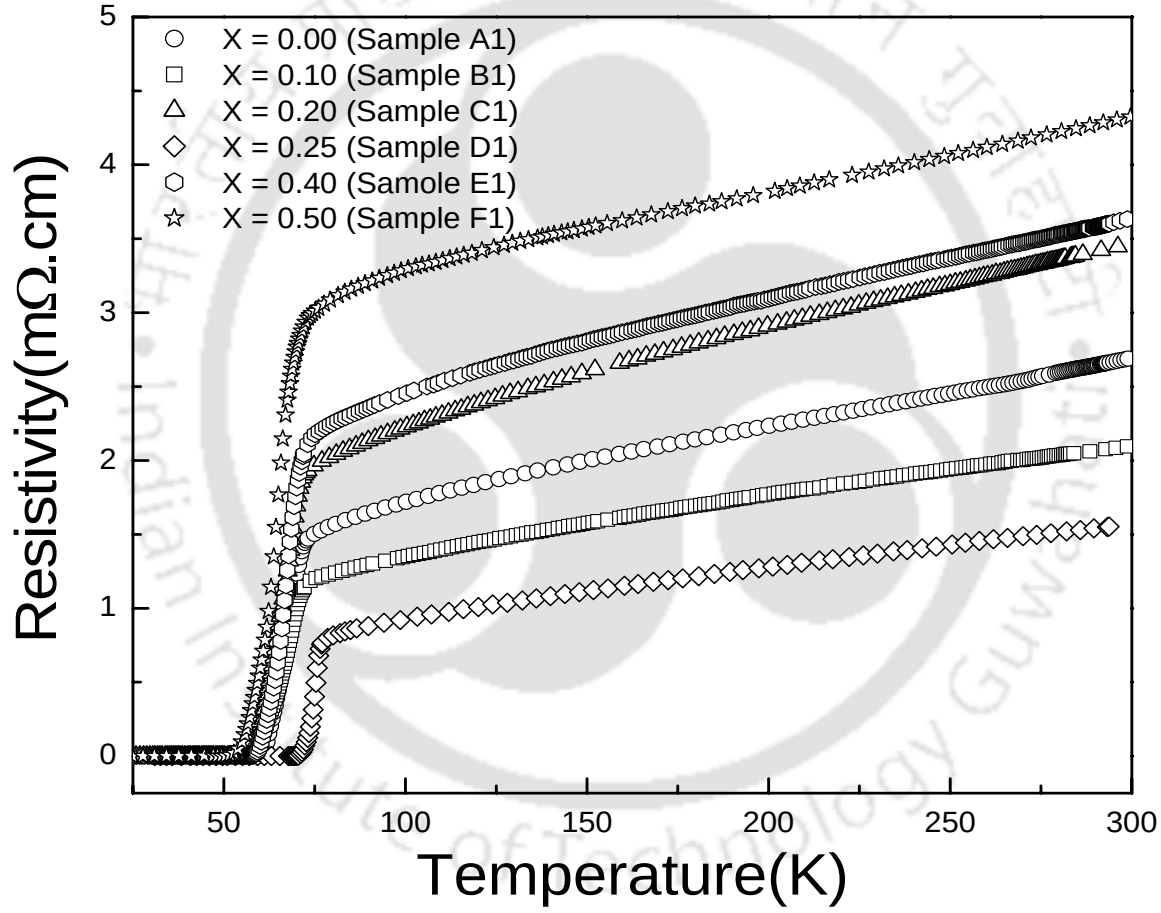

Fig. 2.26. Plots of resistivity versus temperature for Ag doped $(La_{1-x}Y_x)_2Ba_2CaCu_5O_z$ compounds.

(d) AC Susceptibility

Temperature variations of ac susceptibility have been measured for this series of compounds at an ac field amplitude of 23 A/m and are shown in Fig.2.27. All the samples exhibit superconducting transition. The diamagnetic transition temperature varies from 61 to 75 K. Maximum T_c is observed for x = 0.25 sample. AC susceptibility data show the bulk property of the material. By comparing the ac susceptibility of Ag doped samples with those of pure samples (Figs.2.27 & 2.21), we can see that the transition is relatively sharper and χ' approaches towards -1 at higher temperature in Ag doped case. Except x = 0.50 sample, all other Ag doped samples show sharp intragranular transition and on the other hand in pure samples, most of them exhibit broad intragranular diamagnetic transition.

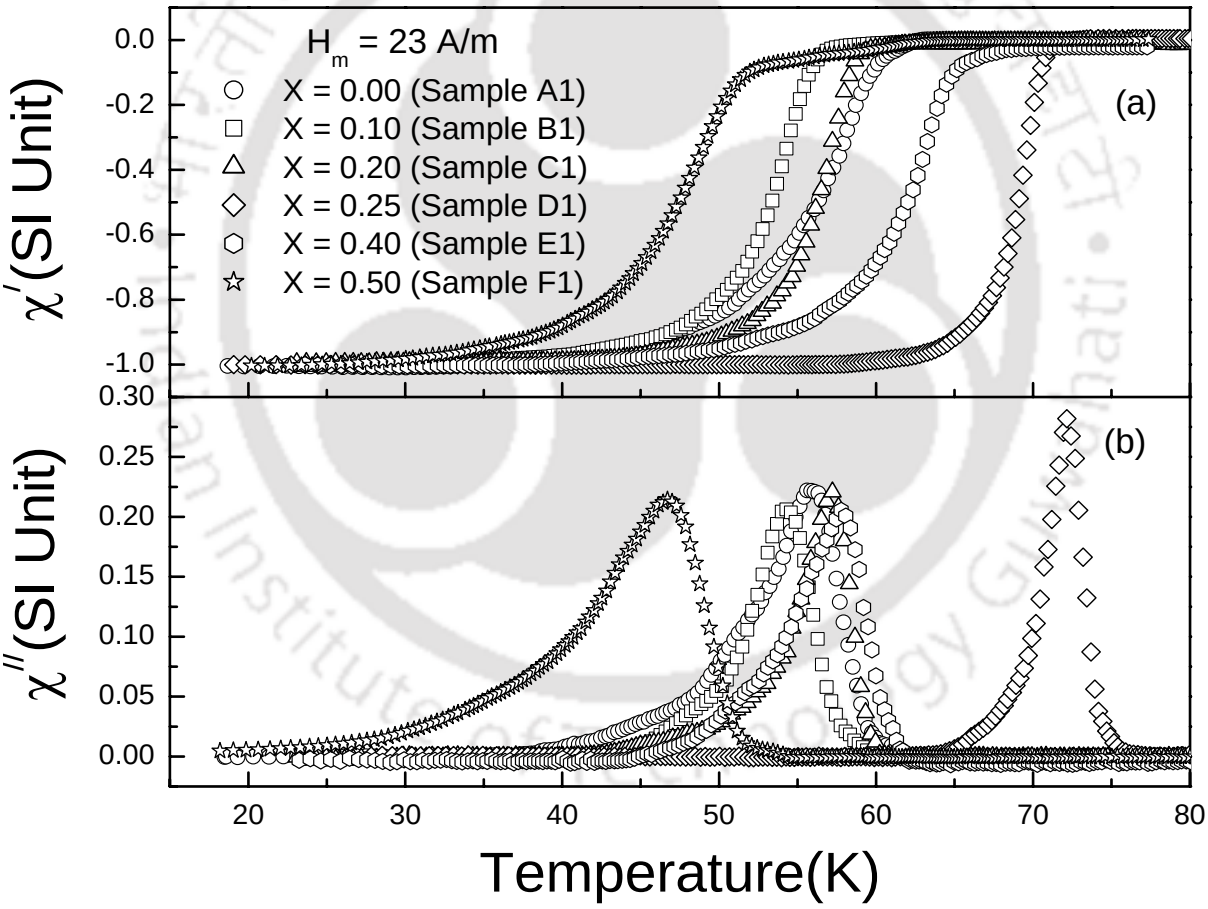

Fig. 2.27. Plots of (a) in phase ac susceptibility (χ') and (b) out of phase ac susceptibility (χ'') of Ag doped $(La_{1-x}Y_x)_2Ba_2CaCu_5O_z$ series as a function of temperature at an ac field amplitude of 23 A/m.

Table 2.5. Parameters obtained from electrical resistivity, low field ac susceptibility and microstructure measurements on pure and Ag doped $(La_{1-x}Y_x)_2Ba_2CaCu_5O_z$ series.

Sl. No	Compositions → Parameters ↓	Pure series						Ag doped series					
		x=0.0 Sample A	x= 0.10 Sample B	x=0.20 Sample C	x=0.25 Sample D	x=0.40 Sample E	x=0.50 Sample F	x=0.0 Sample A1	x=0.10 Sample B1	x=0.20 Sample C1	x=0.25 Sample D1	x=0.40 Sample E1	x=0.50 Sample F1
1	T_c(0) K	59.8	57.4	55	60	53.2	50.4	60.8	58.0	58.9	70.5	57.8	51.4
2	T_c(midpoint)K	63.2	62.8	62.3	73.9	65.3	60.4	68.3	67.8	66.4	75.4	67.6	64.5
3	ΔT_c K (FWHM)	4.15	4.66	8.40	4.23	4.34	5.03	6.21	7.5	6.09	2.03	5.54	5.82
4	ρ_0 (300 K) mΩ.cm	2.985	3.237	4.545	3.863	3.285	4.688	2.681	2.153	3.476	1.567	3.633	4.300
5	T_c(dia) K	62.7	62.3	63.3	69.5	65.7	62.9	61	59.4	62.1	74.8	66	63
6	$T_c(\chi''$peak) K	52.7	48.3	44.2	61.0	48.1	45.4	55.9	54.2	57.0	72.1	57.7	46.8
7	Grain size (μm)	2.6	1.9	2.0	2.2	1.4	1.5	1.8	1.8	1.9	1.7	1.2	1.3

All the samples exhibit superconducting transitions with T_c ranging from 60.4 to 75.4 K. The highest T_c was observed for x = 0.25 sample and is comparable to highest T_c reported in $LaBaCaCu_3O_z$ series reported in literature [127]. The Ag doping results in improved T_c and reduced room temperature resistivity. The temperature variation of ac susceptibility of pure and Ag doped samples show diamagnetic transitions due to intra and intergranular material.

To summarize, both the pure and Ag doped $(La_{1-x}Y_x)_2Ba_2CaCu_5O_z$ series could be prepared in single phase forms for x = 0 to 0.5. The lattice parameters are found to be comparable to that of similar series reported in literature. The intermixing of Ca ions at La and Ba site and, La at La and Ba sites are observed and the level of intermixing is comparable to that reported by Awana et al. [128] from their neutron diffraction studies on undoped $LaBaCaCu_3O_z$ system. The SEM micrographs show uniform morphology with grain size ranging from 1.2 to 2.6 μm and the compositions arrived at from EDAX analysis is close to the nominal starting compositions.

2.2.3. Pure and Ag doped $(La_{1-x}Y_x)_2Ba_2Ca_yCu_{4+y}O_z$(y = 4x, x = 0.15, 0.20)

Unlike the earlier series, where we studied the doping at the rare earth site of optimum hole doped superconducting materials, here we have started with the insulating $La_2Ba_2Cu_4O_z$ compound and simultaneously doped $CaCuO_2$ and rare earth site doping to study the evolution of superconductivity. These are basically under doped materials. This series has been also prepared to have wide range of transition temperatures, so that their physical properties can be studied in detail.

(a) Crystal Structure

Fig.2.28 shows the X-ray diffraction patterns recorded for pure and Ag doped $(La_{1-x}Y_x)_2Ba_2Ca_yCu_{4+y}O_z$ compounds for x = 0.15 and 0.20. All the samples are essentially in single phase form and the XRD patterns could be refined using P4/mmm space group. The typical XRD patterns along with rietveld refinement are shown in Fig.2.29 for pure and Ag doped x = 0.20 sample. The refined parameters such as atomic positions, occupancies and isotropic temperature factors, reliability parameters for pure and Ag doped x = 0.20 sample are given in Table 2.6. The lattice parameters, unit cell volume, bond length, bond angles and total occupancy of each element of this series are given in Table 2.7.

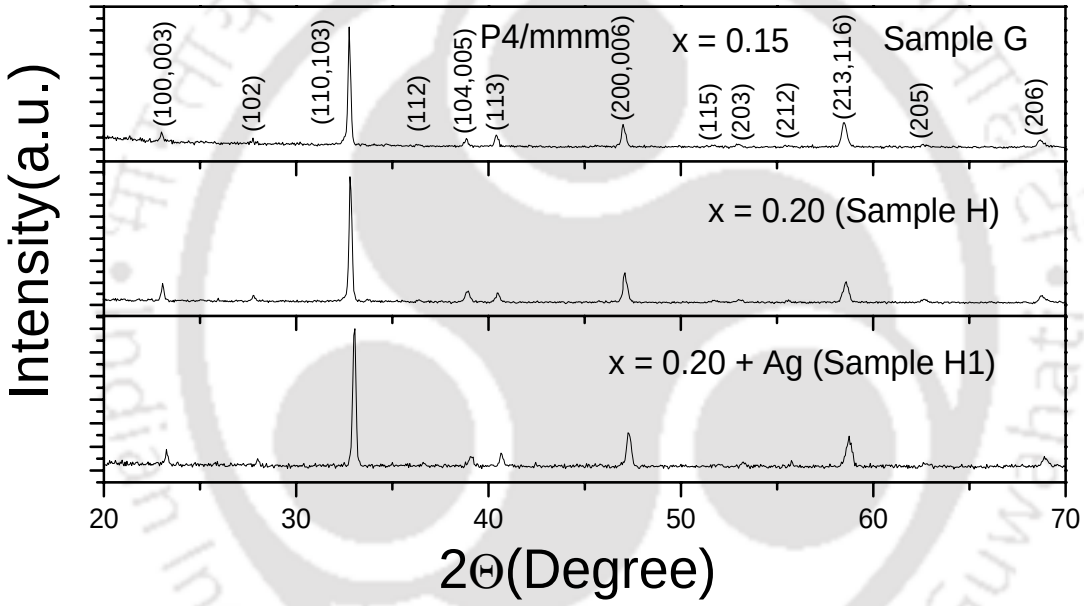

Fig. 2.28. XRD patterns of pure and Ag doped $(La_{1-x}Y_x)_2Ba_2Ca_yCu_{4+y}O_z$ compounds for x = 0.15 and 0.20.

The lattice parameters are marginally smaller compared to the parameters of regular superconducting series discussed in sections 2.2.1 and 2.2.2. This is mostly due to the underdoping of Ca. Moreover, we can see that the occupancy of Ca is comparable to the nominal starting composition. In regular series, Ca occupancy was close to 1 but here it varies from 58% to 80% as per the level of doping. The ratio of occupancy of La & Y are as per our expectation. We can also notice the vacancy in the Cu occupancy.

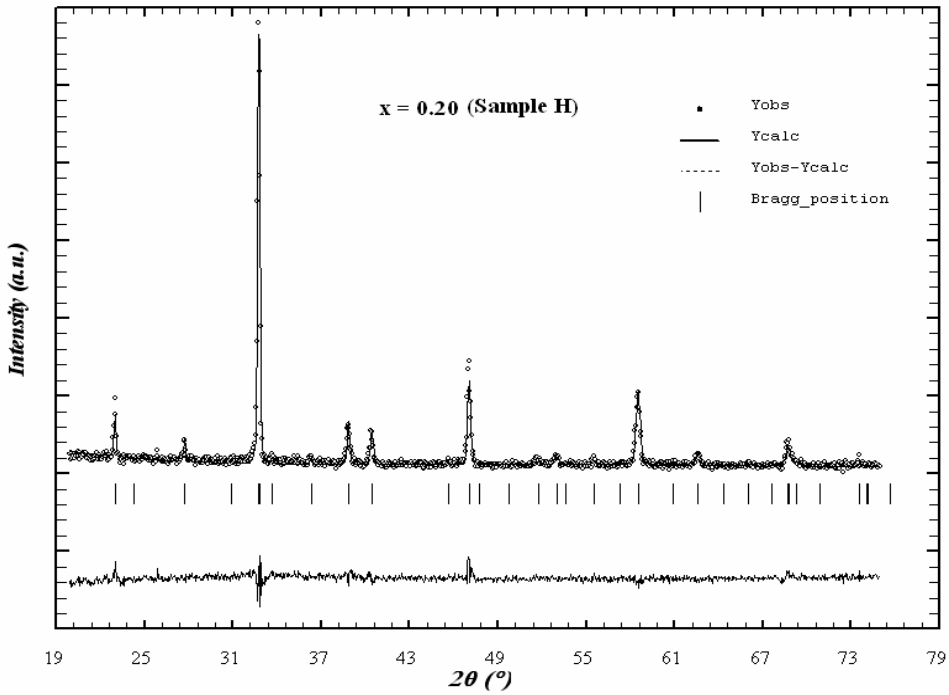

(a)

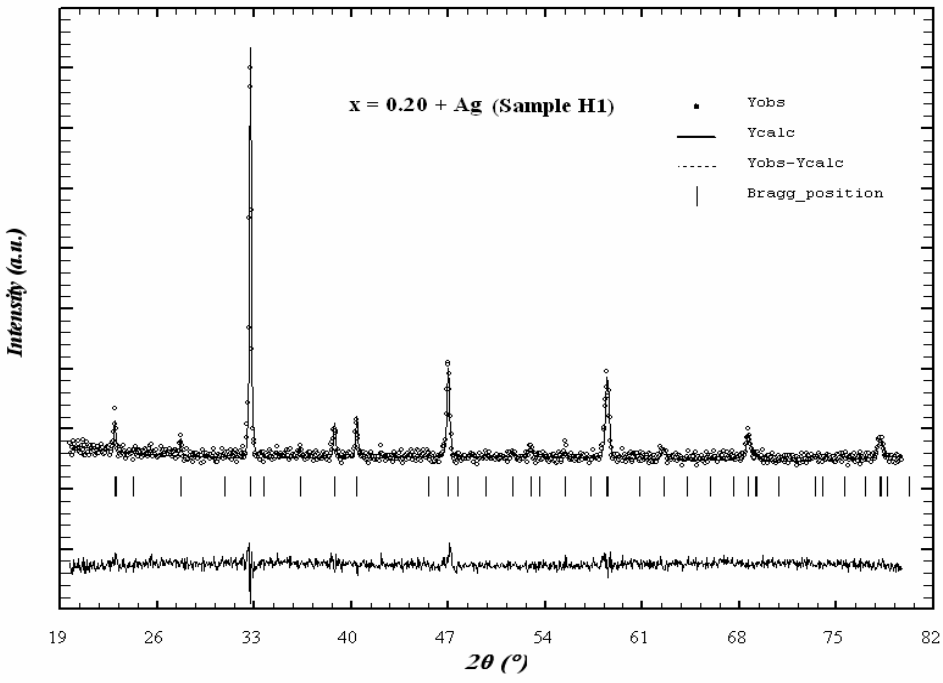

(b)

Fig. 2.29. XRD patterns for the samples (a) pure and (b) Ag doped $(La_{1-x}Y_x)_2Ba_2Ca_yCu_{4+y}O_z$ compounds for x = 0.20. The solid circles represent experimental data and the solid line represents Rietveld refined data. The dotted lines show the difference between experimental and refined data. The possible Bragg positions are marked as vertical lines.

Table 2.6.Parameters such as atomic positions, isotropic temperature factors and occupancies obtained from Rietveld analysis of pure and Ag doped $(La_{1-x}Y_x)_2Ba_2Ca_yCu_{4+y}O_z$ series for x = 0.20. R_p, R_B, R_F and χ^2 are the reliability factors.

x = 0.20 (Sample H)				x = 0.20+Ag (Sample H1)			
Atoms	Site(x, y, z)	Biso (Å^2)	Occupancy	Atoms	Site(x, y, z)	Biso (Å^2)	Occupancy
La Y Ca	(0.5, 0.5, 0.5)	1.16	0.386 0.097 0.405	La Y Ca	(0.5, 0.5, 0.5)	2.64	0.389 0.097 0.405
Ba La Y Ca	(0.5, 0.5, 0.1844)	2.31	0.984 0.405 0.106 0.408	Ba La Y Ca	(0.5 ,0.5, 0.1867)	1.24	0.984 0.403 0.106 0.404
Cu(1)	(0, 0, 0)	0.55	0.811	Cu(1)	(0, 0, 0)	3.26	0.733
Cu(2)	(0, 0, 0.3645)	2.71	1.833	Cu(2)	(0, 0, 0.3514)	3.00	1.883
O(1)	(0.5, 0, 0)	4.60	0.826	O(1)	(0.5, 0, 0)	0.04	1.145
O(2)	(0, 0, 0.1674)	0.05	2.000	O(2)	(0, 0, 0.1496)	0.63	1.500
O(3)	(0.5, 0, 0.3945)	0.01	4.000	O(3)	(0.5, 0, 0.3706)	2.85	4.000
R_p=14.2, R_B=10.5, R_F=12.1, χ^2=1.38				R_p=17.6, R_B=10.7, R_F=11.6, χ^2=1.42			

Table 2.7. Parameters obtained from XRD pattern refinement of pure and Ag doped $(La_{1-x}Y_x)_2Ba_2Ca_yCu_{4+y}O_z$ series. a and c are the lattice parameters. La(G), Y(G), Ba(G), Ca(G), Cu(G) and O(G) are the refined occupancies. ⟨Cu-O⟩ are the bond lengths and ∠Cu-O-Cu is the bond angle.

Sl. No	Parameters	Compositions		
		x=0.15 (Sample G)	x=0.20 (Sample H)	x=0.20+Ag (Sample H1)
1	a = b (Å) c (Å)	3.863 11.575	3.860 11.576	3.865 11.586
2	Volume (Å^3)	172.8	172.5	173.1
3	⟨La-O3⟩ (Å)	2.466	2.284	2.446
4	⟨Cu1-O1⟩ (Å)	1.932	1.930	1.933
5	⟨Cu1-O2⟩ (Å)	1.712	1.938	1.734
6	⟨Cu2-O3⟩ (Å)	1.943	1.961	1.945
7	∠Cu2-O3-Cu2 (deg.)	167.6	159.6	166.8
8	La (G) Y (G)	0.843 0.139	0.792 0.204	0.793 0.203
9	Ba (G)	0.871	0.984	0.985
10	Ca (G)	0.576	0.814	0.809
11	Cu(1) (G) Cu(2) (G)	0.635 1.841	0.811 1.833	0.734 1.884
12	O(1) (G) O(2) (G) O(3) (G)	0.605 1.518 4.000	0.827 2.000 4.000	1.145 1.500 4.000

(b) Microstructure

The typical SEM photographs for pure and Ag doped x = 0.20 samples are given in Fig. 2.30 and 2.31 respectively. The average particle size was found to be 2.7 and 1.9 μm for Sample H and Sample H1 respectively. The EDAX patterns were recorded for these samples to carry out the compositional analysis. The composition of x = 0.20 sample as per EDAX analysis is found to be $(La_{1.68}Y_{0.33})Ba_{2.22}Ca_{0.69}Cu_{4.8}O_{10.6\pm\delta}$ and its corresponding composition in La-1113 form is $(La_{0.84}Y_{0.16})Ba_{1.11}Ca_{0.69}Cu_{2.8}O_{6\pm\delta}$. Similarly, the compositions of Ag doped 0.20 sample as per EDAX analysis is found to be $(La_{1.71}Y_{0.18})Ba_{2.11}Ca_{0.71}Cu_{4.8}O_{10.6\pm\delta}$ or $(La_{0.86}Y_{0.09})Ba_{1.06}Ca_{0.72}Cu_{2.8}O_{6\pm\delta}$ respectively. The above compositions are comparable to the nominal starting compositions. The amount of Ag present in the Ag doped sample is found to be 1.83 wt %.

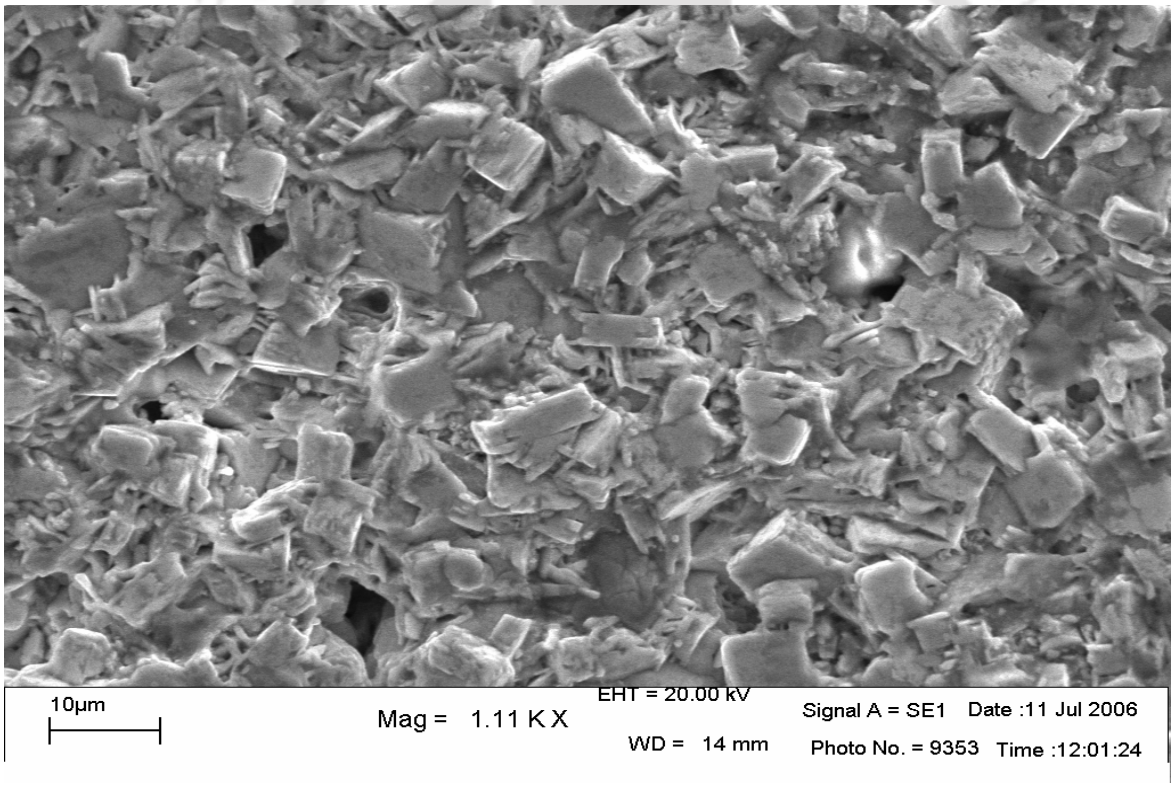

Fig. 2.30: SEM photograph for x = 0.20 (Sample H) in $(La_{1-x}Y_x)_2Ba_2Ca_yCu_{4+y}O_z$ series. The magnification is 1110. The average particle size is 2.7μm.

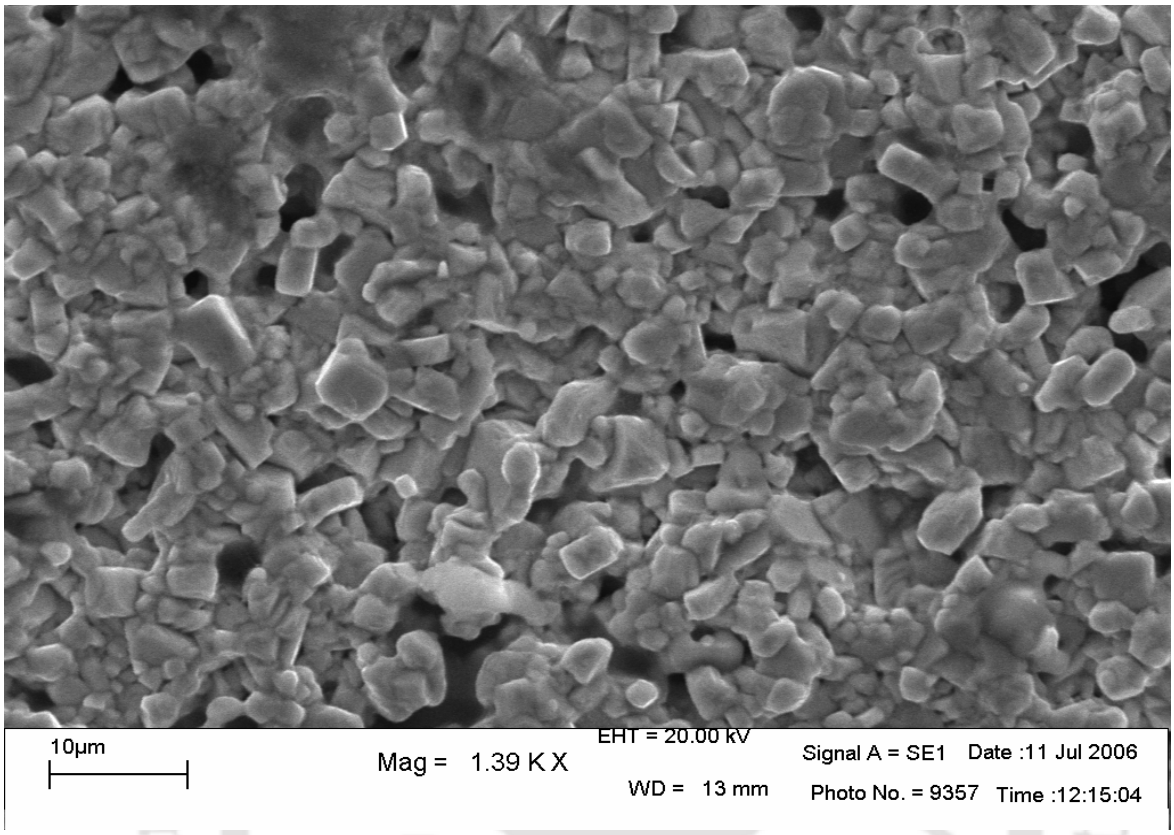

Fig. 2.31: SEM photograph for x = 0.20 (Sample H1) in Ag doped $(La_{1-x}Y_x)_2Ba_2Ca_yCu_{4+y}O_z$ series. The magnification is 1390. The average particle size is 1.9µm.

(c) DC Electrical Resistivity

The temperature variation of electrical resistivity was measured on the samples of the above series and are shown in Fig.2.32. They exhibit superconducting transition with transition temperatures ranging from 49.3 to 73.1 K. We can see that as the doping increases, the T_c increases. Such an increase in T_c with doping has been reported by Kuberkar et al. [124, 343] and can be understood as a result of hole doping by Ca. The transition temperatures and ρ(300 K) are given in Table 2.10. The T_c values of pure and Ag doped x = 0.20 samples are comparable to the T_c reported by Kuberkar et al. [343] in nearby composition. As they have reported only the resistances, the ρ(300 K) could not be compared. The x = 0.20 samples exhibit relatively sharp transition. Unlike in the literature, [124, 343]; where the onset of transition remains same for different doping leading to broad transition, for low T_c samples; here the onset also changes appreciably leading to uniform T_c with relatively sharp transition.

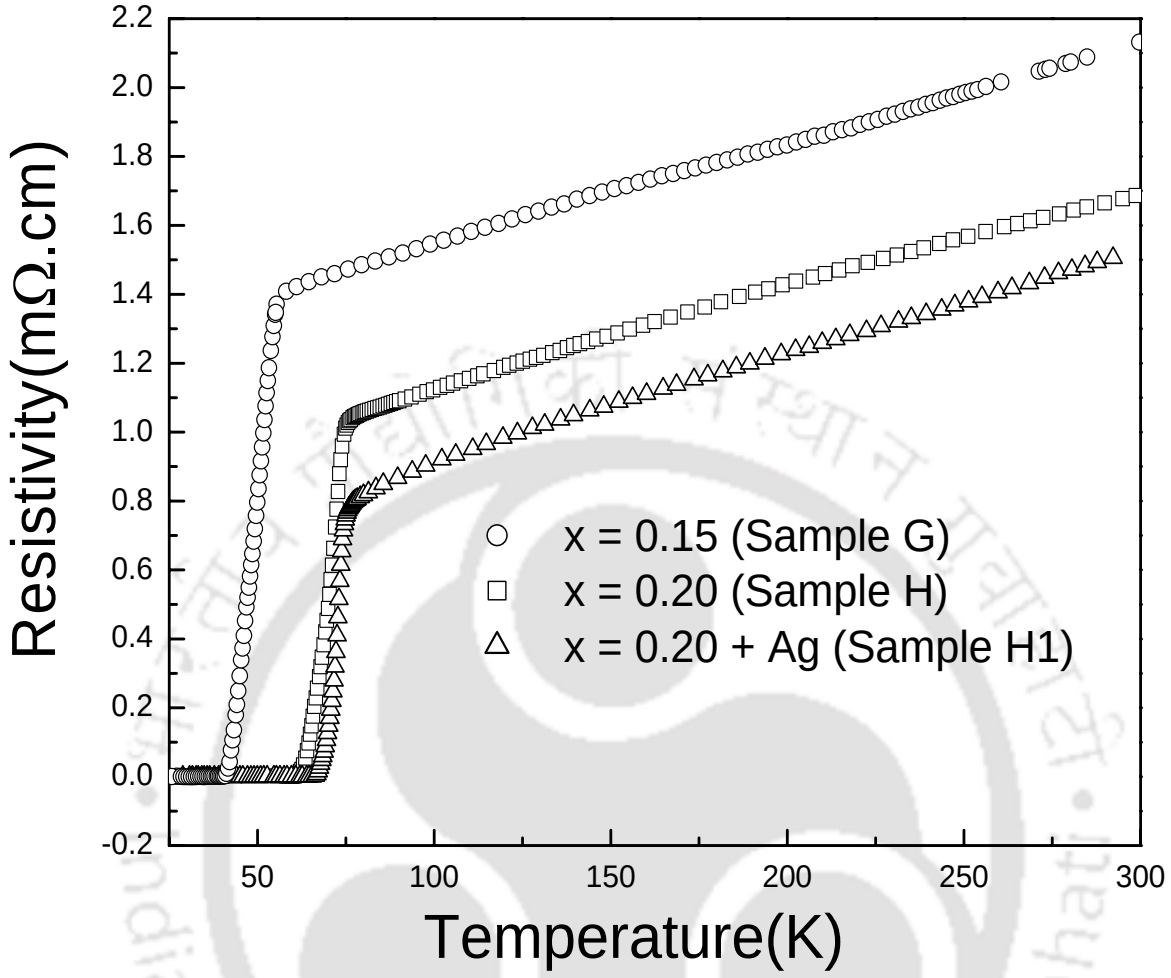

Fig. 2.32. Plots of temperature versus resistivity of pure and Ag doped $(La_{1-x}Y_x)_2Ba_2Ca_yCu_{4+y}O_z$ compounds for sample G(circles), sample H(squares) and sample H1(triangles).

(d) AC Susceptibility

Temperature variations of ac susceptibility at an ac field amplitude of 47 A/m have been measured for this series of compounds, which are shown in Fig.2.33. All the samples exhibit superconducting transition. The diamagnetic transition temperature varies from 44.6 to 70.0 K. . $\chi^{/}$ vs. T plots of x = 0.20 samples approache -1 at low temperatures. The $\chi^{//}$ peak temperatures are found to be 62.5 & 67.7 K respectively for pure and Ag doped x = 0.20 sample.

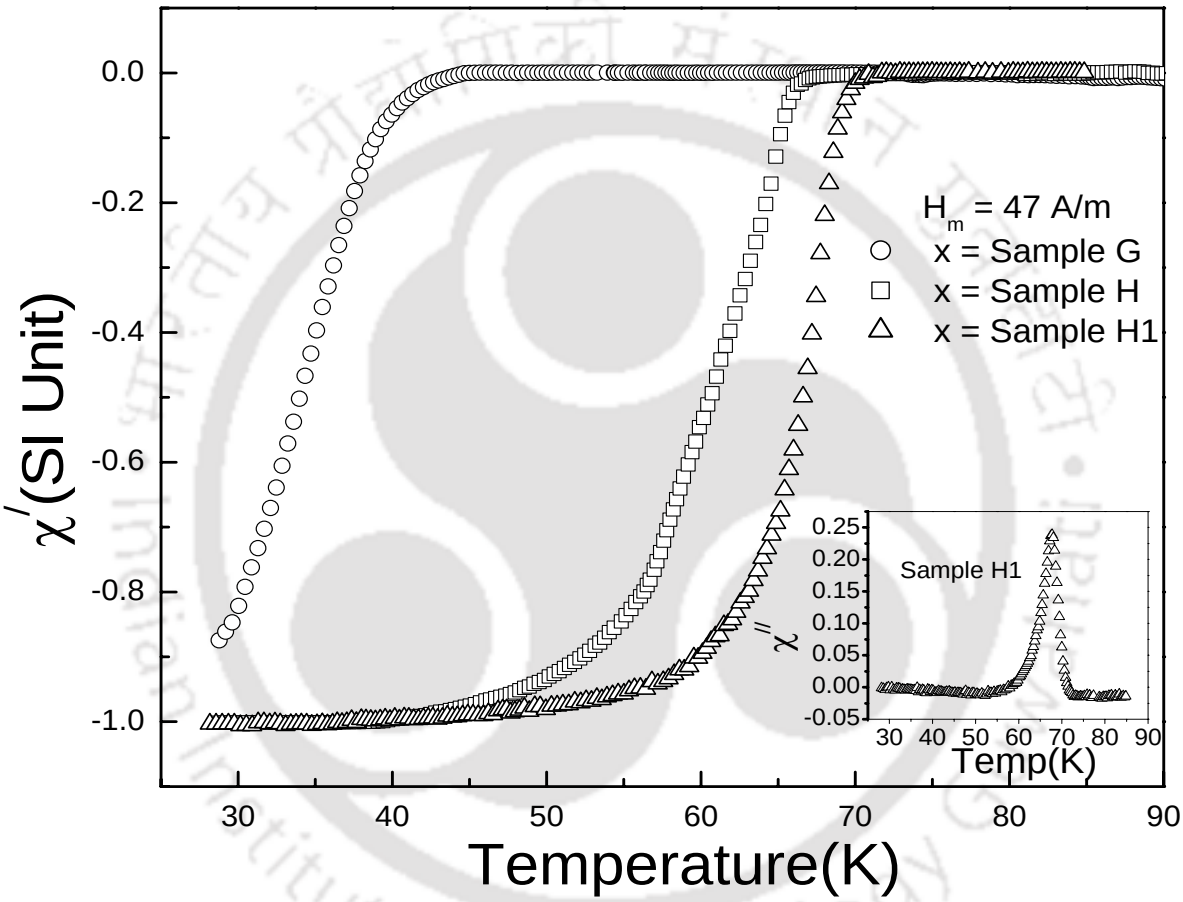

Fig. 2.33. Plots of temperature versus in phase ac susceptibility ($\chi^{/}$) of pure and Ag doped $(La_{1-x}Y_x)_2Ba_2Ca_yCu_{4+y}O_z$ compounds for sample G (circles), sample H (squares) and sample H1 (triangles) at an ac field amplitude of 47 A/m. The inset shows $\chi^{//}$ vs. T plot of sample H1.

2.2.4. Pure and Ag doped $(La_{1-x}Gd_x)_2Ba_2Ca_yCu_{4+y}O_z$ (y= 4x, x = 0.10, 0.20, 0.25)

This series is comparable to that discussed in section 2.2.3 except that the La is partially replaced by Gd rather than Y. This series of compounds have been prepared to see the effect of Gd doping on the superconductivity of the above series.

(a) Crystal Structure

Figs.2.34 shows the X-ray diffraction patterns recorded for pure and Ag doped $(La_{1-x}Gd_x)_2Ba_2Ca_yCu_{4+y}O_z$ compounds for x = 0.10, 0.20 and 0.25. All the samples are essentially in single phase form and the XRD patterns could be refined by using P4/mmm space group. The typical XRD patterns along with rietveld refinement are shown in Fig.2.35 for x = 0.20 and 0.25 samples. The refined parameters such as atomic positions, occupancies and isotropic temperature factors, reliability parameters for pure and Ag doped x = 0.20 and 0.25 samples are given in Table 2.8. The lattice parameters, unit cell volume, bond length, bond angles and total occupancy of each element of this series of compounds are given in Table 2.9.

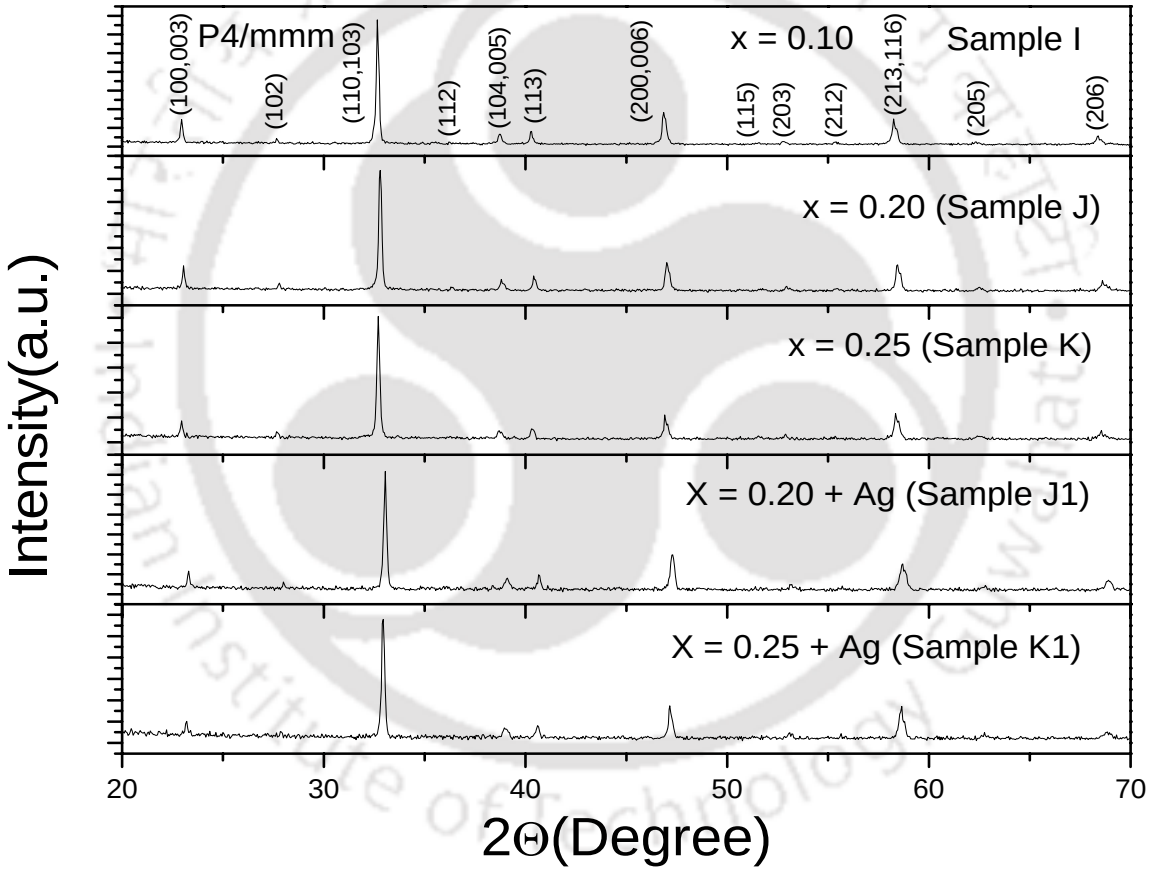

Fig. 2.34. XRD patterns of $(La_{1-x}Gd_x)_2Ba_2Ca_yCu_{4+y}O_z$ compounds for pure x = 0.10 (sample I), x = 0.20 (Sample J), x = 0.25 (Sample K) and Ag doped x = 0.20 (Sample J1), x = 0.25 (Sample K1).

Here the parameters obtained from analysis of XRD patterns are comparable to those of Y doped series discussed in section 2.2.3 except that, the a, b, c parameters are considerably larger and it can be understood on the basis of larger ionic size of Gd compared to that of Y.

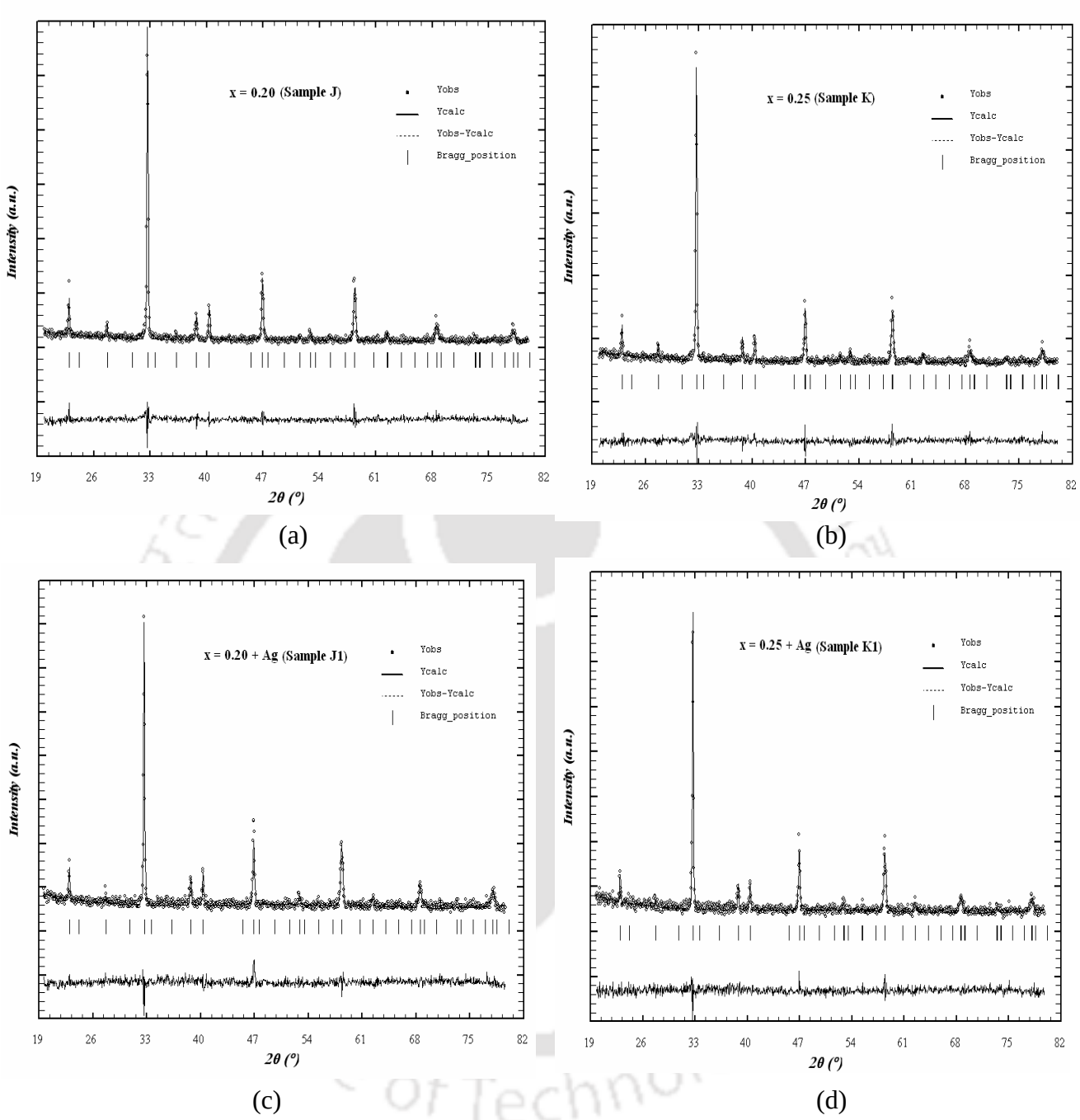

Fig. 2.35. XRD patterns for pure (a) x = 0.20 (Sample J) and (b) x = 0.25 (Sample K) and Ag doped (c) x = 0.20 (Sample J1) (d) x = 0.25 (SampleK1) of $(La_{1-x}Gd_x)_2Ba_2Ca_yCu_{4+y}O_z$ series. The solid circles represent experimental data and the solid line represents Rietveld refined data. The dotted lines show the difference between experimental and refined data. The possible Bragg positions are marked in each figure.

Table 2.8.Parameters such as atomic positions, isotropic temperature factors and occupancies obtained from Rietveld analysis of pure and Ag doped $(La_{1-x}Gd_x)_2Ba_2Ca_yCu_{4+y}O_z$ series for x = 0.20 and x = 0.25 samples. R_p, R_B, R_F and χ^2 are the reliability factors.

x = 0.20 (Sample J)				x = 0.25 (Sample K)			
Atoms	Site(x, y, z)	Biso (Å^2)	Occupancy	Atoms	Site(x, y, z)	Biso (Å^2)	Occupancy
La Gd Ca	(0.5, 0.5, 0.5)	1.02	0.378 0.101 0.413	La Gd Ca	(0.5, 0.5, 0.5)	0.291	0.357 0.119 0.511
Ba La Gd Ca	(0.5, 0.5, 0.1855)	2.03	0.872 0.456 0.094 0.376	Ba La Gd Ca	(0.5 ,0.5, 0.1816)	1.51	0.953 0.424 0.122 0.499
Cu(1)	(0, 0, 0)	0.40	0.689	Cu(1)	(0, 0, 0)	0.85	1.000
Cu(2)	(0, 0, 0.3568)	1.80	1.802	Cu(2)	(0, 0, 0.3712)	2.96	1.992
O(1)	(0.5, 0, 0)	0.01	0.997	O(1)	(0.5, 0, 0)	0.01	0.900
O(2)	(0, 0, 0.1536)	0.01	1.573	O(2)	(0, 0, 0.1741)	0.25	2.167
O(3)	(0.5, 0, 0.3737)	0.08	4.000	O(3)	(0.5, 0, 0.4075)	2.68	4.000
R_p=14.4, R_B=10.6, R_F=13.0, χ^2=1.46				R_p=14.4, R_B=10.9, R_F=13.1, χ^2=1.39			
x = 0.20+Ag (Sample J1)				x = 0.25+Ag (Sample K1)			
Atoms	Site(x, y, z)	Biso (Å^2)	Occupancy	Atoms	Site(x, y, z)	Biso (Å^2)	Occupancy
La Gd Ca	(0.5, 0.5, 0.5)	0.35	0.426 0.098 0.402	La Gd Ca	(0.5, 0.5, 0.5)	0.64	0.427 0.108 0.464
Ba La Gd Ca	(0.5, 0.5, 0.1853)	2.25	0.921 0.394 0.096 0.388	Ba La Gd Ca	(0.5 ,0.5, 0.1845)	1.47	0.952 0.424 0.122 0.499
Cu(1)	(0, 0, 0)	2.00	0.651	Cu(1)	(0, 0, 0)	2.57	1.000
Cu(2)	(0, 0, 0.3574)	1.34	1.792	Cu(2)	(0, 0, 0.3609)	1.85	1.922
O(1)	(0.5, 0, 0)	0.01	0.858	O(1)	(0.5, 0, 0)	0.01	1.000
O(2)	(0, 0, 0.1512)	0.01	1.945	O(2)	(0, 0, 0.1660)	0.02	2.000
O(3)	(0.5, 0, 0.3749)	0.08	4.000	O(3)	(0.5, 0, 0.3887)	0.06	4.000
R_p=15.5, R_B=12.4, R_F=13.4, χ^2=1.26				R_p=15.1, R_B=9.74, R_F=13.2, χ^2=1.18			

Table 2.9. Parameters obtained from XRD pattern refinement of pure and Ag doped $(La_{1-x}Gd_x)_2Ba_2Ca_yCu_{4+y}O_z$ series. a and c are the lattice parameters. La(G), Gd(G), Ba(G), Ca(G),Cu(G) and O(G) are the refined occupancies. ⟨Cu-O⟩ are the bond lengths and ∠Cu-O-Cu is the bond angle.

Sl. No	Parameters	Compositions				
		x = 0.10 Sample I	x = 0.20 Sample J	x = 0.25 Sample K	x = 0.20+Ag Sample J1	x = 0.25+Ag Sample K1
1	a = b (Å) c (Å)	3.878 11.626	3.869 11.613	3.867 11.616	3.871 11.615	3.868 11.594
2	Volume ($Å^3$)	174.9	173.9	173.7	174.1	173.5
3	⟨La-O3⟩ (Å)	2.425	2.427	2.212	2.420	2.324
4	⟨Cu1-O1⟩ (Å)	1.939	1.935	1.934	1.935	1.934
5	⟨Cu1-O2⟩ (Å)	1.862	1.784	2.022	1.756	1.925
6	⟨Cu2-O3⟩ (Å)	1.953	1.945	1.979	1.946	1.961
7	∠Cu2-O3-Cu2 (deg.)	166.5	168.4	155.4	168.0	161.1
8	La (G) Gd (G)	0.831 0.093	0.835 0.195	0.782 0.241	0.820 0.195	0.852 0.230
9	Ba (G)	0.815	0.872	0.953	0.921	0.952
10	Ca (G)	0.392	0.790	1.010	0.790	0.963
11	Cu(1) (G) Cu(2) (G)	0.574 1.660	0.689 1.802	1.000 1.992	0.651 1.792	1.000 1.992
12	O(1) (G) O(2) (G) O(3) (G)	0.756 1.367 4.000	0.997 1.573 4.000	0.900 2.167 4.000	0.858 1.945 4.000	1.000 2.000 4.000

(b) Microstructure

The typical SEM photographs for pure and Ag doped x = 0.25 samples are given in Figs. 2.36 and 2.37. The average particle size was found to be 2.2 and 1.9 μm for pure and Ag doped sample respectively. The EDAX pattern was taken for these samples to find out the compositional analysis. For x = 0.25 (Sample K), the compositions as per EDAX analysis are found to be $(La_{1.44}Gd_{0.41})Ba_{1.95}Ca_{1.36}Cu_5O_{11\pm\delta}$ or $(La_{0.71}Gd_{0.20})Ba_{0.97}Ca_{1.35}Cu_3O_{7\pm\delta}$ (La-1113 form). Similarly for Ag doped x = 0.25 (Sample K1), the compositions are found to be $(La_{1.63}Gd_{0.54})Ba_{2.19}Ca_{0.90}Cu_5O_{11\pm\delta}$ or $(La_{0.82}Gd_{0.27})Ba_{1.10}Ca_{0.91}Cu_3O_{7\pm\delta}$. The above compositions are comparable to the nominal starting compositions. The amount of Ag present in the Ag doped sample is found to be 1.22 wt %.

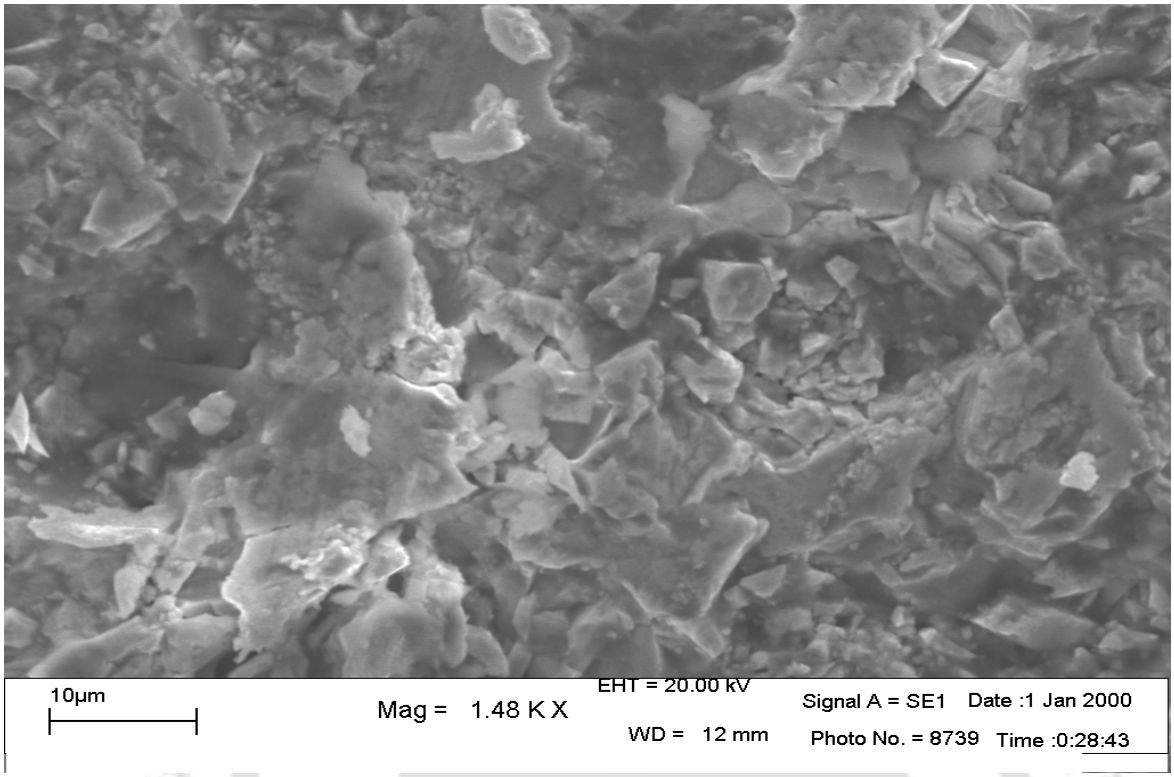

Fig. 2.36: SEM photograph for x = 0.25 (Sample K). The magnification is 1480. The average particle size is 2.2µm.

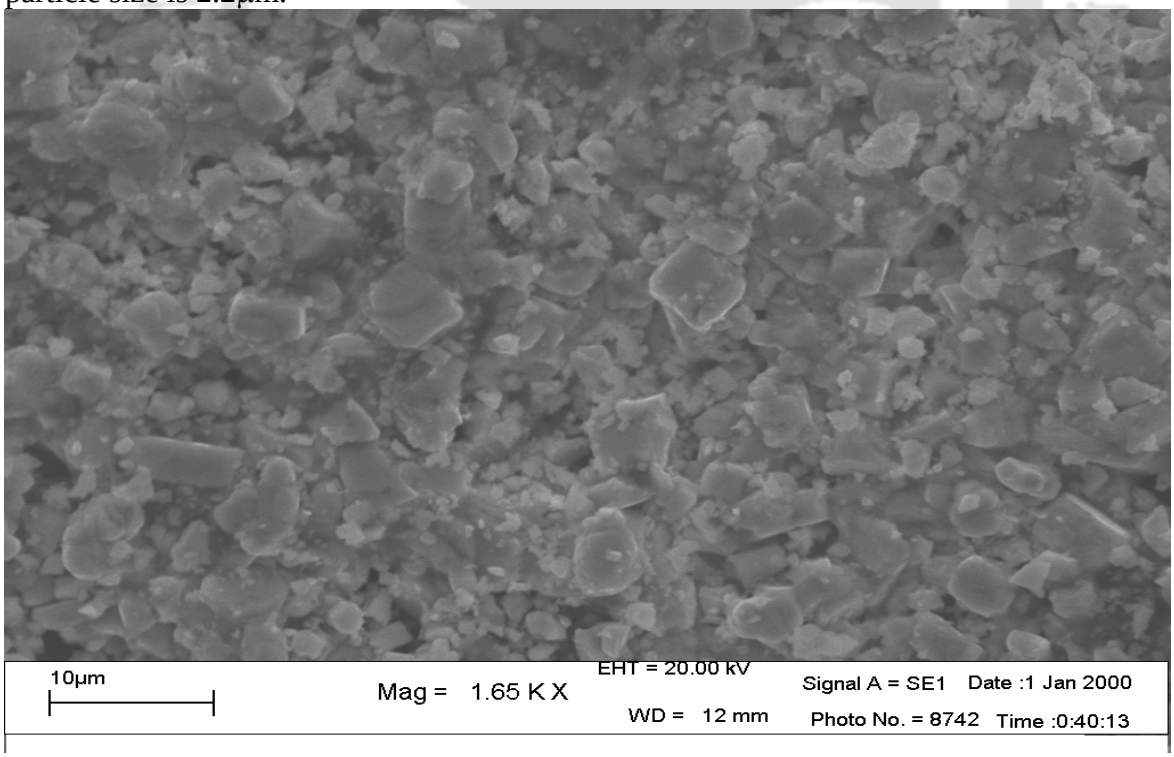

Fig. 2.37: SEM photograph for Ag doped x = 0.25 (Sample K1). The magnification is 1650. The average particle size is 1.9µm.

(c) DC Electrical Resistivity

The temperature variation of electrical resistivity was measured on the samples of the above series and are shown in Fig.2.38. They exhibit superconducting transition with transition temperatures ranging from 56.7 to 70.9 K. The T_c values of some of the compositions are closely comparable to those reported in literature for similar series [124, 343]. Unlike Y doped samples, the transition width is slightly larger and this must be due to magnetic property of Gd atom. Transition width as wide as 25 K has been reported in literature[124] especially on magnetic rare earth doped or magnetic rare earth based superconductors, in the above series namely Pr, Gd & Nd based materials [129, 344, 345].

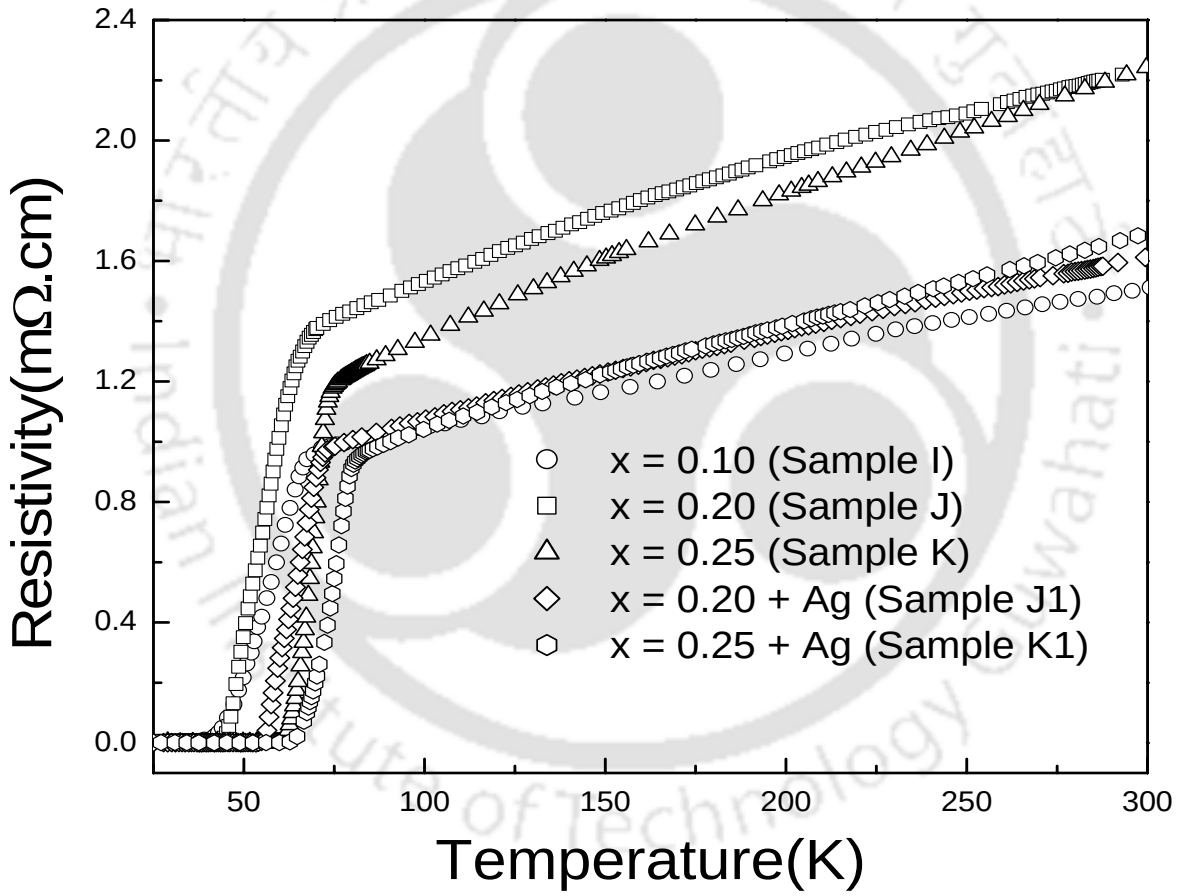

Fig.2.38. Plots of temperature versus resistivity of pure and Ag doped $(La_{1-x}Gd_x)_2Ba_2Ca_yCu_{4+y}O_z$ compounds for x = 0.10 (Sample I), 0.20 (Sample J), 0.25 (Sample K), 0.20 + Ag (Sample J1) and 0.25 + Ag (Sample K1).

(d) AC Susceptibility

Temperature variations of ac susceptibility have been measured for this series of compounds which are shown in Fig.2.39. All the samples exhibit superconducting transition. The diamagnetic transition temperature varies from 44.5 to 62.9 K. We can see the shift of T_c with doping, for a particular doping, Ag doped materials exhibit higher T_c. The diamagnetic T_c are mostly comparable with zero resistivity transition temperature $T_c(0)$ values. The typical $\chi^{//}$ peak temperature are found to be 54.9 & 59.6 K for pure and Ag doped x = 0.25, i.e. sample K and K1 respectively.

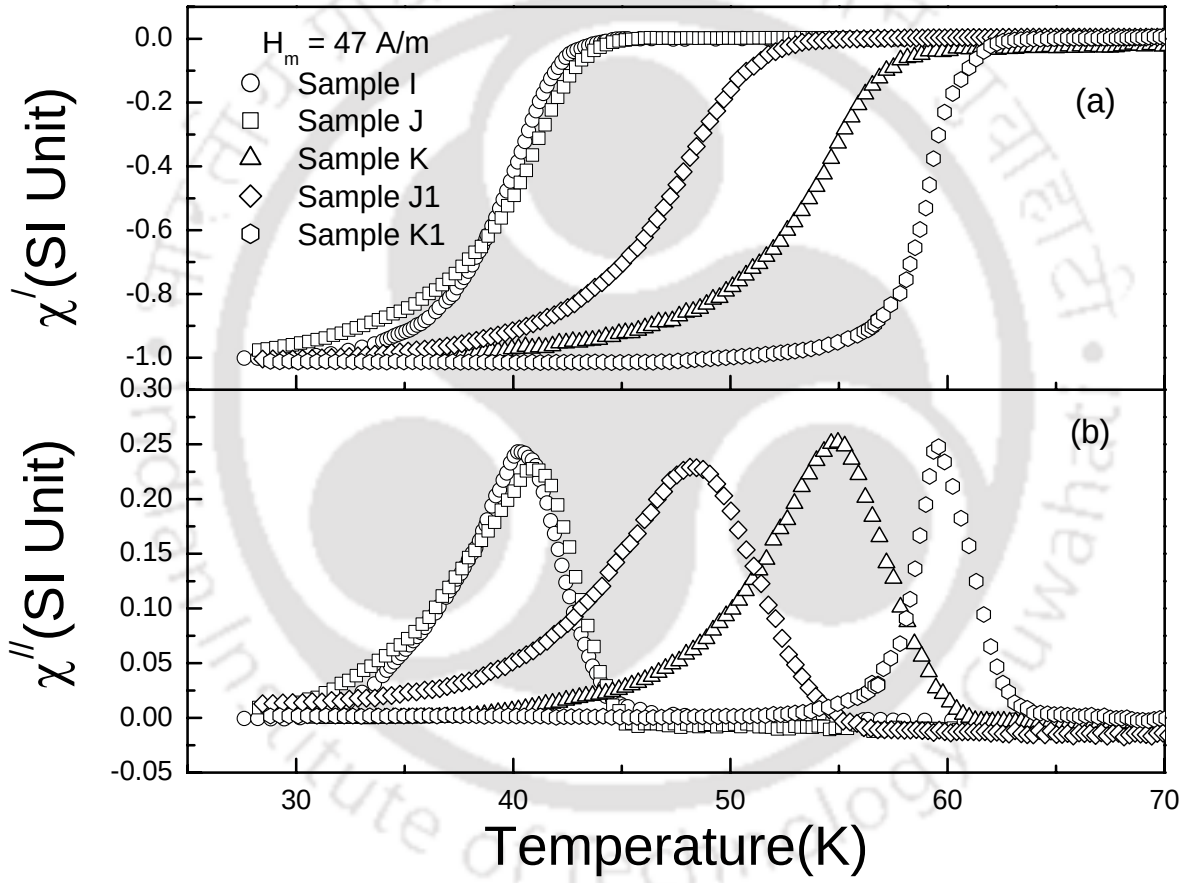

Fig. 2.39. Plots of (a) $\chi^{/}$ and (b) $\chi^{//}$ as a function of temperature for pure and Ag doped $(La_{1-x}Gd_x)_2Ba_2Ca_yCu_{4+y}O_z$ compounds for x = 0.10 (Sample I), 0.20 (Sample J), 0.25 (Sample K), 0.20 + Ag (Sample J1) and 0.25 + Ag (Sample K1) at an ac field amplitude of 47 A/m.

Parameters obtained from electrical resistivity, low field ac susceptibility and microstructure measurements on the above two series of samples are given in Table 2.10. From the Table 2.10, one can see that Ag doped samples show relatively large superconducting

transition temperature compared to pure samples. In case of 'Y' doped series, the sample x = 0.20 with 5 wt % of Ag show maximum transition temperature with ΔT_c of 4.8 K. Similarly, in case of 'Gd' doped series, the sample x = 0.25 with 5 wt % of Ag show maximum transition temperature with ΔT_c of 7.6 K. The estimated grain size of Ag doped samples are relatively small as compared to pure samples. The 'Gd' doped series show low transition temperature compared to 'Y' doped series. This may be due to the magnetic moment of 'Gd', which affects the superconductivity.

Table 2.10. Parameters obtained from electrical resistivity, low field ac susceptibility and microstructure measurements on $(La_{1-x}Y_x)_2Ba_2Ca_yCu_{4+y}O_z$ and $(La_{1-x}Gd_x)_2Ba_2Ca_yCu_{4+y}O_z$ series.

Sl. No	Compositions → Parameters ↓	$(La_{1-x}Y_x)_2Ba_2Ca_yCu_{4+y}O_z$			$(La_{1-x}Gd_x)_2Ba_2Ca_yCu_{4+y}O_z$				
		x=0.15 Sample G	x=0.20 Sample H	x=0.20 + Ag Sample H1	x=0.10 Sample I	x=0.20 Sample J	x=0.25 Sample K	x=0.20 + Ag Sample J1	x=0.25 + Ag Sample K1
1	T_c(0) K	41.2	60.3	66.2	42.9	44.4	60.3	53.5	62.2
2	T_c(midpoint)K	49.3	72.8	73.1	56.7	60.3	70.2	62.4	70.9
4	ΔT_c K (FWHM)	9.1	5.0	4.8	9.1	8.3	7.6	7.8	7.6
5	ρ_0 (300 K) mΩ.cm	3.296	1.686	1.508	1.520	2.237	2.242	1.614	1.712
6	T_c(dia) K	44.6	66.0	70.0	44.5	53.1	60.0	53.5	62.9
7	$T_c(\chi''$ peak) K	35.7	62.5	67.7	40.2	40.9	54.9	48.3	59.6
8	Grain size (μm)	--	2.7	1.9	--	2.0	2.2	1.6	1.9

A brief summary of experimental techniques, sample preparation and characterization are presented below.

I have developed a home made ac susceptometer to carryout temperature and field variation of ac susceptibility. In addition, I have fabricated high temperature furnace, sample insert assembly for resistivity and magneto-resistivity measurements. Three series of compounds with starting compositions $(La_{1-x}Y_x)_2Ba_2CaCu_5O_z$, $(La_{1-x}Y_x)_2Ca_yCu_{4+y}O_z$ (y = 4x) and $(La_{1-x}Gd_x)_2Ca_yCu_{4+y}O_z$ (y = 4x) have been prepared. It may be noted that second and third series are underdoped, where the level of Ca & Cu concentration is less than the optimum level. In addition to that the above series were prepared by doping 5 wt% Ag. All three series could be prepared in single phase form. All of them exhibit similar crystal structure and that could be refined using P4/mmm space group. In Y and Gd doped samples, the lattice parameters mostly decrease with doping due to their smaller ionic size compared to that of La. If we compare the lattice

parameters of Y and Gd underdoped series, the latter series exhibit larger lattice parameters due to relatively larger ionic size of Gd compared to Y. The lattice parameters reported in the present series of compounds are comparable to those reported in literature for similar series. The occupancy of various elements are found to be close to the nominal composition and doping concentration. We have observed the evidence for intermixing of Ca & La ions in the site of La and Ba respectively. Such behavior has been generally observed in this type of series from neutron diffraction studies. The typical Cu2-O3-Cu2 angle is found to be in the range of 162 to 164^0 for the first series and it is about 3 to 5^0 less that observed in tetragonal $YBa_2Cu_3O_7$. The temperature variation of electrical resistivity carried out in the above samples indicate that all of them exhibit superconducting transition with zero resistivity. In the first series, the T_c (transition mid point) was found to vary from 60.4 to 75.4 K and the corresponding range of T_c (zero) was 50.4 to 70.5 K. The transition width of most of the samples in the first series falls within the range of 4 to 6 K. The minimum transition width of 2 K was observed for x = 0.25 with Ag doping ($(La_{1.5}Y_{.5})Ba_2CaCu_5O_z$ + 5 wt% of Ag). The room temperature resistivity is found to be in the range 1.5 to 4.5 mΩ.cm and it is quite small compared to the large values of the order of 57 mΩ.cm reported in the literature. It may be also noted that in literature, most of the authors have reported resistance rather than resistivity. We have observed that Ag doping improves the transition temperature and marginally reduces room temperature resistivity due to improved intergrain coupling and possible reduction in porosity.

In the underdoped series, T_c is found to vary from 49.3 to 73.1 K. The Gd doped samples exhibit wide transition width and it could be due to its magnetic property. Similar behavior has been reported in the literature for magnetic rare earth doping such as Pr,Gd, Nd etc.The ρ(300 K) of under doped series are mostly compared to the first series.

The microstructure has been studied using SEM micrographs on representative samples of each series. The average grain size found to be approximately in the range of 1.0 to 2.5 μm, which is quite small compared to orthorhombic $YBa_2Cu_3O_7$ samples reported in the literature. The compositions of the samples were analyzed by using EDX facility attached with SEM and are mostly comparable to the nominal starting composition of the material.

Temperature variations of low field ac susceptibility measurements have been carried out on the above samples. All samples exhibit diamagnetic transitions and most of the samples show

perfect diamagnetic susceptibility of $\chi^{/}$ = -1 at low temperature. The Ag doped samples show relatively sharp intergranular transition. In the first series the diamagnetic onset temperature varies from 59.4 to 74.8 K and they are mostly comparable to the superconducting transition observed from electrical resistivity measurements. Other than intra & intergranular transitions, no additional transitions have been observed and it shows that the materials are free from other impurity superconducting phases.

EXCESS CONDUCTIVITY AND MAGNETO-CONDUCTIVITY STUDIES

The preparation and characterization of pure and Ag doped superconductors in $(La_{1-x}Y_x)Ba_2CaCu_5O_z$ and $(La_{1-x}R_x)_2Ba_2Ca_{4x}Cu_{4+4x}O_z$ (R = Y, Gd) series have been reported in chapter 2. On a few selected samples, temperature variations of electrical resistivity and magneto-resitivity measurements have been carried out carefully in a close temperature interval. They are analyzed in terms of thermodynamic fluctuations induced excess conductivity ($\Delta\sigma$) and magneto-conductivity ($\Delta\sigma_H$) and, are discussed in detail in the present chapter (Chapter 3).

3.1. Excess conductivity in the Mean Field Regime

The experimental and theoretical studies on excess conductivity ($\Delta\sigma$) in the mean field regime of high T_c superconductors have been extensively reviewed in section 1.4. For convenience some of the important theoretical expressions based on different models are reproduced below. The excess conductivity above T_c is the sum of the direct and indirect contributions of fluctuations induced conductivity. The direct contribution to $\Delta\sigma$ arises from the direct acceleration of fluctuating Cooper pairs, where as the indirect contribution to $\Delta\sigma$ arises from the interaction of fluctuating Cooper pairs with the normal electrons.

Aslamazov and Larkin (AL) [135], expression for the direct contribution to excess conductivity $\Delta\sigma$ is given by,

$$\Delta\sigma = c\varepsilon^{\lambda} \tag{3.1}$$

where c is a constant and its value is $e^2/(16\hbar d)$ and $e^2/(32\hbar\xi(0))$ for 2D and 3D fluctuations of the superconducting order parameter respectively and, the values of λ are -1.0 and -0.5 for 2D and 3D fluctuations respectively. $\varepsilon = (T-T_c/T_c)$ is the reduced temperature; d is the two dimensional characteristic length; $\xi(0)$ is the coherence length at zero Kelvin. Lawrence-Doniach (LD) [140] modified the AL expression for layered superconductors and is given as,

$$\Delta\sigma = \left(\frac{e^2}{16\hbar d}\right)\varepsilon^{-1}\left[1+2\alpha\right]^{-1/2} \tag{3.2}$$

where $\alpha = \alpha_0/\varepsilon = (2\xi_c(0)^2/d^2)/\varepsilon$. The advantage of LD expression is that it reduces to AL-2D and AL-3D at the limiting cases. The cross over from 2D to 3D fluctuations occur at the temperature,

$$T_0 = T_c \exp\left(2\xi_c(0)/d\right)^2 \tag{3.3}$$

The indirect contribution to excess conductivity, which arises mainly due to interaction of fluctuating cooper pairs with normal electrons, was calculated by Maki and Thompson [146,147]. The indirect contribution (MT term) for layered superconductors was derived by Hikami and Larkin [149] and independently by Maki and Thompson [150] and is given below for the zero applied field.

$$\Delta\sigma = \frac{e^2}{8\hbar d(\varepsilon - \alpha\varepsilon/\delta)} \ln\left[\frac{\delta\left(1+\alpha+\sqrt{1+2\alpha}\right)}{\alpha\left(1+\delta+\sqrt{1+2\delta}\right)}\right] \tag{3.4}$$

Where $\delta = \left(16\xi_c(0)^2 \kappa_B T \tau_\phi / (\pi d^2 \hbar)\right)$ is the pair breaking parameter; κ_B is the Boltzman constant and τ_ϕ is the phase breaking time.

For the calculation of experimental excess conductivity; the determination of accurate values of mean field transition temperature, T_c and the background conductivity (σ_n) are very crucial. In the present work, T_c is taken as the temperature at which $d\rho/dT$ versus temperature plot exhibits a peak. The background resistivity (ρ_n) was estimated by fitting the measured resistivity, $\rho(T)$ to the equation;

$$\rho_n = a + bT, \tag{3.5}$$

in the temperature range $2T_c$ to 300K. The excess conductivity was calculated by subtracting the extrapolated background conductivity from the measured conductivity,

$$\Delta\sigma(T) = \frac{1}{\rho(T)} - \frac{1}{\rho_n(T)}. \tag{3.6}$$

The experimental excess conductivity data calculated using above equations were analyzed in terms of AL, LD and MT theories.

3.1.1. Excess Conductivity Analysis of La-Ba-Ca-Cu-O Superconductors

The following samples are chosen for excess conductivity analysis. They are namely,

1. $La_{1.8}Y_{0.2}Ba_2CaCu_5O_z$ (Sample B)
2. $La_{1.2}Y_{0.8}Ba_2CaCu_5O_z$ (Sample E)
3. $LaYBa_2CaCu_5O_z$ (Sample F)
4. $La_{1.8}Y_{0.2}Ba_2CaCu_5O_z$ + 5 wt % of Ag (Sample B1)
5. $La_{1.2}Y_{0.8}Ba_2CaCu_5O_z$ + 5 wt % of Ag (Sample E1)

6. $LaYBa_2CaCu_5O_z$ + 5 wt % of Ag (Sample F1)
7. $La_{1.6}Y_{0.4}Ba_2Ca_{0.8}Cu_{4.8}O_z$ (Sample H)
8. $La_{1.6}Y_{0.4}Ba_2Ca_{0.8}Cu_{4.8}O_z$ + 5 wt % of Ag (Sample H1)
9. $La_{1.5}Gd_{0.5}Ba_2CaCu_5O_z$ (Sample K)

The details of synthesis and characterization of these samples are described in sections 2.1 and 2.2.

3.1.2. Excess Conductivity Calculations

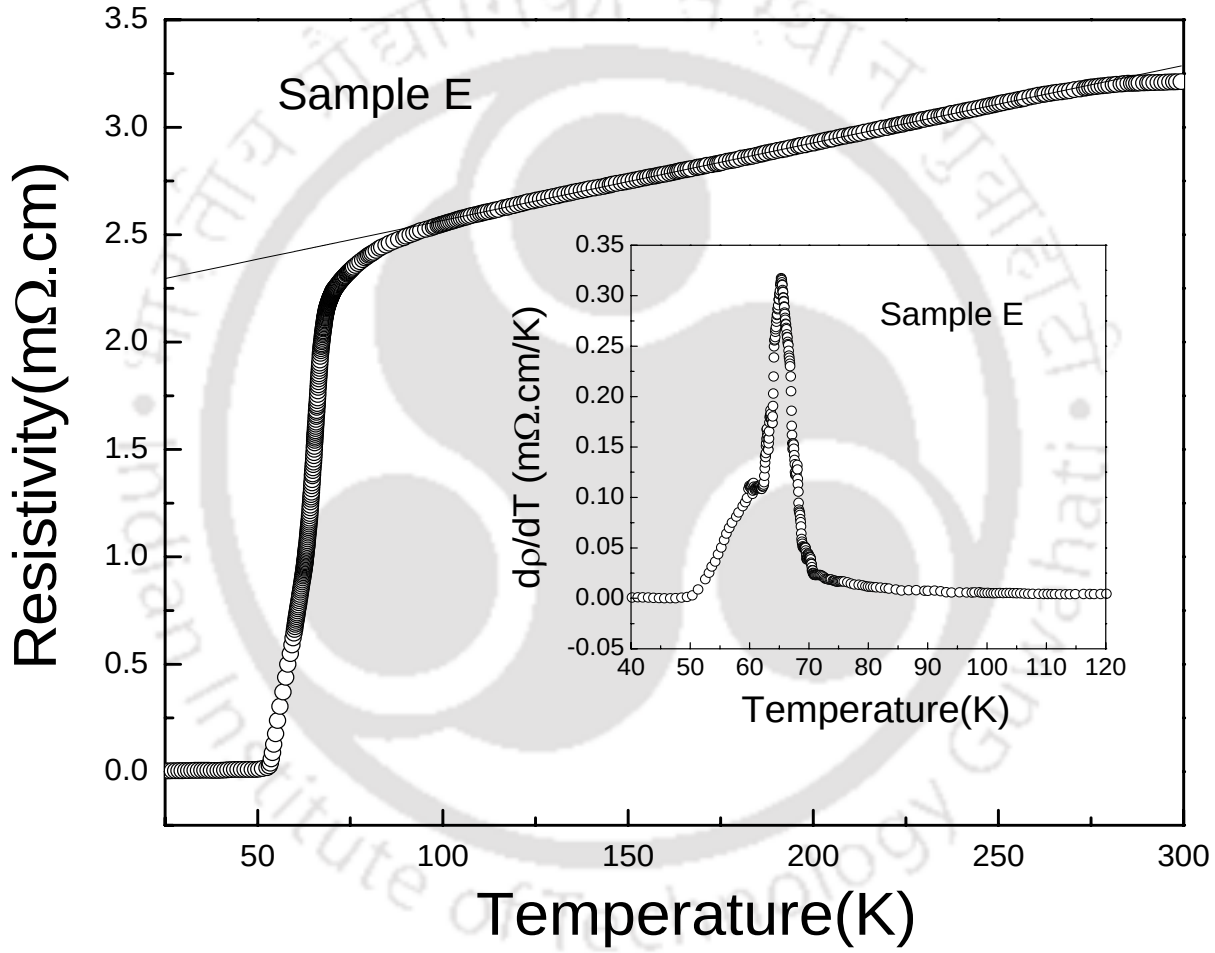

Fig. 3.1. Temperature variation of electrical resistivity of sample E. The solid lines represents the fitted data in the normal state and, extrapolated down to low temperature. dρ/dT vs. T plot is shown in the inset.

The temperature variation of precise dc electrical resistivity measured on sample E is shown in Fig.3.1.This sample exhibits superconducting transition with zero resistivity transition temperature, $T_c(0)$ at 53.2 K. The resistivity at 300 K (ρ(300K)) is found to be 3.285 mΩ.cm.

The inset shows dρ/dT versus temperature plot for this sample. The sample exhibits single prominent peak followed by a low temperature shoulder due to intergranular weak links. The temperature corresponding to peak in dρ/dT vs. T plot is taken as mean field transition temperature, T_c and its value is 65.3 K.

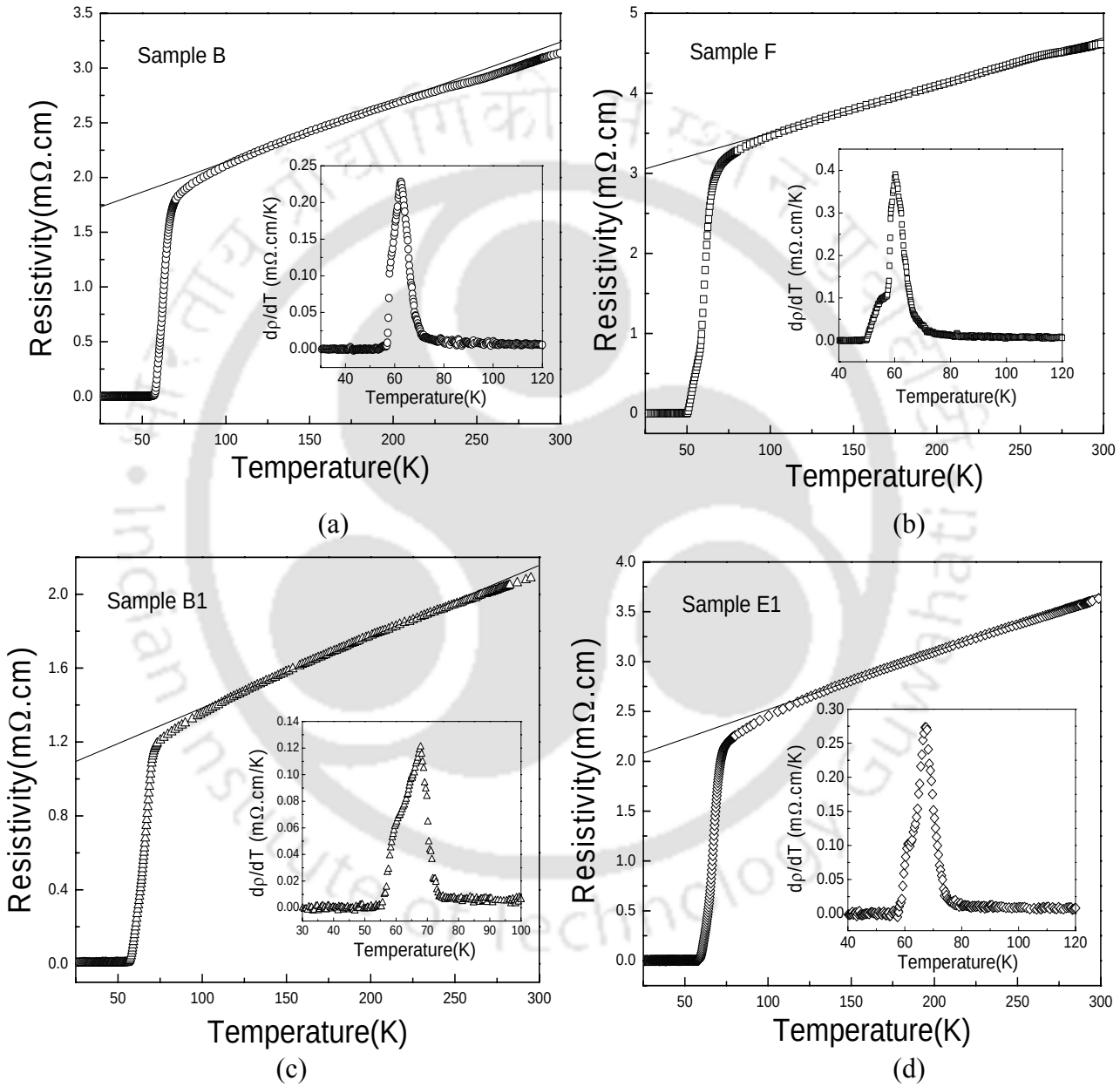

Fig. 3.2. Temperature variations of resistivity of samples B, F, B1and E1. The insets show dρ/dT vs. T plots. The solid lines represent fit to normal state resistivity and their extrapolation down to low temperature.

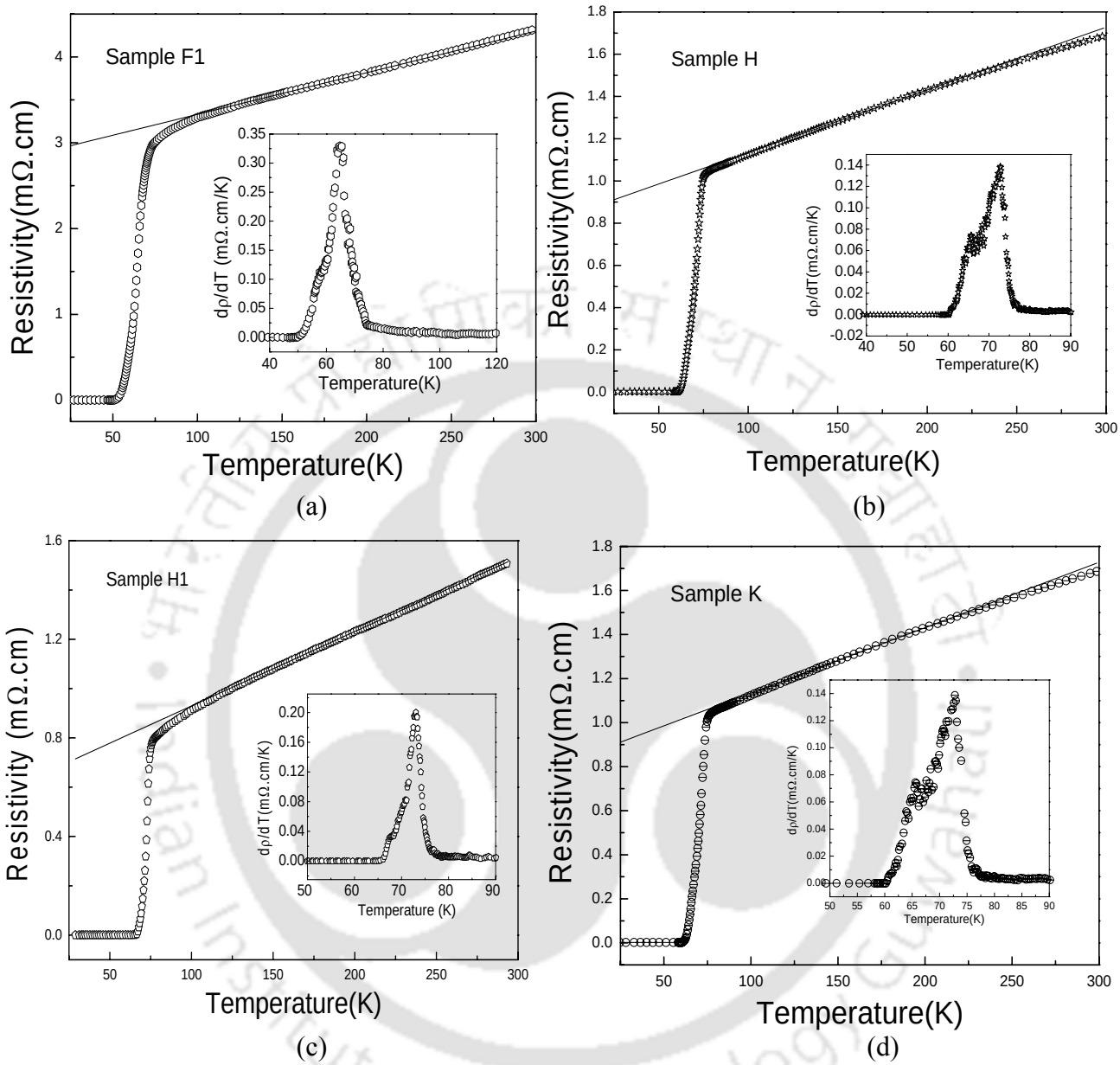

Fig. 3.3. Temperature variations of resistivity of samples F1, H, H1 and K. The insets show dρ/dT vs. T plots. The solid lines represent fit to normal state resistivity and their extrapolation down to low temperature.

The temperature variations of electrical resistivity along with dρ/dT vs. T plots as inset for all other samples are shown in Figs.3.2 & 3.3. Only one third of the experimental data are shown in the plots for clarity. The values of $T_c(0)$, T_c, resistivity at 300 K, ρ(300 K) for all the samples are tabulated in Table-3.1.We can see that all the samples exhibit linear normal state behavior followed by single superconducting transition as the temperature is lowered. In some of

the samples a minor change of slope is observed at around 250 K and such behavior is observed in La-Ba-Ca-Cu-O system [123]. The dρ/dT versus T plots exhibit single peak and for some of the samples a small low temperature shoulder is observed. This is the common feature observed in polycrystalline material due to granular nature.

The measured resistivity data ρ(T) was fitted to the equation 3.5 from $2T_c$ to 300 K with a and b as free parameters of the fit and for some of the samples the fit was restricted up to around 250 K. From the fitted values of a and b, the theoretical $\rho_n(T)$ was calculated using eqn. 3.5 in the entire temperature region, i.e. down to low temperature from 300 K and, they are shown as solid lines in Figs.3.1 to 3.3. We can see that they clearly follow the experimental data in the normal state. The typical fitted parameters a and b for sample E are 2.205 mΩ.cm and 3.61×10^{-3} mΩ.cm/K respectively. The quality of the fit is assessed based on the root mean squared deviation (rmsd) value and it is found to be 0.06% for sample E.

The root mean square deviation (rmsd) is calculated as follows.

$$rmsd = \sqrt{\frac{\sum_{j=1}^{N}(\rho_n(T_j) - \rho(T_j))^2}{N}} \qquad (3.7)$$

where $\rho_n(T_j)$ and $\rho(T_j)$ are theoretically calculated and the measured resistivity respectively. N is the total number of data points. The rmsd is expressed in terms of percentage by dividing the above rmsd value by an average value of $\rho(T_j)$ over the total number of data N, followed by a multiplication of 100. The fitted values of a and b along with rmsd for different samples are given in Table3.1.

The normal state resistivity $\rho_n(T)$ were extrapolated down to T_c and the excess conductivity was calculated from T_c to $2T_c$ using eqn. 3.6. The plots of $\ln(\Delta\sigma/\sigma_0)$ versus $\ln(\varepsilon)$ are shown in Fig.3.4 for sample E. Here σ_0 is the measured conductivity at 300 K and its value is 0.304 $(m\Omega.cm)^{-1}$. The plots of $\ln(\Delta\sigma/\sigma_0)$ versus $\ln(\varepsilon)$ for all other samples are shown in Figs.3.5. & 3.6 .We can see that they all exhibit linear behavior in the mean field regime.

3.1.3. Fit to AL Expression

The Δσ data of sample E were fitted to AL expression ($\Delta\sigma = c\varepsilon^{-\lambda}$) as given in eqn.3.1 in the range of $\ln\varepsilon$ = -4.10 to -1.76 by varying the parameters c and λ. Here the AL expression is taken in logarithmic form. The experimental data could be fitted well with an rmsd of 0.76% and are shown as solid line in Fig.3.4. The value of critical exponent (λ) obtained from the above fit is

found to be -0.84, which is close to two dimensional characteristic value of -1. Thus this material exhibits two dimensional fluctuations in the mean field regime (MFR).

Similarly, the excess conductivity data of all other samples could be fitted well to the AL expression in the mean field regime (MFR). The fitted data are shown as solid lines in Figs.3.5 & 3.6. The fitted parameters c, λ along with the rmsd values are given in Table 3.2. In all the cases, λ is found to be close to two dimensional characteristic value of -1 and thus these materials exhibit two dimensional fluctuations in the MFR.

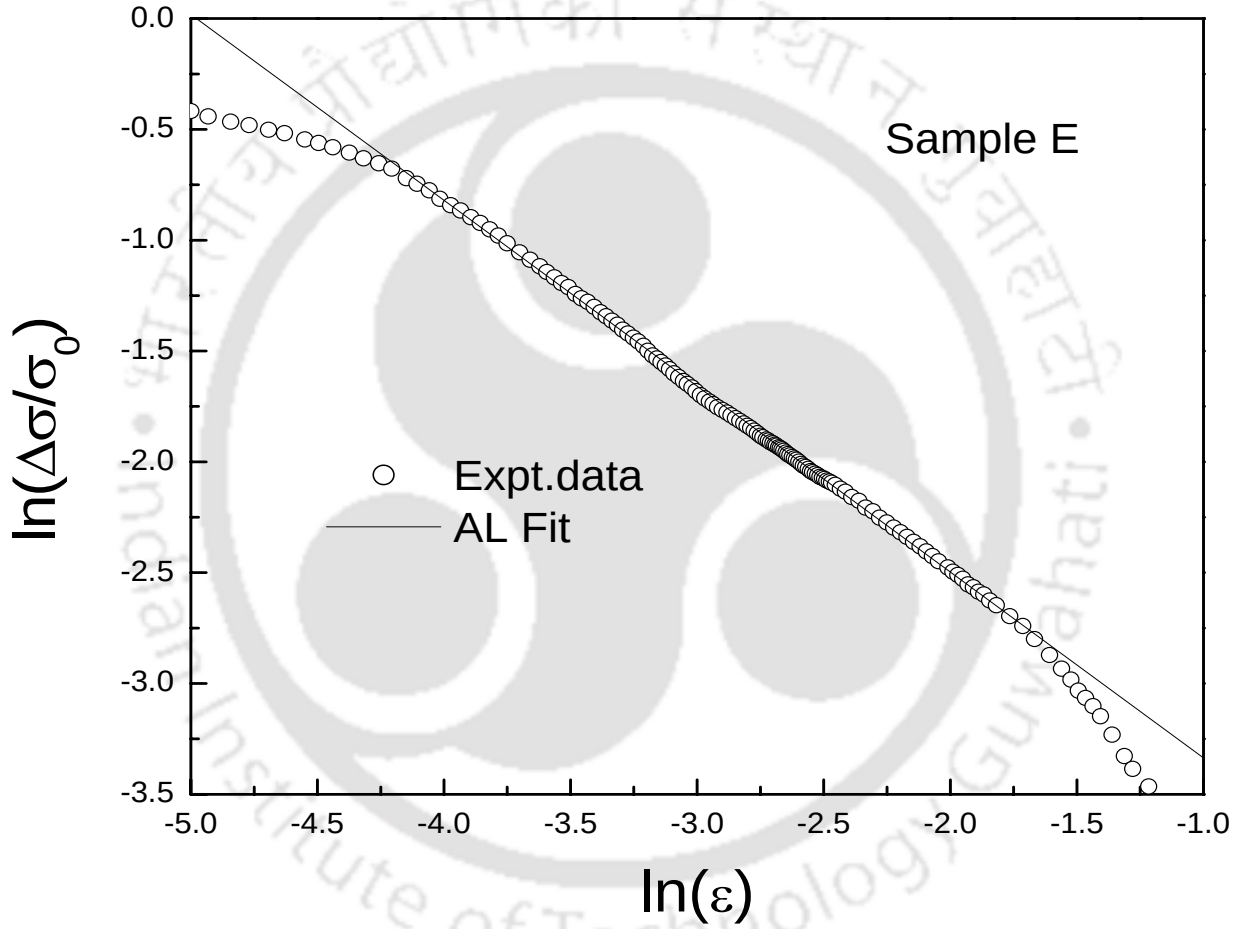

Fig. 3.4. Plots of ln ($\Delta\sigma/\sigma_0$) versus ln (ε) for Sample E. The fitted data using AL expression is shown as solid line.

Table 3.1.Parameters obtained from electrical resistivity measurements and linear fit in the normal state.

Sample Name	$T_c(0)$ (K)	T_c (K)	ρ(300 K) mΩ.cm	a mΩ.cm	b 10^{-3} mΩ.cm/K	rmsd %
Sample B	57.4	62.8	3.237	1.593	5.48	0.17
Sample E	53.2	65.3	3.285	2.205	3.61	0.06
Sample F	50.4	60.4	4.688	2.908	5.95	0.07
Sample B1	58.0	67.8	2.153	0.998	3.86	0.30
Sample E1	57.8	67.6	3.633	1.935	5.82	0.09
Sample F1	51.4	64.5	4.300	2.844	4.86	0.05
Sample H	60.3	72.8	1.686	0.836	2.97	0.11
Sample H1	66.2	73.1	1.508	0.627	3.02	0.06
Sample K	60.3	70.2	2.242	0.990	4.18	0.16

Table-3.2. Parameters obtained from excess conductivity analysis using AL Expression.

Sample Name	Fit to AL model			
	Range of fit (in lnε)	c 10^{-2} (mΩ.cm)$^{-1}$	λ	rmsd (%)
Sample B	-3.52 to -1.50	1.74	-1.05	0.96
Sample E	-4.10 to -1.76	1.53	-0.84	0.76
Sample F	-3.89 to -1.71	1.59	-1.04	1.85
Sample B1	-3.83 to -2.52	1.00	-0.98	0.47
Sample E1	-3.97 to -1.48	2.38	-0.86	0.75
Sample F1	-3.85 to -2.11	1.54	-1.02	0.76
Sample H	-4.33 to -2.87	0.15	-0.94	0.34
Sample H1	-4.46 to -3.20	0.58	-0.91	0.96
Sample K	-3.62 to -2.87	0.43	-1.04	0.73

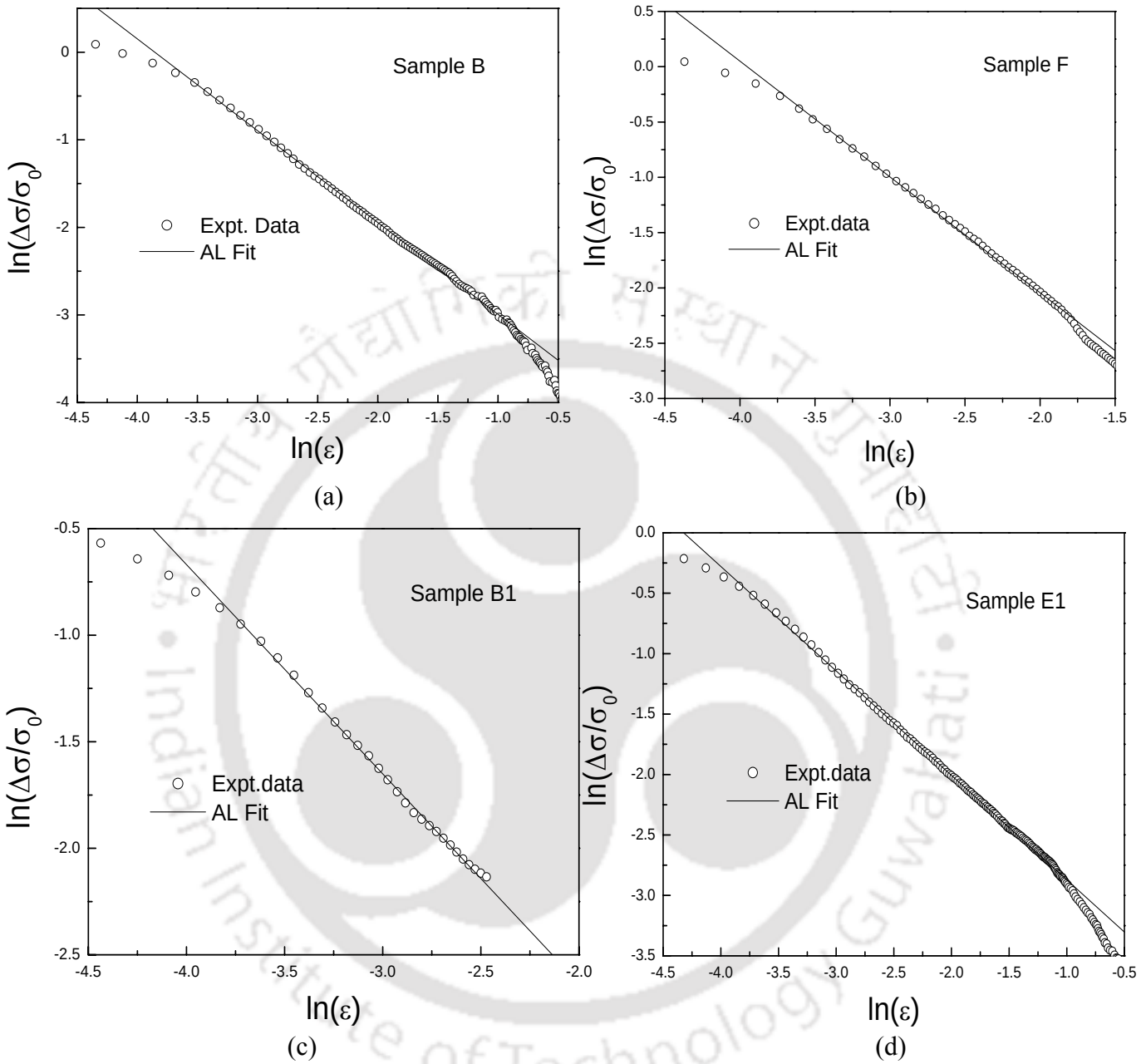

Fig.3.5. Plots of $\ln(\Delta\sigma/\sigma_0)$ versus $\ln(\varepsilon)$ for (a) Sample B, (b) Sample F, (c) Sample B1 and (d) Sample E1. The fitted data using AL expression are shown as solid lines.

AL fit was also carried out in a small temperature region very close to their T_c values, which are not shown in the figures. The values of λ are found to be close to -0.50 for most of the samples. Even though, this exponent value is comparable to the characteristic 3D fluctuations, we could not unequivocally resolve that it is due to 3D in nature because, in this region, the exponent is very sensitive to the choice of T_c. Moreover, according to Lobb [141], in the

temperature region close to T_c, i.e. within 1 K above T_c, the fluctuations enter into critical region with the exponent value of 0.67.

Thus inspite of wide range of T_c observed in La-Ba-Ca-Cu-O system ranging from 60 to 73 K, the dimensionality of order parameter fluctuations is found to be 2D in nature and it reflects the intrinsic property of the materials in the present series.

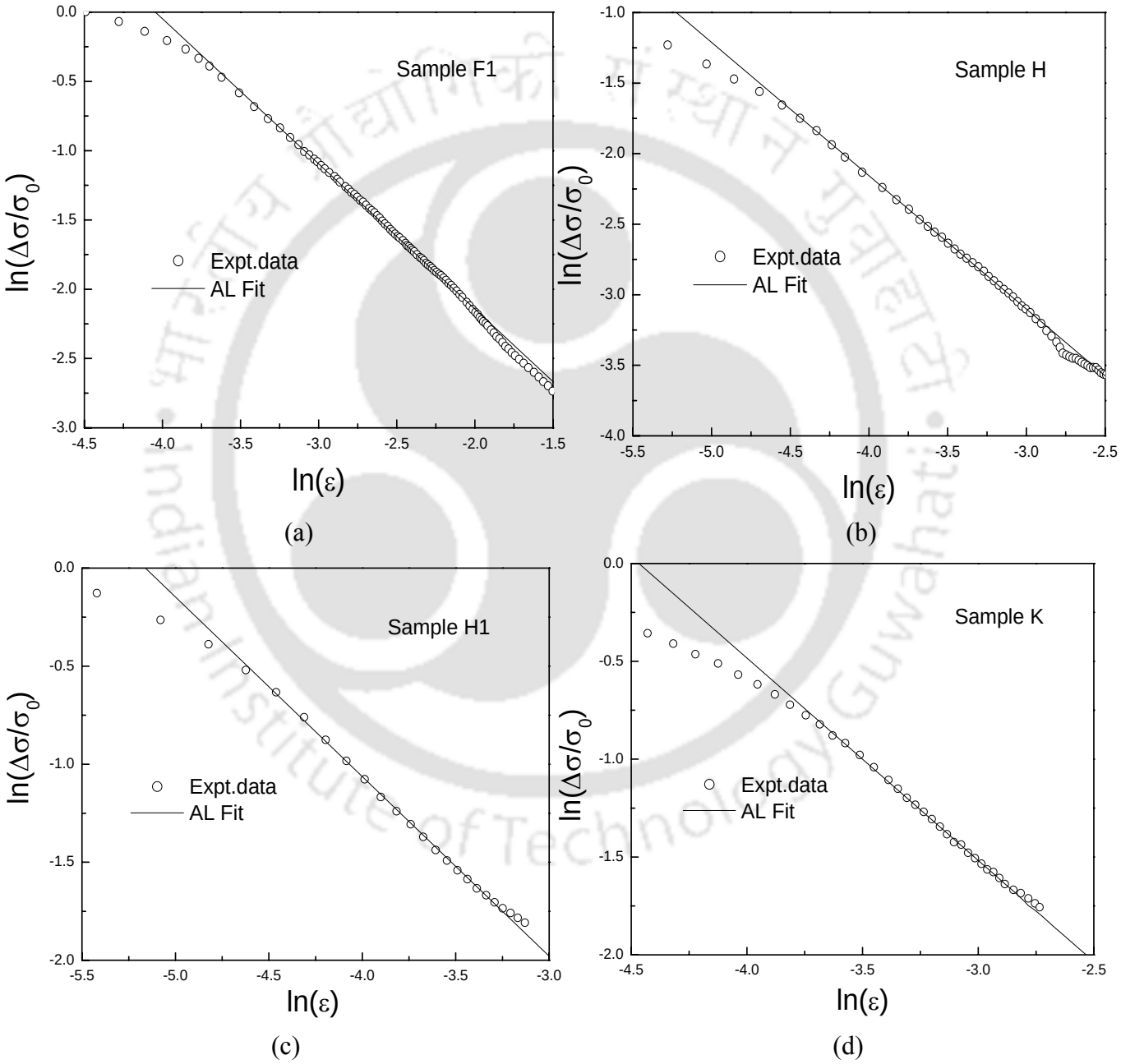

Fig.3.6. Plots of $\ln(\Delta\sigma/\sigma_0)$ versus $\ln(\varepsilon)$ for (a) Sample F1, (b) Sample H, (c) Sample H1 and (d) Sample K. The fitted data using AL expression are shown as solid lines.

3.1.3. Fit to LD Expression

The $\Delta\sigma$ data of sample E were also fitted to the LD expression given by eqn.3.2 in the MFR. The LD fit was carried out to study the dimensionality cross-over and to estimate the relevant parameters. The $\Delta\sigma$ data were fitted to the LD expression by taking the parameters α_o (= $(2\xi_c(0)^2/d^2)$ and the proportionality constant c (=$e^2/16\hbar d$) as free parameters of the fit. The LD model could be fitted well to the experimental data in the region of $\ln\varepsilon$ = -4.25 to -1.76, with an rmsd value of 1.73%. The fitted data are shown as solid line in Fig.3.7. The fitted values of c and α_o are respectively $(1.13 \pm 0.01)\times10^{-2}(m\Omega.cm)^{-1}$ and $(9.50 \pm 0.50)\times10^{-3}$. The error in the parameters was obtained by varying the ranges of fit within the overall fitted region of $\ln\varepsilon$(-4.25 to -1.76). From the fitted value of α_o and by taking d as the c axis length of the unit cell (11.589 Å), the coherence length along c direction of the unit cell at zero Kelvin was estimated and was found to be (0.79 ± 0.04) Å.

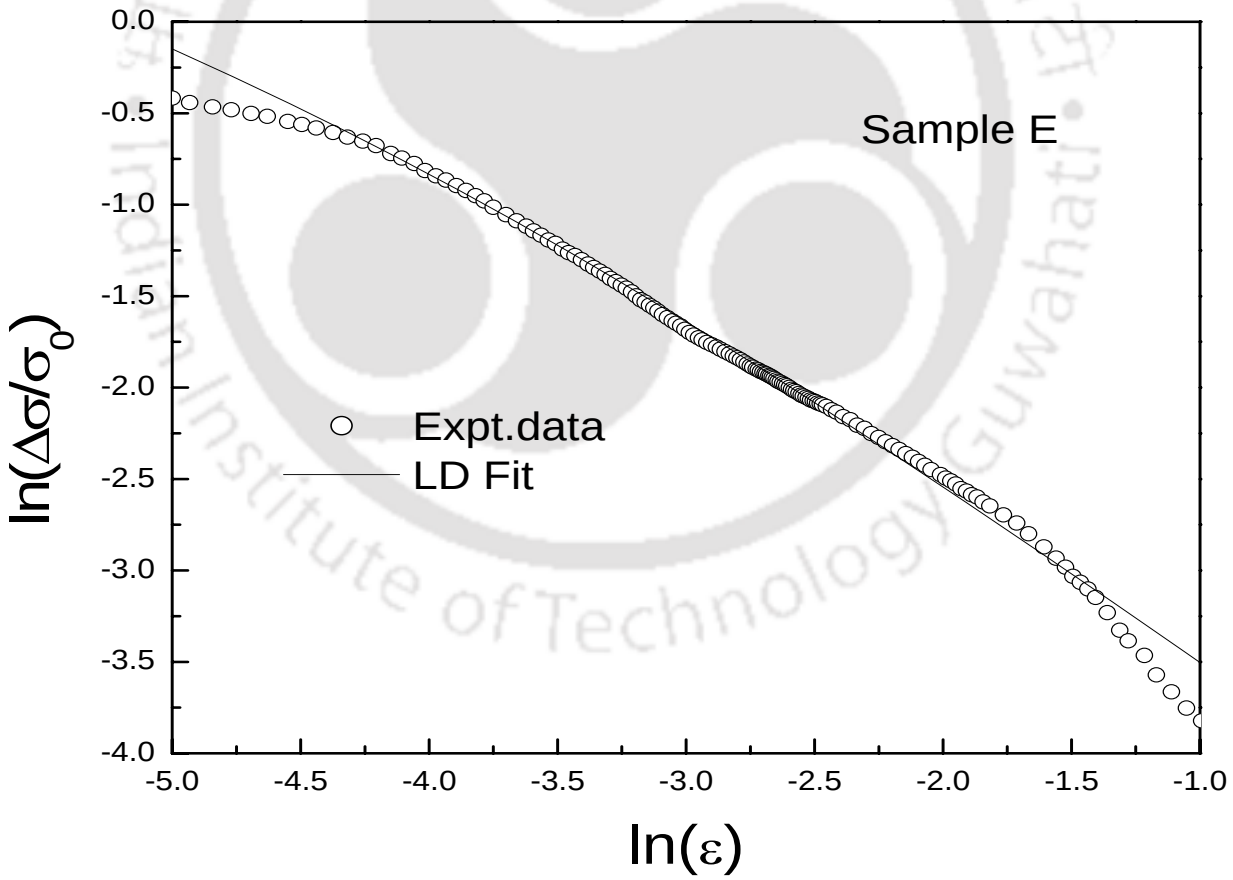

Fig.3.7. Plots of $\ln(\Delta\sigma/\sigma_0)$ versus $\ln(\varepsilon)$ for Sample E. The fitted data using LD expression is shown as solid line.

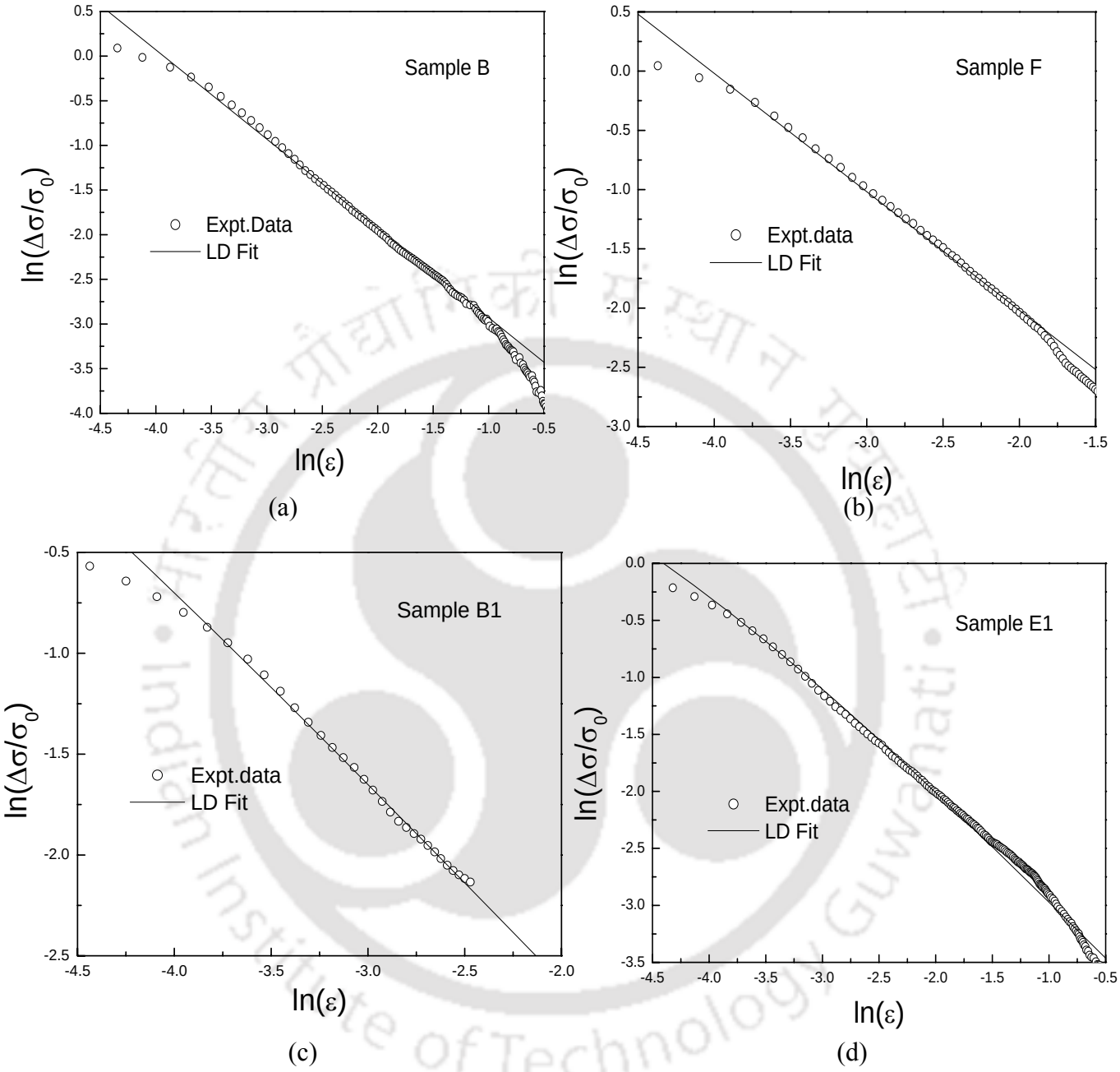

Fig.3.8. Plots of $\ln(\Delta\sigma/\sigma_0)$ versus $\ln(\varepsilon)$ for (a) Sample B, (b) Sample F, and (c) Sample B1, and (d) Sample E1. The fitted data using LD expression are shown as solid lines.

Similarly, the $\Delta\sigma$ data of other samples could also be fitted well to the LD expression in the MFR. The fitted data are shown as solid lines in Figs.3.8 and 3.9. From the fitted values of α_o, the coherence lengths along c direction were calculated and are given in Table 3.3 along with fitted parameters c and the rsmd values. We can see from Table 3.3 that $\xi_c(0)$ values are quite

small and it suggests that the cross-over to 3D fluctuations occur very close to T_c. In other words, these materials exhibit only 2D fluctuations in the MFR and are comparable to the result obtained from AL analysis. To our knowledge, the only report available in literature on fluctuations excess conductivity of $LaBaCaCu_3O_{7-\delta}$ is by Krishnan et al. [245]. In ref. [245], the measured conductivity was fitted to the combination of normal state conductivity and LD model and the value of $\xi_c(0)$ is found to be 0.6 Å. We can see from Table 3.3 that $\xi_c(0)$ values of present series of compounds are comparable to that reported in ref. [245]. Thus, unlike in $YBa_2Cu_3O_7$ superconductors with orthorhombic crystal structure [187,191], where 2D to 3D cross over occurs in the MFR, the present superconductors with tetragonal crystal structure comparable to that of non-superconducting $YBa_2Cu_3O_{6+\delta}$, exhibit two dimensional fluctuations in the entire MFR.

Table-3.3. Parameters obtained from excess conductivity fitting using LD Expression.

Sample Name	Fit to LD model			
	Range of fit (in lnε)	c $10^{-2}(m\Omega.cm)^{-1}$	$\xi_c(0)$ Å	rmsd (%)
Sample B	-3.87 to -1.50	1.95 ± 0.01	0.16 ± 0.01	1.95
Sample E	-4.25 to -1.76	1.13 ± 0.01	0.79 ± 0.04	1.73
Sample F	-4.09 to -1.71	1.79 ± 0.01	0.13 ± 0.01	2.22
Sample B1	-3.95 to -2.52	0.98 ± 0.02	0.33 ± 0.02	1.20
Sample E1	-4.12 to -1.48	1.92 ± 0.05	0.77 ± 0.03	1.84
Sample F1	-3.97 to -2.11	1.66 ± 0.01	0.18 ± 0.02	1.22
Sample H	-4.69 to -2.90	0.13 ± 0.03	0.35 ± 0.03	0.34
Sample H1	-4.46 to -3.20	0.47 ± 0.02	0.40 ± 0.03	1.32
Sample K	-3.62 to -2.87	0.49 ± 0.03	0.30 ± 0.02	1.12

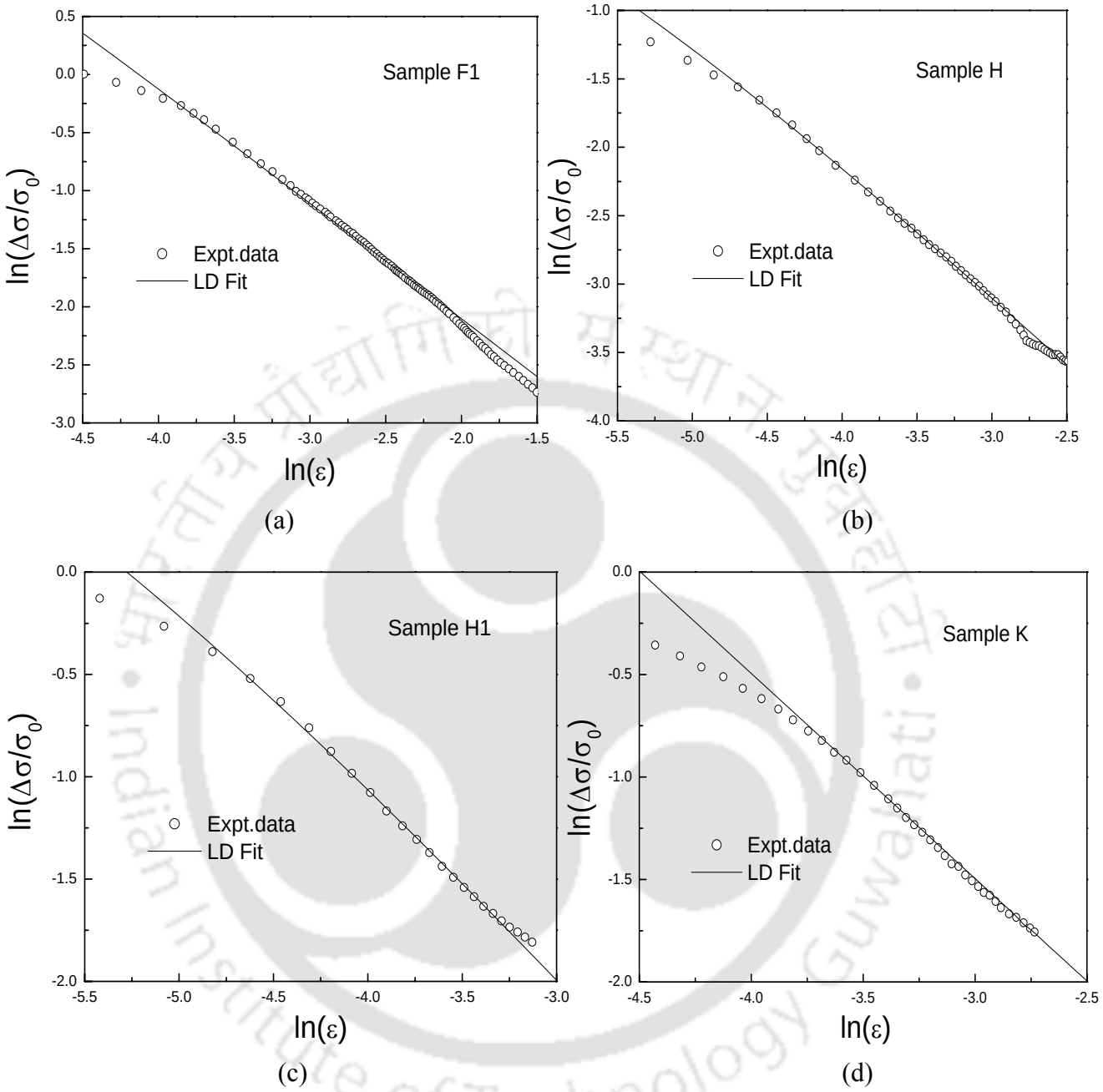

Fig.3.9. Plots of $\ln(\Delta\sigma/\sigma_0)$ versus $\ln(\varepsilon)$ for (a) Sample F1, (b) Sample H, (c) Sample H1 and (d) Sample K. The fitted data using LD expression are shown as solid lines.

3.1.4. Fit to LD+MT Expression

In order to study the contribution of MT term to the excess conductivity, the experimental $\Delta\sigma$ data were also analyzed using the combination of LD and MT expressions,

$$\Delta\sigma = \Delta\sigma_{LD} + \Delta\sigma_{MT} \tag{3.8}$$

Here $\Delta\sigma_{LD}$ and $\Delta\sigma_{MT}$ are taken from eqn.3.2 and eqn.3.4. The fit was carried out in the same temperature region as that of LD fit by taking c = $e^2/16\hbar d$ and $\delta = \left(16\xi_c(0)^2\kappa_B T\tau_\phi/\left(\pi d^2\hbar\right)\right)$ as free parameters for the fit and by fixing ($\alpha_0 = 2\left[\xi_c(0)/d\right]^2$) using the values obtained from LD fit. For sample E, the $\Delta\sigma$ data could be fitted well to eqn. (3.8) in the MFR with an rmsd value of 1.33%. The fitted values of c and δ are respectively $(1.08 \pm 0.01) \times 10^{-2}$(m$\Omega$.cm)$^{-1}$and $(7.30 \pm 0.64) \times 10^{-4}$. The estimated value of c from the LD + MT fit is comparable to that of AL and LD fits. The fitted data along with experimental data are shown in Fig.3.10 for sample E. From the fitted value ofδ, the phase breaking time τ_ϕ(100K) is estimated to be $(2.3 \pm 0.2) \times 10^{-16}$s.

Similarly, the $\Delta\sigma$ data of all other samples were fitted to the sum of LD and MT expressions in the MFR. As described above, the parameters c and δ were taken as free parameters of the fit and by assuming α_0 values obtained from LD fit. The fitted data are shown as solid lines in Figs. 3.11 & 3.12. The parameters c and τ_ϕ along with rmsd values are given in Table 3.4.The value of τ_ϕ is found to be about two orders of magnitude less than that reported for $YBa_2Cu_3O_7$ superconductors. It suggests that in the present series, there is a strong pair breaking effect and the contribution of MT term to $\Delta\sigma$ is insignificant. Such a strong pair breaking behavior has been reported in literature on Bi-Sr-Ca-Cu-O system [228]. It may be noted that there is no prior work on the analysis of $\Delta\sigma$ data of La-Ba-Ca-Cu-O system in terms of LD+MT model.

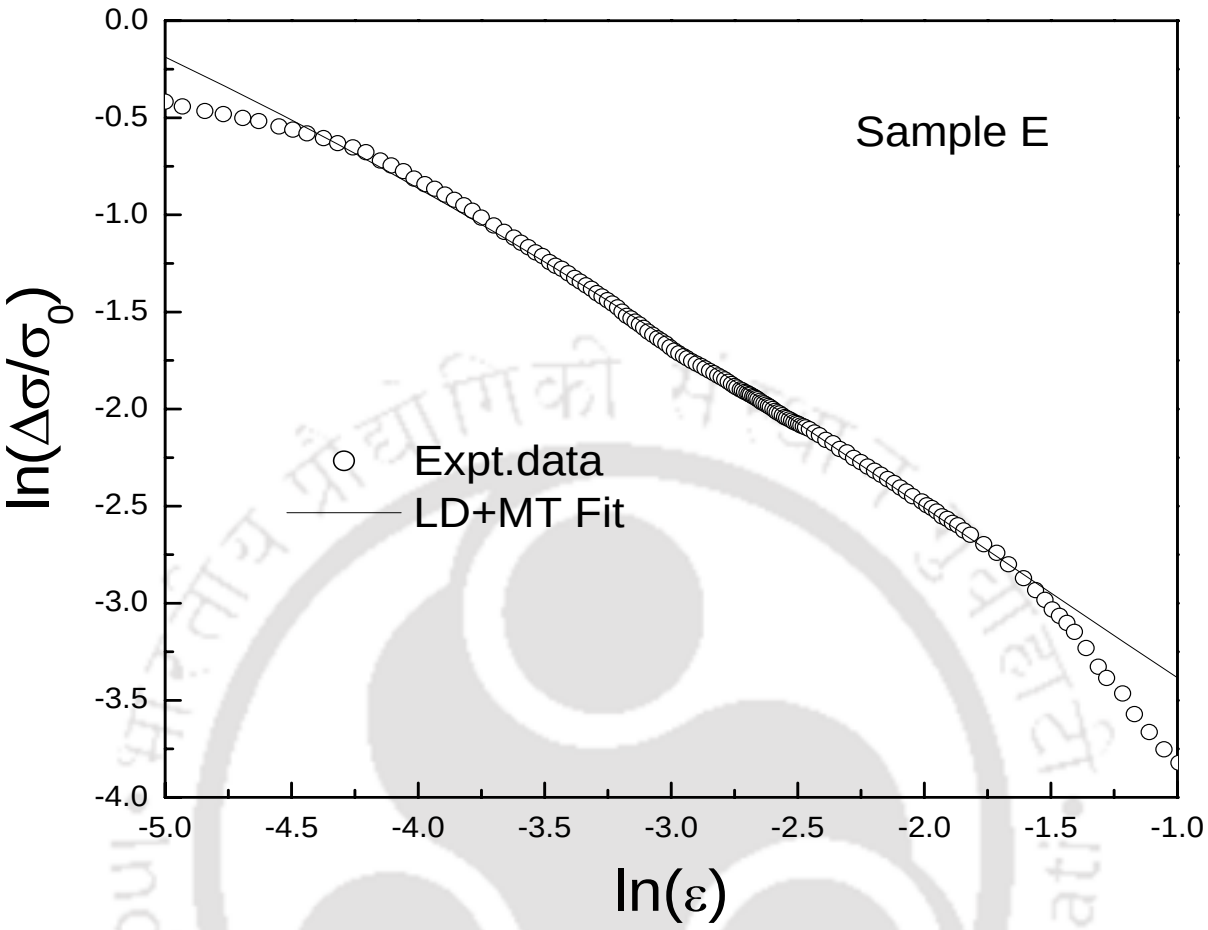

Fig.3.10. Plots of $\ln(\Delta\sigma/\sigma_0)$ versus $\ln(\varepsilon)$ for Sample E. The fitted data using LD+MT expression is shown as solid line.

Table 3.4. Parameters obtained from LD + MT fit to excess conductivity data.

Sample Name	Range of fit (in lnε)	c $10^{-2}(m\Omega.cm)^{-1}$	τ_ϕ (100 K) 10^{-16} s	rmsd (%)
Sample B	-3.87 to -1.50	1.94 ± 0.02	3.4 ± 0.4	2.22
Sample E	-4.25 to –1.76	1.08 ± 0.01	2.3 ± 0.2	1.33
Sample F	-4.09 to -1.71	1.79 ± 0.01	2.7 ± 0.4	2.30
Sample B1	-3.95 to -2.52	0.10 ± 0.01	4.5 ± 1.2	1.17
Sample E1	-4.12 to -1.48	1.80 ± 0.01	1.9 ± 0.1	0.99
Sample F1	-3.97 to -2.11	1.66 ± 0.05	1.3 ± 0.3	1.22
Sample H	-4.69 to -2.90	0.13 ± 0.01	3.9 ± 1.5	0.35
Sample H1	-4.46 to -3.20	0.46 ± 0.05	4.6 ± 3.2	1.36
Sample K	-3.62 to -2.87	0.11 ± 0.01	5.7 ± 4.8	1.22

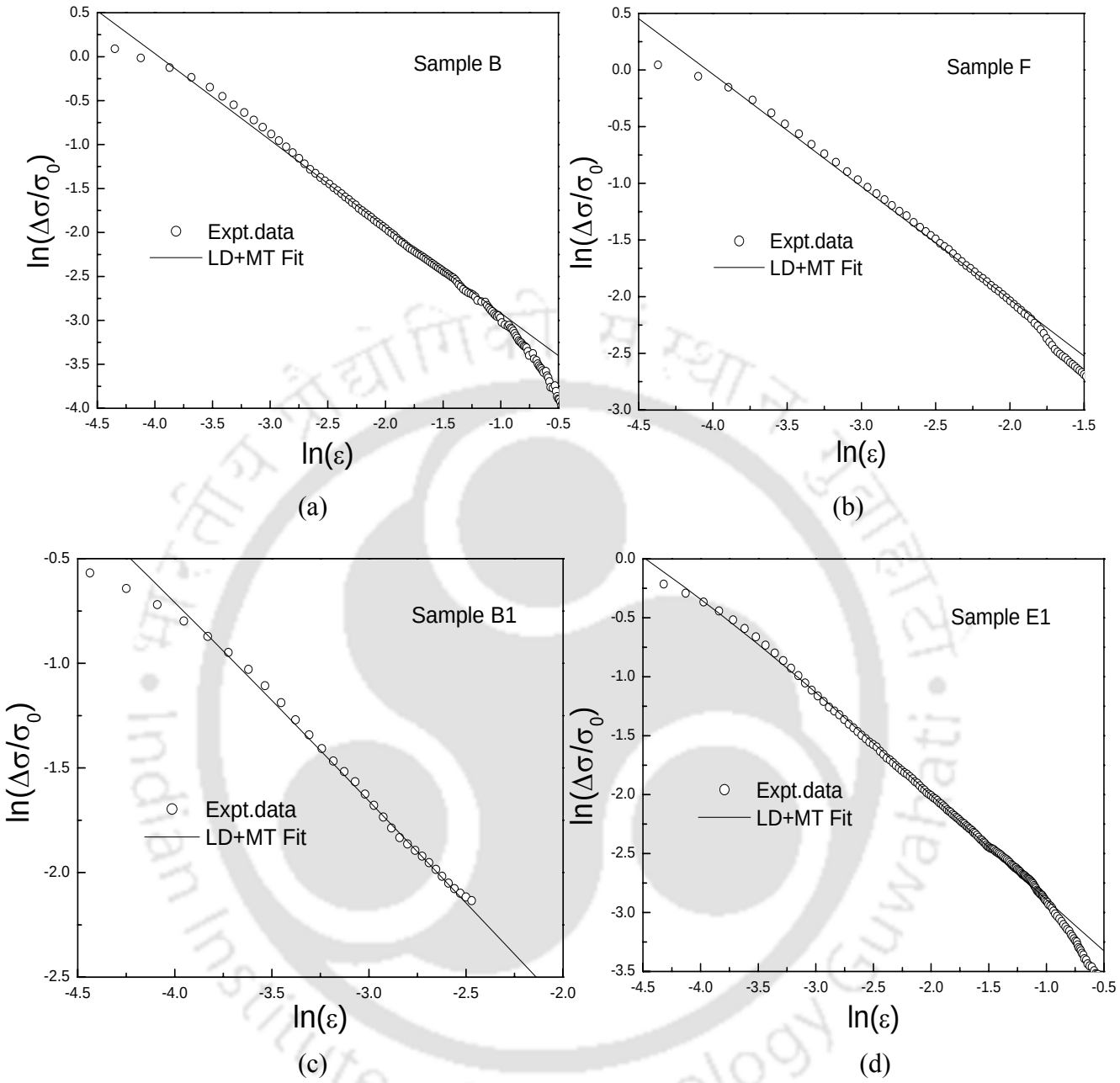

Fig.3.11. Plots of $\ln(\Delta\sigma/\sigma_0)$ versus $\ln(\varepsilon)$ for (a) Sample B, (b) Sample F, (c) Sample B1 and (d) Sample E1. The fitted data using LD+MT expression are shown as solid lines.

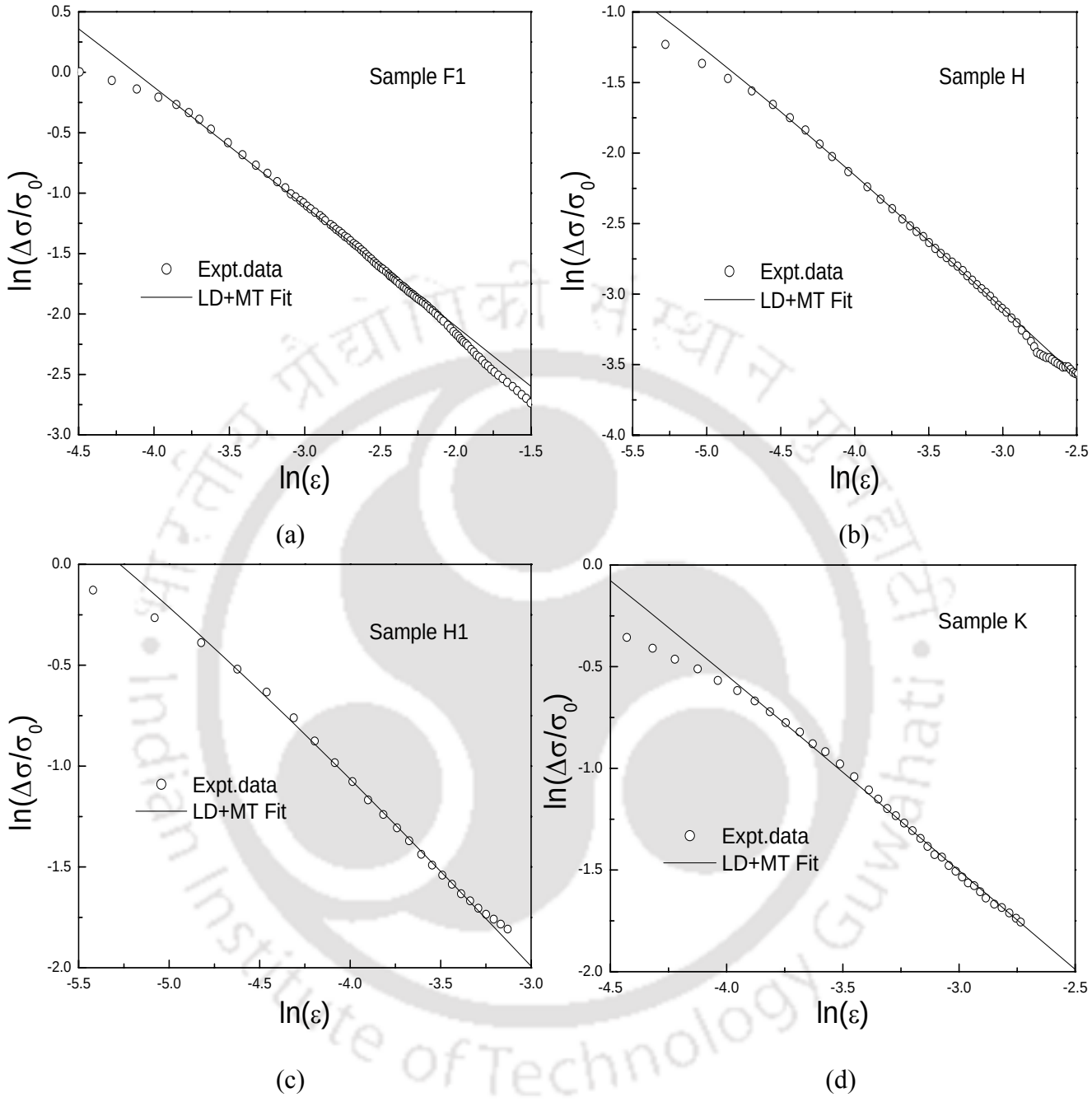

Fig.3.12. Plots of ln ($\Delta\sigma/\sigma_0$) versus ln (ε) for (a) Sample F1, (b) Sample H, (c) Sample H1 and (d) Sample K. The fitted data using LD+MT expression are shown as solid lines.

So from the excess conductivity analysis on the above nine samples using Aslamazov-Larkin (AL), Lawrence-Doniach (LD) and Maki-Thompson (MT) models, we draw some of the conclusions, which are mentioned below. These materials exhibit two dimensional fluctuations in the MFR. Thus unlike orthorhombic superconducting $YBa_2Cu_3O_7$, where a cross over from

2D to 3D fluctuations is observed in the MFR, the present materials with tetragonal structure comparable to the non-superconducting $YBa_2Cu_3O_{6+\delta}$ exhibit only 2D fluctuations in the MFR. This suggests that according to LD model, the interlayer coupling constant $J(T) = (\xi_c (T)/d)^2 << 1/4$ in the present materials. The rather low value of J(T) could be mainly due to reduced $\xi_c(T)$ in the present materials compared to $YBa_2Cu_3O_7$ because; the d values are comparable in both the systems. There is a possibility of large anisotropy and hence a small $\xi_c(T)$ in the present series that lead to 2D fluctuations. It may also be noted that other high T_c superconductors such as Bi-Sr-Ca-Cu-O and Tl-Ba-Ca-Cu-O systems exhibit tetragonal structure with large anisotropy [346, 347] and 2D fluctuations in the MFR [215, 218, 221, 222, 232, 234]. On the other hand, well oxygenated $YBa_2Cu_3O_7$ with orthorhombic structure exhibits relatively low anisotropy [347]. Kleiner and Müller have also reported that $Bi_2Sr_2CaCu_2O_8$ and $Tl_2Ba_2Ca_2Cu_3O_{10}$ superconductors exhibit intrinsic Josephson effect, where each CuO_2 layer behaves like two dimensional superconductors and such effect has not been observed in $YBa_2Cu_3O_7$ [347].

The contribution of Maki-Thompson term to zero field excess conductivity has been studied by a few groups on $YBa_2Cu_3O_7$ superconductors and the estimated value of phase breaking time, τ_ϕ (100 K) is found to be in the order of 10^{-13} to 10^{-14}s, indicating moderate pair breaking effect [195-200]. The coherence length along c-direction at 0 K, (ξ_c) is found to be in the range of 1.0 to 3.0 Å. But here, we found the coherence length is < 1 Å and the phase breaking time τ_ϕ is in the order of 10^{-16}s, which is quite small and is comparable to that reported in Bi-Sr-Ca-Cu-O superconductor with tetragonal structure [228]. The rather small values of τ_ϕ suggests that there is a strong pair breaking effect and the contribution of MT term to $\Delta\sigma$ is negligible.

3.2. Magneto-Conductivity Analysis

The detailed magneto-conductivity studies on high T_c superconductors have been extensively reviewed in section 1.4. For convenience some of the important expressions for fluctuation magneto-conductivity are mentioned below.

The fluctuation magneto-conductivity, $\Delta\sigma_H$ for layered superconductors was theoretically studied by Hikami and Larkin [149], and independently by Maki and Thompson [150]. Their work was based on the pair breaking effect of a magnetic field, which leads to a suppression of

T_c in mean-field theory and decreases the fluctuation conductivity. Hence a positive magneto-resistivity results, which is expressed in terms of a negative magneto-conductivity.

They have worked out the AL and MT contributions in the dirty limit. The AL terms correspond to direct contribution to $\Delta\sigma_H$ and MT terms correspond to indirect contribution to $\Delta\sigma_H$. They have carried out the derivation by considering the interactions of magnetic field with orbital motion of charge carriers and they are represented as $\Delta\sigma_{ALO}$ and $\Delta\sigma_{MTO}$. ALO and MTO refer Aslamazov-Larkin-Orbital and Maki-Thompson-Orbital contributions respectively and are given as follows.

$$\Delta\sigma_{ALO} = \frac{-e^2}{64\hbar d\varepsilon^3}\frac{2+4\alpha+3\alpha^2}{(1+2\alpha)^{5/2}}h^2 \tag{3.9}$$

and

$$\Delta\sigma_{MTO} = \frac{-e^2}{48\hbar d(1-\alpha/\delta)\varepsilon^3}\left[\frac{\delta^2}{\alpha^2}\frac{1+\delta}{(1+2\delta)^{3/2}} - \frac{1+\alpha}{(1+2\alpha)^{3/2}}\right]h^2 \tag{3.10}$$

In the above equation, $h^2 = H_{eff}{}^2(2e\xi_{ab}(0)^2/\hbar)^2$, where H_{eff} is the effective magnetic field to account for angular average of the conducting planes in polycrystalline samples. According to Matsuda et al. [163], $H_{eff}^2 = H^2\langle\cos^2\theta\rangle = H^2/3$, where H is the applied magnetic field. $\xi_{ab}(0)$ is the coherence length along ab plane at 0 K.

Arnov, Hikami and Larkin [164] derived the expression for $\Delta\sigma_H$ by considering the interaction of magnetic field with spin moments of the charge carriers, i.e. Zeeman splitting. It was later modified by Thompson [165]. According to them, the contribution of Zeeman effect on direct ($\Delta\sigma_{ALZ}$) and indirect ($\Delta\sigma_{MTZ}$) components of fluctuations magneto-conductivity can be written as,

$$\Delta\sigma_{ALZ} = -0.526\frac{e^2}{\hbar d\varepsilon^2}\frac{1+\alpha}{(1+2\alpha)^{3/2}}\left[\frac{\omega_s}{4\pi\kappa_B T_c}\right]^2 \tag{3.11}$$

and

$$\Delta\sigma_{MTZ} = \frac{-e^2}{16\hbar d\varepsilon}\left[\frac{1+\delta}{(1+2\delta)^{3/2}} - \frac{1+\delta+\delta/\alpha}{[(1+\delta/\alpha)(1+2\delta+\delta/\alpha)]^{3/2}}\right]\left[\frac{\omega_s\tau_\phi}{\hbar}\right]^2 \tag{3.12}$$

where $\omega_s = g\mu_B H$ is the Zeeman energy, g is the Lande's g factor and μ_B is the Bohr magneton.

3.2.1. Magneto-Conductivity Analysis of La-Ba-Ca-Cu-O Superconductors

In addition to zero field excess conductivity analysis, I have carried out magneto-conductivity analysis on the same set of samples. The magneto-conductivity calculation and analysis are described below. The fluctuation magneto-conductivity is given by the relation,

$$\Delta\sigma_H = \frac{1}{\rho(H)} - \frac{1}{\rho(0)} \tag{3.13}$$

where ρ(H) and ρ(0) are the measured resistivity in the presence and absence of magnetic field. The temperature variations of electrical resistivity for zero field and for the applied magnetic field, H = 1T are shown in Fig.3.13 for sample E1. By the application of magnetic field, T_c (0) shifts from 57.8 to 49.7 K.

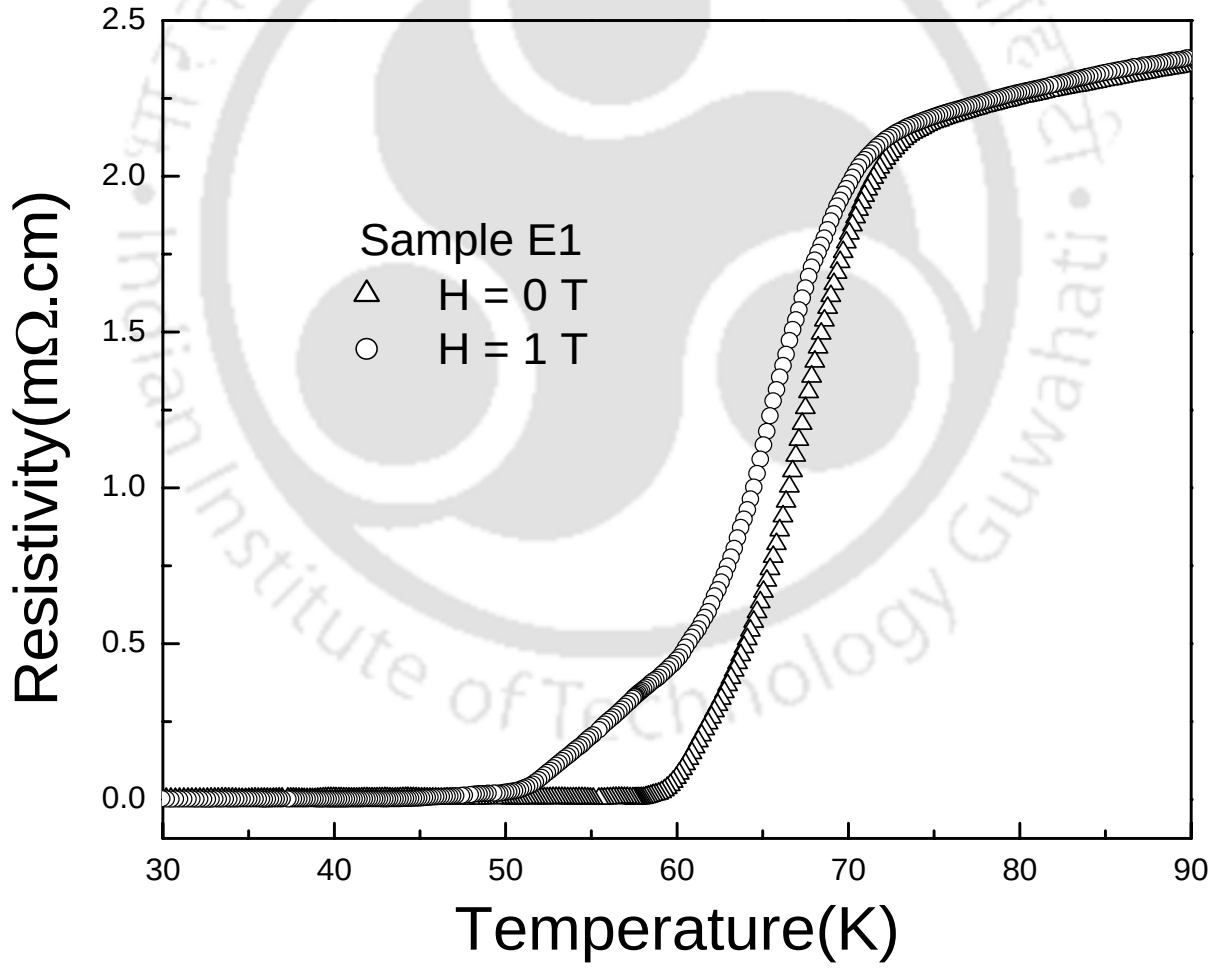

Fig. 3.13. Temperature variation of electrical resistivity measured at H = 0 (triangles) and 1T (circles) for Samples E1.

Figs. 3.14 & 3.15 show the temperature variations of electrical resistivity in the absence and presence of magnetic field for all other samples. Considerable shift in $T_c(0)$ has been observed and it is mainly due to suppression of superconductivity of intergranular weak links, by the applied magnetic field.

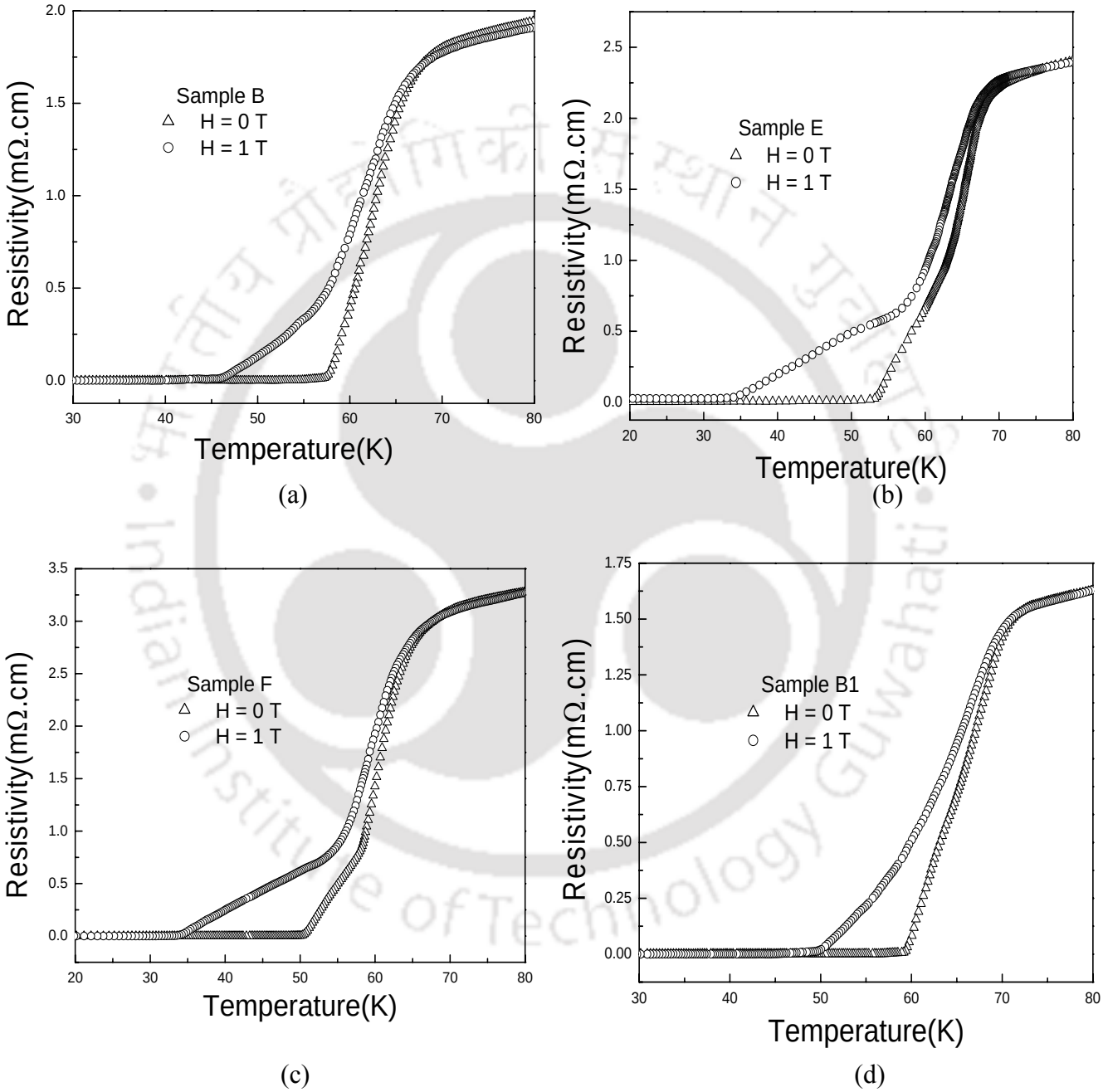

Fig. 3.14. Temperature variation of electrical resistivity measured at H = 0 (triangles) and 1T (circles) for (a) Sample B, (b) Sample E, (c) Sample F and (d) Sample B1.

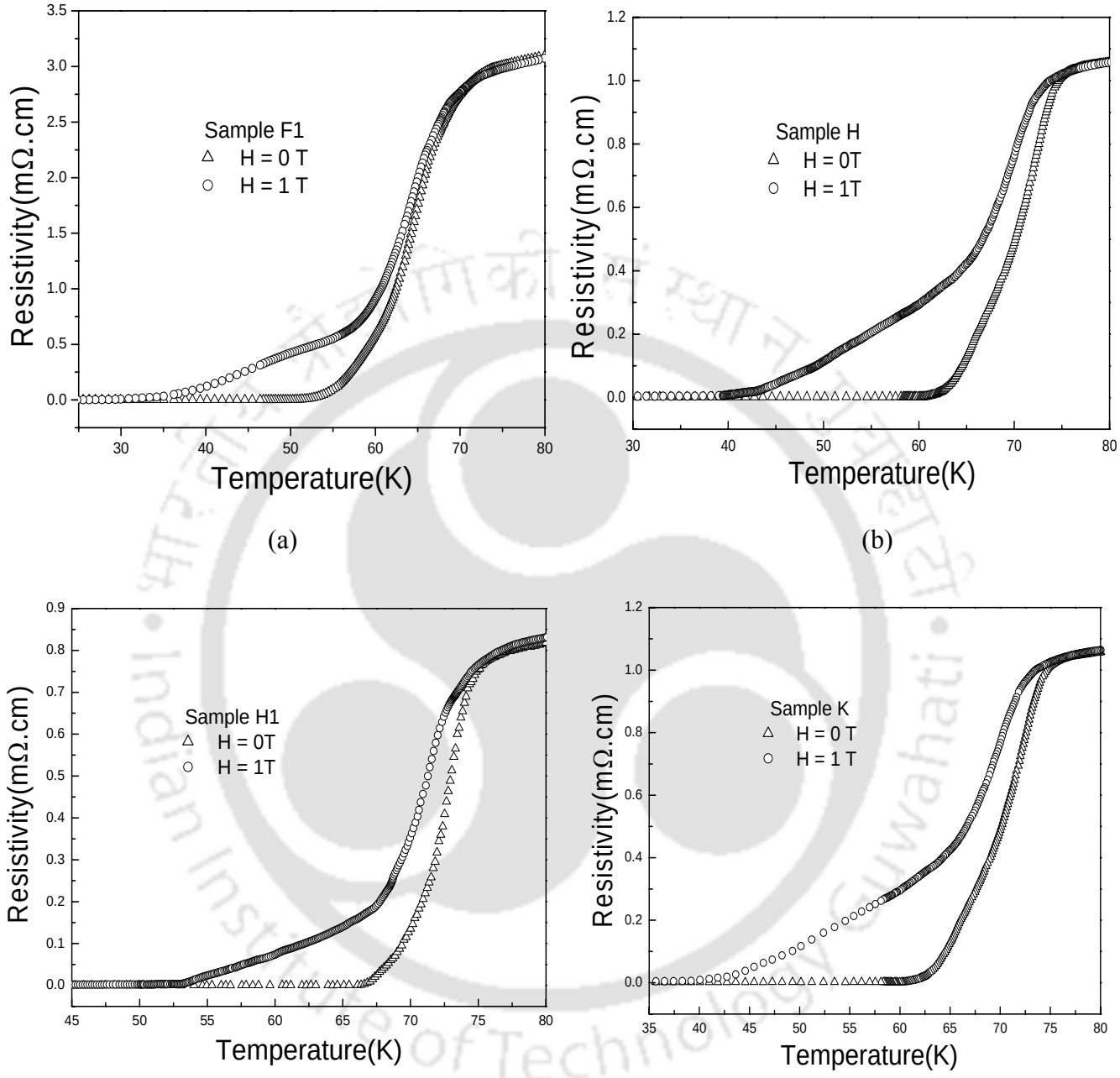

Fig. 3.15. Temperature variation of electrical resistivity measured at H = 0 (triangles) and 1T (circles) for (a) Sample F1, (b) Sample H, (c) Sample H1 and (d) Sample K.

The experimental magneto-conductivity data, $\Delta\sigma_H$ was obtained from the measured resistivity in the absence and presence of magnetic field and, using eqn.3.13. Typical plot of $\ln(-\Delta\sigma_H)$ versus $\ln\varepsilon$ is shown in Fig.3.16 for Sample E1. Initially, $\Delta\sigma_H$ data have been analyzed in terms of only the direct contributions, i.e. the combination of ALO and ALZ terms (eqns. 3.9 & 3.11). This is mainly to estimate the value of α_o. The experimental data could be fitted well to the above models and the fitted data are shown as solid line in Fig. 3.16. From the fitted values of α_o, the coherence length along c direction at 0 K, $\xi_c(0)$ is estimated and it is found to be 0.84 Å. This value is comparable to those obtained from excess conductivity analysis discussed in section 3.1.

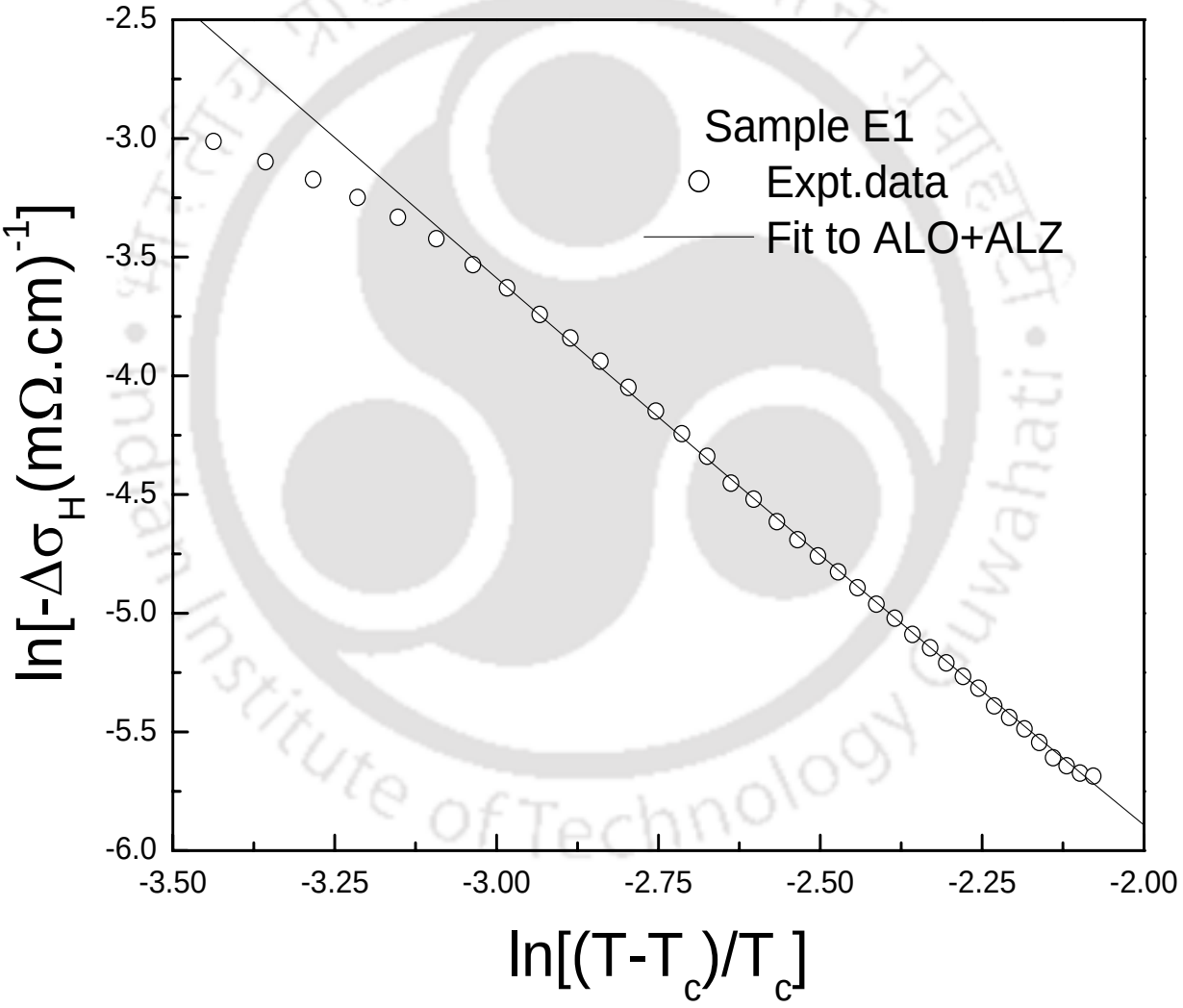

Fig. 3.16. Plot of $\ln(-\Delta\sigma_H)$ versus $\ln\varepsilon$ for Sample E1. The experimental data are shown as symbols. The fitted data as per AL models are shown as solid line.

We can see that this plot exhibits linear behavior in the mean field regime. The $\Delta\sigma_H$ data of all other samples have been also fitted to the combination of eqns. 3.9 & 3.11, i.e. by considering only the direct contribution to $\Delta\sigma_H$. Here the parameters $P_1 = e^2h^2/(64\hbar d)$, $P_2 = (0.526e^2/\hbar d)(\omega_s/4\pi k_B T_c)^2$ and α_0 were taken as free parameters of the fit. Similar to sample E1, the $\Delta\sigma_H$ data of other samples could also be fitted well to the above AL model. These fittings are not shown because similar AL theoretical data are shown in subsequent figures. These fittings were carried out mainly to determine the α_0 values. From the fitted values of α_0 and by taking d as the c axis length of the unit cell (Table 2.2 & 2.4), $\xi_c(0)$ values were estimated and are tabulated in Table 3.5. The $\xi_c(0)$ values obtained for different samples can be compared with their respective values determined from excess conductivity analysis (Table 3.3). We can see that they are mostly comparable to each other and it highlights the consistency of analysis.

The fitting of $\Delta\sigma_H$ was repeated by taking into account the indirect contribution to $\Delta\sigma_H$, i.e. they were fitted to the combination of eqns. 3.9 to 3.12 by taking a C-factor as follows,

$$\Delta\sigma_H = \frac{1}{C}\left[\Delta\sigma_{ALO} + \Delta\sigma_{ALZ} + \Delta\sigma_{MTO} + \Delta\sigma_{MTZ}\right] \qquad (3.14)$$

Here the C-factor is to account for in homogeneity in the current path due to voids, grain boundaries, weak links, etc. in polycrystalline materials. The C-factor was obtained by following Oh et. al. [191] and according to them it is equal to the ratio of slope of normal state resistivity ($d\rho/dT$ at $T>>T_c$) of polycrystalline material to that of single crystals. In high T_c single crystal superconductors, the value of normal state $d\rho/dT$ is generally 0.5 to 0.6 $\mu\Omega$.cm/K. To reduce the number of free parameters of the fit, α_o was fixed using the value obtained from ALO+ALZ fit. The other parameters namely $P_1=e^2h^2/(64\hbar d)$, $P_2=(0.526e^2/\hbar d)(\omega_s/4\pi k_B T_c)^2$, $P_3=\delta$ and $P_4 = \frac{e^2}{16\hbar d}\left(\frac{\omega_s T\tau_\phi}{\hbar}\right)^2$ were varied during the fit. The fitted data in the mean field regime are shown as dashed lines in Fig.3.17 for Sample E1, which closely follow the experimental data. From the fitted parameters, the theoretical data of AL (ALO+ALZ) and MT (MTO+MTZ) terms were calculated. The AL data are shown as solid line in Fig.3.17 and this is indistinguisible from AL+MT data because of insignificant contribution of MT term. Figs. 3.18 & 3.19 show the plots of $\ln(-\Delta\sigma_H)$ versus $\ln\varepsilon$ for other samples. For all these samples, the $\Delta\sigma_H$ data were fitted to eqn.

3.14 by following the above method. The fitted data are shown as dashed lines. From the fitted parameters, AL data (ALO+ALZ) were calculated and are shown as solid lines, which is indistinguisible from the theoretical AL+MT models due to insignificant contribution of MT term.

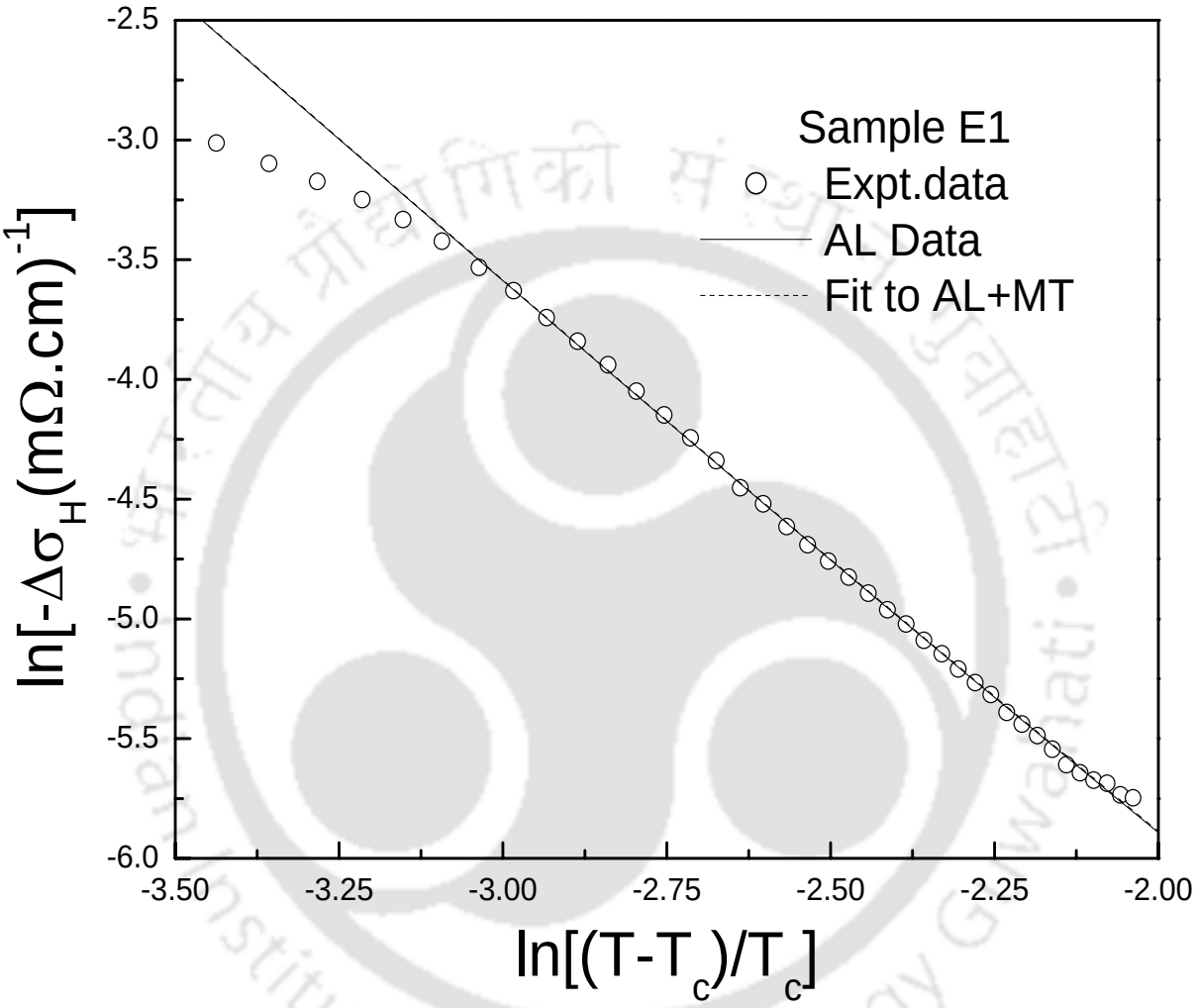

Fig. 3.17. Plot of ln ($-\Delta\sigma_H$) versus lnε for Sample E1. The experimental data are shown as symbols. The theoretical data such as AL and AL+MT are shown as solid and dashed lines respectively and they merge against each other.

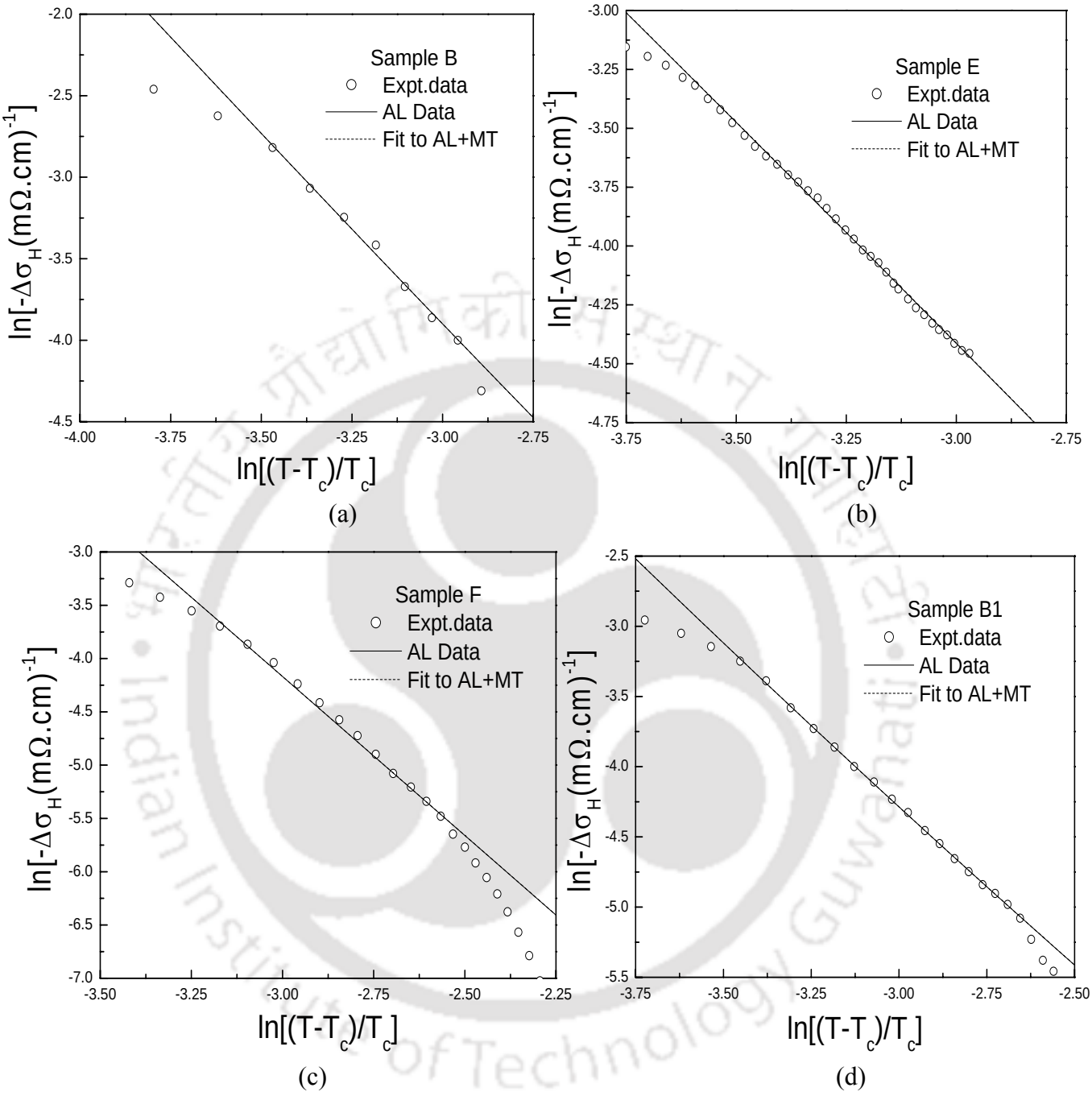

Fig. 3.18. Plots of $\ln(-\Delta\sigma_H)$ versus $\ln\varepsilon$ for (a) Sample B, (b) Sample E, (c) Sample F and (d) Sample B1. The experimental data are shown as symbols. The theoretical data such as AL and AL+MT are shown as solid and dashed lines respectively and they merge against each other.

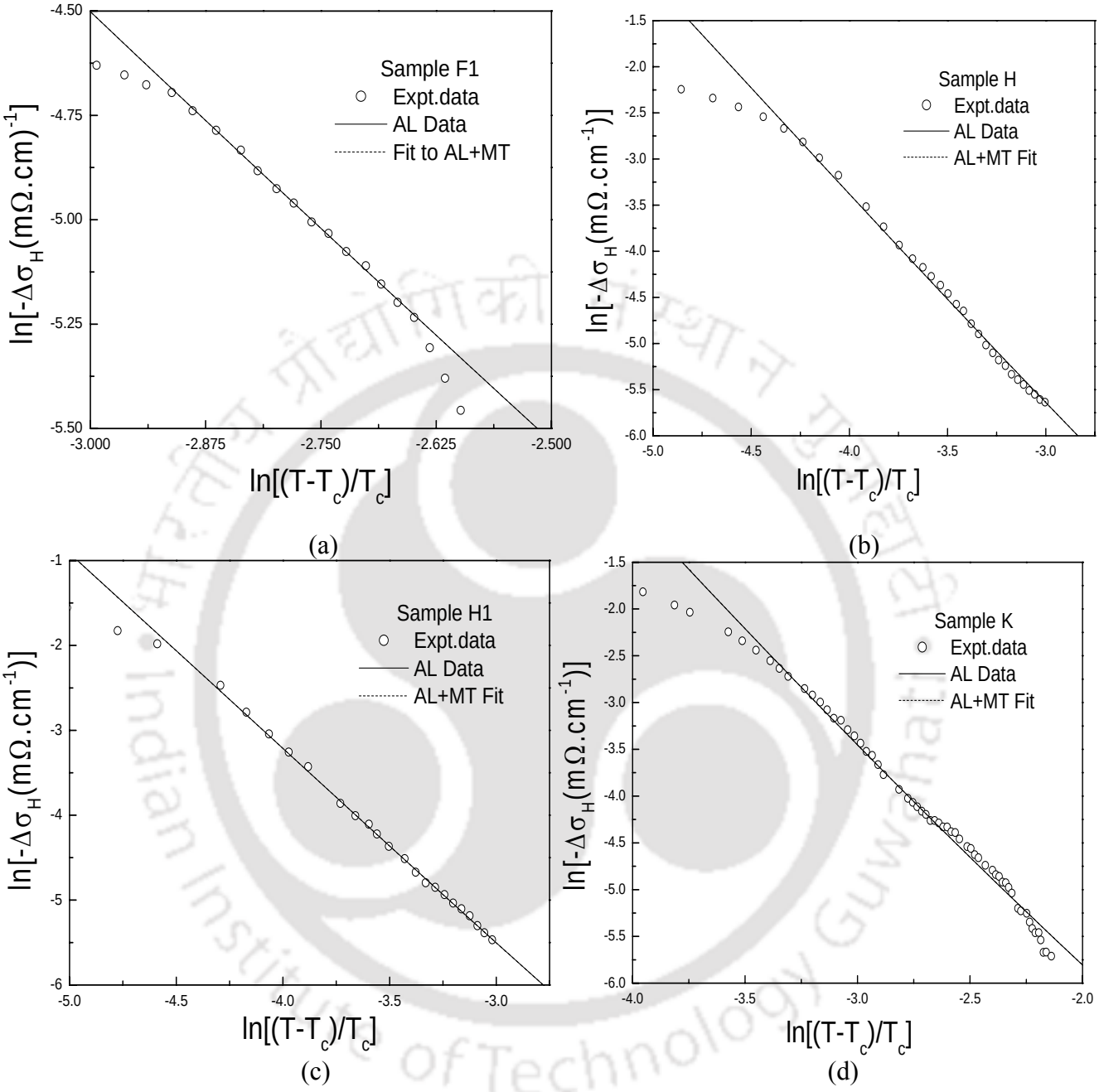

Fig. 3.19. Plots of $\ln(-\Delta\sigma_H)$ versus $\ln\varepsilon$ for (a) Sample F1, (b) Sample H, (c) Sample H1 and (d) Sample K. The experimental data are shown as symbols. The theoretical data such as AL and AL+MT are shown as solid and dashed lines respectively and they merge against each other.

The coherence length along ab plane $\xi_{ab}(0)$ was estimated from the fitted values of P_1 and by taking into account the effective magnetic field. The $\xi_{ab}(0)$ values are tabulated in Table 3.5 and they are comparable to that of $YBa_2Cu_3O_7$ materials [163, 201]. The coherence length can

also be compared with GL coherence length of 20 Å reported by Peng et al. on $LaBaCaCu_3O_z$ superconductor [123]. The values of $\tau_\phi(100K)$ were estimated using δ values obtained from $\Delta\sigma_H$ analysis and they are given in Table 3.5. They are in the order of 10^{-16}s and are comparable to those obtained from zero field excess conductivity analysis. The values of τ_ϕ are found to be about three orders of magnitude less than those reported for orthorhombic $YBa_2Cu_3O_7$ superconductors. However, the τ_ϕ values obtained in the present compounds are comparable to those reported for Bi-Sr-Ca-Cu-O superconductors [228]. According to Aronov et al. [164], τ_ϕ can be compared with the energy relaxation time due to spin-orbit and spin-spin interaction. Accordingly, the energy values $\hbar/\tau_\phi(100K)$ are given in Table 3.5 and it is found that $\frac{\hbar}{\tau_\phi} >> \kappa_B T_c$. The typical value of $\kappa_B T_c$ for a T_c of 70 K is 6.037×10^{-3} eV. This suggests that there is a strong pair breaking effect in the present materials and the contribution of MT term is insignificant.

Table 3.5. Parameters obtained from the analysis of magneto-conductivity using eqn.3.14, i.e. (AL + MT terms).

Sample Name	$\xi_c(0)$ Å	$\xi_{ab}(0)$ Å	$\tau_\phi(100K)$ 10^{-16} s	$\hbar/\tau_\phi(100K)$ eV	rmsd (%)
Sample B	0.46 ± 0.02	28.5 ± 2.0	1.2 ± 0.4	5.22	0.81
Sample E	0.79 ± 0.01	18.7 ± 1.4	5.0 ± 3.2	1.32	0.68
Sample F	0.16 ± 0.01	32.1 ± 0.5	1.2 ± 0.3	5.46	1.63
Sample B1	0.27 ± 0.02	22.8 ± 2.4	4.3 ± 1.3	1.54	0.24
Sample E1	0.84 ± 0.02	33.5 ± 2.8	4.3 ± 0.3	1.54	0.44
Sample F1	0.27 ± 0.03	34.0 ± 3.1	1.4 ± 0.2	4.60	0.10
Sample H	0.35 ± 0.03	14.4 ± 0.9	2.8 ± 0.9	2.35	3.10
Sample H1	0.50 ± 0.03	16.6 ± 1.8	1.1 ± 0.3	5.86	1.25
Sample K	0.30 ± 0.01	30.1 ± 2.5	3.5 ± 1.1	1.89	2.37

Thus, from magneto-conductivity analysis, we have estimated the value of $\xi_c(0)$ and it is quite small and comparable to those obtained from excess conductivity analysis. This suggests that the dimensionality of order parameter fluctuation is 2D in nature. The τ_ϕ value suggests that the contribution of MT term is insignificant.

3.3. Excess conductivity in the Paracoherence Regime

So far we analyzed the excess conductivity arising out of the fluctuations in the magnitude of order parameter in the MFR. Similarly in the paracoherence region, i.e. from zero resistivity transition temperature (T_{c0}) to transition mid-point (T_c), the magnitude of the order parameter assumes an identical non-zero value in each grain. But however, the phase ϕ of the order parameter fluctuates from grain to grain. The fluctuations in the phase of the order parameter give rise to excess conductivity ($\Delta\sigma'$) in the above temperature range, and is given by [248],

$$\Delta\sigma' = \frac{1}{\rho(T)} - \frac{1}{\rho(T_c)} \tag{3.15}$$

where $\rho(T_c)$ is the measured resistivity at T_c. The $\Delta\sigma'$ varies as,

$$\Delta\sigma' \propto \left(\frac{T - T_{c0}}{T_{c0}}\right)^{-\gamma} \tag{3.16}$$

where γ is the critical exponent of excess conductivity.

Excess conductivity analysis in the paracoherence regime has been carried out on a few selected samples as given below. $\Delta\sigma'$ data have been calculated both in the absence and presence of 1 Tesla magnetic field. The detailed analysis are described below.

3.3.1. Excess conductivity in zero field case

In zero field case, eight samples have been taken up for the analysis of excess conductivity in the paracoherene regime. They are as follows,

(i) $La_{1.8}Y_{0.2}Ba_2CaCu_5O_z$ (Sample B)

(ii) $La_{1.2}Y_{0.8}Ba_2CaCu_5O_z$ (Sample E)

(iii) $LaYBa_2CaCu_5O_z$ (Sample F)

(iv) $La_{1.8}Y_{0.2}Ba_2CaCu_5O_z$ + 5 wt % of Ag (Sample B1)

(v) $La_{1.2}Y_{0.8}Ba_2CaCu_5O_z$ + 5 wt % of Ag (Sample E1)

(vi) $LaYBa_2CaCu_5O_z$ + 5 wt % of Ag (Sample F1)

(vii) $La_{1.6}Y_{0.4}Ba_2Ca_{0.8}Cu_{4.8}O_z$ (Sample H)

(viii) $La_{1.6}Y_{0.4}Ba_2Ca_{0.8}Cu_{4.8}O_z$ + 5 wt % of Ag (Sample H1)

The excess conductivity ($\Delta\sigma'$) in the paracoherence region was calculated in the absence of magnetic field using eqn. (3.15), i.e. by subtracting the conductivity at T_c from the measured conductivity at a given temperature. Plot of ln $[\Delta\sigma'/\sigma(T_c)]$ versus ln(ε') is shown in Fig.3.20 for sample E. Here $\sigma(T_c)$ is the conductivity at T_c, $\varepsilon' = (T-T_{c0})/T_{c0}$, is the reduced temperature and T_{c0} is the zero resistivity transition temperature. Here, the plot shows two linear regions with different slopes. The experimental data in the range of lnε = -4.21 to -2.49 were fitted to the linear equation and the fitted data are shown as solid line. The value of critical exponent γ is found to be 1.09 and it is comparable to the value of 1.33 predicted for 3D XY ferromagnet. Thus in the low temperature region (LTR), i.e. in the vicinity of T_{c0}, γ value is comparable to that of 3D XY ferromagnet. The linear behavior observed in the high temperature region (HTR) (lnε = -2.17 to -1.75) was also fitted and the fitted data are shown as dashed lines. The fitted value of γ in the HTR is found to be 2.29 and it is comparable to the value predicted for random site diluted Heisenberg model for ferromagnetism [251] or in other words disordered ferromagnet. The above value is also close to 2.7 reported by several groups on polycrystalline superconducting materials [249, 256]. Thus the above material exhibits cross over from ordered phase fluctuations to disordered phase fluctuations. The $\Delta\sigma'$ data of other samples were also fitted in the LTR & HTR and, they are shown in Figs.3.21 & 3.22. The critical exponents along with the rmsd values are given in Table 3.6.

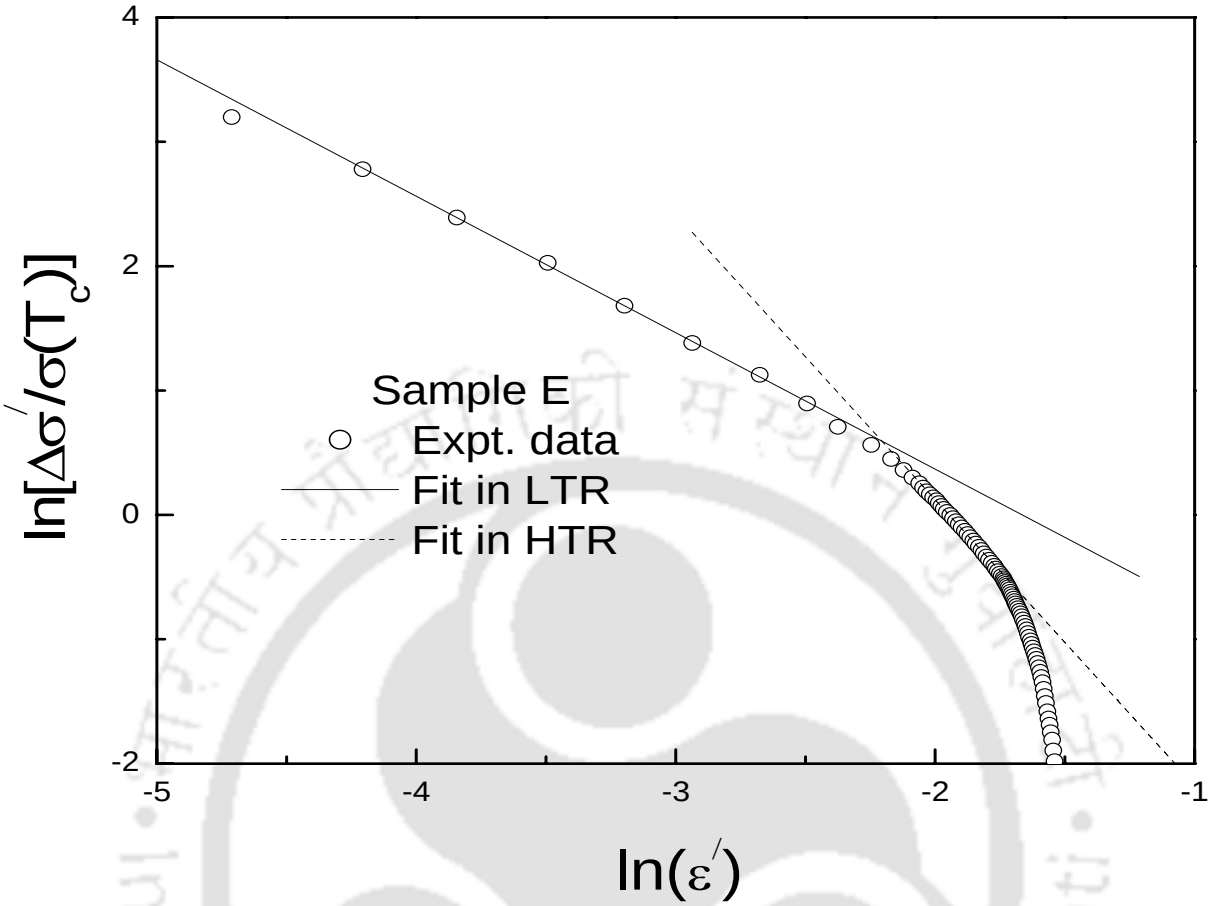

Fig. 3.20. Plots of ln ($\Delta\sigma'/\sigma(T_c)$) versus ln($\varepsilon'$) for sample E. The experimental data are shown as circles. The solid and dashed lines represent the fitted data in the low temperature region (LTR) and high temperature region (HTR) respectively.

All the samples show ordered phase fluctuations in the low temperature region i.e. close to T_{c0} with a crossover to disordered phase fluctuations in the high temperature region i.e. close to T_c. The cross over temperature T_{cr}, from ordered phase fluctuations to disorder phase fluctuations was determined from the plots of $\ln\Delta\sigma'$ versus $\ln\varepsilon'$. The disordered phase fluctuations appear for a much wider temperature region in the case of Ag doped samples compared to that of pure samples. Unlike the pure sample, where the intergranular weak link matrix completely turns into superconducting state as the temperature is lowered, the presence of Ag dilutes the superconducting matrix to some extent, thereby causing disordered phase fluctuations in much wider temperature region. The above argument may appear to contradict the observed enhanced T_{c0} in Ag doped sample and this could be due to the indirect effect of Ag which helps in oxidation of weak link network and thereby enhanced T_{c0}. This property of Ag

has been reported in literature [350]. However, for sample H1, the $\Delta\sigma'$ values falls rather sharply with increase in temperature leaving a small high temperature linear region. The values of T_{c0}, T_{cr}, range of fits and the fitted values of γ are given in Table 3.6.

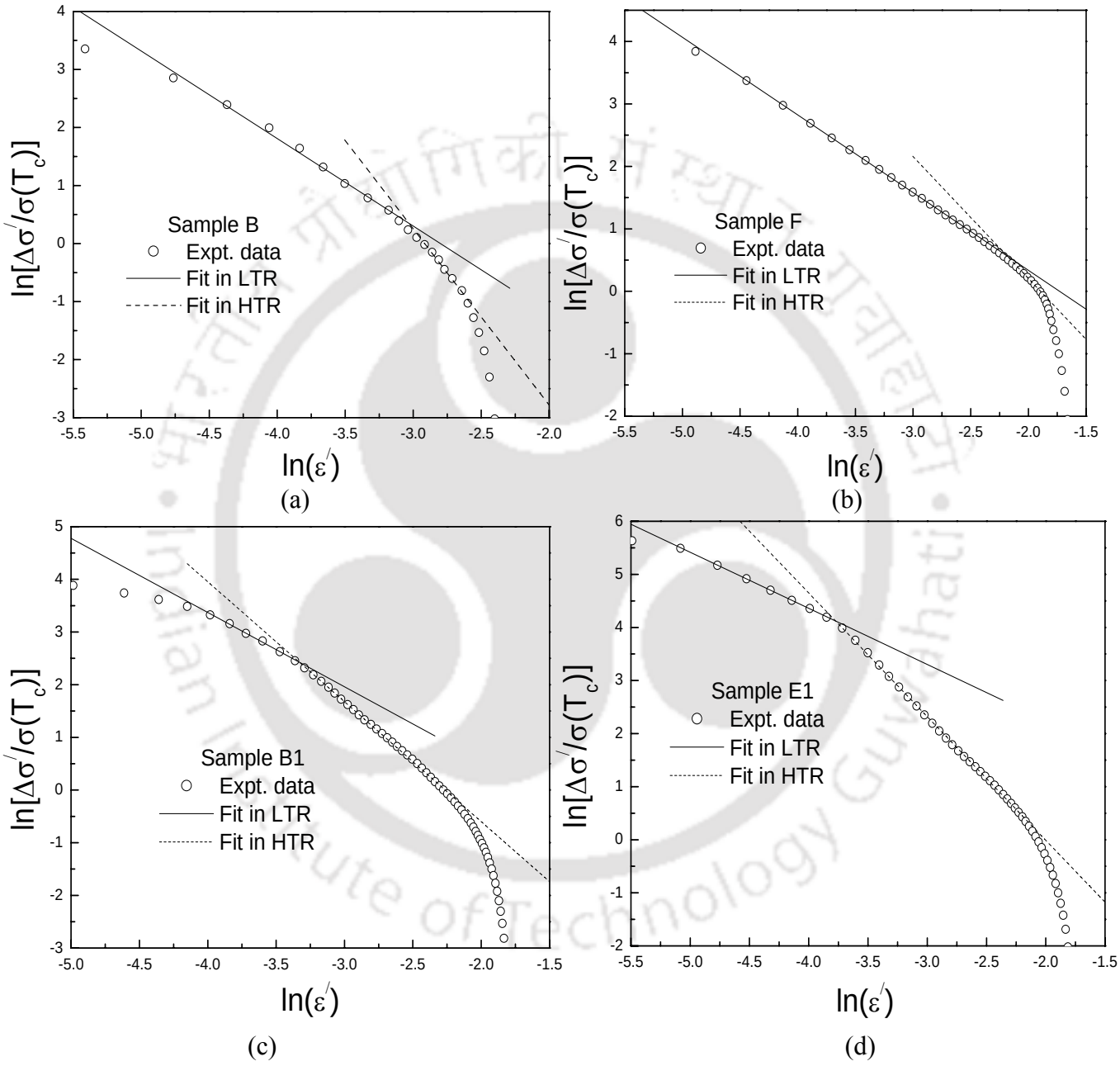

Fig. 3.21. Plots of $\ln(\Delta\sigma'/\sigma(T_c))$ versus $\ln(\varepsilon')$ for (a) sample B, (b) sample F, (c) sample B1 and (d) sample E1. The experimental data are shown as circles. The solid and dashed lines represent the fitted data in the low temperature region (LTR) and high temperature region (HTR) respectively.

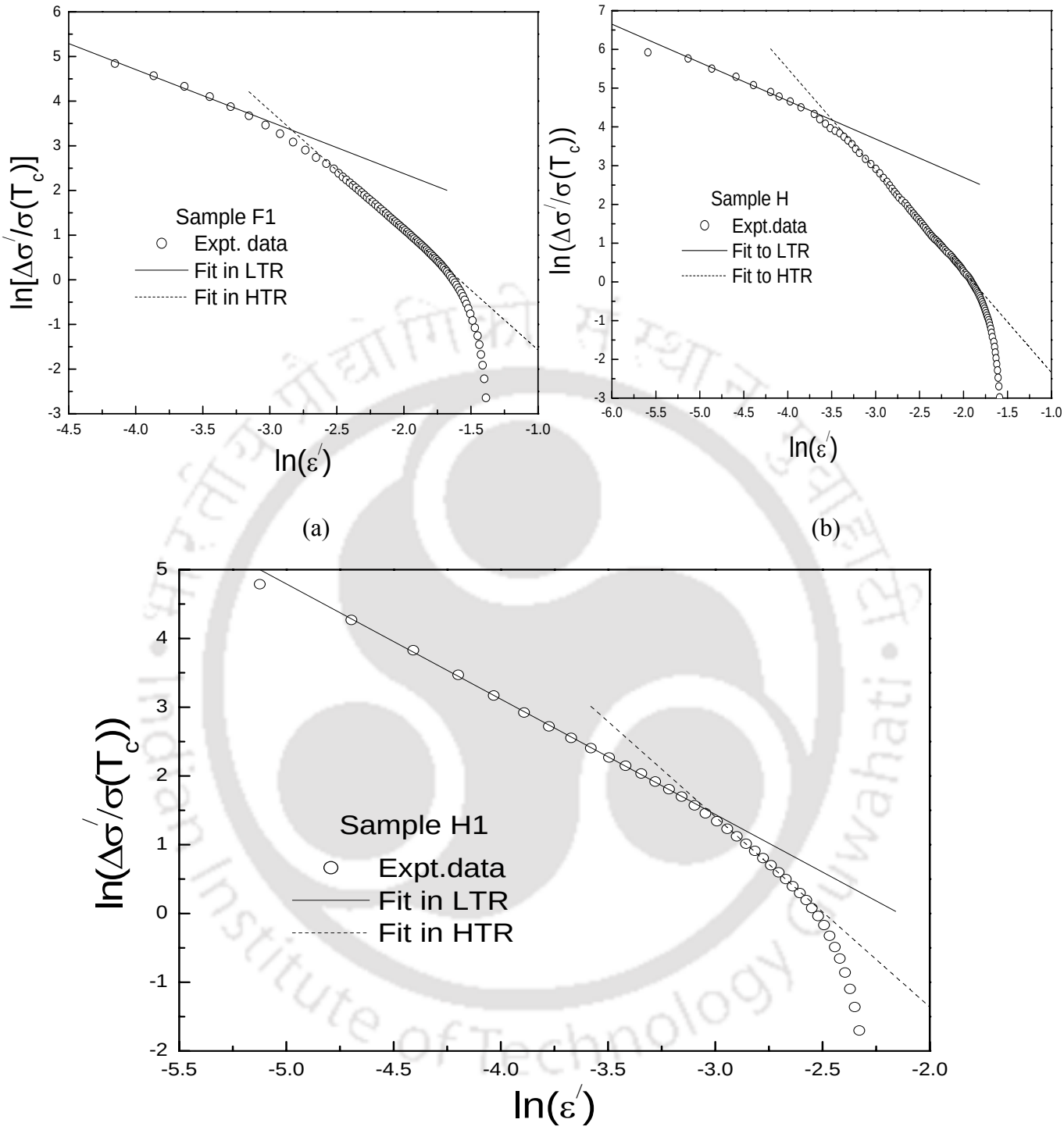

Fig. 3.22. Plots of $\ln(\Delta\sigma'/\sigma(T_c))$ versus $\ln(\varepsilon')$ for (a) sample F1, (b) sample H and (c) sample H1. The experimental data are shown as circles. The solid and dashed lines represent the fitted data in the low temperature region (LTR) and high temperature region (HTR) respectively.

To cross check the critical exponent of phase fluctuations, $[\Delta\sigma'/\sigma(T_c)]^{-1/\gamma}$ versus temperature have been plotted by assuming that $\gamma = 1.33$ and 2.7 respectively. Fig.3.23 (a) shows the plot with $\gamma = 1.33$ for sample E. One can see that the plot exhibits linear behavior only in the LTR confirming the earlier analysis. The linear line is extrapolated down to the temperature axis intercept and it corresponds to Para coherence to coherence transition temperature, T_{c0}' and this value is comparable to T_{c0}. The value of T_{c0}' is given in Table 3.6. The extrapolation of HTR leads a temperature intercept, which is considerably different from T_{c0}. Thus in the low temperature region, the critical exponent is close to 1.33. Fig.3.23 (b) shows the plot with $\gamma = 2.7$, unlike the earlier plot, here the linear behavior is observed in the high temperature region. The intercept of extrapolated linear line from HTR to the temperature axis is taken as T_{c0}'' and it is tabulated in Table 3.6. Here T_{c0}'' value is comparable to T_{c0} and, it confirms that the critical exponent is close to 2.7 in HTR.

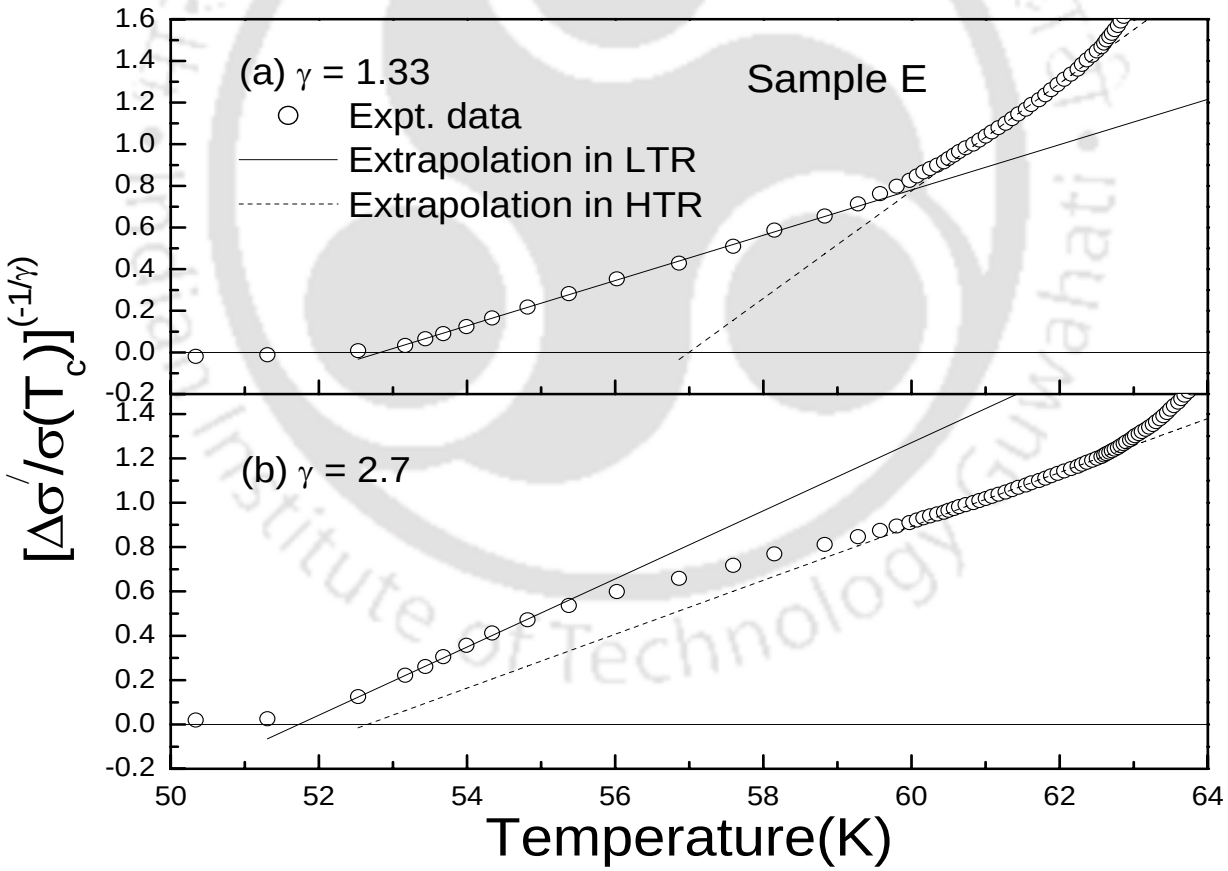

Fig.3.23. Plots of $[\Delta\sigma'/\sigma(T_c)]^{(-1/\gamma)}$ vs. temperature by assuming (a) $\gamma = 1.33$ and (b) $\gamma = 2.7$ for sample E. The open circles show the experimental data, whereas the solid line and dashed lines show the extrapolation of linear behavior in low temperature (LTR) and high temperature regions (HTR) respectively.

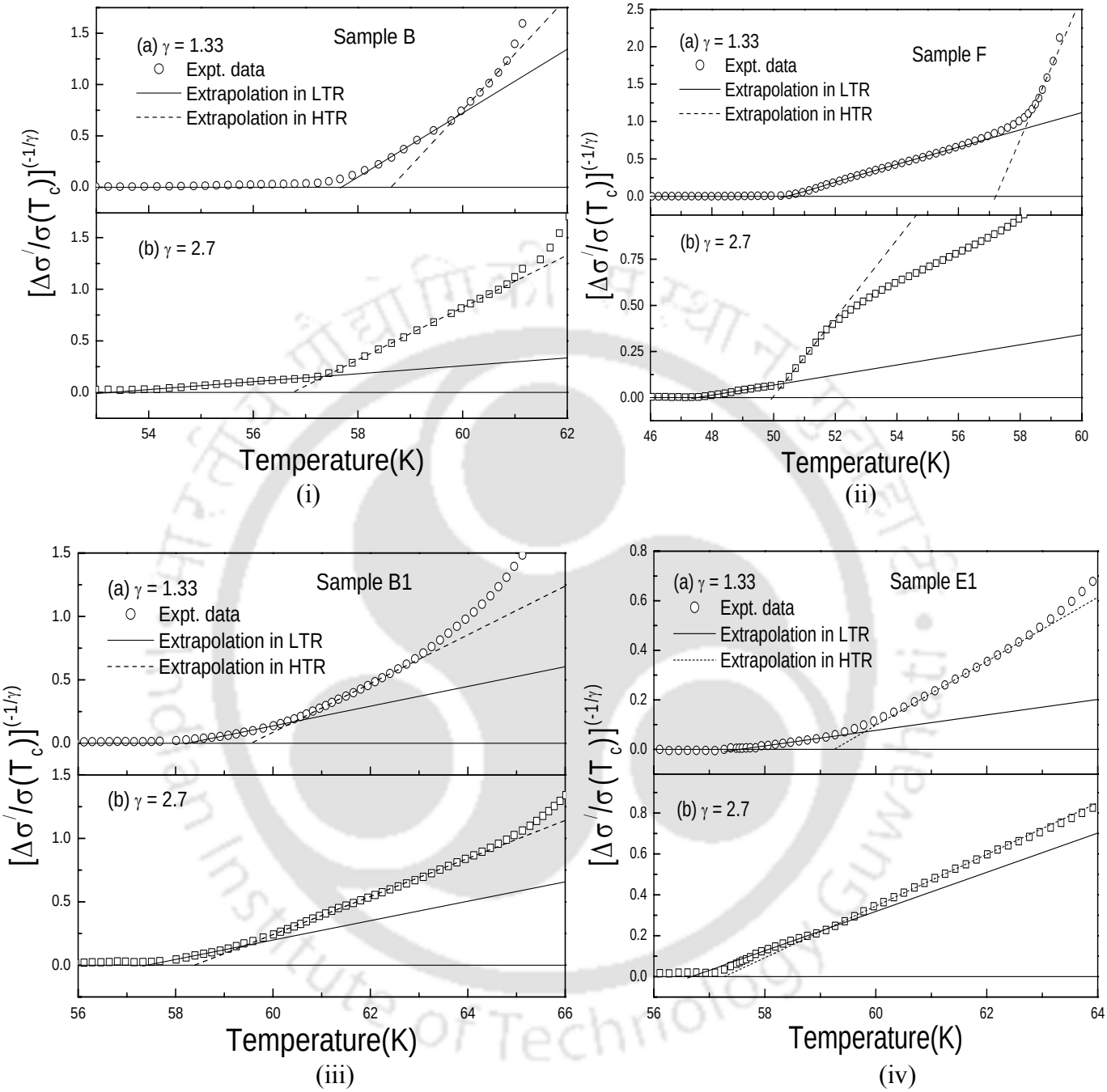

Fig.3.24. Plots of $[\Delta\sigma'/\sigma(T_c)]^{(-1/\gamma)}$ vs. temperature by assuming (a) $\gamma = 1.33$ and (b) $\gamma = 2.7$ for (i) sample B, (ii) sample F, (iii) sample B1 and (iv) sample E1. The open circles and squares show the experimental data, whereas the solid line and dashed lines show the extrapolation of linear behavior in low temperature (LTR) and high temperature regions (HTR) respectively.

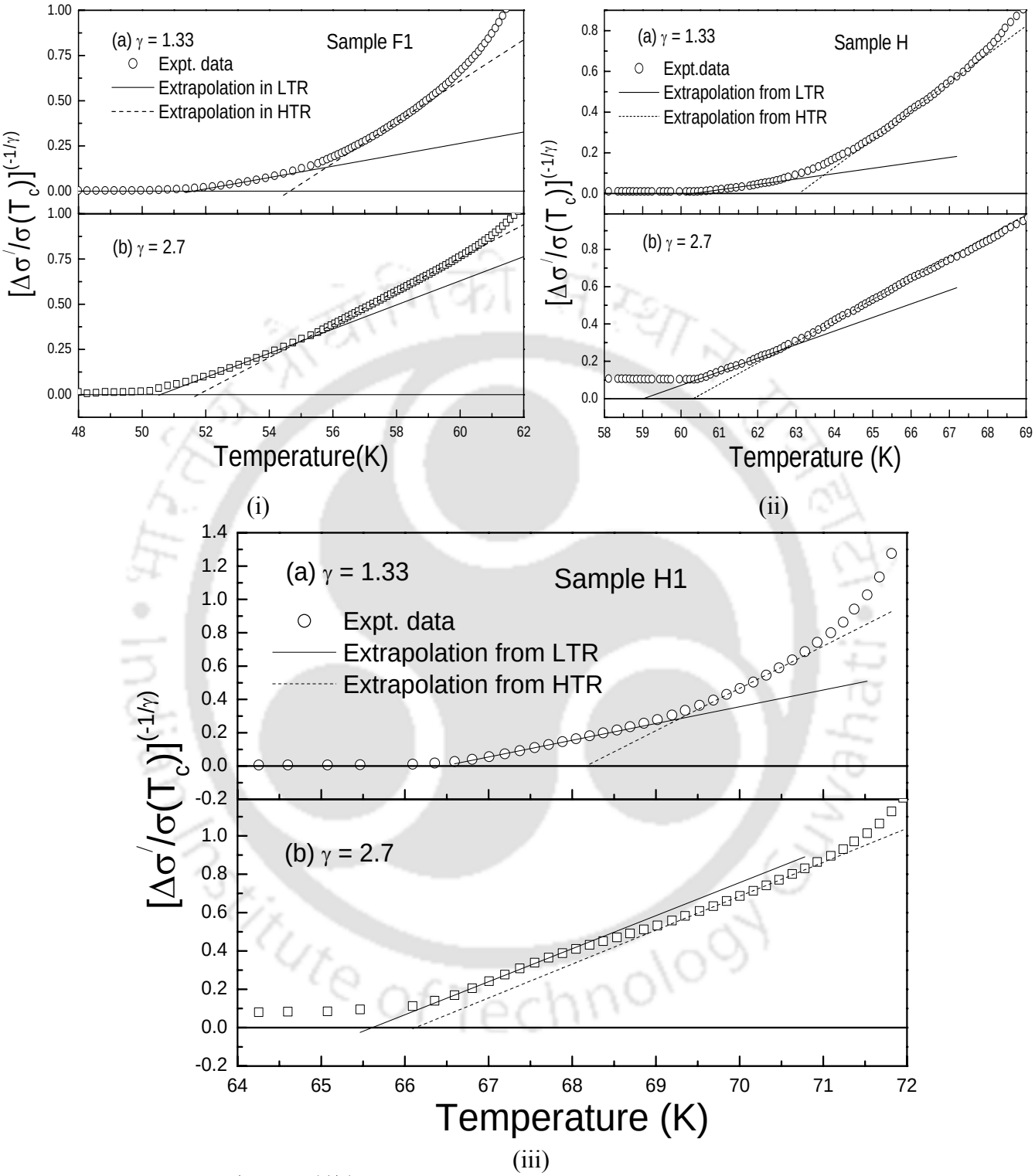

Fig.3.25. Plots of $[\Delta\sigma'/\sigma(T_c)]^{(-1/\gamma)}$ vs. temperature by assuming (a) $\gamma = 1.33$ and (b) $\gamma = 2.7$ for (i) sample F1, (ii) sample H and (iii) sample H1. The open circles and squares show the experimental data, whereas the solid line and dashed lines show the extrapolation of linear behavior in low temperature (LTR) and high temperature regions (HTR) respectively.

Similar exercise was carried out on other samples as shown in Figs. 3.24 & 3.25 of this series and the obtained values of $T_{c0}^{/}$ and $T_{c0}^{//}$ are given in Table 3.7. They confirm that all the samples exhibit a cross over from ordered phase fluctuations to disordered phase fluctuations.

Table 3.6. Parameters obtained from the analysis of excess conductivity in the paracoherence region of La-Ba-Ca-Cu-O superconductors in the absence of magnetic field.

Sample Name	T_{c0} (K)	T_{cr} (K)	LTR				HTR			
			Range of fit (in $\ln(\varepsilon^{/})$)	γ	rmsd (%)	$T_{c0}^{/}$ (K) γ =1.33	Range of fit (in $\ln(\varepsilon^{/})$)	γ	rmsd (%)	$T_{c0}^{//}$ (K) γ = 2.7
B	57.4	T_{c0}+2.7	-4.05 to -3.10	1.50	2.88	57.6	-2.86 to -2.59	3.03	2.35	56.9
E	53.2	T_{c0}+5.6	-4.21 to -2.49	1.09	0.85	52.8	-2.17 to -1.75	2.29	2.06	52.7
F	50.4	T_{c0}+5.7	-4.44 to -2.71	1.24	0.25	50.2	-2.07 to -1.89	1.95	2.53	50.0
B1	58.0	T_{c0}+2.0	-3.98 to -3.36	1.41	0.67	58.0	-3.36 to -2.08	2.27	2.66	58.4
E1	57.8	T_{c0}+1.2	-5.30 to -4.03	1.05	0.11	57.5	-3.86 to -2.21	2.32	1.26	57.3
F1	51.4	T_{c0}+3.0	-4.15 to -3.15	1.16	1.09	51.6	-2.52 to -1.68	2.68	1.83	51.8
H	60.3	T_{c0}+1.8	-5.21 to -3.70	1.00	0.63	60.3	-3.18 to -1.92	2.61	1.45	60.3
H1	66.2	T_{c0}+3.1	-4.68 to -3.15	1.67	0.56	66.4	-2.94 to -2.59	2.76	1.92	66.1

3.3.2. Excess conductivity in the presence of magnetic field (1T)

Excess conductivity in the paracoherence region due to the phase fluctuations in the phase of order parameters has been studied on six samples in the presence of magnetic field, which are mentioned below.

(i) $La_{1.8}Y_{0.2}Ba_2CaCu_5O_z$ (Sample B)

(ii) $La_{1.2}Y_{0.8}Ba_2CaCu_5O_z$ (Sample E)

(iii) $LaYBa_2CaCu_5O_z$ (Sample F)

(iv) $La_{1.8}Y_{0.2}Ba_2CaCu_5O_z$ + 5 wt % of Ag (Sample B1)

(v) $La_{1.2}Y_{0.8}Ba_2CaCu_5O_z$ + 5 wt % of Ag (Sample E1)

(vi) $LaYBa_2CaCu_5O_z$ + 5 wt % of Ag (Sample F1)

In the presence of magnetic field (1T), the excess conductivity in the paracoherence region was calculated using the eqn. (3.15). Here $\rho(T)$, $\rho(T_c)$, T_c & T_{c0} are taken from the temperature variation of resistivity measured in the presence of magnetic field. Plots of $\ln[\Delta\sigma^{/}/\sigma(T_c)]$ versus $\ln(\varepsilon^{/})$ are shown in Fig.3.26 for samples B & E.

Unlike the zero field case, here the plots show only one linear region. The experimental data were fitted to linear equation in this region and the fitted data are shown as solid lines. The

values of critical exponent γ are found to be 1.25 & 1.16 for samples B and E respectively and these are comparable to the value of 1.33. Thus these samples show only ordered phase fluctuations.

Similarly, the experimental data were fitted for other samples in the presence of magnetic field as shown in the Fig. 3.27 and the critical exponents were estimated. The fitted parameters along with the rmsd values are given in Table 3.7. All the samples exhibit only ordered phase fluctuations in the presence of magnetic field. It may be noted that the above critical exponent is observed in the temperature region close to T_c and in the same temperature region, zero field excess conductivity data falls rather sharply without showing any linear behavior. In the above temperature region and in the presence of magnetic field, there is a possibility of some of the defects within the grains turning into normal state leading to intragranular Josephson coupling behaving like ordered phase fluctuations.

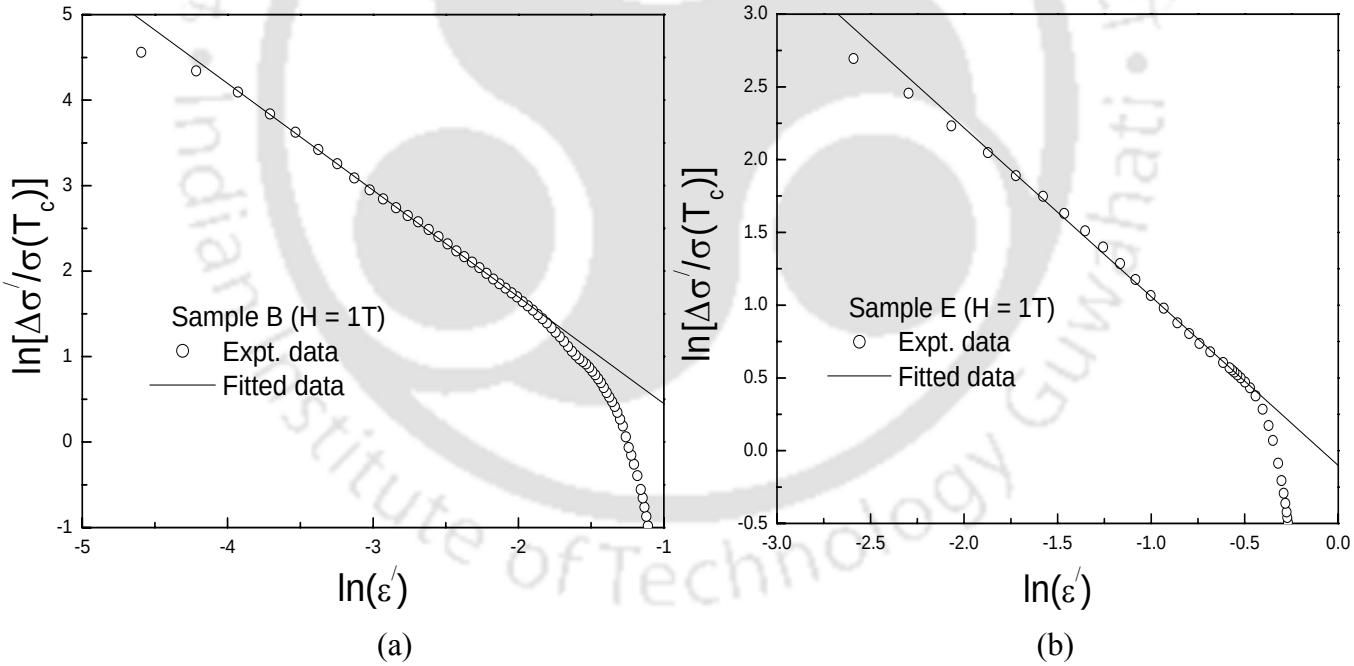

Fig.3.26. Plots of $\ln(\Delta\sigma'/\sigma(T_c))$ versus $\ln(\varepsilon')$ for (a) Sample B and (b) Sample E in presence of magnetic field (1T). The experimental data are shown as circles and the fitted data are shown as solid lines.

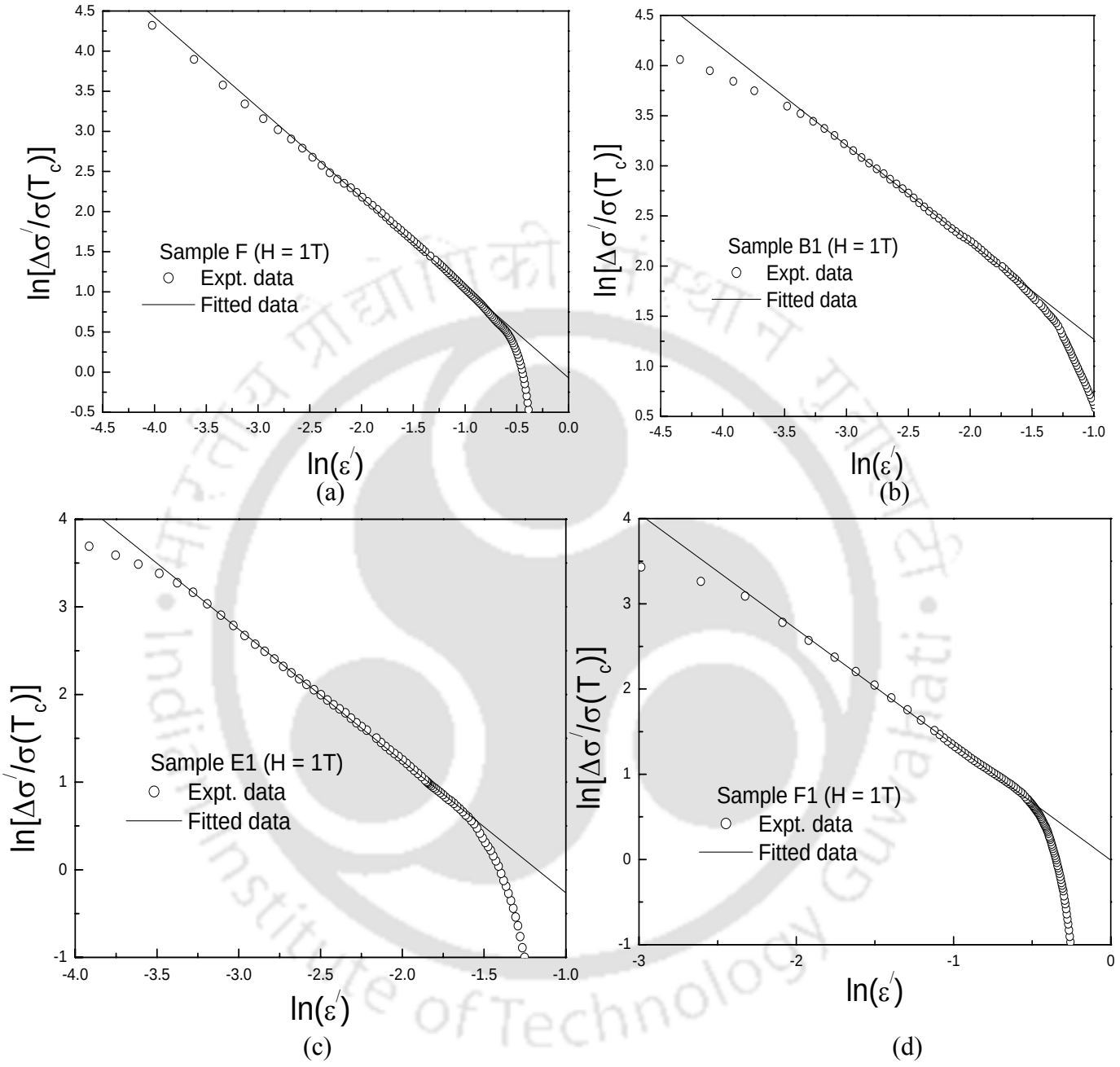

Fig.3.27. Plots of $\ln(\Delta\sigma'/\sigma(T_c))$ versus $\ln(\varepsilon')$ for (a) Sample F, (b) Sample B1, (c) Sample E1 and (d) Sample F1 in the presence of magnetic field (1T). The experimental data are shown as circles and the fitted data are shown as solid lines.

To cross check the critical exponent of phase fluctuations, $[\Delta\sigma'/\sigma(T_c)]^{-1/\gamma}$ versus temperature have been plotted by assuming that $\gamma = 1.33$ for samples B & E as shown in Fig.

3.28. One can see that the plots exhibits linear behavior for a wide temperature range. $T_{c0}^{/}$ values are determined by extrapolating the linear line and they are comparable to their T_{c0} values. The above procedure was repeated by taking $\gamma = 2.7$ but no linear behavior has been observed. For comparison, one plot is shown in Fig. 3.28 by assuming $\gamma = 2.7$ for sample E and one can see that no linearity is observed.

Similar cross checking has been done by assuming that $\gamma = 1.33$ for all other samples, which are shown in Fig. 3.29. The $T_{c0}^{/}$ values for all samples have been obtained in the presence of magnetic field and are given in Table 3.7.

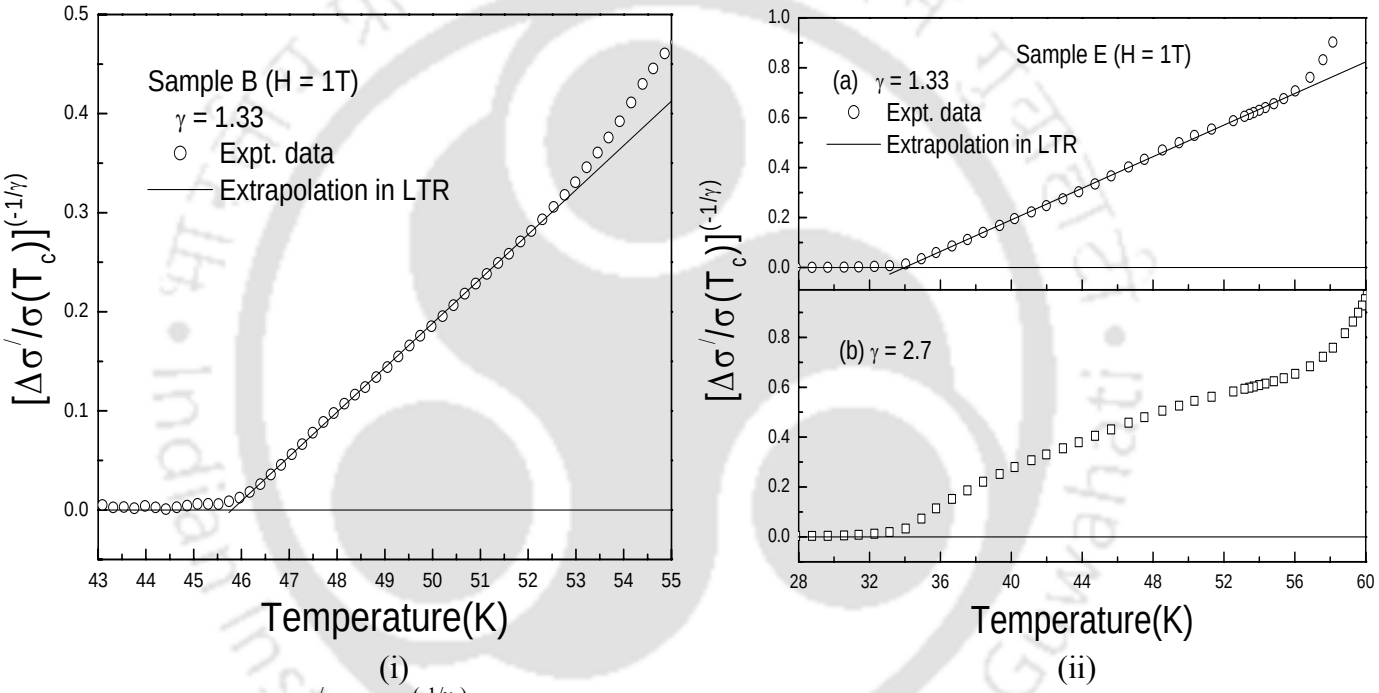

Fig. 3.28. Plots of $[\Delta\sigma^{/}/\sigma(T_c)]^{(-1/\gamma)}$ vs. temperature, (i) by assuming $\gamma = 1.33$ for sample B and (ii) by assuming $\gamma = 1.33$ and 2.7 for Sample E, in presence of magnetic field (1T). The circles and squares show the experimental data, and the solid line shows the extrapolation of linear region.

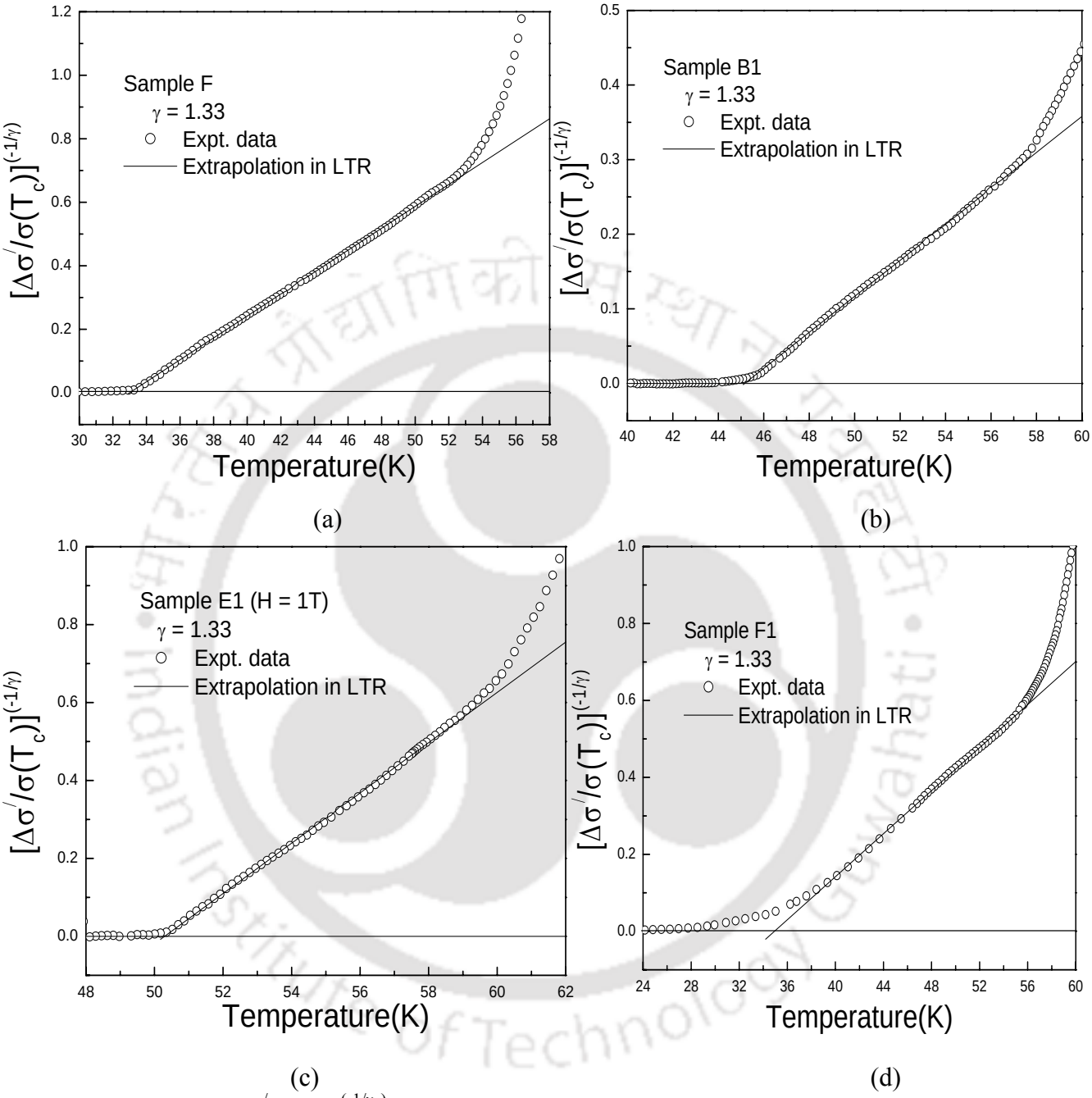

Fig. 3.29. Plots of $[\Delta\sigma'/\sigma(T_c)]^{(-1/\gamma)}$ vs. temperature by assuming $\gamma = 1.33$ for (a) sample F, (b) sample B1, (c) sample E1 and (d) sample F1 in presence of magnetic field (1T). The circles show the experimental data, and the solid line shows the extrapolation of linear region.

Thus in the presence of magnetic field, the excess conductivity in the paracoherence regime show only ordered phase fluctuations and it can be explained on the basis of intragranular Josephson coupling.

Table 3.7. Parameters obtained from the analysis of excess conductivity in the paracoherence region of La-Ba-Ca-Cu-O superconductors in the presence of 1T magnetic field.

Sample Name	T_{c0} (K)	Range of fit (In lnε)	γ	rmsd %	$T_{c0}^{/}$ (K) γ= 1.33
B	45.5	-3.92 to -2.00	1.25	0.49	45.7
E	34.1	-2.30 to -0.46	1.16	1.92	34.0
F	33.9	-2.68 to -0.83	1.12	1.29	33.5
B1	45.3	-3.26 to -1.59	0.97	0.38	45.2
E1	49.7	-3.27 to -1.68	1.50	0.82	50.2
F1	35.0	-2.32 to -0.72	1.35	0.73	34.9

To summarize, I have carried out electrical resistivity and magneto-resistivity measurements on nine different samples in pure and Ag doped $(La_{1-x}Y_x)_2Ba_2CaCu_5O_z$ and underdoped $(La_{1-x}R_x)_2Ba_2Ca_{4x}Cu_{4+4x}O_z$ (R = Y, Gd) series. They have been analyzed in terms of excess conductivity ($\Delta\sigma$) and fluctuation magneto-conductivity ($\Delta\sigma_H$) due to thermo-dynamic fluctuations in the amplitude of order parameter. The $\Delta\sigma$ analysis shows that these materials exhibit 2D fluctuations in the mean field regime. The coherence length along c-direction is found to be mostly in the range of 0.30 to 0.77 Å. The contribution of MT term to $\Delta\sigma$ was found to be insignificant with a strong pair breaking effect and phase breaking time, τ_ϕ(100 K) is found to be in the order of 10^{-16}s. The above behavior is in contrast to the 2D to 3D dimensional cross-over observed in $YBa_2Cu_3O_7$ superconductors in MFR. This could be due to small $\xi_c(0)$ and large anisotropy in the present series of superconductors with tetragonal crystal structure. Such a 2D fluctuations have been reported in other superconductors, with tetragonal crystal structure, such as Bi-Sr-Ca-Cu-O and Tl-Ba-Ca-Cu-O systems.

I have also carried out the analysis of magneto-conductivity of above samples, at an applied magnetic field of 1T. The advantage of magneto-conductivity is that there is no need of estimation of normal state conductivity. The $\Delta\sigma_H$ data were analyzed by using AL and MT terms and by taking into account both Orbital and Zeeman contributions. The values of $\xi_c(0)$ and

τ_ϕ(100 K) are comparable to those obtained from $\Delta\sigma$ analysis and confirms the consistency of analysis. The value $\xi_{ab}(0)$ is found to be in the range of 14 to 34 Å and are comparable to those reported for $YBa_2Cu_3O_7$ samples.

Moreover, I have carried out excess conductivity analysis in the paracoherence regime, i.e. $T_c(0)$ to T_c, where there is fluctuations in the phase of the order parameter. These analysis have been carried out on pure and 5 wt % Ag doped $(La_{1-x}Y_x)_2Ba_2CaCu_5O_z$ superconductors in the absence and presence of 1T magnetic field. In the absence of magnetic field, these materials exhibit cross over from ordered phase fluctuations with the critical exponent comparable to that of pure 3D XY ferromagnet to disordered phase fluctuations with the critical exponent comparable to that of disordered 3D Heisenberg ferromagnetic system. In Ag doped samples, disordered fluctuations are observed for a wider temperature region. This has been explained on the basis of dilution of superconducting matrix by the presence of Ag. In the presence of magnetic field, ordered phase fluctuations have been observed close to T_c and they are attributed to intragranular Josephson coupling. The critical exponent is found to be comparable to that of $YBa_2Cu_3O_7$ sample reported in literature [248]. Excess conductivity in the paracoherence region also has been studied for some samples of under doped series, in the absence of magnetic field. These samples also show cross over from ordered phase fluctuations to disordered phase fluctuations.

AC SUSCEPTIBILITY STUDIES

The detailed review of various theoretical and experimental studies of ac susceptibility using different critical state models have been presented in section 1.5. In this chapter, ac susceptibility data have been analyzed on a few selected single phase samples of pure and 5 wt% of Ag doped $(La_{1-x}Y_x)_2Ba_2CaCu_5O_z$ superconductors for $(0 < x < 0.5)$ and also on some under-doped samples of the above series. Temperature dependence of ac susceptibility measured at different ac field amplitudes and field variation of susceptibility measured at different temperatures have been used for the above analysis. The field dependence of ac susceptibility data have been analyzed using Kim critical state model. The material dependent parameters like critical current density, $J_c(T)$ as a function of temperature and effective volume fraction of superconducting grains have been estimated for these samples.

We have calculated theoretical intergranular matrix susceptibility using the following equations,

$$\chi_m^{/} = \frac{2}{\pi H_m}\int_0^{\pi} M_m(\theta)Cos(\theta)d\theta \qquad (4.1)$$

$$\chi_m^{//} = \frac{2}{\pi H_m}\int_0^{\pi} M_m(\theta)Sin(\theta)d\theta \qquad (4.2)$$

where $M_m(\theta)$ is the magnetization of intergranular matrix derived from Kim critical state model [286]. H_m is the amplitude of the applied ac field.

4.1. Kim Theoretical Susceptibility Calculations

We have derived expressions for real and imaginary components of intergranular matrix susceptibility ($\chi_m^{/}$ and $\chi_m^{//}$) using the expressions for magnetization derived from Kim model. Chen and Goldfarb [286] have derived expressions for magnetization, for an orthorhombic sample geometry with a cross section 2a × 2b using Kim critical state model. The expressions for magnetization as a function of applied field at low, medium and high fields are given in eqns.(1.54) to (1.64). In low field case, the amplitude of applied field (H_m) is less than or equal to the full penetration field (H_p); ($H_m \leq H_p$). For $H_m > H_p$, there are two cases namely high field and medium field. In high field case, the reverse super current completely penetrates to the center of

the superconducting sample before the applied field, H has decreased to 0 and the field amplitude $H_m > H_m^* = (H_0^2+4ka)^{1/2}-H_0$. In the medium field case, the reverse super current does not completely penetrate to the center of the sample even when H is reduced to 0, and this is in the region of $H_p \leq H_m \leq H_m^*$.

The magnetization expressions for low field case are given in eqns.(1.54) and (1.55), in two stages namely Stage I ($0 < H < H_m$) and Stage 2 ($-H_m < H < 0$). Eqns.(1.54) and (1.55) were rearranged by substituting the expressions for S_1, S_3, x_m, x_1, x_2, x_3, R_2, R_3, Q_2, Q_3, Q_4, Q_5 and Q_6. The expressions for R_2 and R_3 were rearranged such that Binomial expansion can be applied and the rearranged expressions are described in Appendix-A. Binomial expansion for R_2^3 and R_3^3 were carried out up to the third order. AC field (H) dependence of magnetization was transformed into a function of phase angle (θ) using the relation $H = H_m\text{Cos}(\theta)$. By substituting the rearranged expressions for magnetization in eqns. (4.1) and (4.2) and by carrying out analytical integrations with respect to θ, by employing Mathematica software, the expressions for $\chi_m^{/}$ and $\chi_m^{//}$ were obtained for the stages I and II. During the integrations, the field limits H_m, 0 and $-H_m$ were taken in terms of phase angles 0, π/2 and π respectively. The obtained expressions for $\chi_m^{/}$ at stages I and II were added to get the final expression for $\chi_m^{/}$ at low field and similarly, the final expression for $\chi_m^{//}$ was obtained. The expressions for $\chi_m^{/}$ and $\chi_m^{//}$ were deduced for orthorhombic sample geometry of dimensions a and b ($b \geq a$). Also, these expressions were converted into a function of full penetration field H_p and, a parameter p using the following eqns.[286],

$$p = \frac{(2ka)^{1/2}}{H_0} \tag{4.3}$$

and

$$H_p = H_0\left[\left(1+p^2\right)^{1/2}-1\right] \tag{4.4}$$

Here H_0 and k are positive constants and '*a*' is the half thickness of the orthorhombic sample. The expressions for $\chi_m^{/}$ and $\chi_m^{//}$ in the low field region are given as follows,

$$\chi_m' = \left[-1-\frac{8a'}{3p^4}-\frac{2}{p^2}-\frac{2a'}{p^2}+\frac{a'}{8p^4p_2^3}-\frac{4}{15p^2p_2^3\pi}-\frac{4a'}{15p^2p_2^3\pi}\right]+\left[\frac{-\frac{1}{16p^2p_1p_2^3}-\frac{a'}{16p^2p_1p_2^3}}{hmp}\right]$$
$$+\left[\begin{array}{l}\frac{a'p_1}{4p^4p_2^3}-\frac{13p_1}{128p^2p_2^3}-\frac{13a'p_1}{128p^2p_2^3}+\frac{3a'p_1}{4p^4p_2}-\frac{p_1}{2p^2p_2}-\frac{a'p_1}{2p^2p_2}+\frac{2p_1p_2}{p^2}\\ +\frac{2a'p_1p_2}{p^2}-\frac{32a'p_1}{9p^4\pi}-\frac{8p_1}{3p^2\pi}-\frac{8a'p_1}{3p^2\pi}+\frac{8\Gamma p_1}{15p^4p_2^3\pi}\end{array}\right]hmp$$
$$+\left[\begin{array}{l}-\frac{a'p_1^2}{p^4}+\frac{13a'p_1^2}{64p^4p_2^3}+\frac{a'p_1^2}{p^4p_2}-\frac{4a'p_1^2p_2}{p^4}+\frac{16a'p_1^2}{15p^4p_2^3\pi}-\frac{43p_1^2}{420p^2p_2^3\pi}-\frac{43a'p_1^2}{420p^2p_2^3\pi}\\ +\frac{16a'p_1^2}{5p^4p_2\pi}-\frac{2p_1^2}{3p^2p_2\pi}-\frac{2a'p_1^2}{3p^2p_2\pi}+\frac{8p_1^2p_2}{3p^2\pi}+\frac{8a'p_1^2p_2}{3p^2\pi}\end{array}\right]hmp^2$$
$$+\left[\frac{23a'p_1^3}{96p^4p_2^3}+\frac{39a'p_1^3}{32p^4p_2}-\frac{4a'p_1^3p_2}{p^4}+\frac{8a'p_1^3p_2^3}{3p^4}-\frac{32a'p_1^3}{9p^4\pi}+\frac{43a'p_1^3}{210p^4p_2^3\pi}+\frac{4a'p_1^3}{3p^4p_2\pi}-\frac{16a'p_1^3p_2}{3p^4\pi}\right]hmp^3$$
$$+\left[-\frac{a'p_1^4}{3p^4}+\frac{59a'p_1^4}{315p^4p_2^3\pi}+\frac{43a'p_1^4}{35p^4p_2\pi}-\frac{16a'p_1^4p_2}{3p^4\pi}+\frac{32a'p_1^4p_2^3}{9p^4\pi}\right]hmp^4 \qquad (4.5)$$

and

$$\chi_m'' = \left[\frac{32a'}{3p^4\pi}-\frac{8}{p^2\pi}-\frac{8a'}{p^2\pi}-\frac{2a'}{15p^4p_2^3\pi}+\frac{1}{6p^2p_2^3\pi}+\frac{a'}{6p^2p_2^3\pi}+\frac{2}{3p^2p_2\pi}+\frac{2a'}{3p^2p_2\pi}\right]$$
$$+\left[\frac{-\frac{16}{3p^2p_1\pi}-\frac{16a'}{3p^2p_1\pi}}{hmp}\right]+\left[\begin{array}{l}\frac{16a'p_1}{p^4\pi}-\frac{16p_1}{3p^2\pi}-\frac{16a'p_1}{3p^2\pi}-\frac{5a'p_1}{9p^4p_2^3\pi}+\frac{p_1}{8p^2p_2^3\pi}+\frac{a'p_1}{8p^2p_2^3\pi}\\ -\frac{4a'p_1}{3p^4p_2\pi}+\frac{p_1}{2p^2p_2\pi}+\frac{a'p_1}{2p^2p_2\pi}\end{array}\right]hmp$$
$$+\left[\begin{array}{l}\frac{12a'p_1^2}{p^4\pi}-\frac{2p_1^2}{3p^2\pi}-\frac{2a'p_1^2}{3p^2\pi}-\frac{61a'p_1^2}{84p^4p_2^3\pi}+\frac{p_1^2}{15p^2p_2^3\pi}+\frac{a'p_1^2}{15p^2p_2^3\pi}-\frac{3a'p_1^2}{p^4p_2\pi}\\ +\frac{3p_1^2}{5p^2p_2\pi}+\frac{3a'p_1^2}{5p^2p_2\pi}+\frac{16a'p_1^2p_2}{3p^4\pi}-\frac{4p_1^2p_2}{p^2\pi}-\frac{4a'p_1^2p_2}{p^2\pi}+\frac{16p_1^2p_2^3}{3p^2\pi}+\frac{16a'p_1^2p_2^3}{3p^2\pi}\end{array}\right]hmp^2$$
$$+\left[\frac{16a'p_1^3}{5p^4\pi}-\frac{17a'p_1^3}{40p^4p_2^3\pi}-\frac{27a'p_1^3}{10p^4p_2\pi}+\frac{12a'p_1^3p_2}{p^4\pi}-\frac{32a'p_1^3p_2^3}{3p^4\pi}\right]hmp^3$$
$$+\left[-\frac{13a'p_1^4}{135p^4p_2^3\pi}-\frac{4a'p_1^4}{5p^4p_2\pi}+\frac{24a'p_1^4p_2}{5p^4\pi}-\frac{16a'p_1^4p_2^3}{3p^4\pi}\right]hmp^4$$

(4.6)

where $p_1 = \sqrt{(1+p^2)} - 1$,

$$p_2 = \sqrt{\frac{1}{{p_1}^2}\frac{{H_p}^2}{{H_m}^2} + \frac{1}{p_1}\frac{H_p}{H_m} + 1}$$

$$hmp = H_m / H_p$$

$$a' = a/b$$

In the high field case, ($H_m > H_m^*$) the expressions for χ_m' and χ_m'' were derived as follows. The expressions for magnetization in high field case are given in eqns.(1.57 to1.60) for four stages namely, Stage I ($H_{prh} < H < H_m$), Stage II ($0 < H < H_{prh}$), Stage III ($-H_p < H < 0$) and Stage IV ($-H_m < H < -H_p$). Here H_{prh} is the reverse full-penetration field for high H_m case and it is the field at which the reverse supercurrent completely penetrates to the center of the sample. H_{prh} is given in eqn.(1.61).

The magnetization expressions at all the four stages were rearranged by substituting the expressions for S_1, S_3, x_1, x_3, R_2, R_4, R_5, R_6, R_7, Q_2, Q_3, Q_4 and Q_5. Binomial expansion up to the third order was applied to the expressions for R_2^3, R_4^3, R_5^3, R_6^3 and R_7^3. The expressions for magnetization were transformed into a function of θ. By substituting the above obtained rearranged expressions for magnetization in eqns.(4.1) and (4.2) and by integrating as a function of θ, the expressions for χ_m' and χ_m'' were obtained for all the four stages. The expressions for H_{prh} and H_p were rearranged such that they can be converted into a function of θ for the limits of the integrations and they are as follows,

$$H_{prh} = H_m \left\{ -\frac{1}{p_1}\frac{H_p}{H_m} + \left[-\frac{2p^2}{{p_1}^2}\frac{{H_p}^2}{{H_m}^2} + \left(1 + \frac{1}{p_1}\frac{H_p}{H_m}\right)^2 \right]^{1/2} \right\} \qquad (4.7)$$

$$H_p = H_m \left(\frac{H_p}{H_m} \right) \qquad (4.8)$$

The limits of the integrations H_m, H_{prh}, 0, $-H_p$ and $-H_m$ were taken in terms of phase angles as 0, $\cos^{-1}\left\{ -\frac{1}{p_1}\frac{H_p}{H_m} + \left[-\frac{2p^2}{{p_1}^2}\frac{{H_p}^2}{{H_m}^2} + \left(1 + \frac{1}{p_1}\frac{H_p}{H_m}\right)^2 \right]^{1/2} \right\}$, $\pi/2$, $\cos^{-1}\left[-\frac{H_p}{H_m} \right]$ and π respectively.

Thus from the above integrations, the expressions for $\chi_m^{/}$ and $\chi_m^{//}$ were obtained for the stages I to IV. By adding all the expressions for $\chi_m^{/}$ obtained in the stages I, II, III and IV, the final expression for $\chi_m^{/}$ was obtained. Similarly the corresponding expression for $\chi_m^{//}$ was also obtained. The above obtained expressions were rearranged using eqns. 4.3 and 4.4. The resultant expressions for $\chi_m^{/}$ and $\chi_m^{//}$ for high field case are given in Annexure B and they are function of H_m/H_p, p and a/b.

In the medium field case, the expressions for $\chi_m^{/}$ and $\chi_m^{//}$ were calculated using the same procedure given in the high field case. The expressions for magnetizations in the medium field case are given in four stages namely Stage I ($0 < H < H_m$), Stage II ($H_{prm} < H < 0$), Stage III ($-H_p < H < H_{prm}$) and Stage IV ($-H_m < H < -H_p$). In Stage I, M(H) has the same expression as in the high field case except that the concerned field interval is ($H_m < H < 0$). For Stages III and IV, the magnetization expressions are same as high field case. The magnetization expression in Stage II is given in eqn. 1.63. H_{prm} is the reverse full penetration field in the medium field case, and the corresponding expression is given in eqn.1.64.

The expression for H_{prm} was rearranged such that it can be transformed into a function of θ as follows,

$$H_{prm} = H_m\left[\frac{1}{p_1}\frac{H_p}{H_m} - \left[\frac{2p^2}{p_1^2}\frac{H_p^2}{H_m^2} + \frac{2}{p_1^2}\frac{H_p^2}{H_m^2} - \left(\frac{1}{P_1}\frac{H_p}{H_m} + 1\right)^2\right]^{1/2}\right] \qquad (4.9)$$

The limits of the integrations H_m, 0, H_{prm}, $-H_p$ and $-H_m$ were taken in terms of phase angles as 0, π/2, $\cos^{-1}\left[\frac{1}{p_1}\frac{H_p}{H_m} - \left[\frac{2p^2}{p_1^2}\frac{H_p^2}{H_m^2} + \frac{2}{p_1^2}\frac{H_p^2}{H_m^2} - \left(\frac{1}{P_1}\frac{H_p}{H_m} + 1\right)^2\right]^{1/2}\right]$, $\cos^{-1}\left[-\frac{H_p}{H_m}\right]$ and π respectively. The expressions for $\chi_m^{/}$ and $\chi_m^{//}$ were obtained by adding their corresponding expressions in all four stages just like high field case. The resultant expressions for $\chi_m^{/}$ and $\chi_m^{//}$ for medium field case are function of H_m/H_p, p and a/b and, are given in Annexure B.

Typical plots of Kim theoretical $\chi_m^{/}$ and $\chi_m^{//}$ versus $\log(H_m/H_p)$ are shown in Fig. 4.1 for p = 5 and a/b = 1. The solid line, dashed lines and dash dotted lines are respectively the theoretical data

calculated in the low, medium and high field cases, and they form a continuous curve as shown in the figure. The $\chi_m^{//}$ versus $\log(H_m/H_p)$ plot exhibits a peak at $(H_m/H_p) = 1$ for p = 5, and the peak value is found to be ≈ 0.32. The corresponding $\chi_m^{/}$ value is -0.25. The values of maximum $\chi_m^{//}$ and the corresponding $\chi_m^{/}$ match with those reported by Chen et al.[266] for the respective a/b and p values and it shows the consistency of our theoretical calculations.

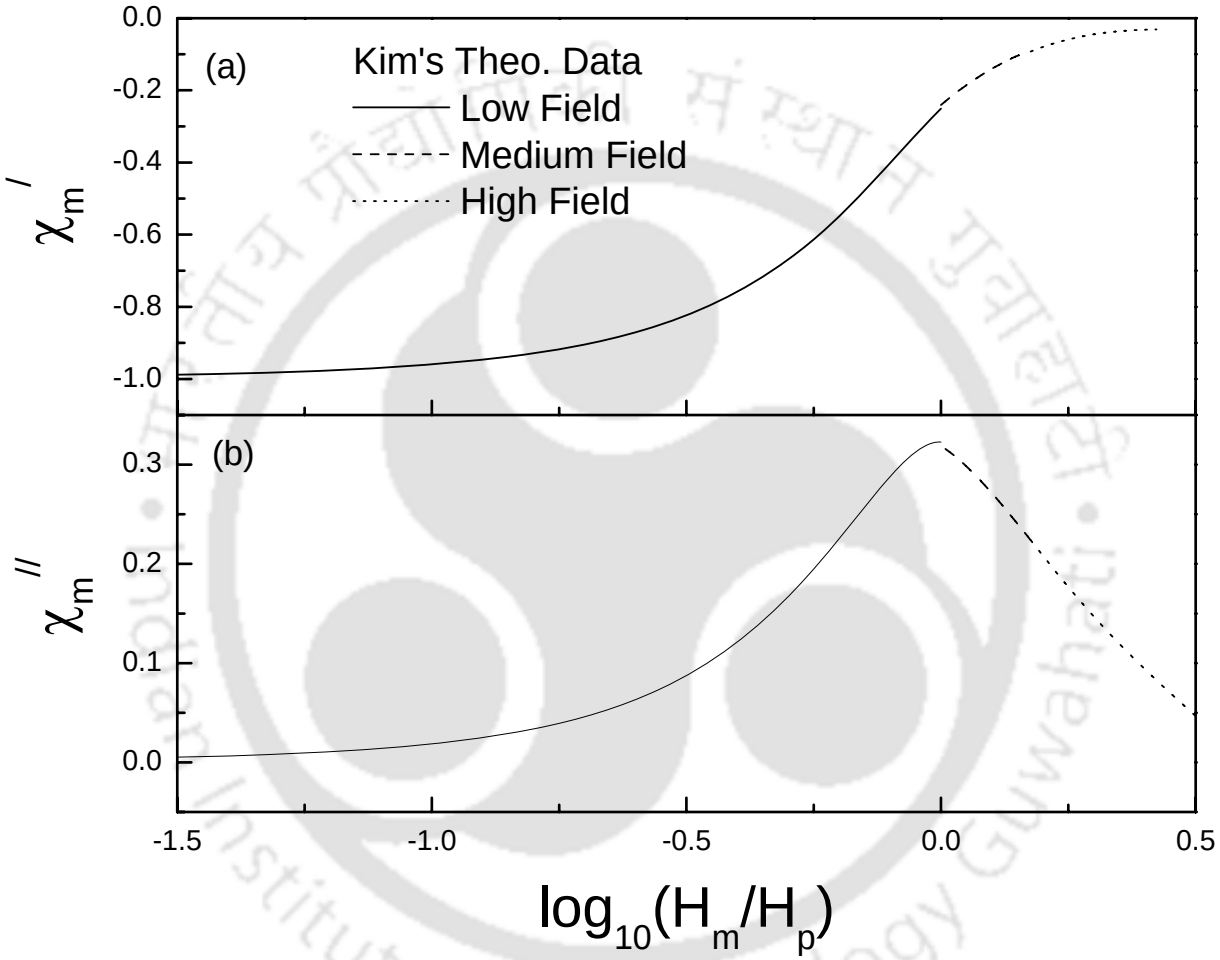

Fig.4.1. Plots of (a) real and (b) imaginary components of intergranular matrix susceptibility as a function of $\log_{10}(H_m/H_p)$ calculated from Kim model at low field (solid line), medium field (dashed lines) and high field (dotted lines) for p = 5 and a/b =1.

4.2.AC Susceptibility Studies in Pure and Ag Doped $(La_{1-x}Y_x)_2Ba_2CaCu_5O_z$ Series

The following samples have been chosen for detailed ac susceptibility analysis.

(i) $La_2Ba_2CaCu_5O_z$ (Sample A) of dimension (2.0 × 2.2 × 8.4) mm^3

(ii) $LaYBa_2CaCu_5O_z$ (Sample F) of dimension (2.0 × 3.3 × 12.7) mm^3

(iii) $La_2Ba_2CaCu_5O_z$ + 5 wt % of Ag (Sample A1) of dimension (1.9 × 2.5 × 8.0) mm^3

(iv) $La_{1.5}Y_{0.5}Ba_2CaCu_5O_z$ + 5 wt % of Ag (Sample D1) of dimension (2.7 × 3.1 × 8.6) mm^3

(v) $LaYBa_2CaCu_5O_z$ + 5 wt % of Ag (Sample F1) of dimension (2.0 × 3.6 × 12.8) mm^3

The details of their preparation procedure and characterizations are described in section 2.1 & 2.2. As per X-ray diffraction and microstructural studies, all the above samples are essentially in single phase form. They all exhibit superconducting transitions with zero resistivity temperatures ranging from 50.4 to 70.5 K.

4.2.1. Field Dependence of Susceptibility

AC field variation of susceptibility measured at different temperatures for these samples are presented in this section. The samples are taken up in the form of orthorhombic geometry with rectangular cross section (2a×2b) where (b > a).

The semi-logarithmic plots of ac field amplitude variations of real and imaginary components of ac susceptibility (χ' and χ'') measured at temperatures 25.0 K, 38.9 K, 42.3 K and 47.0 K for sample A are shown in Fig.4.2. From Fig. 4.2 (a) we can see that the values of $\chi'(H_m)$ at low fields, measured at low temperatures are close to -1, and it's value increases at higher fields due to the transition of intergranular matrix into normal state. We can see that χ' values almost saturate to some non zero negative values at higher fields, for the data recorded at higher temperature (T ≥ 39 K). This marks the completion of superconducting transition of intergranular weak link matrix and at this stage χ' values are mainly due to superconducting grains. To observe the transition of superconducting grains, generally large field is required or the temperature has to be chosen very close to T_c of grains. The plots of $\chi''(H_m)$ versus $\log H_m$ at different temperatures are shown in Fig. 4.2(b). At 47.0 K, $\chi''(H_m)$ versus $\log H_m$ plot exhibits a peak at H_m = 119 A/m and it corresponds to the maximum loss and it occurs when the applied field just penetrates to the center of the bulk material. The peak fields are found to be 315 A/m, 448 A/m

and 1366 A/m respectively at 42.3 K, 38.9 K, and 25.0 K. The peak field increases when the temperature is reduced, i.e. more field is required to fully penetrate to the sample at low temperatures. This is as a result of increase in shielding current density with decrease in temperature. At low temperatures, the values of $\chi^{//}(H_m) \approx 0$ for low applied fields. The $\chi^{//}$ peak at 25.0 K is incomplete because of the limitation in the maximum applied field with the present set up and it is limited to 1500 A/m.

Similarly the plots of measured $\chi^{/}$ and $\chi^{//}$ versus $\log(H_m)$ for samples F, A1, D1 and F1 are shown in Figs.4.3, 4.4, 4.5 and 4.6 respectively. The peak fields are found to be in the range of 445 to 44 A/m for the temperature variation 20.0 to 42.0 K; 1414 to 183 A/m for 25.0 to 47.0 K; 1070 to 68 A/m for 59.0 to 66.1 K and 843 to 19 A/m for 20.0 to 47.0 K for samples F, A1, D1 and F1 respectively. For sample D1, the measurements were carried out only for T > 59 K because the maximum applied field was not enough to observe the transition of intergranular region and in other words this material exhibits larger T_c and larger low temperature J_c. One can see that at a particular temperature, the peak fields of Ag doped samples are higher than those of pure samples. This could be due to the improved intergranular coupling between the grains by the addition of Ag. Thus, at a particular temperature below T_c, the Ag doped samples needs more field for full penetrations and this shows that the Ag doped samples exhibit higher J_c compared to that of pure samples, at a given temperature.

Eventhough, the observed superconducting transitions in the present range of applied fields are mainly due to intergranular weak links, there is a contribution of susceptibility due to superconducting grains. To analyze the intergranular matrix susceptibility, it has to be extracted from the total experimental susceptibility. The experimental intergranular matrix susceptibility ($\chi_m^{/}$ & $\chi_m^{//}$) can be obtained from the measured susceptibility ($\chi^{/}$ & $\chi^{//}$) using the following eqns. [266]

$$\chi^{/} = -f_g + (1 - f_g)\chi_m^{/} \tag{4.10}$$

$$\chi^{//} = (1 - f_g)\chi_m^{//} \tag{4.11}$$

where f_g is the effective volume fraction of superconducting grains. In eqns.(4.10) and (4.11), it is assumed that the grains are perfectly diamagnetic, i.e. $\chi_g^{/} = -1$ and $\chi_g^{//} = 0$ and it would be valid only at temperatures quite below the T_c. At temperatures close to T_c, $\chi_g^{/}$ is no longer equal to -1.

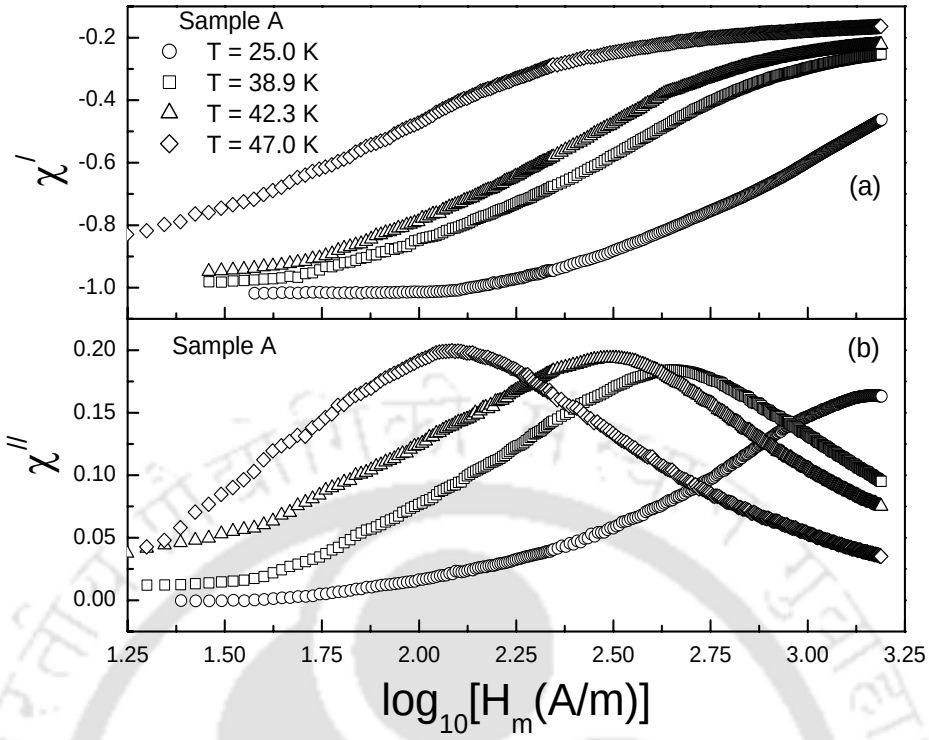

Fig.4.2. Plots of (a) real and (b) imaginary components of the measured susceptibility versus $\log_{10}(H_m)$ at the temperatures 25.0 K (circles), 38.9 K (squares), 42.3 K (triangles) and 47.0 K (diamonds) for sample A.

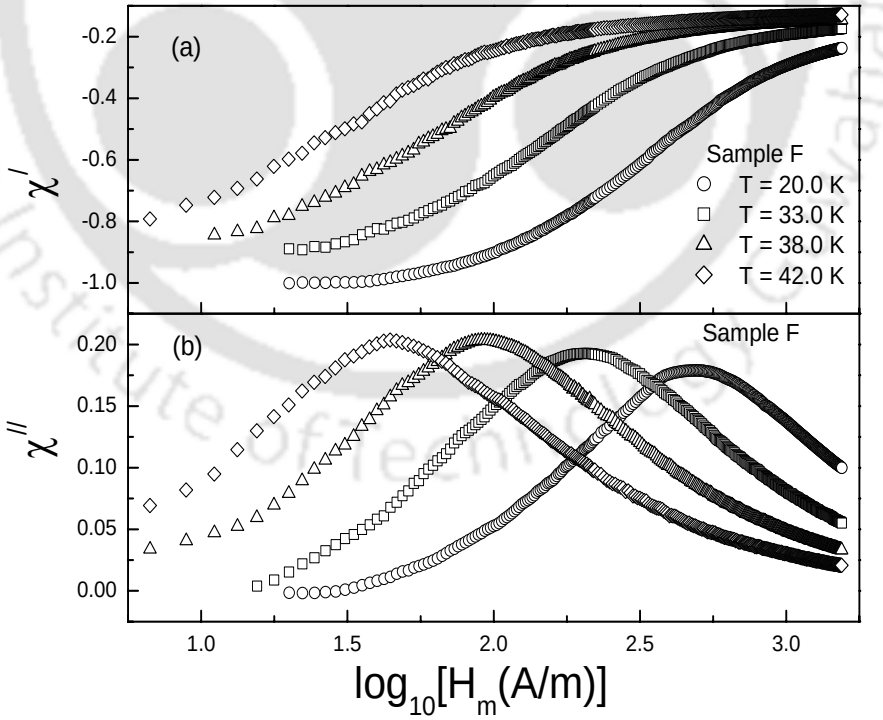

Fig.4.3. Plots of (a) real and (b) imaginary components of the measured susceptibility versus $\log_{10}(H_m)$ at the temperatures 20.0 K (circles), 33.0 K (squares), 38.0 K (triangles) and 42.0 K (diamonds) for sample F.

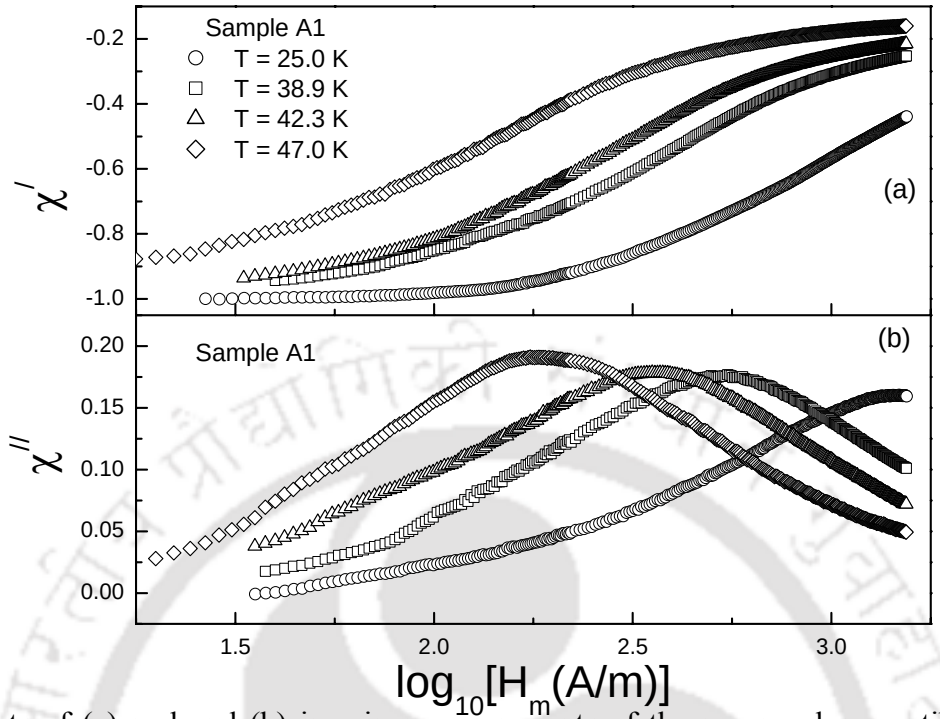

Fig.4.4. Plots of (a) real and (b) imaginary components of the measured susceptibility versus $\log_{10}(H_m)$ at the temperatures 20.0 K (circles), 33.0 K (squares), 38.0 K (triangles) and 42.0 K (diamonds) for sample A1.

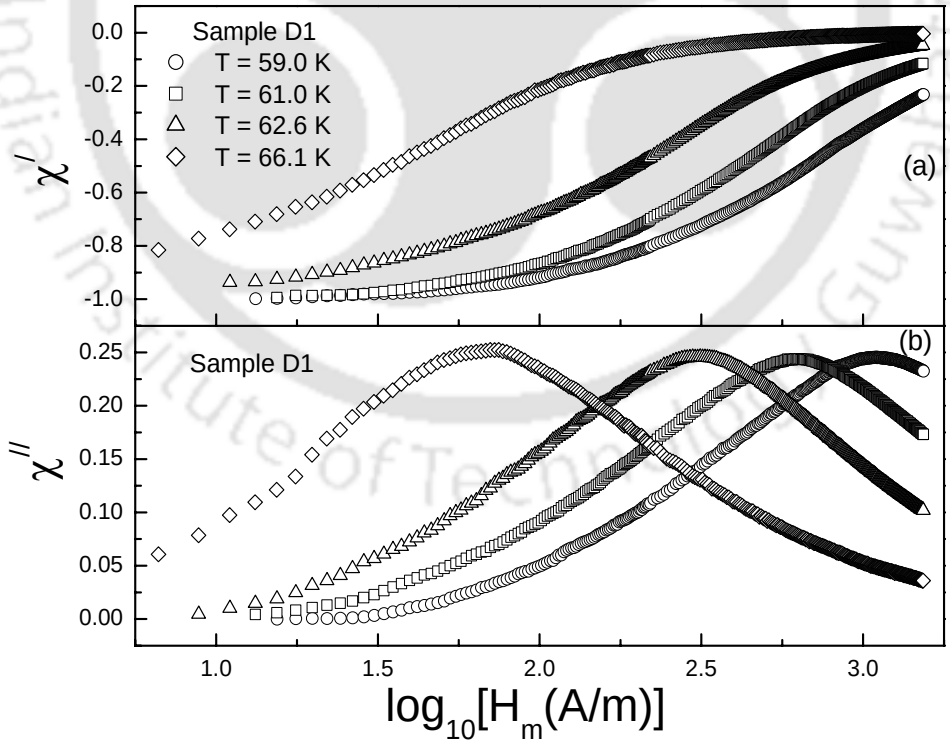

Fig.4.5. Plots of (a) real and (b) imaginary components of the measured susceptibility versus $\log_{10}(H_m)$ at the temperatures 59.0 K (circles), 61.0 K (squares), 62.6 K (triangles) and 66.1 K (diamonds) for sample D1.

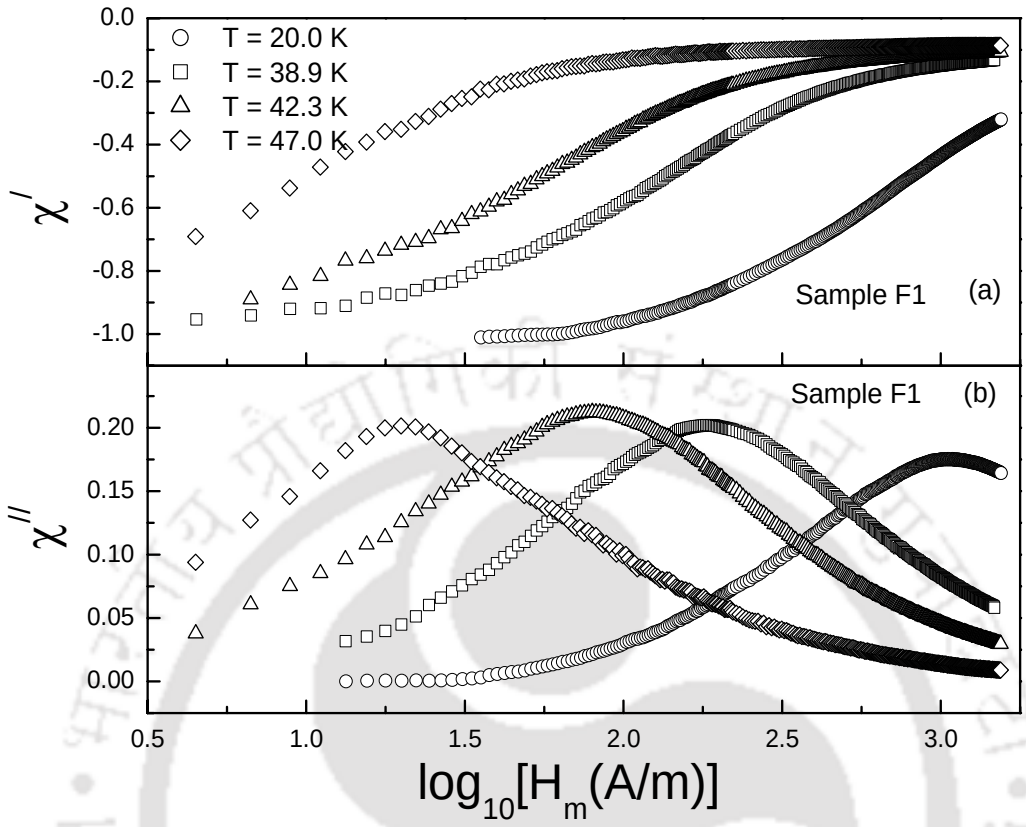

Fig.4.6. Plots of (a) real and (b) imaginary components of the measured susceptibility versus $\log_{10}(H_m)$ at the temperatures 20.0 K (circles), 38.9 K (squares), 42.3 K (triangles) and 47.0 K (diamonds) for sample F1.

For the estimation of f_g values, the following two conditions [348] were used.

(1) χ_m'' as a function of $-\chi_m'$ gives a convex curve with slope $d\chi_m''/d(-\chi_m')$ that tends to ∞ at $\chi_m' = 0$.

(2) The plot of $\log_{10}\chi_m''$ versus $\log_{10}(H_m)$ gives a peak of which both sides are almost linear.

By substituting tentative values of f_g in eqns.(4.10) and (4.11), the values of $\chi_m'(H_m)$ and $\chi_m''(H_m)$ were calculated and the data were tested for the above two conditions. This procedure was repeated for different values of f_g till both the conditions were satisfied and by this process appropriate value of f_g was obtained at a particular temperature. Using this f_g value and by substituting $\chi'(H_m)$ and $\chi''(H_m)$ measured at a particular temperature in eqns. (4.10) and (4.11), the experimental intergranular matrix susceptibility $\chi_m'(H_m)$ and $\chi_m''(H_m)$ were obtained.

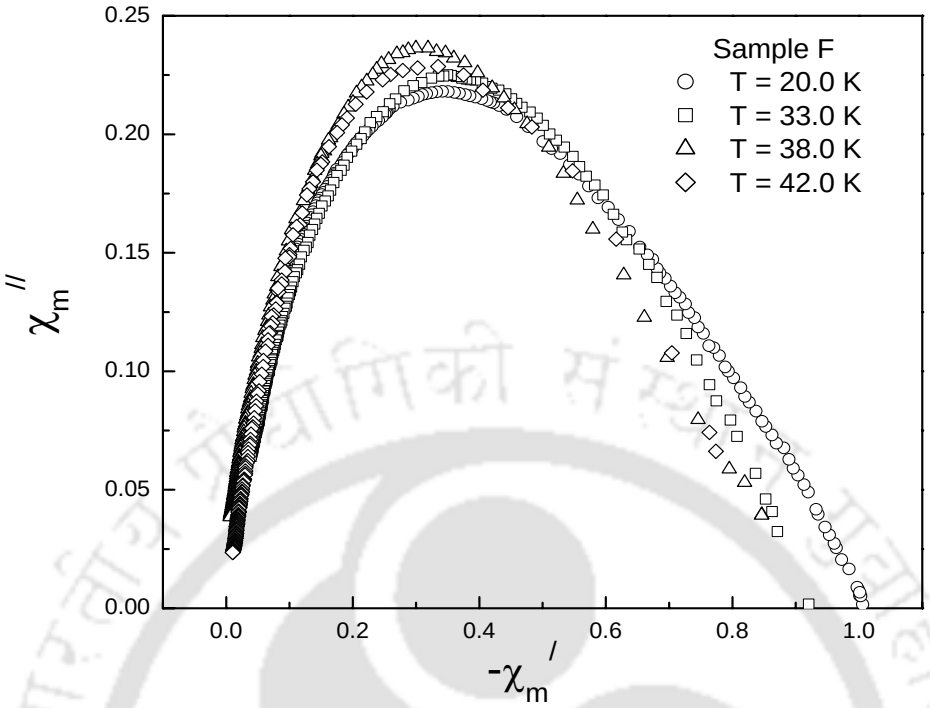

Fig. 4.7. Plots of $\chi_m^{//}$ versus $-\chi_m^{/}$ for sample F at temperatures 20.0 K(circles), 33.0 K(squares), 38.0 K(triangles) and 42.0 K(diamonds).

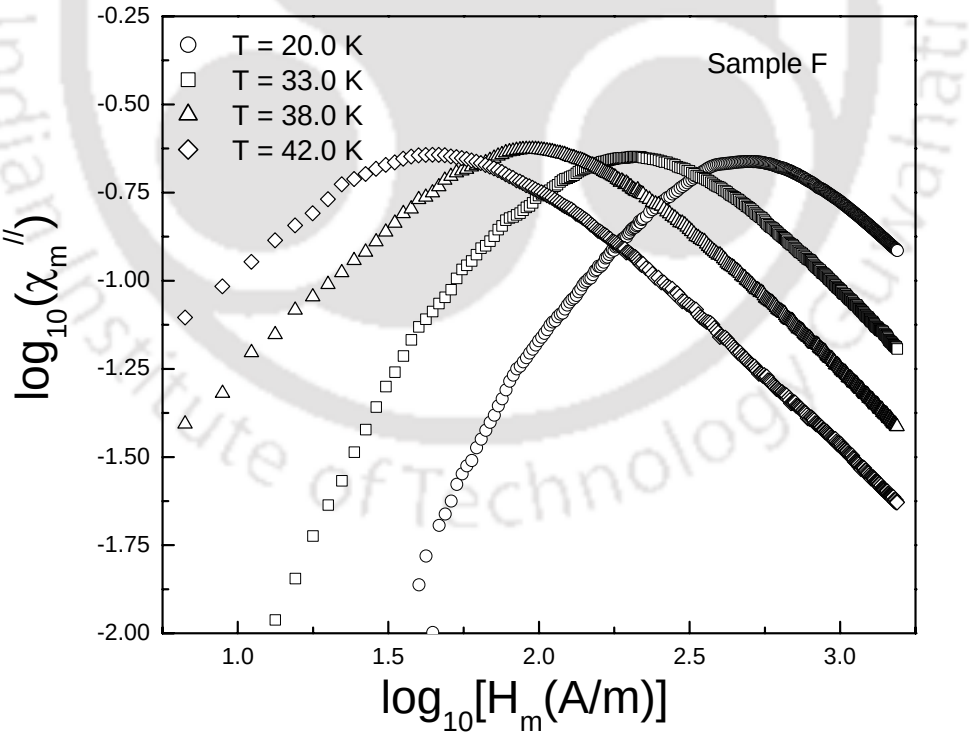

Fig. 4.8. Plots of $\log_{10}\chi_m^{//}$ versus $\log_{10}(H_m)$ for sample B1 at temperatures 20.0 K(circles), 33.0 K(squares), 38.0 K(triangles) and 42.0 K(diamonds). Both sides of the peaks are almost linear.

The estimated f_g values are respectively 0.15, 0.20, 0.20 and 0.24 at temperatures 47.0 K, 42.3 K, 38.9 K and 25.0 K for sample A. The f_g values obtained for various samples at different temperatures are given in Table 4.1. We can see from Table 4.1 that the f_g values mostly vary from about 10 to 25 % with decrease in temperature and for sample D1, the f_g value is found to be zero. On the other hand, in $YBa_2Cu_3O_7$ superconductors, the f_g values are reported to be in the range of 50 to 65 % [266], and in the 110 K phase of Bi-Sr-Ca-Cu-O system it was found to be in the range of 40 to 50 % [318]. To find out the possible reason, we have compared the SEM micrographs of present samples with those of standard $YBa_2Cu_3O_7$. The average grain size of polycrystalline $YBa_2Cu_3O_7$ material is generally in the order of 20 to 40 μm [349]. On the otherhand, we can see from Table 2.5 that the present series exhibit an average grain size of 1.2 to 2.6 μm. So, the rather low f_g can be explained on the basis of finer grains. Here f_g refers the effective volume fraction of superconducting grains, ignoring a shell of thickness of the order of London penetration depth, where there is a penetration of applied field, and $\chi_g \neq -1$. Moreover, within the present series, the f_g values are somewhat comparable to their respective grain size. For example the samples A & A1 have relatively larger grain size and accordingly, their f_g values are also relatively large. The sample F1 has least grain size and corresponding by low f_g value has been observed. How ever, there is an anomaly for the sample D1, in this case even though the average grain size is comparable to that of sample A1, the f_g value is found to be zero in all the temperatures. In this case, there is a probability that superconducting properties of intergranular and intragranular regions are so comparable that the applied magnetic field or magnetic flux lines do not distinguish them. The above argument may be substantiated from the largest diamagnetic T_c observed in sample D1 compared to any other samples in the present pure and Ag doped series. There are also a few reports in the literature, where low f_g values are reported [309,317].

Using the obtained f_g values at different temperatures and eqns.(4.10) and (4.11) the matrix susceptibility $\chi_m'(H_m)$ and $\chi_m''(H_m)$ were calculated at 42.0 K, 38.0 K, 33.0 K and 20.0 K for sample F. The plots of $\chi_m''(H_m)$ versus $-\chi_m'(H_m)$ at these temperatures are shown in Fig. 4.7 and they exhibit convex curve with a slope $d\chi_m''/d(-\chi_m')$ that tends towards ∞ at $-\chi_m' = 0$ as per the first condition given in page 163. The plots of $\log_{10}(\chi_m'')$ versus $\log_{10}(H_m)$ at different temperatures are shown in Fig. 4.8 for sample F. One can see that they all exhibit a peak with almost linear behavior at either side according to the second condition (page 163). The maximum

values of $\chi_m^{//}(H_m)$ i.e. $\chi_{m,max}^{//}$ are respectively 0.214, 0.219, 0.232 and 0.225 and their corresponding values of $-\chi_m^{/}(H_m)$, i.e. $-\chi_m^{/}(\chi_{m,max}^{//})$ are respectively 0.372, 0.381, 0.332 and 0.328. The values of f_g, $\chi_{max}^{//}$ and $-\chi_m^{/}(\chi_{m,max}^{//})$ for sample F at different temperatures are given in Table 4.1.

Similarly by following the above procedure, the f_g values were calculated for the samples A1, D1 and F1. The experimental $\chi_m^{/}(H_m)$ and $\chi_m^{//}(H_m)$ were also calculated at several temperatures below their T_c values. The obtained values of f_g, $\chi_{m,max}^{//}$ and $-\chi_m^{/}(\chi_{m,max}^{//})$ at different temperatures are given in Table 4.1 for samples A1, D1 and F1.

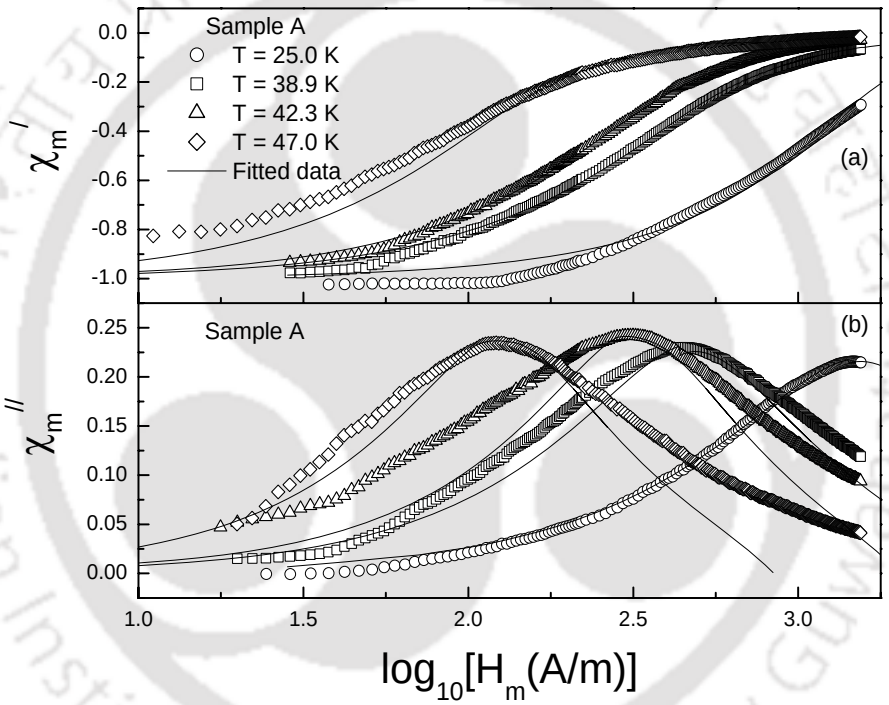

Fig. 4.9. Plots of (a) real and (b) imaginary components of the intergranular matrix susceptibility versus $\log_{10}(H_m)$ at temperatures 25.0 K(circles), 38.9 K(squares), 42.3 K(triangles) and 47.0 K(diamonds) for sample A. The solid lines are the theoretical data calculated using Kim model.

As described in section 4.1, Kim theoretical susceptibility is a function of H_m/H_p, p and a/b. The experimental $\chi_m^{/}(H_m)$ and $\chi_m^{//}(H_m)$ data were fitted to the expressions obtained from the Kim theoretical model by varying the parameters H_p and p. The fitted data are shown as solid lines in Fig.4.9 for sample A. One can see that fitted data closely follow the experimental data especially at low temperature. At higher temperature, $\chi_m^{//}$ data exhibit some deviation from theoretical data.

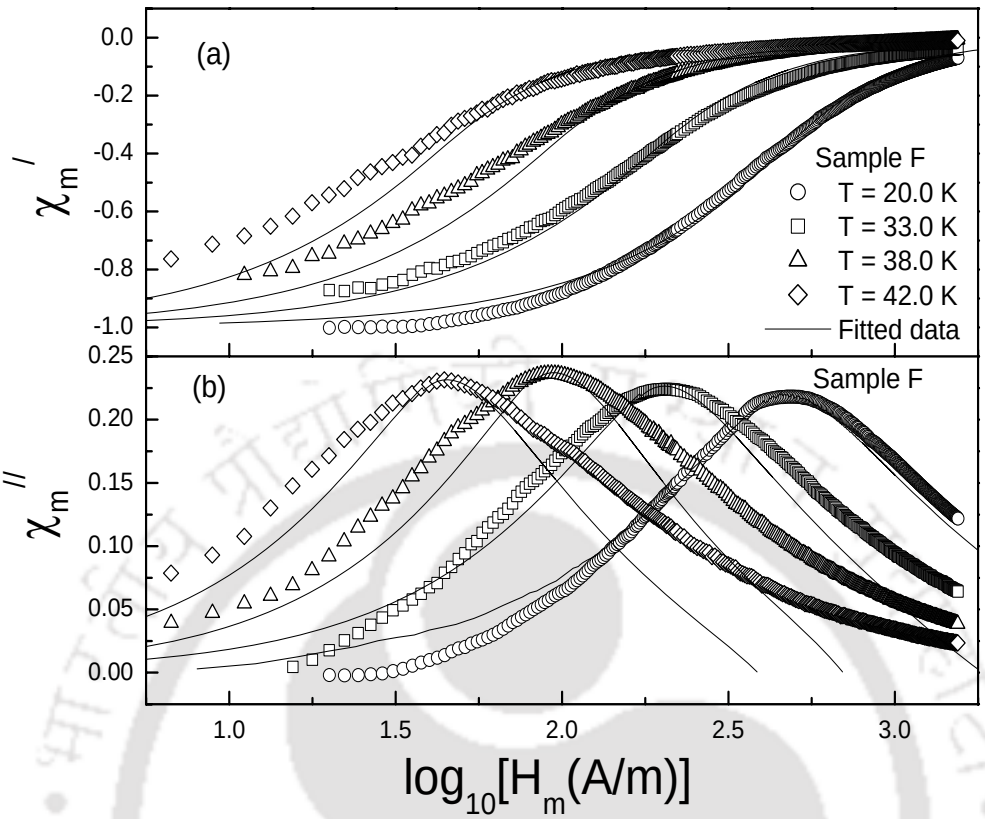

Fig. 4.10. Plots of (a) real and (b) imaginary components of the intergranular matrix susceptibility versus $\log_{10}(H_m)$ at temperatures 20.0 K(circles), 33.0 K(squares), 38.0 K(triangles) and 42.0 K(diamonds) for sample F. The solid lines are the theoretical data calculated using Kim model.

The plots of $\chi_m^{/}$ and $\chi_m^{//}$ as a function of $\log_{10}H_m$ are shown in Fig. 4.10 for sample F at temperatures 20.0 K(circles), 33.0 K(squares), 38.0 K(triangles) and 42.0 K(diamonds). Kim theoretical susceptibility data are shown as solid lines and they fit the experimental data reasonably well. However, at higher temperature (38.0 K and 42.0 K) the experimental data exhibit considerable deviation from the theoretical data. This could be due to one of the following reasons. At higher temperatures, the assumption of perfect diamagnetic property of superconducting grains, such as $\chi_g^{/} = -1$ and $\chi_g^{/} = 0$ may not be valid and as a result, there could be some error in the estimation of f_g from eqns 4.10 & 4.11. Moreever, there is a possibility of some flux creep and/or distribution in critical current density at higher temperatures and that may also contribute for the above deviation. Eventhough there are several reports in literature which make use of critical state model to estimate J_c, only a limited works deal with fitting of measured

susceptibility to the appropriate critical state model. The above fittings are comparable to those reported for Bi-Sr-Ca-Cu-O system [318].

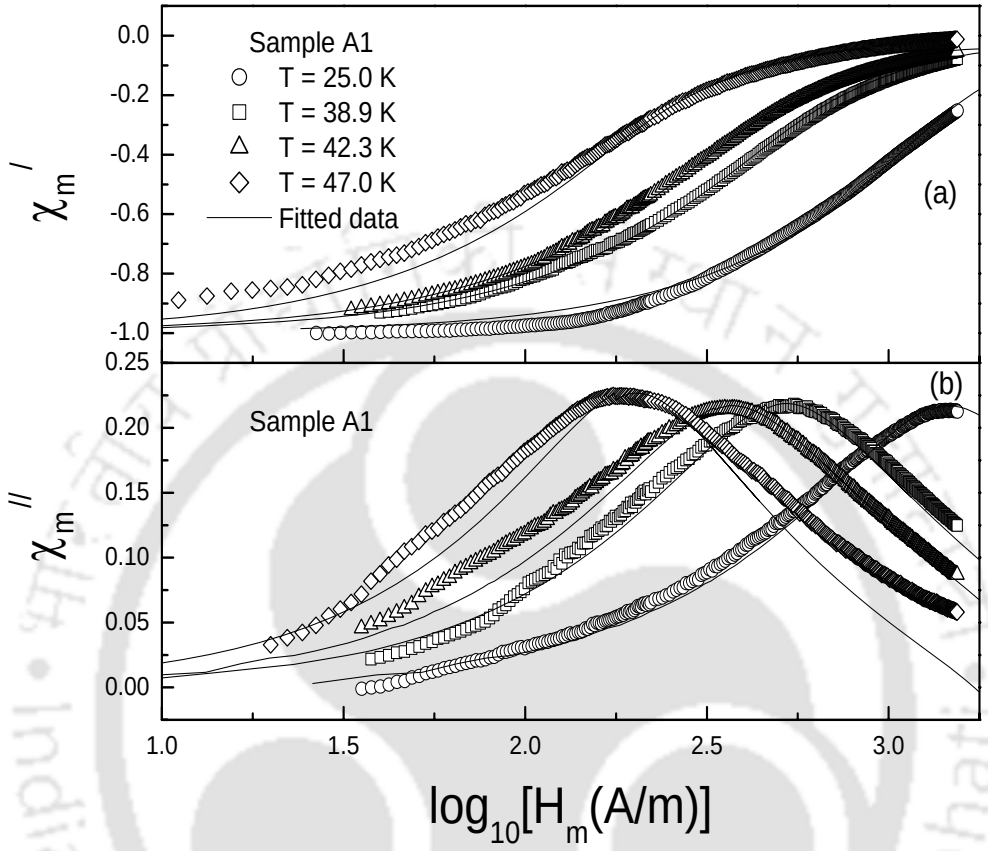

Fig. 4.11. Plots of (a) real and (b) imaginary components of the intergranular matrix susceptibility versus $\log_{10}(H_m)$ at temperatures 25.0 K(circles), 38.9 K(squares), 42.3 K(triangles) and 47.0 K(diamonds) for sample A1. Kim theoretical data are shown solid lines.

Similarly the plots of $\chi_m^{/}$ and $\chi_m^{//}$ versus $\log_{10}H_m$ are shown in Figs.4.11 and 4.12 for samples A1, D1 and F1 at different temperatures below their T_c values. Kim theoretical data could be fitted reasonably well to the experimental data of all the samples especially at low temperatures. For some of the samples, the H_p values were fixed during the fit of $\chi_m^{//}$ data to avoid unreasonable physical parameters. The H_p and p values obtained for various samples from the above analysis are listed in Table 4.1.

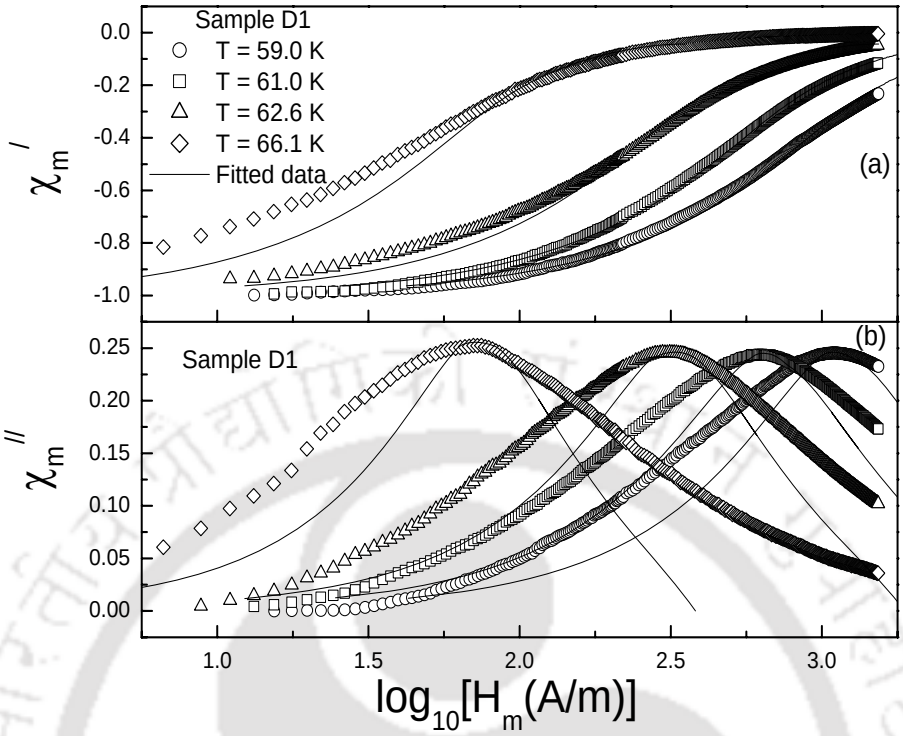

(i)

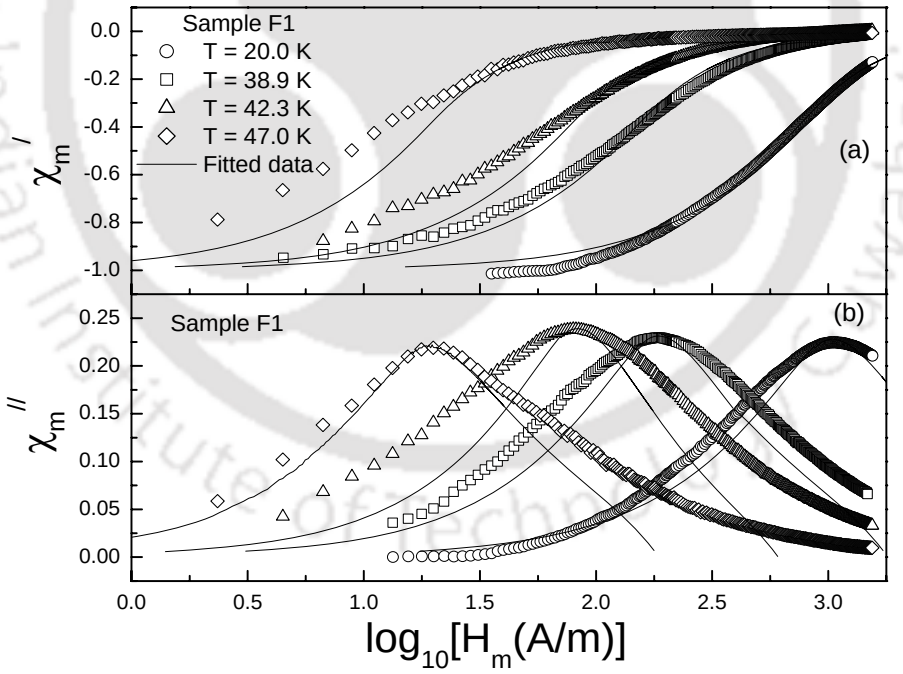

(ii)

Fig. 4.12. (i) Plots of (a) real and (b) imaginary components of the intergranular matrix susceptibility versus $\log_{10}(H_m)$ at temperatures 59.0 K(circles), 61.0 K(squares), 62.6 K(triangles) and 66.1 K(diamonds) for sample D1. (ii) Field variations of $\chi_m^{/}$ and $\chi_m^{//}$ at temperatures 20.0 K(circles), 38.9 K(squares), 42.3 K(triangles) and 47.0 K(diamonds) for sample F1. Kim theoretical data are shown as solid lines.

Table 4.1. List of parameters obtained from the field variation of susceptibility in the samples A, F, A1, D1 and F1at different temperatures.

Sample	T (K)	H_p (A/m)	$-\chi_m^{/}(\chi_{m\ ,max}^{//})$	$\chi_{m\ ,max}^{//}$	f_g	p
A	25.0	1415	0.328	0.215	0.24	0.3
	38.9	443	0.332	0.229	0.20	0.5
	42.3	310	0.330	0.241	0.20	0.8
	47.0	121	0.304	0.234	0.15	0.6
F	20.0	434	0.372	0.214	0.18	0.2
	33.0	180	0.381	0.219	0.14	0.3
	38.0	85	0.332	0.232	0.14	0.7
	42.0	40	0.328	0.225	0.12	0.3
A1	25.0	1463	0.348	0.211	0.25	0.3
	38.9	468	0.366	0.214	0.19	0.3
	42.3	345	0.360	0.214	0.17	0.3
	47.0	179	0.336	0.224	0.15	0.4
D1	59.0	1057	0.342	0.245	0	1.3
	61.0	632	0.337	0.243	0	1.2
	62.6	308	0.354	0.245	0	1.3
	66.1	70	0.300	0.252	0	1.5
F1	20.0	812	0.391	0.219	0.22	0.3
	38.9	152	0.398	0.226	0.12	0.4
	42.3	73	0.345	0.236	0.11	0.7
	47.0	17	0.295	0.216	0.08	0.2

4.2.2. Temperature Dependence of AC Susceptibility

In this section, the temperature variations of real and imaginary components of ac susceptibility measured on several samples such as A, F, A1, D1 and F1 are reported. In each sample, the measurements have been carried out at different ac field amplitudes ranging from 23 A/m to 1527 A/m. The data were analyzed in terms of Kim model. The temperature dependence of critical current density was estimated for these samples.

The plots of $\chi^{/}$ and $\chi^{//}$ versus temperature are shown in Fig.4.13 for sample A. The diamagnetic onset temperature is found to be 62.7 K and it is almost constant for different applied fields. The $\chi^{/}$ value approaches -1 at low temperatures and for low applied fields, and it gradually increases with the increase of applied field. One can see from $\chi^{/}$ vs. T plots that the intergranular and intragranular features are clearly distinguisible at higher applied fields. The first fall of $\chi^{/}$ below diamagnetic onset temperature is due to intragrain and the second fall is due to intergrain. The $\chi^{//}$ peak temperature T_m varies from 53.0 to 26.5 K, when the applied field was increased from 23 A/m to 1516 A/m. The magnitude of $\chi^{//}$ peaks are almost constant at different

temperatures and it suggests that flux line lattice is almost stable and critical state model can be applied. Similar to the field variation of $\chi^{//}$, the peak observed in temperature variation of $\chi^{//}$ can be understood as a result of maximum loss of penetrated flux density as a result of full penetration of applied magnetic field, at the temperature corresponding to peak position.

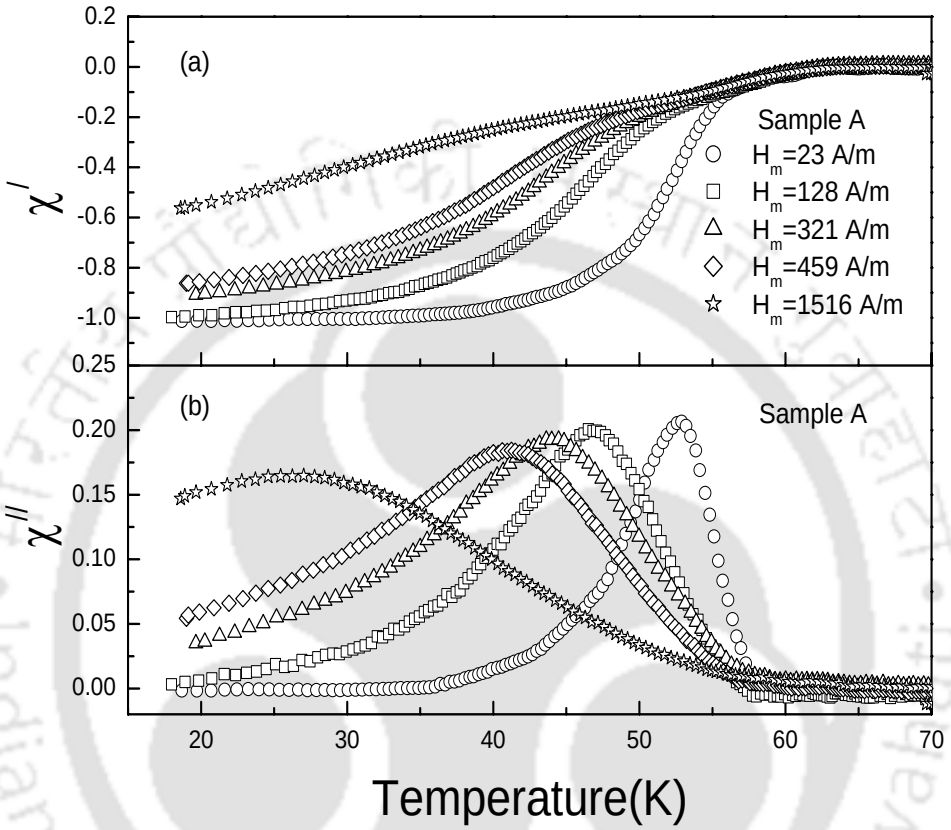

Fig. 4.13. Plots of (a) real and (b) imaginary components of susceptibility versus temperature at ac field amplitudes 23 A/m (circles), 128 A/m (squares), 321 A/m (triangles), 459 A/m(diamonds) and 1516 A/m (stars) for sample A.

According to critical state models as described in section 1.5, the critical current density J_c at $\chi^{//}$ peak temperature T_m can be calculated as follows,

$$J_c(T_m) = H_m/a \qquad (4.12)$$

where, H_m is the amplitude of the applied ac field and 'a' is the radius of the cylindrical sample or half thickness of the orthorhombic sample. The above equation implies that at T_m the applied field H_m is equal to full penetration field H_p, ($H_m = H_p$). The critical current density at $\chi^{//}$ peak temperature, $J_c(T_m)$ are estimated and are given in Table 4.2.

Fig.4.14 shows the plots of temperature variation of real and imaginary parts of ac susceptibility for sample F measured at ac field amplitudes 23 A/m, 44 A/m, 76 A/m, 170 A/m and 443 A/m. The diamagnetic onset temperature is 62.9 K and it is almost constant for different applied fields. The $\chi^{/}$ value is almost close to -1 at low temperatures for low applied fields, and it gradually increases with the increase in applied field. The $\chi^{//}$ peak temperature T_m varies from 45.2 to 24.8 K for sample F, when the applied field was increased from 23 A/m to 443 A/m. The critical current density J_c at T_m have been estimated using eqn.4.12 and are given in Table 4.2.

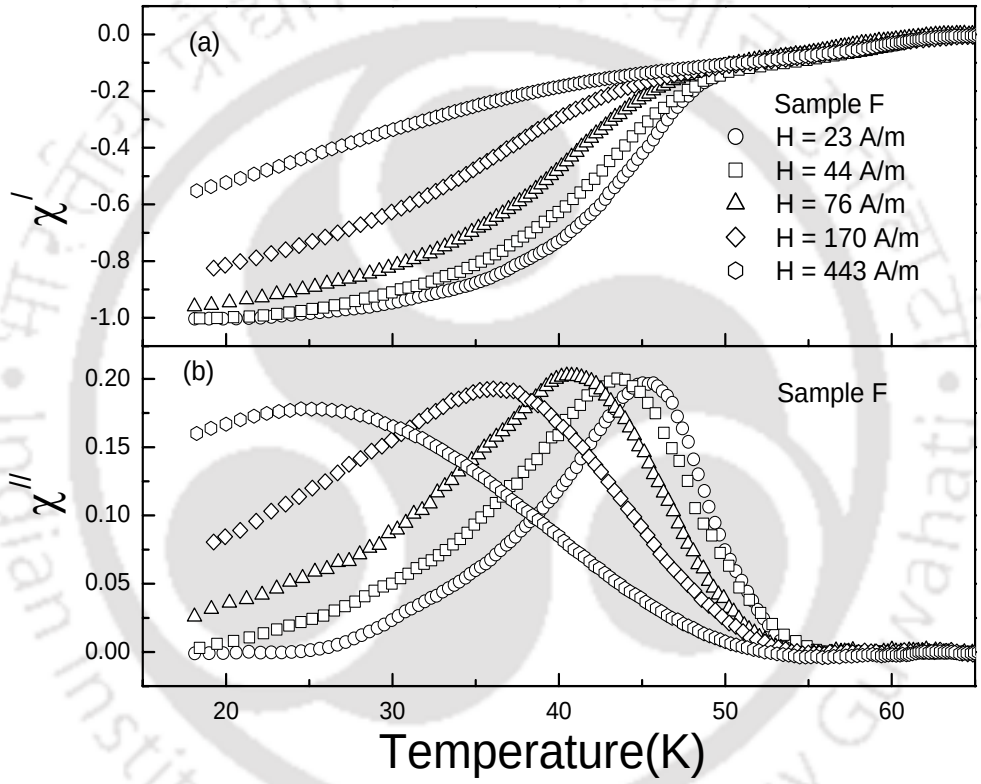

Fig. 4.14. Plots of (a) real and (b) imaginary components of ac susceptibility versus temperature at ac field amplitudes of 23 A/m (circles), 44 A/m (squares), 76 A/m (triangles), 170 A/m (diamonds) and 443 A/m (stars) for sample F.

Similarly, the plots of $\chi^{/}(T)$ and $\chi^{//}(T)$ versus temperature at different ac fields are shown in Figs.4.15, 4.16 and 4.17 for samples A1, D1 and F1 respectively. The diamagnetic onset temperatures are respectively 61.0 K, 74.8 K and 63.0 K. All the samples show intergranular and intragranular features at higher applied fields except for sample D1. The $\chi^{//}$ peak temperature, T_m and $J_c(T_m)$ for different samples are listed in Table 4.2. The $J_c(T_m)$ values are quite low due to

polycrystalline nature of the samples and are comparable to literature in other polycrystalline superconducting series [317, 318, 320, 322].

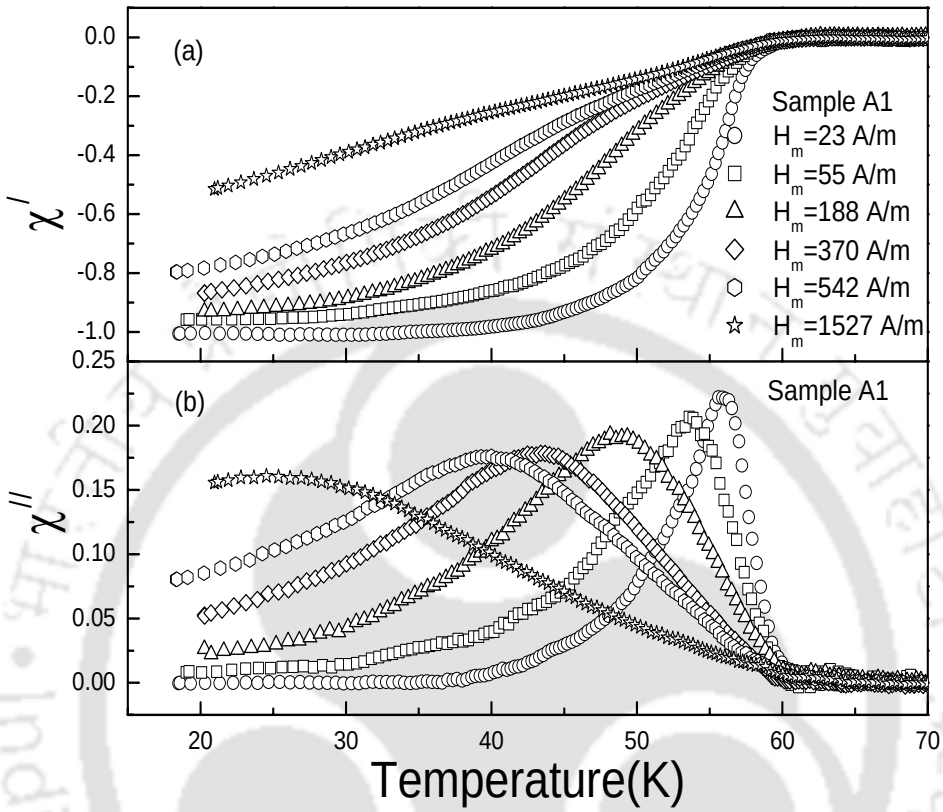

Fig. 4.15. Plots of (a) real and (b) imaginary components of ac susceptibility versus temperature for sample A1 at ac field amplitudes of 23 A/m (circles), 55 A/m (squares), 188 A/m (triangles), 370 A/m(diamonds), 542 A/m (hexoids) and 1527 A/m (stars).

From the $\chi'(T)$ and $\chi''(T)$ measured at different fields and using eqns. (4.10) and (4.11), the intergranular matrix susceptibility $\chi_m'(T)$ and $\chi_m''(T)$ were calculated. For the above calculations, f_g is needed and it was taken from the result of field variation of susceptibility measurement. It was chosen from the analysis of field variation of ac susceptibility carried out at a given temperature, which is in the vicinity of χ'' peak temperature (χ'' vs. T Plot). It is assumed that f_g value is almost constant over a small temperature range on either side of χ'' peak temperature.

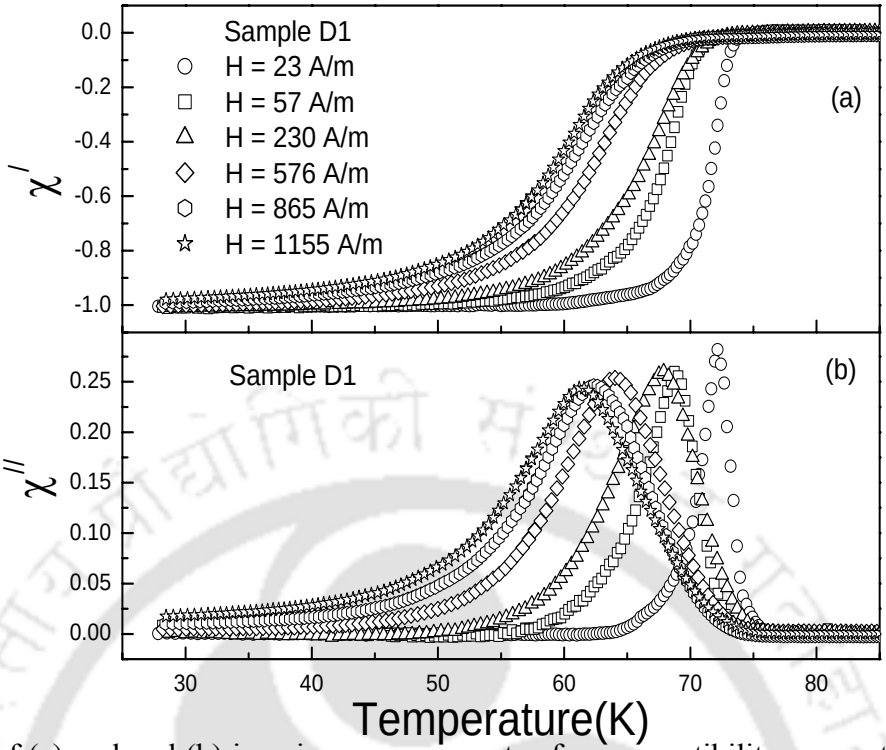

Fig. 4.16. Plots of (a) real and (b) imaginary components of ac susceptibility versus temperature for sample D1 at ac field amplitudes of 23 A/m (circles), 57 A/m (squares), 230 A/m (triangles), 576 A/m(diamonds), 865 A/m (hexoids) and 1155 A/m (stars).

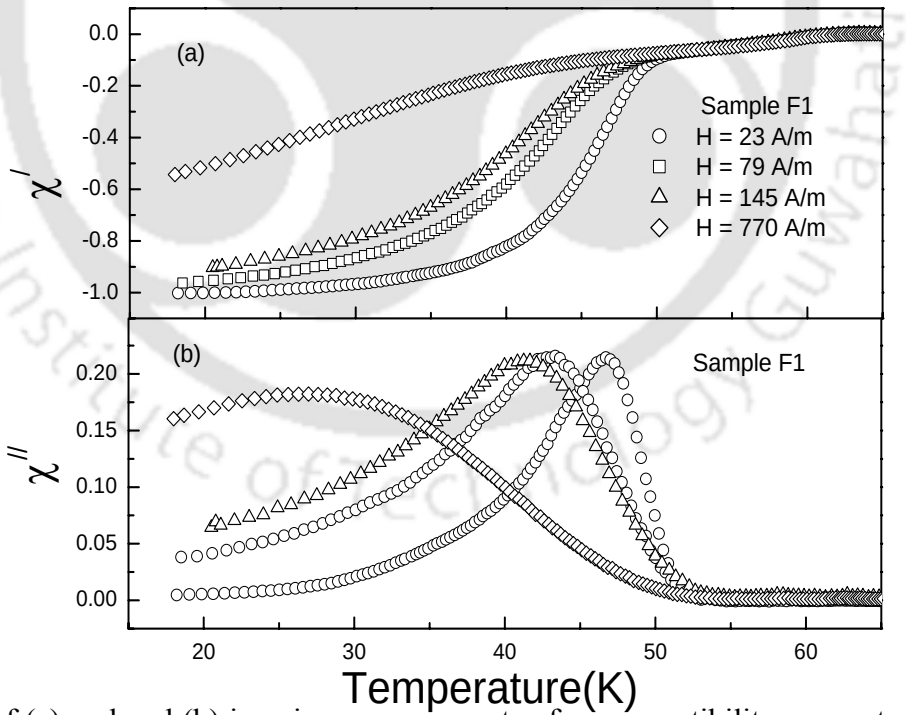

Fig. 4.17. Plots of (a) real and (b) imaginary components of ac susceptibility versus temperature for sample F1 at ac field amplitudes of 23 A/m (circles), 79 A/m (squares), 145 A/m (triangles) and 770 A/m(diamonds).

To estimate the temperature variation of critical current density $J_c(T)$, we use both field and temperature variations of χ'. The theoretical $\chi'(H_m/H_p)$ versus H_m/H_p were calculated using the parameters p and f_g obtained from the fit of field variation of ac susceptibility measured in the vicinity of T_m. By comparing theoretical $\chi'(H_m/H_p)$ versus H_m/H_p with experimental $\chi'(T)$ versus T and by taking H_m as the field at which $\chi'(T)$ was measured, the temperature variation of $H_p(T)$ can be estimated. From $H_p(T)$ and using eqn. 4.12, the $J_c(T)$ values are estimated in the temperature range close to T_m. In the above calculation, it is assumed that f_g is constant in a small temperature range in the vicinity of T_m. The above calculation was repeated in the vicinity of several T_m values, i.e. $\chi'(T)$ measured at different H_m values. Plots of $J_c(T)$ versus temperature estimated from $\chi'(T)$ measured at128 A/m (circles), 321 A/m (squares) and 459 A/m(triangles) are shown in Fig.4.18 for sample A. The $J_c(T)$ estimated using different $\chi'(T)$ data follow a continuous line. The critical current density at χ'' peak temperatures $J_c(T_m)$ (Table 4.1) were estimated using eqn. 4.12, where $H_m = H_p$, and they are given as stars in Fig. 4.18 for a comparison. They closely follow the $J_c(T)$ data estimated from the above analysis.

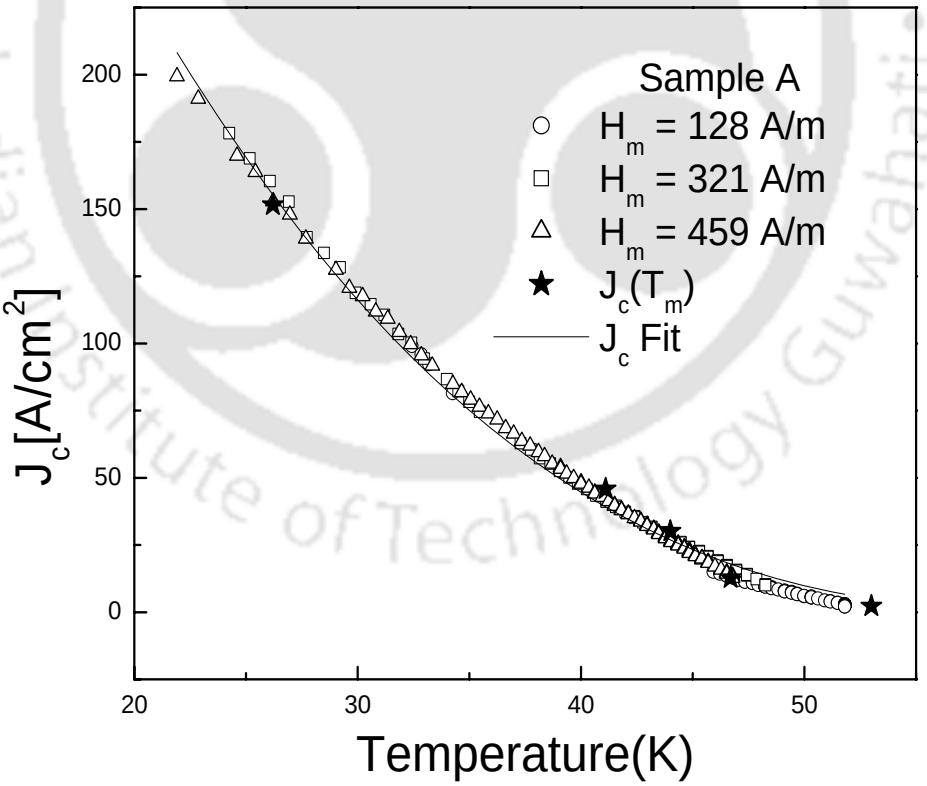

Fig.4.18. Temperature dependence of critical current density estimated from Kim theoretical susceptibility and experimental $\chi'(T)$ at different fields for sample A. $J_c(T_m)$ estimated by applying critical state model at χ'' peaks are shown as stars.

The temperature variation of $J_c(T)$ given in eqn.1.69 is reproduced below,

$$J_c \propto [1-\frac{T}{T_c}]^n \tag{4.13}$$

Here T_c is the superconducting transition temperature (transition mid-point obtained from ρ vs. T plots) and n is a positive constant. The T_c values are reproduced in Table 4.2 for convenience. We have fitted the experimental $J_c(T)$ to the above function. The value of 'n' obtained for sample A is 2.67. This value is comparable to 2 and it suggests that this material exhibits superconductor - metal - superconductor type of junctions [329]. Similar behavior of superconductor-metal-superconductor type of junctions was reported by Salamati et al. [331] on well oxygenated $YBa_2Cu_3O_7$ superconductors.

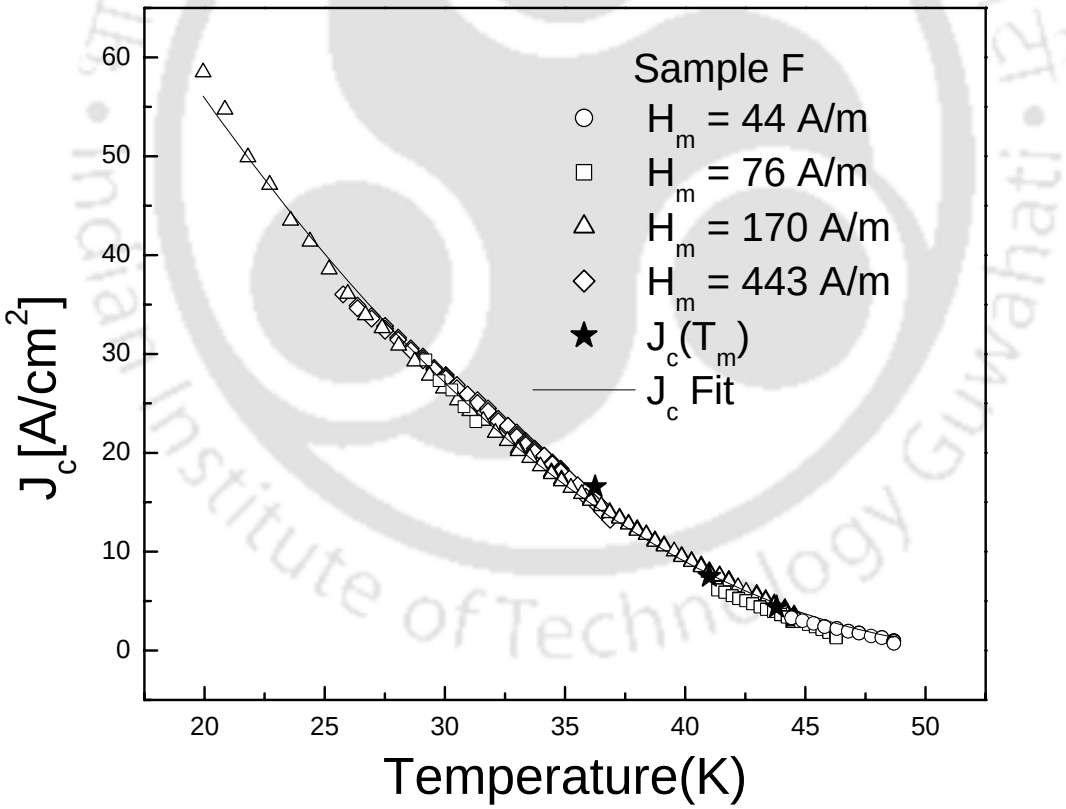

Fig.4.19. Temperature dependence of critical current density estimated by comparing Kim theoretical susceptibility with experimental $\chi'(T)$ at different applied fields for sample F. $J_c(T_m)$ estimated from the temperature variations of susceptibility using eqn. 4.12 are shown as stars.

Similarly $J_c(T)$ as a function of temperature was estimated for other samples such as sample F, A1, D1 & F1 and are shown in Figs.4.19 to 4.22. For all the samples the $J_c(T)$ estimated using different $\chi'(T)$ data follow a continuous line. The $J_c(T)$ data were fitted to eqn. 4.13 by varying the parameters 'n' and the proportionality constant. The fitted data are shown as solid lines in Figs.4.19 to 4.22 and we can see that it closely follows the experimental data. The fitted 'n' values for different samples are given in Table 4.2 and it mostly close to 2. So the 'n' values suggest that these materials exhibit superconductor - metal – superconductor (SNS) type of junctions.

Table 4.2. The list of parameters obtained from the measurement and analysis of temperature variations of ac susceptibility of samples A, F, A1, D1 and F1.

Sample	H_m (A/m)	T_m (K)	$J_c(T_m)$ (A/cm^2)	n	T_c (K)
A	23 128 321 459 1516	53.0 46.7 44.0 41.1 26.2	2.3 12.8 30.1 45.8 151.6	2.67	63.2
F	23 44 76 170 443	45.2 43.8 41.0 36.2 24.8	2.3 4.4 7.6 16.9 44.3	2.35	60.4
A1	55 188 370 542 1527	53.8 48.9 43.2 39.5 22.5	5.8 19.8 38.9 57.1 160.7	2.50	68.3
D1	57 230 576 865 1155	68.7 67.8 64.0 62.3 61.2	4.2 17.0 42.7 64.0 85.6	2.83	75.4
F1	23 79 145 770	46.9 43.3 41.6 26.5	2.3 7.9 14.5 77.0	2.13	64.5

From the above table one can see that the pure samples are having relatively large 'n' values compared to that of Ag doped samples. This suggests that in pure samples, the $J_c(T)$ falls rather sharply with increase in temperature.

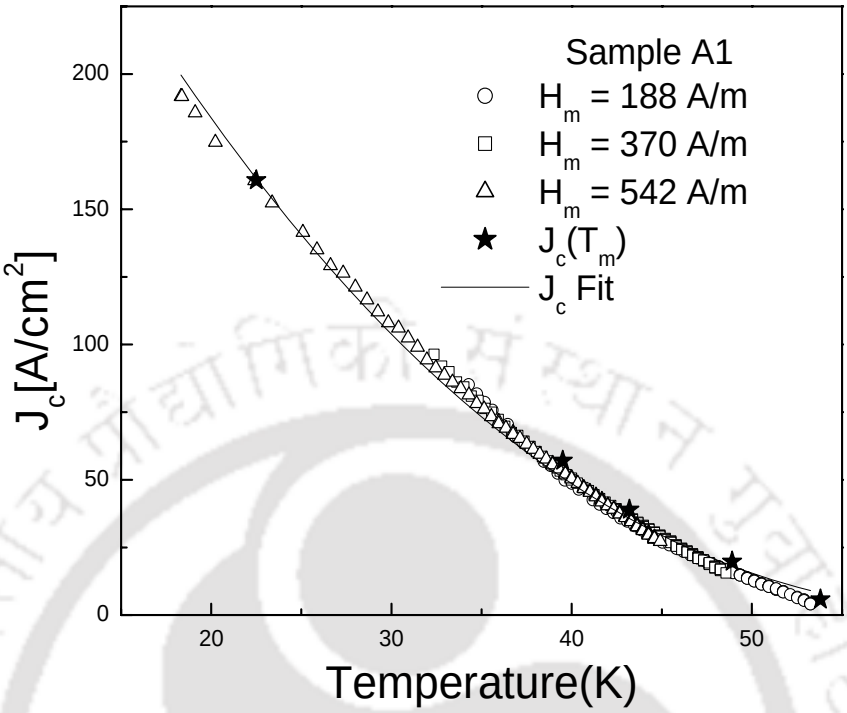

Fig.4.20. Critical current density versus temperature for sample A1. The J_c estimated at T_m are given as stars.

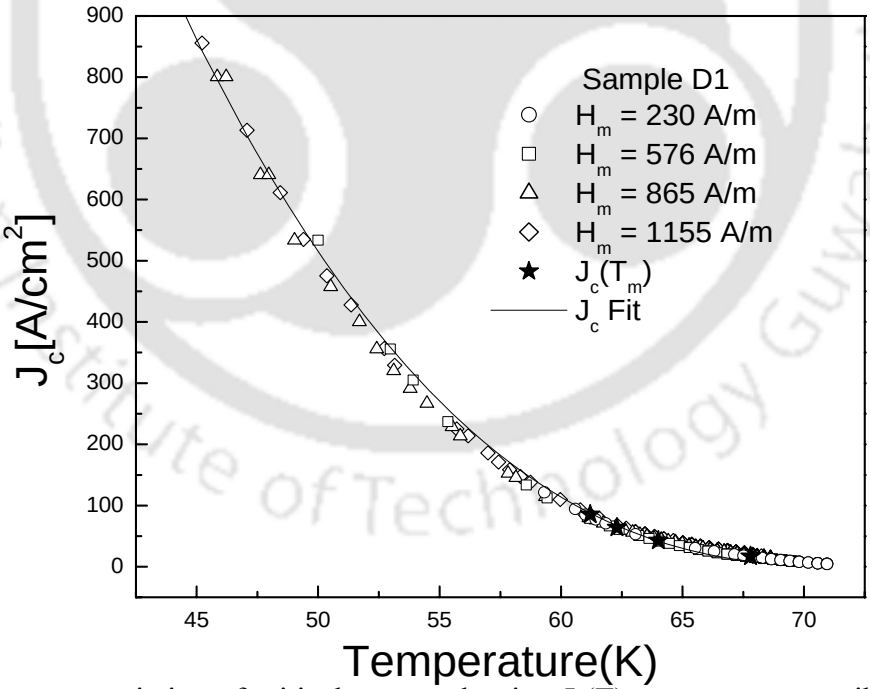

Fig.4.21. Temperature variation of critical current density, $J_c(T)$ as per ac susceptibility analysis for sample D1. $J_c(T_m)$ estimated by applying critical state model at at $\chi^{//}$ peak temperatures are shown as stars.

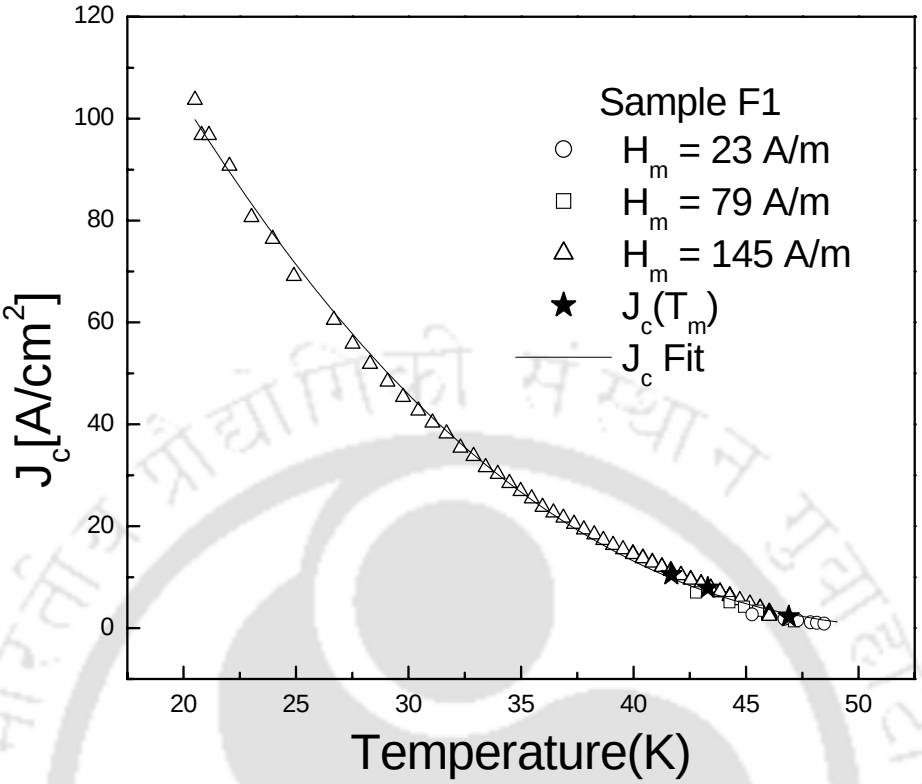

Fig.4.22. $J_c(T)$ versus temperature for sample F1 estimated from the ac susceptibility analysis. $J_c(T_m)$ estimated by using eqn. 4.12 at $\chi^{//}$ peak temperatures are shown as stars.

4.2.3. AC Susceptibility Study in Pure and Ag doped $(La_{1-x}R_x)_2Ba_2Ca_yCu_{4+y}O_z$ (R =Y, Gd, y = 4x, ($0 \leq x \leq 0.25$)) Superconductors

Here three samples of Y substituted and four samples of Gd substituted underdoped series are taken up for detailed ac susceptibility study. They are given as follows,

(i) $La_{1.7}Y_{0.3}Ba_2Ca_{0.6}Cu_{4.6}O_z$ (Sample G) of dimension $(2.7 \times 2.8 \times 8.6)$ mm^3

(ii) $La_{1.6}Y_{0.4}Ba_2Ca_{0.8}Cu_{4.8}O_z$ (Sample H) of dimension $(2.3 \times 3.7 \times 10.8)$ mm^3

(iii) $La_{1.6}Gd_{0.4}Ba_2Ca_{0.8}Cu_{4.8}O_z$ (Sample J) of dimension $(2.2 \times 2.3 \times 8.7)$ mm^3

(iv) $La_{1.5}Gd_{0.5}Ba_2CaCu_5O_z$ (Sample K) of dimension $(2.2 \times 2.3 \times 8.9)$ mm^3

(v) $La_{1.6}Y_{0.4}Ba_2Ca_{0.8}Cu_{4.8}O_z$ + 5 wt % of Ag (Sample H1) of dimension $(2.2 \times 2.3 \times 8.5)$ mm^3

(vi) $La_{1.6}Gd_{0.4}Ba_2Ca_{0.8}Cu_{4.8}O_z$ + 5 wt % of Ag (Sample J1) of dimension $(2.5 \times 2.6 \times 9.0)$ mm^3

(vii) $La_{1.5}Gd_{0.5}Ba_2CaCu_5O_z$ + 5 wt % of Ag (Sample K1) of dimension $(1.9 \times 2.0 \times 7.0)$ mm^3

The temperature variation of real and imaginary components of ac susceptibility measured at different ac field amplitudes such as 47 A/m (circles), 189 A/m (squares) and 473 A/m (triangles) are shown in Fig. 4.23 for sample G. The diamagnetic onset temperature is found to be 44.6 K. One can see from the figure that the $\chi^{/}$ value has not reached -1 at lower temperature and for lowest applied field because of the low level of $CaCuO_2$ doping. The $\chi^{//}$ peak temperature (T_m) varies from 35.7 to 28.5 K, when applied field was increased from 47 A/m to 473 A/m.

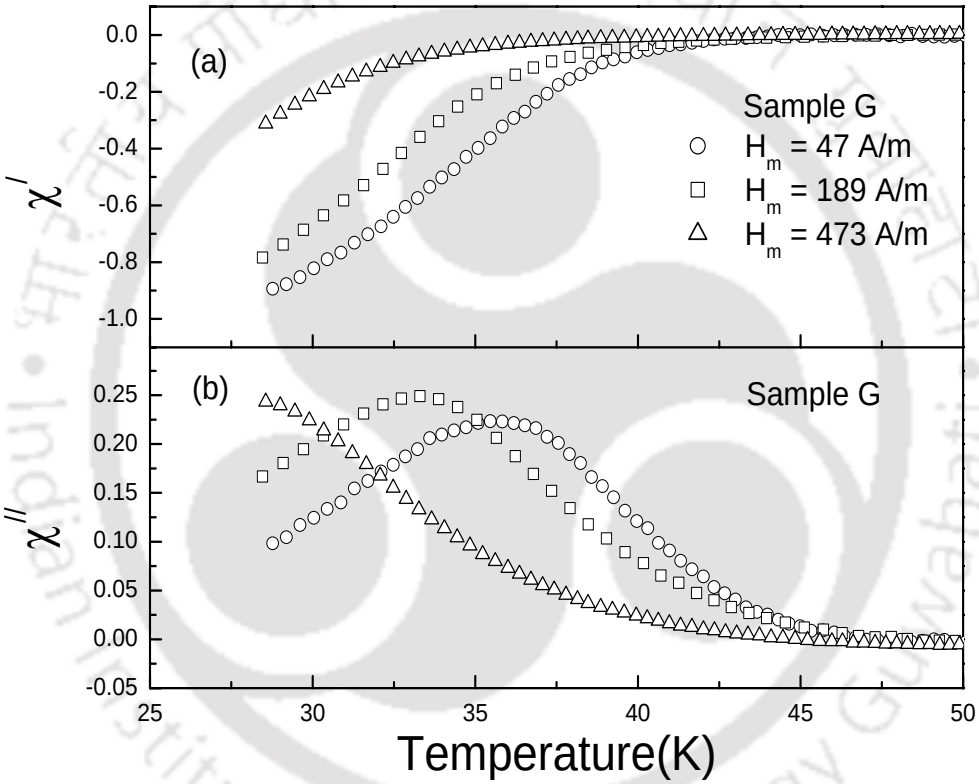

Fig. 4.23. Plots of (a) real and (b) imaginary components of ac susceptibility versus temperature of Sample G at ac field amplitudes of 47 A/m (circles), 189 A/m (squares) and 473 A/m (triangles).

Similarly, $\chi^{/}$ and $\chi^{//}$ as a function of temperature measured at various ac field amplitudes are shown in Figs. 4.24 to 4.29 for all other samples of the above series. For all these samples, $\chi^{/}$ approaches -1 at lower temperature and for low applied field, and its value increases with the increase of applied field. The $\chi^{//}$ peak temperature (T_m) varies from 62.5 to 57.2 K for applied field H_m of 47 A/m to 473 A/m; 40.9 to 31.7 K for H_m = 47 to 473 A/m; 54.9 to 46.0 K for H_m =

47 to 473 A/m; 67.7 to 60.6 K for H_m = 47 to 1353 A/m; 48.3 to 41.4 K for H_m = 47 to 473 A/m and 59.6 to 56.5 K for H_m = 47 to 473 A/m for samples H, J, K, H1, J1 and K1 respectively. The H_m and T_m values for different samples are given in Table 4.3.

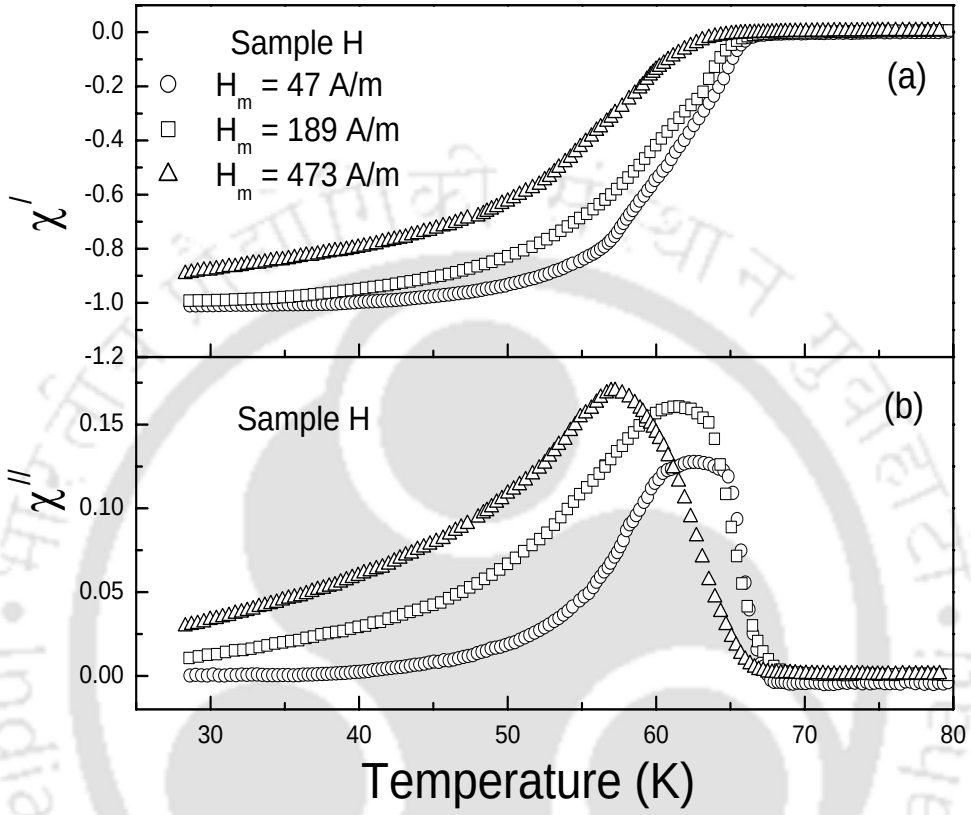

Fig. 4.24. Plots of (a) real and (b) imaginary components of ac susceptibility versus temperature for pure sample H at ac field amplitudes of 47 A/m (circles), 189 A/m (squares) and 473 A/m (triangles).

The critical current density J_c at T_m have been calculated for all these samples using eqn.4.12 and they are given in Table 4.3. At a given temperature, the Ag doped sample exhibits improved critical current density. This may be due to the addition of Ag which suppresses the intergranular weak links between the grains and/or play a role in enhancing the superconducting property of intergranular matrix. According to Xu et al.[350], it is known that Ag addition plays a role in enhancing the oxygenation of the material.

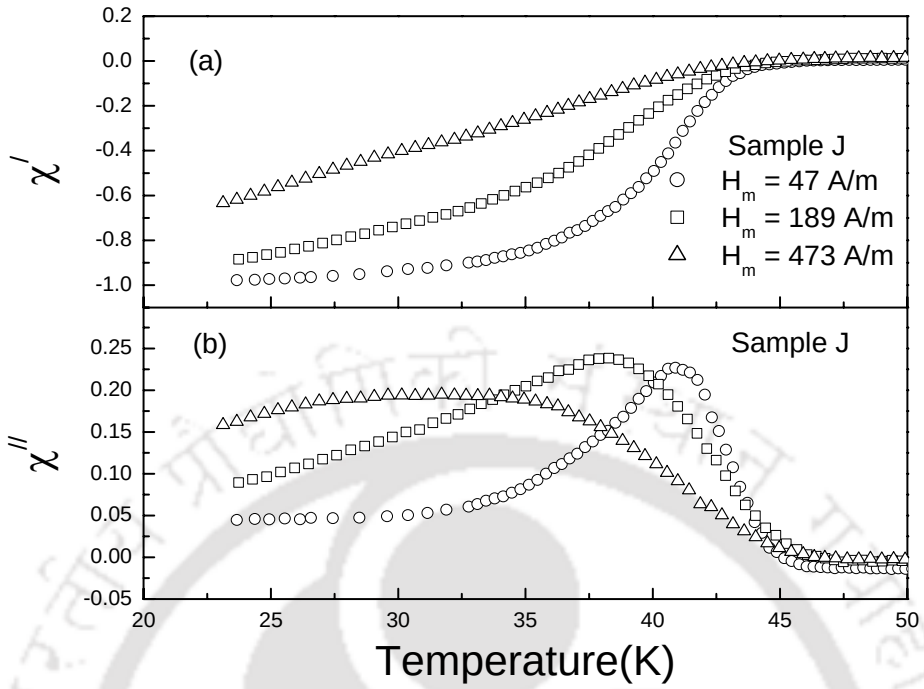

Fig. 4.25. Plots of (a) real and (b) imaginary components of ac susceptibility versus temperature for sample J at ac field amplitudes of 47 A/m (circles), 189 A/m (squares) and 473 A/m (triangles).

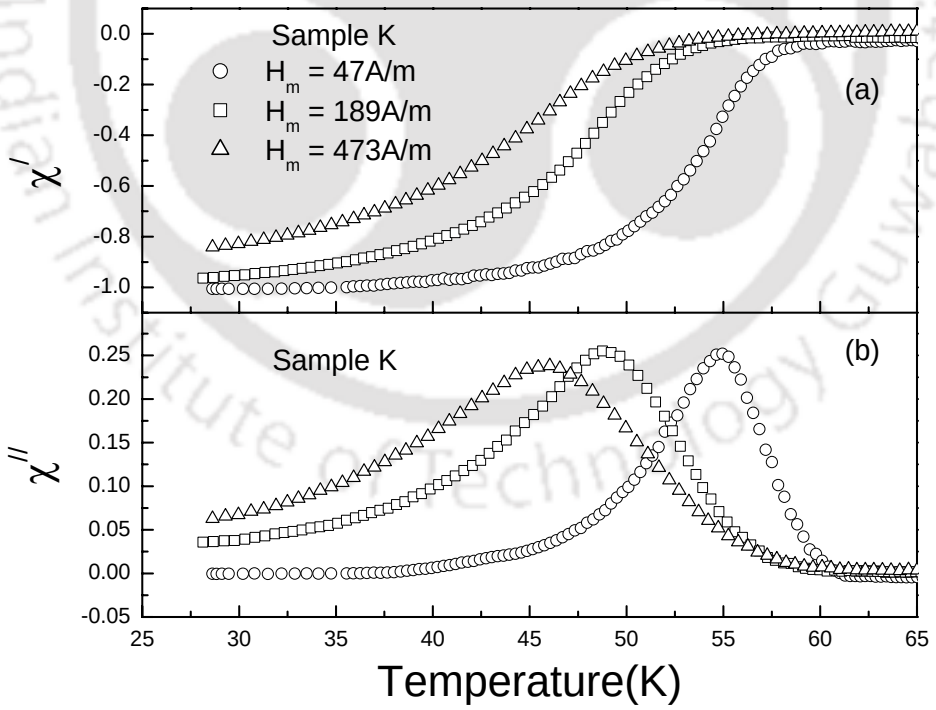

Fig. 4.26. Plots of (a) real and (b) imaginary components of ac susceptibility versus temperature for Sample K at ac field amplitudes of 47 A/m (circles), 189 A/m (squares) and 473 A/m (triangles).

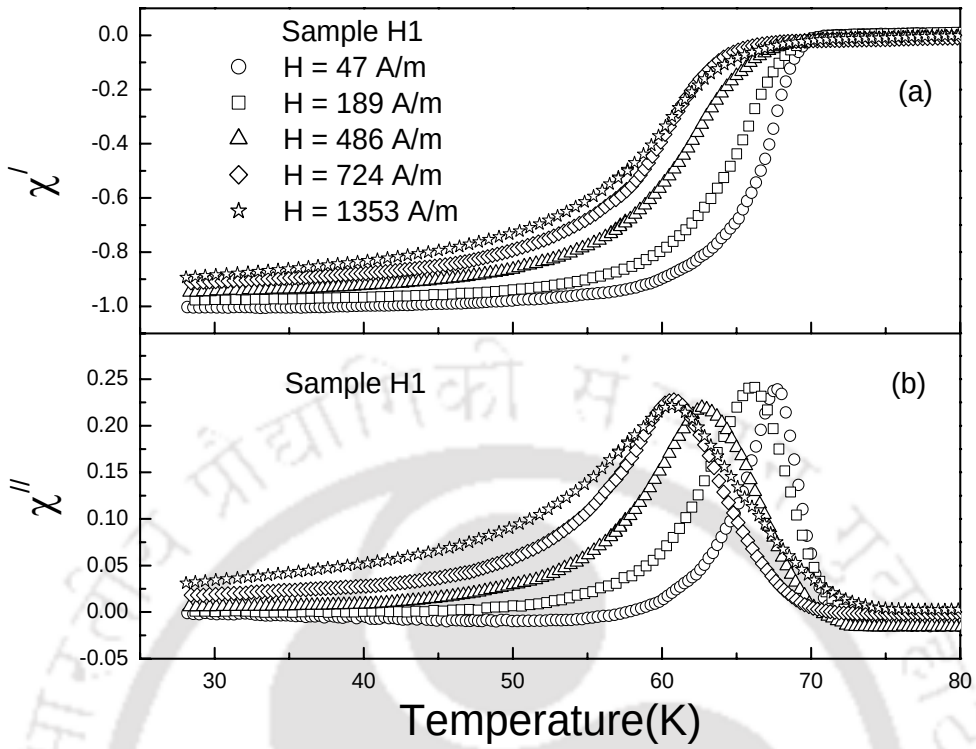

Fig. 4.27. Plots of (a) real and (b) imaginary components of ac susceptibility versus temperature for Sample H1 at ac field amplitudes of 47 A/m (circles), 189 A/m (squares), 486 A/m (triangles), 724 A/m (diamonds) and 1353 A/m (stars).

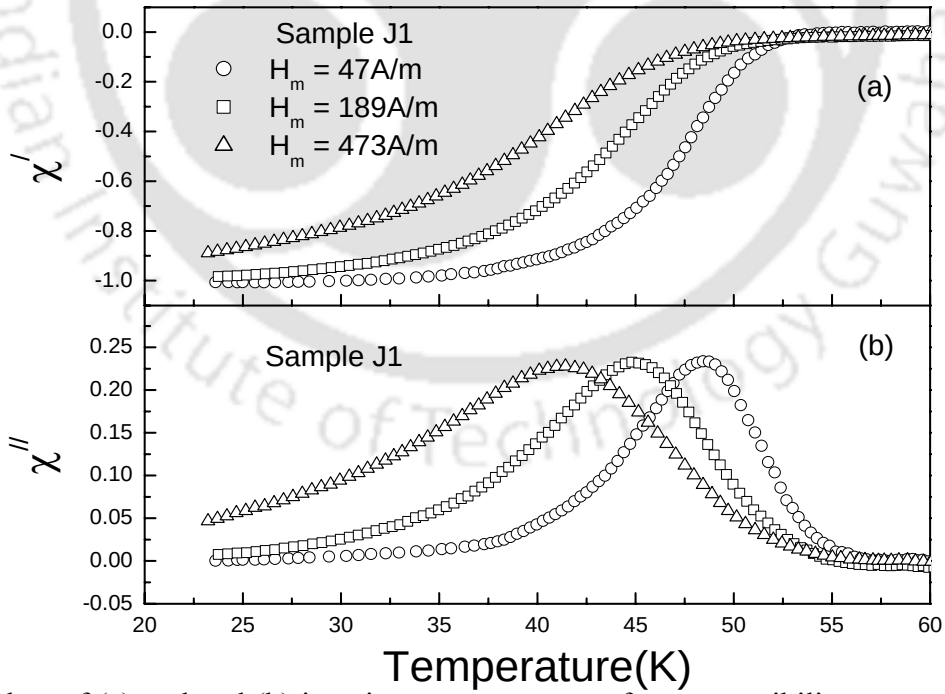

Fig. 4.28. Plots of (a) real and (b) imaginary components of ac susceptibility versus temperature for sample J1 at ac field amplitudes of 47 A/m (circles), 189 A/m (squares) and 473 A/m (triangles).

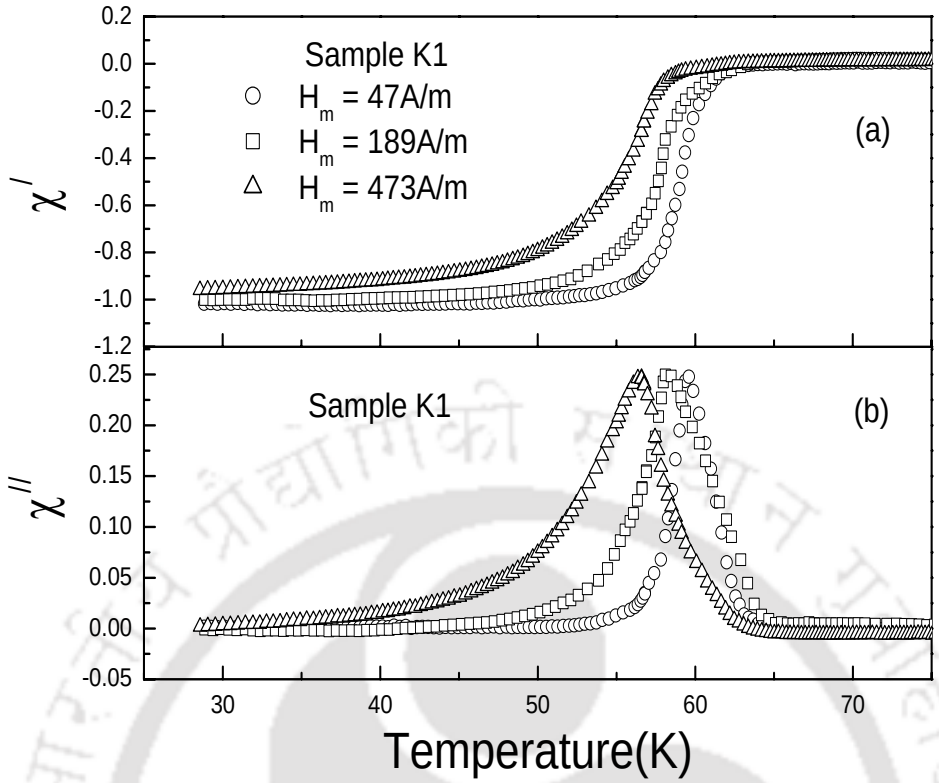

Fig. 4.29. Plots of (a) real and (b) imaginary components of ac susceptibility versus temperature for Sample K1 at ac field amplitudes of 47 A/m (circles), 189 A/m (squares) and 473 A/m (triangles).

Table-4.3: List of parameters obtained from temperature variation of susceptibility of samples G, H, J, K, H1, J1 and K1.

Sample Name	T_m (K)	H_m (A/m)	$J_c(T_m)$ (A/cm^2)
Sample G	35.7	47	3.3
	33.3	189	13.5
	28.5	473	33.7
Sample H	62.5	47	4.0
	61.4	189	16.4
	57.2	473	41.1
Sample J	40.9	47	3.3
	38.3	189	13.5
	31.7	473	33.7
Sample K	54.9	47	4.7
	48.8	189	18.9
	46.0	473	47.3
Sample H1	67.7	47	3.6
	66.2	189	14.7
	62.6	486	37.7
	60.7	724	56.6
	60.6	1353	105.9
Sample J1	48.3	47	3.6
	44.8	189	14.5
	41.4	473	36.3
Sample K1	59.6	47	4.0
	58.3	189	16.4
	56.5	473	41.1

In summary, the temperature and field variations of ac susceptibility have been measured on pure and 5 wt% of Ag doped $(La_{1-x}Y_x)_2Ba_2CaCu_5O_z$ superconductors. The field dependence of ac susceptibility data could be fitted interms of Kim critical state model. From the above analysis, the parameters p, full penetration field H_p and effective volume fractions of the superconducting grains (f_g) have been estimated. The f_g values are found to be quite small and is explained on the basis of finer superconducting grains. By applying Kim critical state model to field variation of susceptibility data and comparing with that of temperature variation of susceptibility data, the intergranular critical current density (J_c) as a function of temperature has been estimated. In addition to that J_c at $\chi^{//}$ peak temperature, T_m has been determined by taking H_m as the full penetration field at T_m. The $J_c(T)$ estimated from both the technique follow the same trend. The Ag doped samples show relatively larger J_c at a given temperature. The magnitude of J_c is comparable to that reported in literature on polycrystalline granular high T_c superconductors [317, 318].

The temperature variation of $J_c(T)$ could be fitted to a power law relation. From the fit, the exponent 'n' has been found out and it is close to 2. This suggests that these materials exhibit superconductor-normal metal-superconductor (SNS) type of junctions. Such a type of feature has been reported on $YBa_2Cu_3O_7$ superconductors [331]. The pure samples are having relatively large 'n' values compared to that of Ag doped samples. This suggests that in pure samples, the $J_c(T)$ falls rather sharply with increase in temperature. So the Ag doped samples show improved intergranular critical current density compared to pure samples. This may be due to the role of Ag in reducing porosity and improving intergranular coupling.

In underdoped series, critical current density at $\chi^{//}$ peak temperature, T_m has been estimated from temperature variations of ac susceptibility carried out at different applied ac fields. It is found to be in the order of 3 to 106 A/cm^2 as the temperature is lowered from T_c. The J_c of underdoped series is relatively lower than that of optimum doped series.

CONCLUSIONS

This chapter gives the summary of results and important conclusions drawn from my research work presented in the thesis.

As reviewed in introduction, even though the La-Ba-Ca-Cu-O superconductors with tetragonal structure is known for about two decades, to our knowledge there is no detailed work on fluctuations induced excess conductivity, fluctuation magneto conductivity and magnetic studies in terms of critical state models. The above compounds are widely reported with several different type of starting compositions such as $La_3Ba_3CaCu_7O_z$, $La_2Ba_2CaCu_5O_z$, $LaBaCaCu_3O_z$ with T_c ranging from 66 to close to 80 K. Even though, there are several reports on the partial replacement of La by several rare earth elements such as Pr, Nd, Gd, Dy etc., there is no report of Y doping to our knowledge except on underdoped materials. The interesting feature of the above compounds are, they exhibit tetragonal structure similar to that of tetragonal $YBa_2Cu_3O_{7-\delta}$ with comparable lattice parameters. However, $YBa_2Cu_3O_{7-\delta}$ in tetragonal form does not exhibit superconductivity for $\delta > 0.5$. So, it would be interesting to study this series of compounds which exhibits tetragonal structure and superconductivity and compare with those of superconducting $YBa_2Cu_3O_7$.

In the present thesis, I have prepared three series of superconductors namely $(La_{1-x}Y_x)_2Ba_2CaCu_5O_z$, $(La_{1-x}Y_x)_2Ba_2Ca_{4x}Cu_{4+4x}O_z$ and $(La_{1-x}Gd_x)_2Ba_2Ca_{4x}Cu_{4+4x}O_z$. Each series has been prepared in pure form and by adding 5 wt % of Ag to enhance intergranular coupling and critical current density. An ac susceptibility set up has been developed to measure the temperature and field variations of ac susceptibility of superconducting materials and it has been calibrated against standard samples as demonstrated in chapter 2. In addition, sample insert assembly for magneto-resistivity measurements and a high temperature furnace have been fabricated.

X-ray diffraction patterns of all samples could be refined using *P4/mmm* space group. Rietveld refinement analysis shows that these materials exhibit tetragonal structure and the typical lattice parameters are found to be a = b = 3.879 Å, c =11.646 Å for x = 0 and a = b = 3.856 Å, c = 11.576 Å for x = 0.5 samples in the first series. The lattice parameters mostly decrease with increase in doping concentration and it can be understood as a result of smaller ionic size of Y compared to La. The Cu2-O3-Cu2 bond angle is found to be mostly in the range

of 162 to 164^{o}. The above bond angle is about 3 to 5^{o} less than that reported for tetragonal $YBa_2Cu_3O_{7-\delta}$ and this deviation could be mainly due to the partial occupation of Ca in La site. About 51 to 55% of Ca is found to occupy the La(Y) site and the remaining Ca occupies the Ba site. The Ba site is also occupied by about 44 to 55 % of La. In the case of Ag doped samples, Ca at La site is found to vary from 52 to 56 % and the La at Ba site is found to be around 48 to 59 %. The occupancy values of doped elements and various other elements are generally comparable to the nominal composition. However, some vacancy has been observed especially in Cu site. Similarly, the under doped series $(La_{1-x}Y_x)_2Ba_2Ca_{4x}Cu_{4+4x}O_z$ and $(La_{1-x}Gd_x)_2Ba_2Ca_{4x}Cu_{4+4x}O_z$ could be prepared in single phase form and their XRD patterns could be refined using *P4/mmm* space groups. Their typical lattice parameters are a = b = 3.860, c = 11.576 Å and, a = b = 3.869, c = 11.613 Å for x = 0.20 in the former and latter series respectively. The Gd doped series exhibit relatively large lattice parameters, compared to Y doped materials because of larger ionic size of Gd. These series also show the signature of intermixing of Ca at La and Ba sites and, La at Ba site.

The samples have been also characterized by recording SEM photographs and EDX analysis. They exhibit uniform morphology with grain size ranging from about 1 to 2.5 μm and the sample compositions are mostly comparable to the nominal starting compositions.

Temperature variation of electrical resistivity measurements show that all the samples exhibit superconducting transitions. In the first series, the transition temperature varies from 60 to 74 K without Ag doping and, about 65 to 75 K with Ag doping. The Ag doping found to enhance the T_c due to improved intergranular coupling etc. The maximum T_c was observed for x = 0.25 sample with Ag doping. The room temperature electrical resistivity is found to be in the range of 1.6 to 4.5 mΩ.cm and it is about one order of magnitude less than that, reported in literature. It shows that the prepared materials are quite homogeneous. It may be also noted that in literature, most of the authors have reported only electrical resistance rather than resistivity, so it could not be compared with many reports. The underdoped series also show superconducting transitions with zero electrical resistivity and, the T_c is found to vary from 49 to 73 K.

The prepared materials have been characterized by measuring low field temperature variation of ac susceptibility. All the samples show diamagnetic transitions and, for most of the samples, χ' approaches -1 at low temperature. Other than intergranular and intragranular superconducting transitions, no other magnetic transition due to any impurity has been observed.

The $\chi^{//}$ versus temperature plots show peak corresponding to maximum loss in the intergranular region. The diamagnetic transitions are mostly comparable to the superconducting transitions observed from electrical resistivity measurements.

The electrical resistivity data measured at close temperature intervals on some selected samples from optimum and underdoped series have been analyzed in terms of fluctuations induced excess conductivity in the mean field regime, by using Aslamazov-Larkin (AL), Lawrence-Doniach (LD) and Maki-Thompson (MT) models. The fluctuations in the amplitude of order parameter are found to be two dimensional in nature. This is in contrast to 2D to 3 D cross-over reported in orthorhombic superconducting $YBa_2Cu_3O_7$ in the mean field regime. This suggests that; according to LD model, the interlayer coupling constant $J(T) = (\xi_c(T)/d)^2 << 1/4$ in the present materials. The rather low value of J(T) could be mainly due to reduced $\xi_c(T)$ in the present materials compared to $YBa_2Cu_3O_7$ because, the d values are comparable in both the systems. There is a possibility of large anisotropy and hence a small $\xi_c(T)$ in the present series that lead to 2D fluctuations. The coherence length along c-direction at 0 K is found to be mostly in the range of 0.30 to 0.77 Å. The phase breaking time, $\tau_\phi(100K)$ is found to be in the order of 10^{-16}s, which indicates that the contribution of Maki-Thompson term to zero field excess conductivity is rather insignificant.

The magneto-resistivity as a function of temperature was measued at an applied magnetic field of 1T on above samples, where excess conductivity have been analyzed. The magneto-resistivity data were analyzed in terms of fluctuation magneto-conductivity ($\Delta\sigma_H$) by using AL and MT models for layered superconductors and by taking into account both Orbital and Zeeman terms. The values of $\xi_c(0)$ and $\tau_\phi(100\ K)$ are comparable to those obtained from $\Delta\sigma$ analysis. These materials exhibit strong pair breaking effect and the typical phase breaking time at 100 K is found to be in the order of 10^{-16}s. The magnitude of coherence lengths along ab plane, $\xi_{ab}(0)$ is found to be in the range of 14 to 34 Å and are comparable to those reported for $YBa_2Cu_3O_7$ samples.

Moreover, I have carried out excess conductivity analysis in the paracoherence regime, i.e. $T_c(0)$ to T_c, where there is fluctuations in the phase of the order parameter. This analysis has been carried out on pure and 5 wt % Ag doped $(La_{1-x}Y_x)_2Ba_2CaCu_5O_z$ superconductors, in the absence and presence of 1T magnetic field. In the absence of magnetic field, these materials exhibit cross over from ordered phase fluctuations with the critical exponent comparable to that

of pure 3D XY ferromagnet to disordered phase fluctuations with the critical exponent comparable to that of disordered 3D Heisenberg ferromagnetic system. The disordered phase fluctuations appear for a much wider temperature region in the case of Ag doped samples compared to that of pure samples. Unlike the pure sample, where the intergranular weak link matrix completely turns into superconducting state as the temperature is lowered, the presence of Ag dilutes the superconducting matrix to some extent, thereby causing disordered phase fluctuations in much wider temperature region. The above argument may appear to contradict the observed enhanced T_{c0} in Ag doped sample and this could be due to the indirect effect of Ag, which helps in oxidation of weak link network and thereby enhanced T_{c0}.

In the presence of magnetic field, all the samples exhibit only ordered phase fluctuations. It may be noted that the above critical exponent is observed in the temperature region close to T_c and in the same temperature region, zero field excess conductivity data falls rather sharply without showing any linear behavior. In the above temperature region and in the presence of magnetic field, there is a possibility of some of the defects within the grains turning into normal state leading to intragranular Josephson coupling behaving like ordered phase fluctuations.

Excess conductivity in the paracoherence regime also has been analyzed on some of the underdoped series in the absence of magnetic field. These samples also show cross-over from ordered phase fluctuations to disordered phase fluctuations.

I have derived expressions for real and imaginary components of intergranular matrix susceptibility ($\chi_m^{/}$ and $\chi_m^{//}$) using the expressions for magnetization derived from Kim critical state model. The expressions for complex ac susceptibility derived from Kim model are a function of H_m/H_p, p and a/b, where H_m is the amplitude of the applied ac field, H_p is the full penetration field and p is a constant.

From the measured field variation of susceptibility data at different temperatures, the field dependence of intergranular matrix susceptibility ($\chi_m^{/}$ and $\chi_m^{//}$) have been obtained by choosing the appropriate values of f_g. Similarly, temperature variations of intergranular matrix susceptibility ($\chi_m^{/}$ and $\chi_m^{//}$) at different ac fields have been obtained from the measured susceptibility data by using the f_g values obtained from the analysis of field variation $\chi^{/}$ and $\chi^{//}$ carried out in the vicinity of $\chi^{//}$ peak temperature. The f_g values for different samples are found to be in the range of 10 to 25 %. It is quite small compared to $YBa_2Cu_3O_7$ and it is explained on the

basis of finer superconducting grains. Such a small value of f_g has been also reported in literature especially for Nd-123 and Bi-Sr-Ca-Cu-O system.

After calculating the intergranular matrix susceptibility ($\chi_m^{/}$ and $\chi_m^{//}$) from field variation and temperature variation of ac susceptibility, these data have been analyzed using critical state models. Field variation of susceptibility data could be fitted to Kim critical state model. The temperature variation of critical current density $J_c(T)$ was calculated by using both field and temperature variations of $\chi_m^{/}$ data. The temperature variation of J_c estimated from the above analysis has been studied by fitting to standard theoretical expression. The exponent 'n' obtained from J_c fit is close to the value 2 and it suggests that these materials exhibit superconductor - metal – superconductor (SNS) type of junctions. Ag doped samples show improved intergranular critical current density compared to pure samples.

----------XXX----------

LIST OF PUBLICATIONS

(a) In National/International Journals:

(1) Study of Crystal Structure and Characterization of Pure and Ag doped $(La_{1-x}Y_x)_2Ba_2CaCu_5Oz$ $(0 \leq x \leq 0.5)$ Superconductors.

P. K. Nayak and S. Ravi

Accepted in Journal of the American Ceramic Society (2007).

(2) Excess Conductivity and Magneto-conductivity Studies in pure and Ag doped $(La_{1-x}Y_x)_2Ba_2CaCu_5O_z$ superconductors.

P. K. Nayak and S. Ravi

Supercond. Sci. Technol. **19** (2006) 1209-1214.

(3) Excess Conductivity in the Paracoherence Regime of pure and Ag doped $(La_{1-x}Y_x)_2Ba_2CaCu_5O_z$ superconductors.

P. K. Nayak and S. Ravi

Solid State Commun. **140** (2006) 464-468.

(4) Fluctuation Magneto-Conductivity in La-Ba-Ca-Cu-O Superconductors**.**

P. K. Nayak and S. Ravi

Journal of Superconductivity and Novel Magnetism, **19**, 6 (2006) 515-520.

(5) AC susceptibility and intergranular critical current density study in pure and Ag doped $(La_{1-x}Y_x)_2Ba_2CaCu5O_z$ Superconductors.

P. K. Nayak and S. Ravi

Solid State Communications, **138** (2006) 377-381.

(6) Excess Conductivity in the Mean Field and Paracoherence Regimes of $(La_{1.6}Y_{0.4})Ba_2\,Ca_{0.8}\,Cu_{4.8}O_z$ Superconductors.

P. K. Nayak and S. Ravi

Modern Physics Letters B, **20** (2006)111-122.

(7) AC susceptibility study in the single phase Bi-2223 system.

S. Keshri, V. Dayal, S. Ravi and **P. K. Nayak**

Czechoslovak Journal of Physics, **55** (2005) 73-84.

(8) Transport & Thermal properties of $Bi_{1.2}Pb_{0.33}Sr_{1.54}Ca_{2.06}Cu_3O_y$ superconductor.

V. Dayal, S. Keshri, **P. K. Nayak** and S. Ravi

Indian Journal of Cryogenics, **28** (2003) 122-126.

(b) In Refereed Conference Proceedings:

(1) Study of Critical Current Density from ac Susceptibility Measurements in $(La_{1-x}Y_x)_2Ba_2CaCu_5O_z$ Superconductors.

P. K. Nayak and S. Ravi

Proceedings of Physics Academy of North East (India) 2007 in Press.

(2) Excess conductivity, magneto-conductivity and ac susceptibility studies in La-Ba-Ca-Cu-O Superconductors.

P. K. Nayak

Proceedings of Solid State Physics (India) **51** (2006) 1005-1006.

(3) Fluctuations induced magneto-conductivity study in Pure and Ag doped $(La_{1.6}Y_{0.4})Ba_2(Ca_{0.8}Cu_{4.8})O_z$ Compounds.

P. K. Nayak and S. Ravi

Proceedings of Solid State Physics (India) **50** (2005) 649-650.

(4) AC Susceptibility and Critical Current Density in $(La_{1.5}Y_{0.5})Ba_2CaCu_5O_{11}$ compound.

P. K. Nayak and S. Ravi

Proceedings of Solid State Physics (India) **46** (2003) 615-616.

----------XXX----------

REFERENCES

[1] H. Kamerlingh Onnes, Leiden commun. **1206**, 1226 (1911).

[2] W. Meissner and R. Ochenfeld, Naturwiss **21**, 787 (1933).

[3] T. V. Ramakrishnan and C. N. R. Rao, Superconductivity Today, p.12, p.26-54,Wiley Eastern Ltd., India (1992).

[4] F. B. Silsbee and J. Wash. Acad Sci: **6**, 597 (1916).

[5] Werner Buckel, Superconductivity-Fundamentals and applications, p.150, p.20, (VCH, Weinheim Germany) 1991.

[6] E. Maxwell, Phys Rev. **78,** 477 (1950).

[7] C. A. Reynolds, B. Serin, W. H. Wright and L .B. Nesbitt, Phys. Rev. **78**, 487 (1950).

[8]. R. Doll and M Näbauer, Phys. Rev. Lett. **7**, 51 (1961).

[9] B. S. Deaver, Jr. and W. M. Fairbank, Phys. Rev. Lett. **7**, 43 (1961).

[10] F. London, Superfluids, Vol 1, page 152, Wiley 1950.

[11] R. E. Glover, III and M.Tinkham, Phys. Rev. **108**, 243 (1957) (Werner Buckel, Superconductivity, VCH-1991, p 54).

[12] I. Giaever, Phys. Rev. Lett. **5**, 464 (1960).

[13] J. C. Fisher and I. Giaever, J. Appl. Phys. **32**, 172 (1961).

[14] B. D. Josephson, Phys. Rev. Lett **1**, 251 (1962).

[15] I. Giaever, Phys .Rev. Lett **14**, 904 (1965).

[16] A. C. Roseinnes and E. H. Rhoderick, Introduction to Superconductivity, p 175, p 54 (pergamen press, 1894).

[17] C. P. Poole Jr, H. A. Farach, R. J. Creswick, Superconductivity, p 61-89 (Academic Press, London, 1995).

[18] B. T. Matthias, Phys .Rev. **97**, 74 (1955).

[19] F. London and H. London, Z. Phys **96**, 359 (1935).

[20] A. J. Rutgers, Physica C **3**, 999 (1936).

[21] A. B. Pippard, Proc. Royal. Soc. (London) A **216**, 547 (1953).

[22] V. L. Ginzburg and L. D. Landau, Zh. Eksperim. i. Teor. Fiz **20**, 1064 (1950).

[23] J. Bardeen, L. N. Cooper and J. R. Schrieffer, Phys. Rev. **108**, 1175 (1957).

[24] L. P. Gor'kov, Soviet Phys. –JETP **9**, 1364 (1959).

[25] M. Tinkham, Introduction to superconductivity, second edition, p 110-147(McGrew-Hill International Edition, 1996).

[26] H. Frölich, Proc. Royal Soc. (London) A **215**, 291 (1952).

[27] A. A. Abrikosov, J. Experim. Theoret. Phys. (USSR) **32**, p. 1442, 1957 (translation: Soviet Phys.-JETP 5, p. 1174, 1957).

[28] J. R. Gavoler, Appl. Phys. Lett. **23**, 480 (1973).

[29] J. G. Bednorz and K. A. Müller, Z. Phys. B Conden. Matter **64**, 189 (1986).

[30] S. Uchida, H. Takagi, K. Kitagawa and S. Tanaka, Jpn. J. Appl. Phys **26**, L1 (1987).

[31] H. Takagi, S. Uchida, K. Kitagawa and S. Tanaka, Jpn. J. Appl. Phys **26**, L123 (1987).

[32] R. J. Cava, R. B. Van Dover, B. Batlogg and E. A. Rietman, Phys. Rev. Lett. **58**, 408 (1987).

[33] D. W. Capone, D. G. Hinks, J. D. Jorgansen, Appl. Phys. Lett. **50**, 543 (1987).

[34] C. W. Chu, P. H. Her, R. L. Meng, L. Gao and Z. G. Huang, Science **235**, 567 (1987).

[35] J. M. Tarascon, L. H. Greene, P. Barboux, W. R. McKinnon, G. W. Hull, T. P. Orlando, K. A. Delin, S. Foner and E. J. Mc Niff, Jr. Phys. Rev. B **36**, 8393 (1987).

[36] G. Xiao, A. Bakhshai, M. Z. Cieplak, Z. Tesanovic and C. L. Chien, Phys. Rev. B **39**, 315 (1989).

[37] M. K. Wu, J. R. Ashburn, C. J. Torng, P. H. Hor, R. L. Meng, L. Gao, Z. J. Huang, Y. Q. Wang and C. W. Chu, Phys. Rev. Lett. **58**, 908 (1987).

[38] R. J. Cava, B. Batlogg, R. B. Van Dover, D. W. Murphy, S. Sunshine, T. Siegrist, J. P. Remeika, E. A. Rietman, S. Zahurak and G. P. Espinosa, Phys. Rev. Lett. **58**, 1676 (1987).

[39] R. M. Hazen, L. W. Finger, R. J. Angel, C.T. Prewitt, N. L. Ross, H. K. Mao, C. G. Hadichiacos, P. H. Hor, R.L. Meng and C.W. Chu, Phys. Rev. B **35**, 7238 (1987).

[40] P. M. Grant, R. Beyers, E. M. Engler, G. Lim, S. S. P Parkin, M. L. Ramirez, V. Y. Lee, A. Nazal, J. E. Vasquez and R. J. Savoy, Phys. Rev. B **35**, 7242 (1987).

[41] T. Siegrist, S. Sunshine, D. W. Murphy, R. J. Cava and S. M. Zahurak, Phys. Rev. B **35**, 7137 (1987).

[42] M. A. Beno, L. Soderholm, D. W. Capone II, D. G. Hinks, J. D. Jorgensen, I. K. Schüller, C. V. Segre, K. Zhang and J. D. Grace, Appl. Phys. Lett. **51**, 6 (1987).

[43] P. H. Hor, R. L. Meng, Y. Q. Wang, L. Gao, Z. J. Huang, J. Bechtold, K. Forster and C. W. Chu, Phys. Rev. Lett. **58**, 1891 (1987).

[44] J. M. Tarascon, W. R. McKinnon, L. H. Greene, G. W. Hull and E. M. Vogel, Phys. Rev. B **36**, 226 (1987).

[45] Z. Fisk, J. D. Thompson, E. Zirngiebel, J. L. Smith and S. W. Cheong, Solid State Commun. **62**, 743 (1987).

[46] S. Hasoya, S. I. Shamoto, M. K. Onoda and M. Sato, Jpn. J. Appl. Phys. **26**, L325 (1987).

[47] D. W. Murphy, S. Sunshine, R. B. Van Dover, R. J. Cava, B. Batlogg, S. M. Zahurak and L. F. Schneemeyer, Phys. Rev. Lett. **58**, 1888 (1987).

[48] J. R. Thompson, S. T. Sekula, D. K. Christen, B. C. Sales, L. A. Boatner and Y. C. Kim, Phys. Rev. **B 36**, 718 (1987).

[49] A. R. Modenbaugh, M. Suenaga, T. Asano, R. N. Shelton, H. C. Ku, R. W. McCallum and P. Klavin, Phys. Rev. Lett. **58**, 1885 (1987).

[50] R. J. Cava, B. Batlogg, C. H. Chen, E. A. Rietman, S. M. Zahurak and D. Werder, Phys. Rev. B **36**, 5719 (1987).

[51] P. K. Gallagher, H. M. O'Bryan, S. A. Sunshine, D. W. Murphy, Mat. Res. Bull. **22**, 995 (1987).

[52] C. N. R. Rao, Int. Conf. on Superconductivity, p. 72, ed. S. K. Joshi, C. N. R. Rao and S. V. Subramanyam, World Scientific 1990.

[53] G. K. Bichile, D. G. Kuberkar, A. K. Rajarajan, S. S. Shah, L. C. Gupta and R. Vijaya Raghavan, Bull. Mater. Sci., **14**, 195 (1991).

[54] A. F. Marshall, R. W. Barton, K. Char, A. Kapitulnik, B. Oh, R. H. Hammond, S. S. Lachermann, Phys. Rev. B **37**, 9353 (1988).

[55] H. W. Zandbergen, R. Gronsky, K. Wang and G. Thomas, Nature **331**, 596 (1988).

[56] J. Karpinski, E. Kaldis, E. Jilek, S. Rusiechi and B. Bucher, Nature **336**, 660 (1988).

[57] D. E. Morris, J. H. Nickel, J. Y. Wei, N. G. Asmar, J. S. Scott, U. M. Scheven, C. T. Hultgren, A. G. Markelz, J. E. Post, P. J. Heaney, D. R. Veblen and R. M. Hazen, Phys. Rev. B **39**, 7347 (1989).

[58] R. J. Cava, J. J. Krajewski, W. F. Peck Jr, B. Batlogg, L. W. Rupp Jr, R. M. Fleming, A. C. W. P. James and P. Marsh, Nature **338**, 328 (1989).

[59] P. Bordet, C. Chaillout, J. Chenavas, J. L. Hodeau, M. Marezio, J. Karpinski and E. Kardis, Nature **334**, 596 (1988).

[60] C. Michel, H. Hervieu, M. M. Borel, A. Gradin, F. Deslandes, J. Provst and B. Raveau, Z. Für. Phys. Cond. Matt. **68**, 421 (1987).

[61] H. Maeda, Y. Tanaka, M. Fukutomi and T. Asano, Jpn. J. Appl. Phys. **27**, L209 (1988).

[62] H. W. Zanbergen, Y. K. Huang, M. J. V. Menken, JN, K. Kadouaki, A. A. Menovsky, G. Van Tendeloo and S. Amelinckx, Nature **332**, 620 (1988).

[63] R. Ramesh, C. J. D. Hetherington, G. Thomas, S. M. Green, C. Jiang, M. L. Rudee and H. L. Luo, Appl. Phys. Lett. **53**, 615 (1988).

[64] J. L. Tallon, R. G. Buckley, P. W. Gilberd, M. R. Presland, I. W. M. Brown, M. E. Bowden, L. A. Christian and R. Goguel, Nature **333**, 153 (1988).

[65] E. Takayama-Muromachi, Y. Uchida, Y. Matsui, M. Onoda and K. Kato, Jpn. J. Appl. Phys. **27**, L556 (1988).

[66] M. Hervieu, C. Michel, B. Domengues, Y. Laligant, A. Lebail, G. Feress and B. Raveau, Mod. Phys. Letters. B **2**, 491 (1988).

[67] J. M. Tarascon, W. R. McKinnon, P. Barboux, D. M. Hwang, B. G. Bagley, L. H. Greene, G. W. Hull, Y. LePage, N. Stoffel and M. Giroud, Phys. Rev. B **38**, 8885 (1988).

[68] S. A. Sunshine, T. Siegrist, L. F. Schneemeyer, D. W. Murphy, R. J. Cava, R. B. Van Dover, R. M. Fleming, S. H. Glarum, S. Nakahara, R. Farrow, J. J. Krajewski, S. M. Zahurak, J. V. Waszczak, J. H. Marshall, P. Marsh, L. H. Rupp Jr., and W. F. Peck, Phys. Rev. B **38**, 893 (1988).

[69] R. J. Cava, B. Batlogg, S. A. Sunshine, T. Siegrist, R. M. Fleming, K. Rabe, L. F. Schneemeyer, D. W. Murphy, R. B. Van Dover, P. K. Gallagher, S. H. Glarum, S. Nakahara, R. C. Farrow, J. J. Krajewski, S. M. Zahurak, J. V. Waszczak, J. H. Marshall, P. Marsh, L. W. Rupp, Jr.,W. F. Peck and E. A. Rietman, Physica C **153-155**, 560 (1988).

[70] M. Takano, Nature **333**, 200 (1988).

[71] F. Shi, T. S. Rong, S. Z. Zhou, X. F. Wu, J. Du, Z. H. Shi, C. G. Cui, R. Y. Jin, J. L. Zhang, Q. Z. Ran and N. C. Shi, Phys. Rev. B **41**, 6541 (1990).

[72] V. Seshu Bai, S. Ravi, T. Rajasekharan and R. Gopalan, J. Appl. Phys. **70**,4378 (1991).

[73] Z. Z. Sheng and A. M. Herman, Nature **332**, 55 (1988).

[74] Z. Z. Sheng and A. M. Herman, A. El. Ali, C. Almasan, J. Estrada, T. Datta, R. J. Matson, Phys. Rev. Lett. **60**, 937 (1988).

[75] Z. Z. Sheng and A. M. Herman, Nature **332**, 138 (1988).

[76] R. M. Hazen, L. W. Finger, R. J. Angel, C. T. Prewitt, N. L. Ross, C. G. Hadidiacos, P. J. Heaney, D. R. Veblen, Z. Z. Sheng, A. El Ali and A. M. Hermann, Phys. Rev. Lett **60**, 1657 (1988).

[77] M. A. Subramanian, J. C. Calabrese, C. C. Toradi, J. Gopalakrishnan, T. R. Askew, R. B. Flippen, K. J. Morrissey, V. Chowdhry and A. W. Sleight, Nature **332**, 420 (1988).

[78] C. C. Torardi, M. A. Subramanian, J. C. Calabrese, J. Gopalakrishnan, K. J. Morrissey, T. R. Askew, R. B. Flippen, V. Chowdhry and A. W. Sleight, Science **240**, 631 (1988).

[79] S. S. Parkin, V. Y. Lee, E. M. Engler, A. I. Nazzal, T. C. Huang, G. Gorman, R. Savoy and R. Beyers, Phys. Rev. Lett. **60**, 2539 (1988).

[80] S. S. Parkin, V. Y. Lee, A. I. Nazzal, R. Savoy, R. Beyers and S. J. La Placa, Phys. Rev. Lett. **61**, 750 (1988).

[81] M. Herview, A. Maignan, C. Martin, C. Michel, J. Provost and B. Raveau, J. Solid State Chem. **75**, 212 (1988).

[82] S. N. Putillin, E. V. Antipov, O. Chmaissem and M. Marezio, Nature **362**, 226 (1993).

[83] A. Schilling, M. Cantoni, J. D. Guo and H. R. Ott, Nature **363**, 56 (1993).

[84] H. Ihara, K. Tokiwa, H. Ozawa, M. Hirabayashi, A. Negishi, H. Matuhata, Y. S. Song, Jpn. J. Appl. Phys. **33**, 503 (1994).

[85] H. Ihara, K. Tokiwa, K. Tanaka, T. Tukamoto, T. Watanabe, H. Yamamoto, A. Iyo, M. Tokumotu, M. Umeda, Physica C **283-287**, 957 (1997).

[86] H. Yamamoto, K. Tanaka, K. Tokiwa, H. Hirabayashi, M. Tukamoto, N. A. Khan, H. Ihara, Physica C **302**, 137 (1998).

[87] L. Bauernfeind, W. Widder and H. F. Braun, Physica C **254**, 151 (1995).

[88] L. Bauenfeind, W. Widder, H. F. Braun, J. Low Temp. Physics **105**, 1605 (1996).

[89] I. Felner, U. Asaf, Y. Levi and O. Millo, Phys. Rev. B **55**, R3374 (1997).

[90] C. Bernhard, J. L. Tallon, Ch. Niedermayer, Th. Blasius, A. Golnik, E. Brücher, R. K. Kremer, D. R. Noakes, C. E. Stronach and E. J. Ansaldo, Phys. Rev. B **59**, 14099 (1999).

[91] I. Felner, U. Asaf, S. Reich and Y. Tsabba, Physica C **311**, 163 (1999).

[92] J. L. Tallon, C. Bernhard, J. W. Loram, J. Low Temp. Physics **117**, 823 (1999).

[93] C. A. Cardoso, A. J. C. Lanfredi, A. J. Chiquito, F. M. Araűjo-Moreira, V. P. S. Awana, H. Kishan, R. L. de Almeida and O. F. de Lima, Phys. Rev. B **71**, 134509 (2005).

[94] Y. Tokura, H. Takagi and S. Uchida, Nature **337**, 345 (1989).

[95] Y. Hikada and M. Suzuki, Nature, **338**, 635 (1989).

[96] J. T. Markert and M. B. Maple, Solid state Commun. **70**, 145 (1989).

[97] E. A. Early, N. Y. Ayoub, J. Beille, J. T. Markert and M. B. Maple, Physica C **160**, 320 (1989).

[98] N. Y. Ayoub, J. T. Markert, E. A. Early, C. L. Seaman, L. M. Paulius and M. B. Maple, Physica C **165**, 469 (1990).

[99] P. Fournier, P. Mohanty, E. Maiser, S. Darzens, T. Venkatesan, C. J. Lobb, G. Czjzek, R. A. Webb and R. L. Greene, Phys. Rev. Lett. **81**, 4720 (1998).

[100] A. Sawa, M. Kawasaki, H. Tagaki, Y. Tokura, Phys. Rev. B **66**, 14531 (2002).

[101] C. Mazumdar, R. Nagarajan, C. Godart, L. C. Gupta, M. Latroche, S. K. Dhar, C. Levy-Clement, B. D. Padalia and R. Vijayaraghavan, Solid State Commun. **87** ,413 (1993).

[102] R. Nagarajan, C. Mazumdar, Z. Hossain, S. K. Dhar, K. V. Gopalakrishnan, L. C. Gupta, C. Godart, B. D. Padalia and R. Vijayaraghavan, Phys. Rev. Lett. **72**, 274 (1994).

[103] R. J. Cava, H. Takagi, B. Batlogg, H. W. Zandbergen, J. J. Krajewski, W. F. Peck, Jr., R. B. Van Dover, R. J. Felder, T. Siegrist, K. Mizuhashi, J. O. Lee, H. Eisaki, S. A. Carter and S. Uchida, Nature **367**, 146 (1994).

[104] R. J. Cava, H. Takagi, H. W. Zandbergen, J. J. Krajewski, W. F. Peck, Jr., T. Siegrist, B. Batlogg, R. B. Van Dover, R. J. Felder, K. Mizuhashi, J. O. Lee, H. Eisaki and S. Uchida, Nature **367**, 252 (1994).

[105] R. J. Cava, B. Batlogg, T. Siegrist, J. J. Krajewski, W. F. Peck, Jr., S. Carter, R. J. Felder, H. Takagi, R. B. Van Dover, Phys. Rev. B **49,** 12384 (1994).

[106] T. Siegrist, H. W. Zandbergen, R. J. Cava, J. J. Krajewski and W. F. Peck Jr., Nature **367**, 254 (1994).

[107] J. Akimitsu, *Symposium on Transition Metal Oxides (Sendai, Japan, 10 January 2001).*

[108] J. D. Jorgensen, H. B. Schüttler, D. G. Hinks, D. W. Capone II, K. Zhang, M. B. Brodsky and D. J. Scalopino, Phys. Rev. Lett. **58**, 1024 (1987).

[109] H. Takagi, S. Uchida, K. Kitazawa and S. Tanaka, Jpn. J. Appl. Phys. **26**, L123 (1987).

[110] Y. LePage, W.R. McKinnon, J. M. Tarascon, L. H. Greene, G. W. Hall and D. M. Huang, Phys. Rev. B **35**,7245 (1987).

[111] R. M. Hazen,"Crystal Structures of High-Temperature Superconductors", *In Physical Properties of High Temperature Superconductors II*, D. M. Ginsberg, ed., World Scientific, Singapore (1990).

[112] J. J. Capponi, C. Chaillout, A. W. Hewat, P. Lejay, M. Murezio, N. Nguyen, B. Raveau, J. L. Soubeyroux, J. L. Tholence and R. Tournier, Euro Phys. Lett. **3**, 1301 (1987).

[113] F. Izumi, H. Asano, T. Ishigaki, E. Takayama-Muromachi, Y. Uchida, N. Watanabe and T. Nishikawa, Jpn. J. Appl. Phys. **26**, L649 (1987).

[114] F. Beech, S. Miraglia, A. Santoro and R. S. Roth, Phys. Rev. B **35**, 8778 (1987).

[115] C. C. Torardi, E. M. McCarron, P. E. Bierstedt and A. W. Sleight and D. E. Cox, Solid State Commun. **64**, 497 (1987).

[116] K. Imai, I. Nakai, T. Kawashima, S. Sueno and A. Ono, Jpn. J. Appl. Phys. **27**, L1661 (1988).

[117] M. Onoda and M. Sato, Solid State Commun. **67**, 799 (1988).

[118] J. K. Liang, S. S. Xie, G. C. Che, J. Q. Huang, Y. L. Zhang and Z. X. Zhao, Mod. Phys. Lett. B **2**, 483 (1988).

[119] L. Er-Rakho, C. Michel, J. Provost and B. Raveau, J. Solid State Chem. **37,** 151 (1981).

[120] S. Engelsberg, Physica C **176,** 451 (1991).

[121] D. M. De Leeuw, C. A. H. A. Mutsaers, H. A. M. Van Hal, H. Verweij, A. H. Carim and H. C. A. Smoorenburg, Physica C **156,** 126 (1988).

[122] A. H. Carim, A. F. de Jong and D. M. de Leeuw, Phys. Rev. B **38**, 7009 (1988).

[123] J. L. Peng, P. Klavins, R. N. Shelton, H. B. Radousky, P. A. Hahn, L. Bernardez and M. Costantino, Phys. Rev. B **39**, 9074 (1989).

[124] D.G. Kuberkar, N. A. Shah, M. R. Gonal, R. Prasad and R. G. Kulkarni, J. Supercond. **13,** 37 (2000).

[125] W. I. F David, W. T. A Harrison, R. M. Ibberson, M. T. Weller, J. R. Grasmeder and P. Lanchester, Nature **328,** 328 (1987).

[126] R. A. Gunasekaran, I. K. Gopalakrishnan, P. V. P. S. S. Sastry, J. V. Yakhmi and R. M. Iyer, Physica C **199,** 240 (1992).

[127] R. Singh, A. V. Narlikar, V. P. S. Awana, J. Horvat and S. X. Dou, Physica C **301,** 48 (1998).

[128] V. P. S. Awana, S. X. Dou, S. K. Malik, R. Singh, A. V. Narlikar, D. A. L. Tellez, J. M. Ferreira, J. A. Aguiar, S. Uma, E. Gmelin and W. B. Yelon, J. Mag. Magn. Mat. **187,** 192 (1998).

[129] M. Kariminezhad and M. Akhavan, Eur. Phys. J. B **47,** 47 (2005).

[130] V. L. Ginzburg, Sov. Phys.-Solid State **2**, 1824 (1960).

[131] R. E. Glover, Phys. Lett. **25 A**, 542 (1967).

[132] D. G. Naugle and R. E. Glover, Phys. Lett. **28 A**, 110 (1968).

[133] M. Strongin, O. F. Kammerer, J. Crow, R. S. Thompson and H. L. Fine, Phys. Rev. Lett.**20**, 922 (1968).

[134] R. O. Smith, B. Serin and E. Abrahams, Phys. Lett. A **28** , 224 (1968).

[135] L. G. Aslamazov and A. I. Larkin, Phys. Lett. A **26**, 238 (1968).

[136] M. Tinkham, Introduction to Superconductivity, Mc Graw-Hill, New York, **230** (1975).

[137] W. J. Skocpol and M. Tinkham, Rep. Prog. Phys. **38**, 1049 (1975).

[138] P. C. Hohenberg, Proc. Of 12th Int. Conf. Low Temp. Phys., Kyoto, Japan, 1970, ed. E. Kanda (Keigaku, Tokyo). P.211.

[139] Y. Iye, Studies on high temperature superconductors Vol. I, ed. A. Narlikar, Nova Science Publishers N. Y (1989), p.166.

[140] J. Lawrence and S. Doniach, in Proc. 12th Int. Conf. on Low Temperature Physics, Kyoto,1970 ed. E. Kanda (Keigaka, Tokyo,1971) P.361.

[141] C. J. Lobb, Phys. Rev. B **36,** 3930 (1987).

[142] W. E. Masker and R. D. Parks, Phys. Rev. B **1**, 2164 (1970).

[143] A. K. Bhatnagar, P. Kahn and T. J. Zammit, Solid State Commun. **8**, 79 (1970).

[144] K. Kajimura and N. Mikoshiba, Phys. Lett. **32A**, 216 (1970).

[145] B. Serin, R. O. Smith and T. Mizusaki, Physica **55**, 224 (1971).

[146] K. Maki, Prog. Theor. Phys. **39**, 897 (1968).

[147] R. S. Thompson, Phys. Rev. B **1**, 327 (1970).

[148] J. E. Crow, R. S. Thompson, M. A. Klenin and A. K. Bhatnagar, Phys. Rev. Lett. **24**, 371 (1970).

[149] S. Hikami and A. I. Larkin, Mod. Phys. Lett. B **2,** 693 (1988).

[150] K. Maki and R. S. Thompson, Phys. Rev. B **39,** 2767 (1989).

[151] V. V. Dorin, R. A. Klemm, A. A. Varlamov, A. I. Buzdin and D. V. Livanov, Phys. Rev. B **48**, 12951 (1993).

[152] W. L. Johnson and C. C. Tsuei, Phys. Rev. B **13**, 4827 (1976).

[153] W. L. Johnson, C. C. Tsuei and P. Chaudhuri, Phys. Rev. B **17**, 2884 (1978).

[154] A. Schmid, Phys. Rev. **180**, 527 (1969).

[155] T. P. Gollub, M. R. Beasley and M. Tinkham, Phys. Rev. Lett. **25**, 1646 (1970).

[156] J. P. Gollub, M. R. Beasley, R. Callarotti and M. Tinkham, Phys. Rev. B **7**, 3039 (1973).

[157] C. Carballeira, S. R. Currás, J. Viña, J. A. Veira, M. V. Ramallo, and F. Vidal, Phys. Rev. B **63**, 144515 (2001).

[158] B. R. Patton, V. Ambegaoker, J. W. Wilkins, Solid State Commun. **7,** 1287 (1969).

[159] B. R. Patton and J. W. Wilkins, Phys. Rev. B **6**, 4349 (1972).

[160] S. B. Nam, Phys. Rev. Lett. **26**, 1369 (1971).

[161] J. Viña, J. A. Campá, C. Carballeira, S. R. Currás, A. Maignan, M. V. Ramallo, I. Rasines, J. A. Veira, P. Wagner and F. Vidal, Phys. Rev. B **65**, 212509 (2002).

[162] W. Lang, Physica C **235-240**, 1447 (1994).

[163] Y. Matsuda, T. Hirai and S. Komiyama, Solid State Commun. **68,** 103 (1988).

[164] A. G. Aronov, S. Hikami and A. I. Larkin, Phys. Rev. Lett. **62,** 965 (1989).

[165] R. S. Thompson, Phys. Rev. Lett. **66**, 2280 (1991).

[166] J. B. Bieri and K. Maki, Phys. Rev.B **42**, 4854 (1990).

[167] P. P. Freitas, C. C. Tsuei & T. S. Plaskett, Phys. Rev. B **36,** 833 (1987).

[168] R. Srinivasan, Int. Conf. Superconductivity, Jan. 10-14, 1990, Bangalore, India, P. 147, ed. S. K. Joshi, C. N. R. Rao and S. V. Subramanyam, World Scientific.

[169] J. A. Veira, J. Maza and F. Vidal, Phys. Lett. A **131**, 310 (1988).

[170] V. V. Gridin, T. W. Krause and W. R. Datars, J. Appl. Phys. **68**, 675 (1990).

[171] S. J. Hagen, Z. Z. Wang and N. P. Ong, Phys. Rev. B **38,** 7137 (1988).

[172] P. W. Anderson and Z. Zou, Phys. Rev. Lett. **60**, 132 (1988).

[173] J. A. Veira and F. Vidal, Physica C **159**, 468 (1989).

[174] L. R. Testardi, W. A. Reed, P. C. Hohenberg, W. H. Haemmerk and G. F. Brennert, Phys. Rev. **181**, 800 (1969).

[175] J. F. Kovel and M. E. Fisher, Physical Review **136A** , 1626 (1964).

[176] P. Pureur, R. M. Costa, P. Rodrigues, Jr., J. Schaf, and J. V. Kunzler, Phys. Rev. B **47**, 11420 (1993).

[177] A. R. Jurelo, C. L. de Araújo, E. C. Siqueira, and M. P. Cantão, Brazilian J. of Physics, **35**, 587 (2005).

[178] J. A. Veira and F. Vidal, Physica C **159**, 468 (1989).

[179] N. Goldenfeld, P. D. Olmsted, T. A. Friedmann and D. M. Ginsberg, Solid State Commun. **65**, 465 (1988).

[180] F. Vidal, J. A. Veira, J. Maza, F. Miguélez, E. Morán and M. A. Alario, Solid State Commun. **66**, 421 (1988).

[181] S. E. Inderhees, M. B. Salamon, N. Goldenfeld, J. P. Rice, B. G. Pazol, D. M. Ginsberg, J. Z. Liu and G. W. Crabtree, Phys. Rev. Lett. **60**, 1178 (1988).

[182] F. Vidal, J. A. Veira, J. Maza, F. Garcia-Alvarado, E. Moran and M. A. Alario, J. Phys. C. **21**, L599 (1988).

[183] T. K. Dey, K. Radha, H. K. Barik, D. Bhattacharya and K. L. Chopra, Solid State Commun. **74,** 1315 (1990).

[184] V. P. N. Padmanaban and K. Shahi, Physica C **172,** 427 (1991).

[185] A. K. Ghosh, S. K. Bandyopadhyay, P. Barat, P. Sen and A. N. Basu, Physica C **264**, 255 (1996).

[186] A. Wahl, V. Hardy, F. Warmont, A. Maignan, M. P. Delamare and Ch. Simon, Phys. Rev. B **55**, 3929 (1997).

[187] T. A. Friedmann, J. P. Rice, J. Giapintzakis and D. M. Ginsberg, Phys. Rev. B **39,** 4258 (1989).

[188] N. P. Ong, Z. Z. Wang, S. Hagen, T. W. Jing, J. Clayhold and J. Horvath, Physica C **153-155**, 1072 (1988).

[189] G. Weigang and K. Winzer, Z. Phys. B **77**,11 (1989).

[190] D. M. Ginsberg, J. P. Rice, T. A. Friedmann and J. M. Mochel, Proceedings of second ISSP international symposium on physics and chemistry of oxide superconductors, Tokyo, Japan, 1991.

[191] B. Oh, K. Char, A. D. Kent, M. Naito, M.R. Beasley, T. H. Geballe, R.H. Hammond, A. Kapitulnik and J. M. Graybeal, Phys. Rev. B **37,** 7861 (1988).

[192] A. Kapitulnik, Physica C **153-155**, 520 (1988).

[193] W. Lang ,G. Heine, H. Jodlbauer, V. Schlosser, M. Markowitsch, P. Schwab, Y. Z. Wang and D. Bäuerle, Physica C **185-189,** 1315 (1991).

[194] Q. Y. Ying and H. S. Kwok, Phys. Rev. B **42**, 2242 (1990).

[195] J. J. Kim, J. Kim, H. J. Shin, H. J. Lee and K. K. Ja, Solid State Commun. **75**, 921 (1990).

[196] M. Ausloos, F. Gillet, Ch. Laurent and P. Clippe, Z. Phys. B **84**, 13 (1991).

[197] Y. Matsuda, T. Hirai, S. Komiyama, T. Terashima, Y. Bando, K. Lijima, K. Yamamoto and K. Hirata, Phys. Rev. B, **40** 5176 (1989).

[198] N. Overend and H. A. Howson, J. Phys.: Condens. Matter **4**, 9615(1992).

[199] K. Winzer and G. Kumm, Z. Phys. B **82**, 317 (1991).

[200] W. Lang, G. Heine, P. Schwab, X. Z. Wang and D. Bäuerle, Phys. Rev. B **49**, 4209 (1994).

[201] M. Andersson and Ö. Rapp, Phys. Rev. B **44,** 7722 (1991).

[202] M. Hikita and M. Suzuki, Phys. Rev. B **39**, 4756 (1989).

[203] M. Hikita and M. Suzuki, Phys. Rev. B **41,** 834 (1990).

[204] K. Semba, T. Ishii and A. Matsuda, Phys. Rev. Lett. **67,** 769 (1991).

[205] W. Holm, M. Andersson, Ö. Rapp, M. A. Kulikov and I. Makarenko, Phys. Rev. B **48,** 4227 (1993).

[206] A. Pomar, M.V. Ramallo, J. Maza and F. Vidal, Physica C **225**, 287 (1994).

[207] J. Axnäs, B. Landqvist and Ö. Rapp, Phys. Rev. B **58**, 6628 (1998).

[208] K. Semba and A. Matsuda, Phys. Rev. B **55**, 11103 (1997).

[209] J. Sugawara, H. Iwasaki, N. Kobayashi, H. Yamane, and T. Hirai, Phys. Rev. B **46**, 14818 (1992).

[210] C. Sekirnjak, W. Lang, S. Proyer, and P. Schwab, Physica C **243**, 60 (1995).

[211] W. Holm, Ö. Rapp, C. N. Johnson and U. Helmersson, Phys. Rev. B **52,** 3748 (1995).

[212] W. Lang, Physica C **245**, 69 (1995).

[213] W. Göb, W. Lang, W. Kula and R. Sobolewski, Superlattices and Microstructures **21,** 345 (1997).

[214] N. Senthilkumaran, S. Ravi, K. Sethupati, V. Sankaranarayanan, G. Rangarajan, and K. Sreenivas, IEEE Transactions on Magnetics **32**, 4663 (1996).

[215] F. Vidal, J. A. Veira, J. Maza, J. J. Ponte, F. Garcia-Alvarado, E. Moran, J. Amador, C. Cascales, A. Castro, M.T. Casais and I. Rasines, Physica C **156,** 807 (1988).

[216] A. Poddar, P. Mandal, A. N. Das, B. Ghosh and P. Choudhury, Physica C **159**, 231 (1989).

[217] A. Poddar, P. Mandal, A. N. Das, B. Ghosh and P. Choudhury, Physica C **161**, 567 (1989).

[218] G. Balestrino, A. Nigro, R.Vaglio and M. Marinelli, Phys. Rev. B **39,** 12264 (1989).

[219] W. Schnelle, E. Braun, H. Broicher, H. Weiss, H. Geus, S. Ruppel, M. Galffy, W. Braunisch, A. Waldorf, F. Seidler and D. Wohlleben, Physica C **161**, 123 (1989).

[220] M. Akinaga and L. Rinderer, Physica B **165-166**, 1373 (1990).

[221]. S. Ravi and V. Seshu Bai, Physica C **182** 345 (1991).

[222]. S. Ravi and V. Seshu Bai, Solid State Commun. **83** 117 (1992).

[223] P. Mandal, A. Poddar, A. N. Das, B. Ghosh and P. Choudhury, Physica C **169**, 43 (1990).

[224] S. Martin, A. T. Fiory, R. M. Fleming, G. P. Espinosa and A. S. Cooper, Phys. Rev. Lett. **62**, 677 (1989).

[225] W. Lang, G. Heine, W. Kula and R. Sobolewski, Phys. Rev. B **51**, 9180 (1995).

[226] S. H. Han and Ö. Rapp, Solid State Commun. **94**, 661 (1995).

[227] A. K. Ghosh and A. N. Basu, Phys. Rev.B, **59** 11193 (1999).

[228] S. Ravi and V. Seshu Bai, Mod. Phys. Lett. B **6**, 1857 (1992).

[229] W. Lang, G. Heine, W. Kula and R. Sobolewski, Phys. Rev. B **51**, 9180 (1995).

[230] S. N. Bhatia, Pramana Journal of Physics, **58**, 817 (2002).

[231] J. Viña, J. A. Campa, C. Carballeira, S. R. Currás, A. Maignan, M. V. Ramallo, I. Rasines, J. A. Veira, P. Wagner and F. Vidal, Phys. Rev. B **65**, 212509-1 (2002).

[232] D. H. Kim, A. M. Goldman, J. H. Kang, K. E. Gray and R.T. Kampwirth, Phys. Rev. B **39,** 12275 (1989).

[233] S. N. Bhatia, R. Walia, , I. K. Gopalakrishnan, P. V. P. S. S. Sastry, J. V. Yakhmi and R. M. Iyer, Solid State Commun.**75**, 415 (1990).

[234] H. M. Duan,W. Kiehl, C. Dong, A.W. Cordes, M. J. Saeed, D. L. Viar and A. M. Hermann, Phys. Rev. B **43,** 12925 (1991).

[235] R. Srinivasan, H. Krishnan, V. Sankaranarayanan, I. K. Gopalakrishnan, P. V. P. S. S. Sastry, J. V. Yakhmi and R. M. Iyer, Physica C **159**, 747 (1989).

[236] A. Poddar, P. Mandal and S. Das, J. Phys. Condens. Matter **7**, 1351 (1995).

[237] D. H. Kim, K. E. Gray, R. T. Kampwirth and D. M. McKay, Phys. Rev. B **43**, 2910 (1991).

[238] H. J. Kim, P. Chowdhury, W. N. Kang, D. J. Zang and S. I. Lee, Phys. Rev. B **67**, 144502 (2003).

[239] H. J. Kim, P. Chowdhury, S. K. Gupta, N. H. Dan and S. I. Lee, Phys. Rev. B **70,** 144510 (2004).

[240] J. Axnäs, I. Bryntse, I. Safonova and Ö. Rapp, Physica B **284-288**, 1009 (2000).

[241] M. O. Mun, S. Lee, M. K. Bae and S. I. Lee, Solid State Commun. **90**, 603 (1994).

[242] H. J. Kim, K. H. Kim, W. N. Kang, H. S. Lee, K. H. P. Kim, E. M. Choi, H. J. Kim, S. I. Lee and M. O. Mun, Physica C **408-410**, 72 (2004).

[243] F. Vidal, J. A. Veira, C. Torron, J. J. Ponte, F. Miguelez, J. Maza, G. Domarco, J. Amador, M.T. Casais, C. Cascales, A. Castro, M. De pedro and I. Rasines, J. Less-Commun Mat. **151**,165 (1989).

[244] N. Sudhakar, M. K. Pillai, A. Banerjee, D. Bahadur, A. Das, K. P. Gupta, S. V. Sharma and A. K. Majumdar, Solid State Commun. **77,** 529 (1991).

[245] H. Krishnan, R. Srinivasan, V. Sankaranarayanan, C. K. Subramaniam and G. V. Subba Rao, Bull. Mater. Science **14**, 747 (1991).

[246] J. Rosenblatt, P. Peyral and A. Raboutou, Physics Letters **98A,** 463 (1983).

[247] J. Rosenblatt, P. Peyral, A. Raboutou and C. Lebeau, Physica B **152,** 95 (1988).

[248] H. Krishnan, V. Sankaranarayanan and R. Srinivasan, Physica C **194,** 163 (1992).

[249] A Raboutou, P. Peyral, C. Lebeau and J. Rosenblatt, Physica A **157,** 159 (1989).

[250] J. C. Le Guillou and Z. Zinn-Justin, Phys. Rev. Lett. **39,** 95 (1977).

[251] G. S. Rushbroke, R. A. Muse, R. L. Stephenson and K. Pirnie, J. Phys.C **5,** 3371 (1972).

[252] E. Brown, J. W. Essam and C. M. Place, J. Phys. **C 8**, 321 (1975).

[253] M. K. Marhas, K. Balakrishnan, V. Ganesan, R. Srinivasan, D. Kanjilal, G. K. Muralidhar, G. Mohan Rao, S. Nathan and S. Mohan, Bull. Mater. Sci.**17**, 585 (1994).

[254] N. Senthilkumaran, S. Ravi, K. Sethupati, V. Sankaranarayanan and G. Rangarajan, "Advances in Superconductivity-New Materials, Critical currents and Devices" New Age International Ltd. New Delhi, 1st edition, edited by Pinto et al.(1997) p.239.

[255] S. V. Sharma, T. K. Nath and A. K. Majumdar, Physica C **290**, 229 (1997).

[256] E. Isaac Samuel, S. Ravi and V. Seshu Bai, Solid State Commun. **96,** 441 (1995).

[257] P. Levy, C. Acha and V. Bekeris, Solid State Commun. **80,** 849 (1991).

[258] R. B. Goldfarb, A. F. Clark, A. Z. Braginski and A. J. Panson, Cryogenics **27**, 475 (1987).

[259] M. Nikolo and R. B. Goldfarb, Phys. Rev. B **39**, 6615 (1989).

[260] A. F. Khoder, M. Couach, B. Barbara, Physica C **153-155**, 1477 (1988).

[261] H. Dersch and G. Blatter, Phys. Rev. B **38**, 11391 (1988).

[262] H. Mazaki, M. Takano, R. Kanno and Y. Takeda, Jpn. J. Appl. Phys. **26**, L780 (1977).

[263] H. Küper, I. Apfelstedt, W. Schuer, R. Flükiger, R. Meier Hirmer and H. Wühl Z. Phys. B **69**, 159 (1987).
[264] F. Gömöry and P. Lobotka, Solid State Commun. **66,** 645 (1988).
[265] S. D. Murphy, K. Renouard, R. Crittenden and S. M. Bhagat, Solid State Commun. **69**, 367 (1989).
[266] D. X. Chen, J. Nogues and K.V. Rao, Cryogenics **29,** 800 (1989).
[267] P. W. Anderson, Phys. Rev. Lett. **9**, 309 (1962).
[268] H. Mazaki, M. Takano, X. Ikeda, Y. Bando, R. Kanno,Y. Takeda and O. Yamamoto, Jpn. J. Appl. Phys. **26**, L1749 (1987).
[269] D. X. Chen, R. B. Goldfarb, J. Nogues and K. V. Rao, J. Appl. Phys. **63**, 980 (1988).
[270] S. L. Shindé, J. Morrill, D. Goland, D. A. Chance and T. McGuire, Phys. Rev. B **41**, 8838 (1990).
[271] C. Ree and W. K. Choo, Physica C **166**, 221 (1990).
[272] C. P. Bean, Rev. Mod. Phys. **36**, 31 (1964).
[273] Y. B. Kim, C. F. Hempstead and A. R. Strnad, Phys Rev Lett **9,** 306 (1962).
[274] J. H. P Watson, J. Appl. Phys. **39**, 3406 (1968).
[275] F. Irie and K. Yamafuji, J. Phys. Soc. Jpn.**23**, 255 (1967).
[276] I. M. Green and P. Hlawiczka, Proc. IEEE **114**, 1329 (1967).
[277] W. A. Fietz, M. R. Beasley, J. Silcox and W. W. Webb, Phys. Rev. **136,** A 335 (1964).
[278] V. R. Karasik, N. G. Vasil'ev and V. G. Ershov, Sov. Phys. JEPT, **32**, 433 (1971).
[279] J. R. Clem, Physica C **153-155**, 50 (1988).
[280] K. –H. Müller, Physica C **159**, 717 (1989).
[281] L. Ji, R. H. Sohn, G. C. Spalding, C. J. Lobb and M. Tinkham, Phys. Rev. B **40**, 10936 (1989).
[282] T. Ishida and R. B. Goldfarb, Phys. Rev. B **41**, 8937 (1990).
[283] Ming Xu, Donglu Shi, and Ronald F. Fox, Phys. Rev. B **42**, 10773 (1990).
[284] Q. H. Lam, Y. Kim and C. D. Jeffries, Phys. Rev. B **42**, 4846 (1990).
[285] G. Ravi Kumar and P. Chaddah, Phys. Rev. B **39**, 4704 (1989).
[286] D. X. Chen and R. B. Goldfarb, J. Appl. Phys. **66,** 2489 (1989).
[287] K. Yamamoto, H. Mazaki and H. Yasuoka, Phys. Rev. B **47,** 915 (1993).
[288] D. -X. Chen, A. Sanchez, and J. S. Muñoz, J. Appl. Phys. **67**, 3430 (1990).
[289] D. -X. Chen, and A. Sanchez, J. Appl. Phys. **70**, 5463 (1991).

[290] Z. Koziol, J. J. M. Franse, P. F. de Châtel, and A. A. Menovsky, Phys. Rev. B **50**, 15978 (1994).

[291] T. H. Johansen, M. R. Koblischka, H. Bratsberg, and P. O. Hetland, Phys. Rev. B **56**, 11273 (1997).

[292] P. O. Hetland, T. H. Johansen and H. Bratsberg, Cryogenics **36**, 41 (1996).

[293] D. -X. Chen, K. -Y. Wang and A. Hernando, Phisica C **274**, 39 (1997).

[294] S. Ravi, Manoranjan Kar and G. Rangarajan, Proceedings of Solid State Physics (India) **43**, 428 (2000).

[295] S. Uma, S. Ravi and G. Rangarajan, Physica C **253**, 225 (1995).

[296] S. Senoussi, C. Aguillon and P. Manuel, Physica C **175**, 202 (1991).

[297] M. A. R. Le Blanc and J. P. Lorrain, Cryogenics **24**, 143 (1984).

[298] W. I. Dunn and P. Hlawiczka, Br. J. Appl. Phys. **1**, 1649 (1968).

[299] D.D. Stancil, T. E. Schlesinger, A. K. Stamper, and D. Wong, J. Appl. Phys. **64**, 5899 1988.

[300] D. X. Chen, R. W. Cross, and A. Sanchez, Crygenics **33**, 695 (1993).

[301] Y. Kimishima and Y. Ichiyanagi, Physica C **353**, 111 (2001).

[302] Y. Kimishima, K. Kamimura and Y. Ichiyanagi, Physica C **329**, 17 (2000).

[303] P. Fabbricatore, G. Gemme, R. Musenich, M. Occhetto and R. Porodi,Cryogenics **32**, 559 (1992).

[304] C. P. Bean and J. D. Livingston, Phys. Rev. Lett. **12**, 14 (1964).

[305] J. R. Clem, J. Appl. Phys. **50**, 3518 (1979).

[306] D. -X. Chen and A. Sanchez, Phys. Rev. B **45**, 10793 (1992).

[307] D. -X. Chen, R. B. Goldfarb, R. W. Cross and A. Sanchez, Phys. Rev. B **48**, 6426 (1993).

[308] Q. H. Lam, C. D. Jeffries, P. Berdahl, R. E. Russo and R. P. Reade, Phys. Rev. B **46**, 437 (1992).

[309] B. V. Kumaraswamy, R. Lal and A. V. Narlikar, Phys. Rev. B **53**, 6759 (1996).

[310] Q. H. Lam, C. D. Jeffries, Physica C **194**, 47 (1992).

[311] L. A. Angurel, F. Lera, C. Rillo, and R. Navarro, Cryogenics (1992).

[312] S. Shatz, A. Shaulov and Y. Yeshurun, Phys. Rev. B **48**, 13871 (1993).

[313] N. Hari Babu, T. Rajasekharan, S. Ravi, V. Seshu Bai, Phys. Rev. B **52**, 13605 (1995).

[314] S. Ravi Physica C **295**, 277 (1998).

[315] A. Sedky, M. I. Youssif, S. M. Khalil and A. Sawalha, Solid State Commun. **139,** 126 (2006).

[316] D. X. Chen, Y. Mei and H. L. Luo, Physica C **167**, 317 (1990).

[317] S. Ravi and V. Seshu Bai, Physica C **230,** 51 (1994).

[318] S. Ravi and V. Seshu Bai, Phys. Rev. B **49,** 13082 (1994).

[319] Y. Kimishima, K. Inagaki, K. Tanabe and Y. Ichiyanagi, Supercond. Sci. & Technol. **13**, 295 (2000).

[320] V. Mihalache, G. Aldica, S. Popa and A. Crisan, Physica C **384**, 451 (2003).

[321] E. Aksu, A. Gencer, H. Yilmaz and S. Nezir, Physica C **391**, 67 (2003).

[322] P. Kameli, H. Salamati and M. Eslami, Solid State Commun. **137**, 30 (2006).

[323] E. Aksu, A. Gencer, N. Calinli, H. Koralay and S. Cavdar, Physica B **363**, 158 (2005).

[324] M. K. Bae, M. S. Choi, M. O. Mun, S. Lee, S. I. Lee and W. C. Lee, Physica C **234**, 207 (1994).

[325] C. C. Lam, K. C. Hung, J. Feng, X. Jin and H. M. Shao, Physica C **282-287**, 2307 (1997).

[326] A. Crisan, P. Badica, M. Hirai, H. Kito, A. Iyo and Y. Tanaka, Physica C **388-389**, 421 (2003).

[327] O. F. Schilling, K. Aihara, A. Soeta, T. Kamo and S. Matsuda, Phys. Rev. B **47,** 8096 (1993).

[328] S. Ravi, Physica C **330**, 58 (2000).

[329] P. G. De Gennes, Rev. Mod. Phys. **36**, 225 (1964).

[330] V. Ambegaokar, A. Baratoff, Phys. Rev. Lett. **10**, 486 (1963).

[331] H. Salamati, P. Kameli, Solid State Commun. **125**, 407 (2003).

[332] *The Rietveld Method, edited by* R. A. Young, *International Union of Crystallography* (Oxford University Press, NewYork, 1995).

[333] "Ballistic and Bridge Methods of Magnetic Measurements of Materials", D. –X. Chen, China Metorology, Beijing (1990), Page-526.

[334] R. B. Goldfarb, M. Lelental and C. A. Thompson,"Magnetic Susceptibility of superconductors and Other Spin Systems", Edited by R. A. Hein, Plenum Press, New York, 1991, Page-49.

[335] D. -X. Chen and A. Sanchez, J. Appl. Phys. **70**, 5463 (1991).

[336] M. I. Youssif, A. A. Bahgat and I. A. Ali, Egypt. J. Sol. **23**, 231 (2000).

[337] M. Sato and Y. Ishii, J. Appl. Phys. **66,** 983 (1989).

[338] R. B. Goldfarb and J. V. Minervini, *Rev. Sci. Instr.* **55,** 761 (1984).

[339] L. Sagnotti et al. Physics of the Earth and Planetary Interiors **138**, 25 (2003).

[340] "Introduction to Solid State Physics", Charles Kittel, John-Wiley Sons, 7th Edition, 2000.

[341] A. Earnshaw "Introduction of Magnetochemistry", Academic Press, London, 1968.

[342] I. Nakai, S. Sueno, F. P. Okamura and A. Uno, Jpn. J. Appl. Phys. **26**, L788 (1987).

[343] D. G. Kuberkar, N. A. Shah, M. V. Subbarao, A. G. Joshi and R. G. Kulkarni, Physica B **259-261,** 538 (1999).

[344] R. Ganguly, I. K. Gopalakrishnan and J. V. Yakhmi, Physica C **256,** 51 (1996).

[345] M. V. Subbarao, D. G. Kuberkar, G. J. Baldha and R. G. Kulkarni, Physica C **288,** 57 (1997).

[346] M. J. Naughton, R. C. Yu, P. K. Davies, J. E. Fischer, R. V. Chamberlin, Z. Z. Wang, T. W. Jing, N. P. Ong and P. M. Chaikin, Phys. Rev. B **38,** 9280 (1988).

[347] R. Kleiner and P. Müller, Phys. Rev. B **49,** 1327 (1994).

[348] D. -X. Chen, A. Sanchez, T. Puig, L. M. Martinez and J. S. Muñoz, Physica C **168**, 652 (1990).

[349] H. Küpfer, I. Apfelstedt, R. Flükiger, C. Keller, R. Meier-Hirmer, B. Runtsch, A. Turowski, U. Wiech and T. Wolf, Cryogenics **28**, 650 (1988).

[350] Q. Y. Xu, R. P. Wang and Z. Zhang, Phys. Rev. B **71,** 092401 (2005).

----------XXX----------

Appendix A

We have rearranged the expressions for R_2, R_3, R_4, R_5, R_6 and R_7 in (eqns.1.54 to 1.60) in such a way that Binomial expansion can be applied. The rearranged expressions are as follows.

$$R_2 = H_m p_2 \left[1 + \frac{H^2 + 2H_0 H - H_m{}^2}{2H_m{}^2 p_2{}^2}\right]^{1/2} \tag{A.1}$$

$$R_3 = H_m p_2 \left[1 + \frac{2H_0 H - H^2 - H_m{}^2}{2H_m{}^2 p_2{}^2}\right]^{1/2} \tag{A.2}$$

$$R_4 = H_m p_3 \left[1 + \frac{2H_0 H_m - 2p^2 H_0{}^2}{H_m{}^2 p_3{}^2}\right]^{1/2} \tag{A.3}$$

$$R_5 = H_m p_3 \left[1 + \frac{H^2 + 2H_0 H - H_m{}^2}{H_m{}^2 p_3{}^2}\right]^{1/2} \tag{A.4}$$

$$R_6 = H_m p_3 \left[1 + \frac{2H_0 H - H^2 - H_m{}^2}{H_m{}^2 p_3{}^2}\right]^{1/2} \tag{A.5}$$

$$R_7 = H_m p_3 \left[1 + \frac{H^2 - 2H_0 H - 2p^2 H_0{}^2 - H_m{}^2}{H_m{}^2 p_3{}^2}\right]^{1/2} \tag{A.6}$$

where $p_1 = \sqrt{1+p^2} - 1$, $p_2 = \left[\frac{1}{p_1{}^2}\frac{H_p{}^2}{H_m{}^2} + \frac{1}{p_1}\frac{H_p}{H_m} + 1\right]^{1/2}$ and $p_3 = \left[\frac{1}{p_1{}^2}\frac{H_p{}^2}{H_m{}^2} + \frac{p^2}{p_1{}^2}\frac{H_p{}^2}{H_m{}^2} + 1\right]^{1/2}$

Expressions for $R_2{}^3$, $R_3{}^3$, $R_4{}^3$, $R_5{}^3$, $R_6{}^3$ and $R_7{}^3$ were obtained by applying Binomial expansion up to third order and are given as follows.

$$R_2{}^3 = H_m{}^3 p_2{}^3 + \frac{3}{4}\left(H^2 + 2H_0 H - H_m{}^2\right) H_m p_2 + \frac{3}{32}\frac{\left(H^2 + 2H_0 H - H_m{}^2\right)^2}{H_m p_2} - \frac{1}{128}\frac{\left(H^2 + 2H_0 H - H_m{}^2\right)^3}{H_m{}^3 p_2{}^3} \tag{A.7}$$

$$R_3^{\,3} = H_m^{\,3} p_2^{\,3} + \frac{3}{4}\left(2H_0H - H^2 - H_m^{\,2}\right)H_m p_2 + \frac{3}{32}\frac{\left(2H_0H - H^2 - H_m^{\,2}\right)^2}{H_m p_2} - \frac{1}{128}\frac{\left(2H_0H - H^2 - H_m^{\,2}\right)^3}{H_m^{\,3} p_2^{\,3}} \quad \text{(A.8)}$$

$$R_4^{\,3} = H_m^{\,3} p_3^{\,3} + 3\left(H_0H_m - p^2H_0^{\,2}\right)H_m p_3 + \frac{3}{2}\frac{\left(H_0H_m - p^2H_0^{\,2}\right)^2}{H_m p_3} - \frac{1}{2}\frac{\left(H_0H_m - p^2H_0^{\,2}\right)^3}{H_m^{\,3} p_3^{\,3}} \quad \text{(A.9)}$$

$$R_5^{\,3} = H_m^{\,3} p_3^{\,3} + \frac{3}{4}\left(H^2 + 2H_0H - H_m^{\,2}\right)H_m p_3 + \frac{3}{8}\frac{\left(H^2 + 2H_0H - H_m^{\,2}\right)^2}{H_m p_3} - \frac{1}{16}\frac{\left(H^2 + 2H_0H - H_m^{\,2}\right)^3}{H_m^{\,3} p_3^{\,3}} \quad \text{(A.10)}$$

$$R_6^{\,3} = H_m^{\,3} p_3^{\,3} + \frac{3}{2}\left(2H_0H - H^2 - H_m^{\,2}\right)H_m p_3 + \frac{3}{8}\frac{\left(2H_0H - H^2 - H_m^{\,2}\right)^2}{H_m p_3} - \frac{1}{16}\frac{\left(2H_0H - H^2 - H_m^{\,2}\right)^3}{H_m^{\,3} p_3^{\,3}} \quad \text{(A.11)}$$

$$R_7^{\,3} = H_m^{\,3} p_3^{\,3} + \frac{3}{2}\left(H^2 - 2H_0H - 2p^2H_0^{\,2} - H_m^{\,2}\right)H_m p_3 + \frac{3}{8}\frac{\left(H^2 - 2H_0H - 2p^2H_0^{\,2} - H_m^{\,2}\right)^2}{H_m p_3} - \frac{1}{16}\frac{\left(H^2 - 2H_0H - 2p^2H_0^{\,2} - H_m^{\,2}\right)^3}{H_m^{\,3} p_3^{\,3}} \quad \text{(A.12)}$$

Appendix B

Expressions for $\chi_m^{/}$ and $\chi_m^{//}$ derived from Kim model at high field region are given as follows.

```
χm/ = -1 - (8*ab)/(3.*p**4) + 2/p**2 + (2*ab)/p**2 - (64*ab)/(75.*p**4*p3**3*Pi) -
  16/(15.*p**2*p3**3*Pi) + (16*ab)/(75.*p**2*p3**3*Pi) -
(4*tp)/(p**2*Pi) -
  (4*ab*tp)/(p**2*Pi) + (ab*tr)/(8.*p**4*p2**3*Pi) -
  Sin(tp)/(16.*p3**3*Pi) + (9*ab*Sin(tp))/(80.*p3**3*Pi) -
  (2*ab*Sin(tp))/(15.*p**4*p3**3*Pi) + (5*Sin(tp))/(4.*p**2*p3**3*Pi) +
  (2*ab*Sin(tp))/(5.*p**2*p3**3*Pi) - Sin(tp)/(2.*p3*Pi) +
  (13*ab*Sin(tp))/(10.*p3*Pi) + (12*ab*Sin(tp))/(5.*p**4*p3*Pi) -
  (22*ab*Sin(tp))/(5.*p**2*p3*Pi) + (4*p3*Sin(tp))/Pi -
  (4*ab*p3*Sin(tp))/(5.*Pi) - (16*ab*p3*Sin(tp))/(5.*p**2*Pi) -
  (2*Sin(2*tp))/(p**2*Pi) - (2*ab*Sin(2*tp))/(p**2*Pi) +
  Sin(3*tp)/(32.*p3**3*Pi) - (11*ab*Sin(3*tp))/(480.*p3**3*Pi) -
  (4*ab*Sin(3*tp))/(45.*p**4*p3**3*Pi) + (5*Sin(3*tp))/(24.*p**2*p3**3*Pi) +
  (ab*Sin(3*tp))/(6.*p**2*p3**3*Pi) + Sin(3*tp)/(6.*p3*Pi) +
  (ab*Sin(3*tp))/(10.*p3*Pi) + (4*ab*Sin(3*tp))/(15.*p**4*p3*Pi) -
  (2*ab*Sin(3*tp))/(3.*p**2*p3*Pi) - Sin(5*tp)/(160.*p3**3*Pi) -
  (7*ab*Sin(5*tp))/(800.*p3**3*Pi) - (2*ab*Sin(5*tp))/(75.*p**4*p3**3*Pi) +
  Sin(5*tp)/(40.*p**2*p3**3*Pi) + (3*ab*Sin(5*tp))/(50.*p**2*p3**3*Pi)-
(5*ab*Sin(tr))/(24.*p**4*p2**3*Pi) + Sin(tr)/(32.*p**2*p2**3*Pi) +
  (ab*Sin(tr))/(32.*p**2*p2**3*Pi) + (3*Sin(tr))/(4.*p**2*p2*Pi) +
  (3*ab*Sin(tr))/(4.*p**2*p2*Pi) - (ab*Sin(tr))/(2.*p**4*p3**3*Pi) -
  Sin(tr)/(8.*p**2*p3**3*Pi) + (13*ab*Sin(tr))/(8.*p**2*p3**3*Pi) +
  (8*ab*Sin(tr))/(5.*p3*Pi) + (2*ab*Sin(tr))/(5.*p**4*p3*Pi) -
  (7*Sin(tr))/(2.*p**2*p3*Pi) - (57*ab*Sin(tr))/(10.*p**2*p3*Pi) +
  (4*p3*Sin(tr))/Pi - (4*ab*p3*Sin(tr))/(5.*Pi) -
  (16*ab*p3*Sin(tr))/(5.*p**2*Pi) +
  ((-4*ab)/(5.*p3**3) + p**2/p3**3 + (ab*p**2)/(3.*p3**3) +
     (4*ab*tp)/(5.*p3**3*Pi) - (p**2*tp)/(p3**3*Pi) -
     (ab*p**2*tp)/(3.*p3**3*Pi) + (2*ab*Sin(2*tp))/(5.*p3**3*Pi) -
     (p**2*Sin(2*tp))/(2.*p3**3*Pi) - (ab*p**2*Sin(2*tp))/(6.*p3**3*Pi)-
8*ab*Sin(tr))/(5.*p3**3*Pi) + (2*p**2*Sin(tr))/(p3**3*Pi) +
     (2*ab*p**2*Sin(tr))/(3.*p3**3*Pi))/hr**3 +
  ((8*ab*p**2*Sin(tp))/(15.*p3**3*Pi) - (2*p**4*Sin(tp))/(3.*p3**3*Pi)+
(2*ab*p**4*Sin(tp))/(15.*p3**3*Pi) +
     (8*ab*p**2*Sin(tr))/(15.*p3**3*Pi) - (2*p**4*Sin(tr))/(3.*p3**3*Pi) +
     (2*ab*p**4*Sin(tr))/(15.*p3**3*Pi))/hr**4 +
  ((-3*Sin(tp))/(2.*p3**3*Pi) - (19*ab*Sin(tp))/(10.*p3**3*Pi) +
     (6*ab*Sin(tp))/(5.*p**2*p3**3*Pi) - (p**2*Sin(tp))/(4.*p3**3*Pi) +
     (9*ab*p**2*Sin(tp))/(20.*p3**3*Pi) + (8*ab*Sin(tp))/(5.*p3*Pi) -
     (2*p**2*Sin(tp))/(p3*Pi) + (2*ab*p**2*Sin(tp))/(5.*p3*Pi) -
     Sin(3*tp)/(6.*p3**3*Pi) - (3*ab*Sin(3*tp))/(10.*p3**3*Pi) +
     (2*ab*Sin(3*tp))/(15.*p**2*p3**3*Pi) +
     (p**2*Sin(3*tp))/(12.*p3**3*Pi) +
     (ab*p**2*Sin(3*tp))/(36.*p3**3*Pi) - (2*Sin(tr))/(p3**3*Pi) -
     (14*ab*Sin(tr))/(5.*p3**3*Pi) + (8*ab*Sin(tr))/(5.*p**2*p3**3*Pi)+
(8*ab*p**2*Sin(tr))/(15.*p3**3*Pi) + (8*ab*Sin(tr))/(5.*p3*Pi) -
     (2*p**2*Sin(tr))/(p3*Pi) + (2*ab*p**2*Sin(tr))/(5.*p3*Pi))/hr**2 +
  (ab*Sin(2*tr))/(12.*p**4*p2**3*Pi) -
  (5*ab*Sin(3*tr))/(144.*p**4*p2**3*Pi) - Sin(3*tr)/(192.*p**2*p2**3*Pi) -
  (ab*Sin(3*tr))/(192.*p**2*p2**3*Pi) + Sin(3*tr)/(12.*p**2*p2*Pi) +
  (ab*Sin(3*tr))/(12.*p**2*p2*Pi) + (23*ab*Sin(3*tr))/(180.*p**4*p3**3*Pi) +
```

```
  Sin(3*tr)/(48.*p**2*p3**3*Pi) - (ab*Sin(3*tr))/(240.*p**2*p3**3*Pi) -
  (2*ab*Sin(3*tr))/(15.*p**4*p3*Pi) - Sin(3*tr)/(6.*p**2*p3*Pi) +
  (ab*Sin(3*tr))/(30.*p**2*p3*Pi) + (ab*Sin(4*tr))/(96.*p**4*p2**3*Pi)+
(1/(4.*p3**3) - (9*ab)/(20.*p3**3) - ab/(5.*p**4*p3**3) +
     1/(4.*p**2*p3**3) + (19*ab)/(20.*p**2*p3**3) + 2/p3 +
     (6*ab)/(5.*p3) - (8*ab)/(5.*p**2*p3) - tp/(4.*p3**3*Pi) +
     (9*ab*tp)/(20.*p3**3*Pi) - tp/(2.*p**2*p3**3*Pi) -
     (9*ab*tp)/(10.*p**2*p3**3*Pi) - (2*tp)/(p3*Pi) -
     (6*ab*tp)/(5.*p3*Pi) + (8*ab*tp)/(5.*p**2*p3*Pi) -
     tr/(16.*p**2*p2**3*Pi) - (ab*tr)/(16.*p**2*p2**3*Pi) +
     (ab*tr)/(5.*p**4*p3**3*Pi) + tr/(4.*p**2*p3**3*Pi) -
     (ab*tr)/(20.*p**2*p3**3*Pi) - (4*Sin(tp))/Pi -
     (32*ab*Sin(tp))/(15.*p**4*Pi) + (2*ab*Sin(2*tp))/(5.*p3**3*Pi) -
     Sin(2*tp)/(3.*p**2*p3**3*Pi) -
     (11*ab*Sin(2*tp))/(15.*p**2*p3**3*Pi) - Sin(2*tp)/(p3*Pi) -
     (3*ab*Sin(2*tp))/(5.*p3*Pi) + (4*ab*Sin(2*tp))/(5.*p**2*p3*Pi) +
     Sin(4*tp)/(16.*p3**3*Pi) + (7*ab*Sin(4*tp))/(80.*p3**3*Pi) -
     Sin(4*tp)/(24.*p**2*p3**3*Pi) -
     (17*ab*Sin(4*tp))/(120.*p**2*p3**3*Pi) -
     (8*ab*Sin(tr))/(5.*p3**3*Pi) - (8*ab*Sin(tr))/(15.*p**4*p3**3*Pi)+
(2*Sin(tr))/(3.*p**2*p3**3*Pi) +
     (46*ab*Sin(tr))/(15.*p**2*p3**3*Pi) + (4*Sin(tr))/(p3*Pi) +
     (12*ab*Sin(tr))/(5.*p3*Pi) - (16*ab*Sin(tr))/(5.*p**2*p3*Pi) -
     Sin(2*tr)/(24.*p**2*p2**3*Pi) - (ab*Sin(2*tr))/(24.*p**2*p2**3*Pi)+
(2*ab*Sin(2*tr))/(15.*p**4*p3**3*Pi) + Sin(2*tr)/(6.*p**2*p3**3*Pi) -
     (ab*Sin(2*tr))/(30.*p**2*p3**3*Pi) - Sin(4*tr)/(192.*p**2*p2**3*Pi) -
     (ab*Sin(4*tr))/(192.*p**2*p2**3*Pi) +
     (ab*Sin(4*tr))/(60.*p**4*p3**3*Pi) + Sin(4*tr)/(48.*p**2*p3**3*Pi)-
(ab*Sin(4*tr))/(240.*p**2*p3**3*Pi))/hr -
  (ab*Sin(5*tr))/(240.*p**4*p2**3*Pi) - Sin(5*tr)/(320.*p**2*p2**3*Pi)-
(ab*Sin(5*tr))/(320.*p**2*p2**3*Pi) +
  (7*ab*Sin(5*tr))/(300.*p**4*p3**3*Pi) + Sin(5*tr)/(80.*p**2*p3**3*Pi)-
(ab*Sin(5*tr))/(400.*p**2*p3**3*Pi) +
  hr*((-11*ab)/(24.*p**4*p3**3) + 13/(32.*p**2*p3**3) -
     (21*ab)/(160.*p**2*p3**3) + (8*ab)/(5.*p**4*p3) + 1/(p**2*p3) -
     ab/(p**2*p3) + (8*ab*p3)/(5.*p**4) - (2*p3)/p**2 -
     (14*ab*p3)/(5.*p**2) - (32*ab)/(9.*p**4*Pi) - 8/(3.*p**2*Pi) -
     (8*ab)/(3.*p**2*Pi) + (11*ab*tp)/(15.*p**4*p3**3*Pi) -
     (13*tp)/(16.*p**2*p3**3*Pi) + (17*ab*tp)/(80.*p**2*p3**3*Pi) -
     (6*ab*tp)/(5.*p**4*p3*Pi) - (2*tp)/(p**2*p3*Pi) +
     (6*ab*tp)/(5.*p**2*p3*Pi) + (4*p3*tp)/(p**2*Pi) +
     (12*ab*p3*tp)/(5.*p**2*Pi) + (ab*tr)/(24.*p**4*p2**3*Pi) -
     tr/(128.*p**2*p2**3*Pi) - (ab*tr)/(128.*p**2*p2**3*Pi) +
     (3*ab*tr)/(4.*p**4*p2*Pi) - tr/(8.*p**2*p2*Pi) -
     (ab*tr)/(8.*p**2*p2*Pi) + (2*p2*tr)/(p**2*Pi) +
     (2*ab*p2*tr)/(p**2*Pi) + (11*ab*tr)/(120.*p**4*p3**3*Pi) +
     tr/(32.*p**2*p3**3*Pi) - (ab*tr)/(160.*p**2*p3**3*Pi) -
     (ab*tr)/(p**4*p3*Pi) + tr/(4.*p**2*p3*Pi) - (ab*tr)/(20.*p**2*p3*Pi) -
     (8*ab*p3*tr)/(5.*p**4*Pi) - (2*p3*tr)/(p**2*Pi) +
     (2*ab*p3*tr)/(5.*p**2*Pi) - (12*ab*Sin(tp))/(p**4*Pi) +
     (3*Sin(tp))/(p**2*Pi) + (3*ab*Sin(tp))/(p**2*Pi) +
     (3*ab*Sin(2*tp))/(5.*p**4*p3**3*Pi) -
     (31*Sin(2*tp))/(64.*p**2*p3**3*Pi) +
     (43*ab*Sin(2*tp))/(320.*p**2*p3**3*Pi) -
     (4*ab*Sin(2*tp))/(5.*p**4*p3*Pi) - Sin(2*tp)/(p**2*p3*Pi) +
     (ab*Sin(2*tp))/(p**2*p3*Pi) + (2*p3*Sin(2*tp))/(p**2*Pi) +
     (6*ab*p3*Sin(2*tp))/(5.*p**2*Pi) - (4*ab*Sin(3*tp))/(3.*p**4*Pi) +
```

```
     Sin(3*tp)/(3.*p**2*Pi) + (ab*Sin(3*tp))/(3.*p**2*Pi) +
     (3*ab*Sin(4*tp))/(20.*p**4*p3**3*Pi) -
     (3*Sin(4*tp))/(64.*p**2*p3**3*Pi) -
     (ab*Sin(4*tp))/(320.*p**2*p3**3*Pi) -
     (ab*Sin(4*tp))/(10.*p**4*p3*Pi) + (ab*Sin(4*tp))/(5.*p**2*p3*Pi) +
     (ab*Sin(6*tp))/(45.*p**4*p3**3*Pi) - Sin(6*tp)/(192.*p**2*p3**3*Pi) -
     (11*ab*Sin(6*tp))/(960.*p**2*p3**3*Pi) -
     (ab*Sin(tr))/(16.*p**4*p2**3*Pi) - (3*ab*Sin(tr))/(2.*p**4*p2*Pi)-
(8*ab*Sin(tr))/(15.*p**4*p3**3*Pi) + (16*ab*Sin(tr))/(5.*p**4*p3*Pi) -
     (16*ab*Sin(tr))/(5.*p**2*p3*Pi) + (16*ab*p3*Sin(tr))/(5.*p**4*Pi)-
(4*p3*Sin(tr))/(p**2*Pi) - (28*ab*p3*Sin(tr))/(5.*p**2*Pi) +
     (ab*Sin(2*tr))/(96.*p**4*p2**3*Pi) + Sin(2*tr)/(512.*p**2*p2**3*Pi) +
     (ab*Sin(2*tr))/(512.*p**2*p2**3*Pi) + (ab*Sin(2*tr))/(2.*p**4*p2*Pi) +
     (p2*Sin(2*tr))/(p**2*Pi) + (ab*p2*Sin(2*tr))/(p**2*Pi) +
     (3*ab*Sin(2*tr))/(32.*p**4*p3**3*Pi) -
     Sin(2*tr)/(128.*p**2*p3**3*Pi) + (ab*Sin(2*tr))/(640.*p**2*p3**3*Pi) -
     (4*ab*Sin(2*tr))/(5.*p**4*p3*Pi) - (4*ab*p3*Sin(2*tr))/(5.*p**4*Pi) -
     (p3*Sin(2*tr))/(p**2*Pi) + (ab*p3*Sin(2*tr))/(5.*p**2*Pi) +
     (ab*Sin(3*tr))/(96.*p**4*p2**3*Pi) - (ab*Sin(3*tr))/(6.*p**4*p2*Pi) -
     (ab*Sin(4*tr))/(96.*p**4*p2**3*Pi) + Sin(4*tr)/(512.*p**2*p2**3*Pi) +
     (ab*Sin(4*tr))/(512.*p**2*p2**3*Pi) +
     (ab*Sin(4*tr))/(16.*p**4*p2*Pi) + Sin(4*tr)/(32.*p**2*p2*Pi) +
     (ab*Sin(4*tr))/(32.*p**2*p2*Pi) +
     (7*ab*Sin(4*tr))/(160.*p**4*p3**3*Pi) -
     Sin(4*tr)/(128.*p**2*p3**3*Pi) + (ab*Sin(4*tr))/(640.*p**2*p3**3*Pi) -
     (3*ab*Sin(4*tr))/(20.*p**4*p3*Pi) - Sin(4*tr)/(16.*p**2*p3*Pi) +
     (ab*Sin(4*tr))/(80.*p**2*p3*Pi) +
     (ab*Sin(5*tr))/(160.*p**4*p2**3*Pi) -
     (ab*Sin(6*tr))/(288.*p**4*p2**3*Pi) -
     Sin(6*tr)/(1536.*p**2*p2**3*Pi) -
     (ab*Sin(6*tr))/(1536.*p**2*p2**3*Pi) +
     (19*ab*Sin(6*tr))/(1440.*p**4*p3**3*Pi) +
     Sin(6*tr)/(384.*p**2*p3**3*Pi) - (ab*Sin(6*tr))/(1920.*p**2*p3**3*Pi)) \
+ hr**2*((-7*ab)/p**4 + (1172*ab)/(525.*p**4*p3**3*Pi) -
     43/(105.*p**2*p3**3*Pi) + (43*ab)/(525.*p**2*p3**3*Pi) +
     (304*ab)/(75.*p**4*p3*Pi) - 4/(3.*p**2*p3*Pi) +
     (4*ab)/(15.*p**2*p3*Pi) + (32*ab*p3)/(15.*p**4*Pi) +
     (8*p3)/(3.*p**2*Pi) - (8*ab*p3)/(15.*p**2*Pi) + (6*ab*tp)/(p**4*Pi) +
     (ab*tr)/(64.*p**4*p2**3*Pi) + (ab*tr)/(4.*p**4*p2*Pi) -
     (4*ab*p2*tr)/(p**4*Pi) - (77*ab*Sin(tp))/(30.*p**4*p3**3*Pi) +
     (179*Sin(tp))/(384.*p**2*p3**3*Pi) -
     (143*ab*Sin(tp))/(1920.*p**2*p3**3*Pi) -
     (7*ab*Sin(tp))/(2.*p**4*p3*Pi) + (3*Sin(tp))/(2.*p**2*p3*Pi) -
     (ab*Sin(tp))/(10.*p**2*p3*Pi) + (32*ab*p3*Sin(tp))/(5.*p**4*Pi) -
     (3*p3*Sin(tp))/(p**2*Pi) - (9*ab*p3*Sin(tp))/(5.*p**2*Pi) +
     (32*ab*p3**3*Sin(tp))/(15.*p**4*Pi) + (4*ab*Sin(2*tp))/(p**4*Pi) -
     (53*ab*Sin(3*tp))/(120.*p**4*p3**3*Pi) +
     (23*Sin(3*tp))/(384.*p**2*p3**3*Pi) -
     (7*ab*Sin(3*tp))/(384.*p**2*p3**3*Pi) -
     (9*ab*Sin(3*tp))/(20.*p**4*p3*Pi) + Sin(3*tp)/(6.*p**2*p3*Pi) -
     (ab*Sin(3*tp))/(15.*p**2*p3*Pi) + (16*ab*p3*Sin(3*tp))/(15.*p**4*Pi) -
     (p3*Sin(3*tp))/(3.*p**2*Pi) - (ab*p3*Sin(3*tp))/(5.*p**2*Pi) +
     (ab*Sin(4*tp))/(2.*p**4*Pi) - (13*ab*Sin(5*tp))/(200.*p**4*p3**3*Pi) +
     (7*Sin(5*tp))/(1920.*p**2*p3**3*Pi) -
     (19*ab*Sin(5*tp))/(9600.*p**2*p3**3*Pi) +
     (ab*Sin(5*tp))/(100.*p**4*p3*Pi) - (ab*Sin(5*tp))/(50.*p**2*p3*Pi)-
(ab*Sin(7*tp))/(140.*p**4*p3**3*Pi) +
```

```
     Sin(7*tp)/(2688.*p**2*p3**3*Pi) +
     (11*ab*Sin(7*tp))/(13440.*p**2*p3**3*Pi) -
     (3*ab*Sin(tr))/(128.*p**4*p2**3*Pi) +
     (5*Sin(tr))/(3072.*p**2*p2**3*Pi) +
     (5*ab*Sin(tr))/(3072.*p**2*p2**3*Pi) -
     (3*ab*Sin(tr))/(8.*p**4*p2*Pi) + Sin(tr)/(32.*p**2*p2*Pi) +
     (ab*Sin(tr))/(32.*p**2*p2*Pi) + (6*ab*p2*Sin(tr))/(p**4*Pi) -
     (p2*Sin(tr))/(2.*p**2*Pi) - (ab*p2*Sin(tr))/(2.*p**2*Pi) +
     (8*p2**3*Sin(tr))/(3.*p**2*Pi) + (8*ab*p2**3*Sin(tr))/(3.*p**2*Pi)-
(29*ab*Sin(tr))/(960.*p**4*p3**3*Pi) -
     (5*Sin(tr))/(768.*p**2*p3**3*Pi) + (ab*Sin(tr))/(768.*p**2*p3**3*Pi) +
     (19*ab*Sin(tr))/(20.*p**4*p3*Pi) - Sin(tr)/(16.*p**2*p3*Pi) +
     (ab*Sin(tr))/(80.*p**2*p3*Pi) + (2*ab*p3*Sin(tr))/(p**4*Pi) +
     (p3*Sin(tr))/(2.*p**2*Pi) - (33*ab*p3*Sin(tr))/(10.*p**2*Pi) -
     (8*p3**3*Sin(tr))/(3.*p**2*Pi) + (8*ab*p3**3*Sin(tr))/(15.*p**2*Pi) -
     (ab*Sin(2*tr))/(256.*p**4*p2**3*Pi) - (2*ab*p2*Sin(2*tr))/(p**4*Pi) +
     (ab*Sin(3*tr))/(128.*p**4*p2**3*Pi) -
     Sin(3*tr)/(1024.*p**2*p2**3*Pi) -
     (ab*Sin(3*tr))/(1024.*p**2*p2**3*Pi) +
     (ab*Sin(3*tr))/(16.*p**4*p2*Pi) - Sin(3*tr)/(64.*p**2*p2*Pi) -
     (ab*Sin(3*tr))/(64.*p**2*p2*Pi) +
(2*ab*p2*Sin(3*tr))/(3.*p**4*Pi)+(p2*Sin(3*tr))/(6.*p**2*Pi) +
(ab*p2*Sin(3*tr))/(6.*p**2*Pi) -
     (ab*Sin(3*tr))/(192.*p**4*p3**3*Pi) + Sin(3*tr)/(256.*p**2*p3**3*Pi) -
     (ab*Sin(3*tr))/(1280.*p**2*p3**3*Pi) -
     (5*ab*Sin(3*tr))/(24.*p**4*p3*Pi) + Sin(3*tr)/(32.*p**2*p3*Pi) -
     (ab*Sin(3*tr))/(160.*p**2*p3*Pi) - (2*ab*p3*Sin(3*tr))/(3.*p**4*Pi) -
     (p3*Sin(3*tr))/(6.*p**2*Pi) + (ab*p3*Sin(3*tr))/(30.*p**2*Pi) -
     (ab*Sin(4*tr))/(256.*p**4*p2**3*Pi) -
     (ab*Sin(4*tr))/(16.*p**4*p2*Pi) +
     (ab*Sin(5*tr))/(640.*p**4*p2**3*Pi) +
     Sin(5*tr)/(3072.*p**2*p2**3*Pi) +
     (ab*Sin(5*tr))/(3072.*p**2*p2**3*Pi) +
     (3*ab*Sin(5*tr))/(80.*p**4*p2*Pi) + Sin(5*tr)/(320.*p**2*p2*Pi) +
     (ab*Sin(5*tr))/(320.*p**2*p2*Pi) +
     (19*ab*Sin(5*tr))/(4800.*p**4*p3**3*Pi) -
     Sin(5*tr)/(768.*p**2*p3**3*Pi) +
     (ab*Sin(5*tr))/(3840.*p**2*p3**3*Pi) -
     (13*ab*Sin(5*tr))/(200.*p**4*p3*Pi) - Sin(5*tr)/(160.*p**2*p3*Pi)+
(ab*Sin(5*tr))/(800.*p**2*p3*Pi) +
     (ab*Sin(6*tr))/(768.*p**4*p2**3*Pi) -
     (ab*Sin(7*tr))/(896.*p**4*p2**3*Pi) -
     Sin(7*tr)/(21504.*p**2*p2**3*Pi) -
     (ab*Sin(7*tr))/(21504.*p**2*p2**3*Pi) +
     (5*ab*Sin(7*tr))/(1344.*p**4*p3**3*Pi) +
     Sin(7*tr)/(5376.*p**2*p3**3*Pi) -
(ab*Sin(7*tr))/(26880.*p**2*p3**3*Pi)\) + hr**3*((-9*ab)/(20.*p**4*p3**3) -
(5*ab)/(4.*p**4*p3) +
     (16*ab*p3)/(5.*p**4) + (16*ab*p3**3)/(15.*p**4) -
     (32*ab)/(9.*p**4*Pi) + (107*ab*tp)/(120.*p**4*p3**3*Pi) +
     (12*ab*tp)/(5.*p**4*p3*Pi) - (24*ab*p3*tp)/(5.*p**4*Pi) +
     (5*ab*tr)/(768.*p**4*p2**3*Pi) + (3*ab*tr)/(32.*p**4*p2*Pi) -
     (ab*p2*tr)/(p**4*Pi) + (8*ab*p2**3*tr)/(3.*p**4*Pi) +
     (ab*tr)/(240.*p**4*p3**3*Pi) + (ab*tr)/(20.*p**4*p3*Pi) -
     (4*ab*p3*tr)/(5.*p**4*Pi) - (16*ab*p3**3*tr)/(15.*p**4*Pi) -
     (5*ab*Sin(tp))/(2.*p**4*Pi) + (19*ab*Sin(2*tp))/(30.*p**4*p3**3*Pi) +
     (8*ab*Sin(2*tp))/(5.*p**4*p3*Pi) - (16*ab*p3*Sin(2*tp))/(5.*p**4*Pi) -
```

```
     (5*ab*Sin(3*tp))/(12.*p**4*Pi) +
     (13*ab*Sin(4*tp))/(120.*p**4*p3**3*Pi) +
     (ab*Sin(4*tp))/(5.*p**4*p3*Pi) - (2*ab*p3*Sin(4*tp))/(5.*p**4*Pi)-
(ab*Sin(5*tp))/(20.*p**4*Pi) + (ab*Sin(6*tp))/(90.*p**4*p3**3*Pi) +
     (ab*Sin(8*tp))/(960.*p**4*p3**3*Pi) -
     (5*ab*Sin(tr))/(1536.*p**4*p2**3*Pi) - (ab*Sin(tr))/(16.*p**4*p2*Pi) +
     (ab*p2*Sin(tr))/(p**4*Pi) - (16*ab*p2**3*Sin(tr))/(3.*p**4*Pi) +
     (16*ab*p3*Sin(tr))/(5.*p**4*Pi) +
     (32*ab*p3**3*Sin(tr))/(15.*p**4*Pi) -
     (ab*Sin(2*tr))/(384.*p**4*p2**3*Pi) -
     (3*ab*Sin(2*tr))/(128.*p**4*p2*Pi) +
     (4*ab*p2**3*Sin(2*tr))/(3.*p**4*Pi) +
     (ab*Sin(2*tr))/(480.*p**4*p3**3*Pi) +
     (3*ab*Sin(2*tr))/(80.*p**4*p3*Pi) - (4*ab*p3*Sin(2*tr))/(5.*p**4*Pi) -
     (8*ab*p3**3*Sin(2*tr))/(15.*p**4*Pi) +
     (ab*Sin(3*tr))/(512.*p**4*p2**3*Pi) +
     (ab*Sin(3*tr))/(32.*p**4*p2*Pi) - (ab*p2*Sin(3*tr))/(3.*p**4*Pi) -
     (ab*Sin(4*tr))/(768.*p**4*p2**3*Pi) -
     (3*ab*Sin(4*tr))/(128.*p**4*p2*Pi) + (ab*p2*Sin(4*tr))/(4.*p**4*Pi) -
     (ab*Sin(4*tr))/(480.*p**4*p3**3*Pi) -
     (ab*Sin(4*tr))/(80.*p**4*p3*Pi) - (ab*p3*Sin(4*tr))/(5.*p**4*Pi) -
     (ab*Sin(5*tr))/(1536.*p**4*p2**3*Pi) -
     (ab*Sin(5*tr))/(160.*p**4*p2*Pi) +
     (ab*Sin(6*tr))/(1152.*p**4*p2**3*Pi) +
     (ab*Sin(6*tr))/(128.*p**4*p2*Pi) -
     (ab*Sin(6*tr))/(1440.*p**4*p3**3*Pi) -
     (ab*Sin(6*tr))/(80.*p**4*p3*Pi) +
     (ab*Sin(7*tr))/(10752.*p**4*p2**3*Pi) -
     (ab*Sin(8*tr))/(6144.*p**4*p2**3*Pi) +
     (ab*Sin(8*tr))/(1920.*p**4*p3**3*Pi)) +
  hr**4*(-ab/(3.*p**4) + (428*ab)/(1575.*p**4*p3**3*Pi) +
     (472*ab)/(525.*p**4*p3*Pi) - (32*ab*p3)/(15.*p**4*Pi) +
     (64*ab*p3**3)/(45.*p**4*Pi) - (101*ab*Sin(tp))/(320.*p**4*p3**3*Pi) -
     (ab*Sin(tp))/(p**4*p3*Pi) + (2*ab*p3*Sin(tp))/(p**4*Pi) -
     (9*ab*Sin(3*tp))/(160.*p**4*p3**3*Pi) -
     (ab*Sin(3*tp))/(6.*p**4*p3*Pi) + (ab*p3*Sin(3*tp))/(3.*p**4*Pi) -
     (7*ab*Sin(5*tp))/(800.*p**4*p3**3*Pi) -
     (ab*Sin(5*tp))/(50.*p**4*p3*Pi) + (ab*p3*Sin(5*tp))/(25.*p**4*Pi)-
(3*ab*Sin(7*tp))/(4480.*p**4*p3**3*Pi) -
     (ab*Sin(9*tp))/(17280.*p**4*p3**3*Pi) -
     (7*ab*Sin(tr))/(6144.*p**4*p2**3*Pi) -
     (5*ab*Sin(tr))/(256.*p**4*p2*Pi) + (ab*p2*Sin(tr))/(4.*p**4*Pi) -
     (2*ab*p2**3*Sin(tr))/(3.*p**4*Pi) - (ab*Sin(tr))/(640.*p**4*p3**3*Pi) -
     (3*ab*Sin(tr))/(160.*p**4*p3*Pi) + (ab*p3*Sin(tr))/(5.*p**4*Pi) +
     (4*ab*p3**3*Sin(tr))/(15.*p**4*Pi) +
     (7*ab*Sin(3*tr))/(9216.*p**4*p2**3*Pi) +
     (3*ab*Sin(3*tr))/(256.*p**4*p2*Pi) - (ab*p2*Sin(3*tr))/(8.*p**4*Pi) +
     (2*ab*p2**3*Sin(3*tr))/(9.*p**4*Pi) +
     (ab*Sin(3*tr))/(1440.*p**4*p3**3*Pi) +
     (ab*Sin(3*tr))/(160.*p**4*p3*Pi) - (ab*p3*Sin(3*tr))/(30.*p**4*Pi)-
(4*ab*p3**3*Sin(3*tr))/(45.*p**4*Pi) -
     (ab*Sin(5*tr))/(3072.*p**4*p2**3*Pi) -
     (ab*Sin(5*tr))/(256.*p**4*p2*Pi) +
(ab*p2*Sin(5*tr))/(40.*p**4*Pi)+(ab*Sin(5*tr))/(800.*p**4*p3*Pi) -
(ab*p3*Sin(5*tr))/(50.*p**4*Pi) +
     (ab*Sin(7*tr))/(12288.*p**4*p2**3*Pi) +
     (ab*Sin(7*tr))/(1792.*p**4*p2*Pi) -
```

```
     (ab*Sin(7*tr))/(8960.*p**4*p3**3*Pi) -
     (ab*Sin(7*tr))/(1120.*p**4*p3*Pi) -
     (ab*Sin(9*tr))/(110592.*p**4*p2**3*Pi) +
     (ab*Sin(9*tr))/(34560.*p**4*p3**3*Pi))
```

and $\chi_m^{//}$= -2/(p**2*Pi) - (2*ab)/(p**2*Pi) - (7*ab)/(480.*p**4*p2**3*Pi)+
1/(30.*p**2*p2**3*Pi) + ab/(30.*p**2*p2**3*Pi) + 1/(3.*p**2*p2*Pi) +
ab/(3.*p**2*p2*Pi) + 4/(15.*p3**3*Pi) - (4*ab)/(25.*p3**3*Pi) -
(24*ab)/(25.*p**4*p3**3*Pi) + 2/(15.*p**2*p3**3*Pi) +
(22*ab)/(15.*p**2*p3**3*Pi) + 4/(3.*p3*Pi) + (4*ab)/(5.*p3*Pi) +
(16*ab)/(15.*p**4*p3*Pi) - 4/(3.*p**2*p3*Pi) - (76*ab)/(15.*p**2*p3*Pi) +
(5*Cos(tp))/(16.*p3**3*Pi) - (13*ab*Cos(tp))/(80.*p3**3*Pi) -
(2*ab*Cos(tp))/(15.*p**4*p3**3*Pi) - Cos(tp)/(4.*p**2*p3**3*Pi) +
(3*Cos(tp))/(2.*p3*Pi) - (7*ab*Cos(tp))/(10.*p3*Pi) -
(4*ab*Cos(tp))/(5.*p**4*p3*Pi) + (2*ab*Cos(tp))/(5.*p**2*p3*Pi) -
(4*p3*Cos(tp))/Pi + (4*ab*p3*Cos(tp))/(5.*Pi) +
(16*ab*p3*Cos(tp))/(5.*p**2*Pi) + (2*Cos(2*tp))/(p**2*Pi) +
(2*ab*Cos(2*tp))/(p**2*Pi) - (5*Cos(3*tp))/(96.*p3**3*Pi) -
(ab*Cos(3*tp))/(160.*p3**3*Pi) - Cos(3*tp)/(8.*p**2*p3**3*Pi) +
(ab*Cos(3*tp))/(30.*p**2*p3**3*Pi) - Cos(3*tp)/(6.*p3*Pi) -
(ab*Cos(3*tp))/(10.*p3*Pi) - (4*ab*Cos(3*tp))/(15.*p**4*p3*Pi) +
(2*ab*Cos(3*tp))/(3.*p**2*p3*Pi) + Cos(5*tp)/(160.*p3**3*Pi) +
(7*ab*Cos(5*tp))/(800.*p3**3*Pi) + (2*ab*Cos(5*tp))/(75.*p**4*p3**3*Pi) -
Cos(5*tp)/(40.*p**2*p3**3*Pi) - (3*ab*Cos(5*tp))/(50.*p**2*p3**3*Pi)+
(ab*Cos(tr))/(24.*p**4*p2**3*Pi) - Cos(tr)/(32.*p**2*p2**3*Pi) -
(ab*Cos(tr))/(32.*p**2*p2**3*Pi) - Cos(tr)/(4.*p**2*p2*Pi) -
(ab*Cos(tr))/(4.*p**2*p2*Pi) + (31*ab*Cos(tr))/(30.*p**4*p3**3*Pi) +
Cos(tr)/(8.*p**2*p3**3*Pi) - (13*ab*Cos(tr))/(8.*p**2*p3**3*Pi) -
(8*ab*Cos(tr))/(5.*p3*Pi) - (6*ab*Cos(tr))/(5.*p**4*p3*Pi) +
(5*Cos(tr))/(2.*p**2*p3*Pi) + (59*ab*Cos(tr))/(10.*p**2*p3*Pi) -
(4*p3*Cos(tr))/Pi + (4*ab*p3*Cos(tr))/(5.*Pi) +
(16*ab*p3*Cos(tr))/(5.*p**2*Pi) +
((-6*ab)/(5.*p3**3*Pi) + (3*p**2)/(2.*p3**3*Pi) +
   (ab*p**2)/(2.*p3**3*Pi) - (2*ab*Cos(2*tp))/(5.*p3**3*Pi) +
   (p**2*Cos(2*tp))/(2.*p3**3*Pi) +
(ab*p**2*Cos(2*tp))/(6.*p3**3*Pi)+(8*ab*Cos(tr))/(5.*p3**3*Pi) -
(2*p**2*Cos(tr))/(p3**3*Pi) -
   (2*ab*p**2*Cos(tr))/(3.*p3**3*Pi))/hr**3 +
((-8*ab*p**2*Cos(tp))/(15.*p3**3*Pi) + (2*p**4*Cos(tp))/(3.*p3**3*Pi)-
(2*ab*p**4*Cos(tp))/(15.*p3**3*Pi) -
   (8*ab*p**2*Cos(tr))/(15.*p3**3*Pi) + (2*p**4*Cos(tr))/(3.*p3**3*Pi) -
   (2*ab*p**4*Cos(tr))/(15.*p3**3*Pi))/hr**4 +
(-4/(3.*p3**3*Pi) - (12*ab)/(5.*p3**3*Pi) +
   (16*ab)/(15.*p**2*p3**3*Pi) + (2*p**2)/(3.*p3**3*Pi) +
   (2*ab*p**2)/(9.*p3**3*Pi) + Cos(tp)/(2.*p3**3*Pi) +
   (ab*Cos(tp))/(10.*p3**3*Pi) - (2*ab*Cos(tp))/(5.*p**2*p3**3*Pi) +
   (3*p**2*Cos(tp))/(4.*p3**3*Pi) -
   (17*ab*p**2*Cos(tp))/(60.*p3**3*Pi) - (8*ab*Cos(tp))/(5.*p3*Pi) +
   (2*p**2*Cos(tp))/(p3*Pi) - (2*ab*p**2*Cos(tp))/(5.*p3*Pi) +
  Cos(3*tp)/(6.*p3**3*Pi) + (3*ab*Cos(3*tp))/(10.*p3**3*Pi) -
   (2*ab*Cos(3*tp))/(15.*p**2*p3**3*Pi) -
   (p**2*Cos(3*tp))/(12.*p3**3*Pi) -
   (ab*p**2*Cos(3*tp))/(36.*p3**3*Pi) + (2*Cos(tr))/(p3**3*Pi) +
   (14*ab*Cos(tr))/(5.*p3**3*Pi) - (8*ab*Cos(tr))/(5.*p**2*p3**3*Pi)-
   (8*ab*p**2*Cos(tr))/(15.*p3**3*Pi) - (8*ab*Cos(tr))/(5.*p3*Pi) +
   (2*p**2*Cos(tr))/(p3*Pi) - (2*ab*p**2*Cos(tr))/(5.*p3*Pi))/hr**2 -
(ab*Cos(2*tr))/(24.*p**4*p2**3*Pi) + (ab*Cos(3*tr))/(48.*p**4*p2**3*Pi) -

```
Cos(3*tr)/(192.*p**2*p2**3*Pi) - (ab*Cos(3*tr))/(192.*p**2*p2**3*Pi)-
Cos(3*tr)/(12.*p**2*p2*Pi) - (ab*Cos(3*tr))/(12.*p**2*p2*Pi) -
(ab*Cos(3*tr))/(20.*p**4*p3**3*Pi) + Cos(3*tr)/(48.*p**2*p3**3*Pi) -
(ab*Cos(3*tr))/(240.*p**2*p3**3*Pi) + (2*ab*Cos(3*tr))/(15.*p**4*p3*Pi) +
Cos(3*tr)/(6.*p**2*p3*Pi) - (ab*Cos(3*tr))/(30.*p**2*p3*Pi) -
(ab*Cos(4*tr))/(96.*p**4*p2**3*Pi) +
(-8/(3.*p**2*Pi) - (8*ab)/(3.*p**2*Pi) - 5/(192.*p**2*p2**3*Pi) -
   (5*ab)/(192.*p**2*p2**3*Pi) - 3/(16.*p3**3*Pi) -
   (117*ab)/(80.*p3**3*Pi) - (9*ab)/(20.*p**4*p3**3*Pi) +
   9/(16.*p**2*p3**3*Pi) + (219*ab)/(80.*p**2*p3**3*Pi) + 3/(p3*Pi) +
   (9*ab)/(5.*p3*Pi) - (12*ab)/(5.*p**2*p3*Pi) + (4*Cos(tp))/Pi +
   (32*ab*Cos(tp))/(15.*p**4*Pi) + Cos(2*tp)/(4.*p3**3*Pi) -
   (ab*Cos(2*tp))/(20.*p3**3*Pi) + Cos(2*tp)/(6.*p**2*p3**3*Pi) +
   (ab*Cos(2*tp))/(6.*p**2*p3**3*Pi) + Cos(2*tp)/(p3*Pi) +
   (3*ab*Cos(2*tp))/(5.*p3*Pi) - (4*ab*Cos(2*tp))/(5.*p**2*p3*Pi) -
   Cos(4*tp)/(16.*p3**3*Pi) - (7*ab*Cos(4*tp))/(80.*p3**3*Pi) +
   Cos(4*tp)/(24.*p**2*p3**3*Pi) +
   (17*ab*Cos(4*tp))/(120.*p**2*p3**3*Pi) +
   (8*ab*Cos(tr))/(5.*p3**3*Pi) + (8*ab*Cos(tr))/(15.*p**4*p3**3*Pi)-
   (2*Cos(tr))/(3.*p**2*p3**3*Pi) -
   (46*ab*Cos(tr))/(15.*p**2*p3**3*Pi) - (4*Cos(tr))/(p3*Pi) -
   (12*ab*Cos(tr))/(5.*p3*Pi) + (16*ab*Cos(tr))/(5.*p**2*p3*Pi) +
   Cos(2*tr)/(48.*p**2*p2**3*Pi) + (ab*Cos(2*tr))/(48.*p**2*p2**3*Pi)-
   (ab*Cos(2*tr))/(15.*p**4*p3**3*Pi) - Cos(2*tr)/(12.*p**2*p3**3*Pi)+
   (ab*Cos(2*tr))/(60.*p**2*p3**3*Pi) + Cos(4*tr)/(192.*p**2*p2**3*Pi) +
   (ab*Cos(4*tr))/(192.*p**2*p2**3*Pi) -
   (ab*Cos(4*tr))/(60.*p**4*p3**3*Pi) - Cos(4*tr)/(48.*p**2*p3**3*Pi)+
   (ab*Cos(4*tr))/(240.*p**2*p3**3*Pi))/hr +
(ab*Cos(5*tr))/(240.*p**4*p2**3*Pi) + Cos(5*tr)/(320.*p**2*p2**3*Pi)+
(ab*Cos(5*tr))/(320.*p**2*p2**3*Pi) -
(7*ab*Cos(5*tr))/(300.*p**4*p3**3*Pi) - Cos(5*tr)/(80.*p**2*p3**3*Pi)+
(ab*Cos(5*tr))/(400.*p**2*p3**3*Pi) +
hr*(-8/(3.*p**2*Pi) - (8*ab)/(3.*p**2*Pi) - (7*ab)/(180.*p**4*p2**3*Pi) -
   5/(768.*p**2*p2**3*Pi) - (5*ab)/(768.*p**2*p2**3*Pi) -
   (17*ab)/(48.*p**4*p2*Pi) - 3/(32.*p**2*p2*Pi) -
   (3*ab)/(32.*p**2*p2*Pi) + p2/(p**2*Pi) + (ab*p2)/(p**2*Pi) -
   (85*ab)/(144.*p**4*p3**3*Pi) + 31/(192.*p**2*p3**3*Pi) -
   (7*ab)/(960.*p**2*p3**3*Pi) + (63*ab)/(20.*p**4*p3*Pi) +
   3/(16.*p**2*p3*Pi) - (243*ab)/(80.*p**2*p3*Pi) +
   (12*ab*p3)/(5.*p**4*Pi) - (3*p3)/(p**2*Pi) - (21*ab*p3)/(5.*p**2*Pi) +
   (4*ab*Cos(tp))/(p**4*Pi) - Cos(tp)/(p**2*Pi) -
   (ab*Cos(tp))/(p**2*Pi) - (2*ab*Cos(2*tp))/(15.*p**4*p3**3*Pi) +
   (21*Cos(2*tp))/(64.*p**2*p3**3*Pi) -
   (5*ab*Cos(2*tp))/(64.*p**2*p3**3*Pi) +
   (2*ab*Cos(2*tp))/(5.*p**4*p3*Pi) + Cos(2*tp)/(p**2*p3*Pi) -
   (ab*Cos(2*tp))/(5.*p**2*p3*Pi) - (2*p3*Cos(2*tp))/(p**2*Pi) -
   (6*ab*p3*Cos(2*tp))/(5.*p**2*Pi) + (4*ab*Cos(3*tp))/(3.*p**4*Pi) -
   Cos(3*tp)/(3.*p**2*Pi) - (ab*Cos(3*tp))/(3.*p**2*Pi) -
   (ab*Cos(4*tp))/(12.*p**4*p3**3*Pi) + Cos(4*tp)/(32.*p**2*p3**3*Pi)-
   (ab*Cos(4*tp))/(32.*p**2*p3**3*Pi) + (ab*Cos(4*tp))/(10.*p**4*p3*Pi) -
   (ab*Cos(4*tp))/(5.*p**2*p3*Pi) - (ab*Cos(6*tp))/(45.*p**4*p3**3*Pi) +
   Cos(6*tp)/(192.*p**2*p3**3*Pi) +
   (11*ab*Cos(6*tp))/(960.*p**2*p3**3*Pi) +
   (ab*Cos(tr))/(16.*p**4*p2**3*Pi) + (ab*Cos(tr))/(2.*p**4*p2*Pi) +
   (8*ab*Cos(tr))/(15.*p**4*p3**3*Pi) - (16*ab*Cos(tr))/(5.*p**4*p3*Pi) +
   (16*ab*Cos(tr))/(5.*p**2*p3*Pi) - (16*ab*p3*Cos(tr))/(5.*p**4*Pi)+
   (4*p3*Cos(tr))/(p**2*Pi) + (28*ab*p3*Cos(tr))/(5.*p**2*Pi) -
```

```
     (ab*Cos(2*tr))/(32.*p**4*p2**3*Pi) +
     (5*Cos(2*tr))/(512.*p**2*p2**3*Pi) +
     (5*ab*Cos(2*tr))/(512.*p**2*p2**3*Pi) -
     (ab*Cos(2*tr))/(4.*p**4*p2*Pi) + Cos(2*tr)/(8.*p**2*p2*Pi) +
     (ab*Cos(2*tr))/(8.*p**2*p2*Pi) - (p2*Cos(2*tr))/(p**2*Pi) -
     (ab*p2*Cos(2*tr))/(p**2*Pi) + (ab*Cos(2*tr))/(480.*p**4*p3**3*Pi)-
     (5*Cos(2*tr))/(128.*p**2*p3**3*Pi) +
     (ab*Cos(2*tr))/(128.*p**2*p3**3*Pi) + (ab*Cos(2*tr))/(5.*p**4*p3*Pi) -
     Cos(2*tr)/(4.*p**2*p3*Pi) + (ab*Cos(2*tr))/(20.*p**2*p3*Pi) +
     (4*ab*p3*Cos(2*tr))/(5.*p**4*Pi) + (p3*Cos(2*tr))/(p**2*Pi) -
     (ab*p3*Cos(2*tr))/(5.*p**2*Pi) + (ab*Cos(3*tr))/(96.*p**4*p2**3*Pi) +
     (ab*Cos(3*tr))/(6.*p**4*p2*Pi) - Cos(4*tr)/(256.*p**2*p2**3*Pi) -
     (ab*Cos(4*tr))/(256.*p**2*p2**3*Pi) -
     (ab*Cos(4*tr))/(16.*p**4*p2*Pi) - Cos(4*tr)/(32.*p**2*p2*Pi) -
     (ab*Cos(4*tr))/(32.*p**2*p2*Pi) -
     (ab*Cos(4*tr))/(240.*p**4*p3**3*Pi) + Cos(4*tr)/(64.*p**2*p3**3*Pi) -
     (ab*Cos(4*tr))/(320.*p**2*p3**3*Pi) +
     (3*ab*Cos(4*tr))/(20.*p**4*p3*Pi) + Cos(4*tr)/(16.*p**2*p3*Pi) -
     (ab*Cos(4*tr))/(80.*p**2*p3*Pi) -
     (ab*Cos(5*tr))/(160.*p**4*p2**3*Pi) +
     (ab*Cos(6*tr))/(288.*p**4*p2**3*Pi) +
     Cos(6*tr)/(1536.*p**2*p2**3*Pi) +
     (ab*Cos(6*tr))/(1536.*p**2*p2**3*Pi) -
     (19*ab*Cos(6*tr))/(1440.*p**4*p3**3*Pi) -
     Cos(6*tr)/(384.*p**2*p3**3*Pi) + (ab*Cos(6*tr))/(1920.*p**2*p3**3*Pi)) \
+ hr**2*((-3*ab)/(2.*p**4*Pi) - 2/(3.*p**2*Pi) - (2*ab)/(3.*p**2*Pi) -
     (337*ab)/(13440.*p**4*p2**3*Pi) + 1/(105.*p**2*p2**3*Pi) +
     ab/(105.*p**2*p2**3*Pi) - (17*ab)/(80.*p**4*p2*Pi) +
     2/(15.*p**2*p2*Pi) + (2*ab)/(15.*p**2*p2*Pi) +
     (2*ab*p2)/(3.*p**4*Pi) - (4*p2)/(3.*p**2*Pi) -
     (4*ab*p2)/(3.*p**2*Pi) + (8*p2**3)/(3.*p**2*Pi) +
     (8*ab*p2**3)/(3.*p**2*Pi) - (8*ab)/(525.*p**4*p3**3*Pi) +
     4/(105.*p**2*p3**3*Pi) - (4*ab)/(105.*p**2*p3**3*Pi) +
     (112*ab)/(75.*p**4*p3*Pi) + 4/(15.*p**2*p3*Pi) -
     (4*ab)/(15.*p**2*p3*Pi) + (16*ab*p3)/(3.*p**4*Pi) -
     (4*p3)/(3.*p**2*Pi) - (28*ab*p3)/(15.*p**2*Pi) +
     (7*ab*Cos(tp))/(15.*p**4*p3**3*Pi) -
     (53*Cos(tp))/(384.*p**2*p3**3*Pi) -
     (7*ab*Cos(tp))/(1920.*p**2*p3**3*Pi) +
     (7*ab*Cos(tp))/(10.*p**4*p3*Pi) - Cos(tp)/(2.*p**2*p3*Pi) -
     (ab*Cos(tp))/(10.*p**2*p3*Pi) + (p3*Cos(tp))/(p**2*Pi) +
     (3*ab*p3*Cos(tp))/(5.*p**2*Pi) - (32*ab*p3**3*Cos(tp))/(15.*p**4*Pi) -
     (2*ab*Cos(2*tp))/(p**4*Pi) + (31*ab*Cos(3*tp))/(120.*p**4*p3**3*Pi) -
     (19*Cos(3*tp))/(384.*p**2*p3**3*Pi) +
     (ab*Cos(3*tp))/(128.*p**2*p3**3*Pi) +
     (29*ab*Cos(3*tp))/(60.*p**4*p3*Pi) - Cos(3*tp)/(6.*p**2*p3*Pi) -
     (16*ab*p3*Cos(3*tp))/(15.*p**4*Pi) + (p3*Cos(3*tp))/(3.*p**2*Pi) +
     (ab*p3*Cos(3*tp))/(5.*p**2*Pi) - (ab*Cos(4*tp))/(2.*p**4*Pi) +
     (9*ab*Cos(5*tp))/(200.*p**4*p3**3*Pi) -
     Cos(5*tp)/(384.*p**2*p3**3*Pi) +
     (41*ab*Cos(5*tp))/(9600.*p**2*p3**3*Pi) -
     (ab*Cos(5*tp))/(100.*p**4*p3*Pi) + (ab*Cos(5*tp))/(50.*p**2*p3*Pi)+
     (ab*Cos(7*tp))/(140.*p**4*p3**3*Pi) -
     Cos(7*tp)/(2688.*p**2*p3**3*Pi) -
     (11*ab*Cos(7*tp))/(13440.*p**2*p3**3*Pi) +
     (5*ab*Cos(tr))/(128.*p**4*p2**3*Pi) -
     (35*Cos(tr))/(3072.*p**2*p2**3*Pi) -
```

```
     (35*ab*Cos(tr))/(3072.*p**2*p2**3*Pi) +
     (3*ab*Cos(tr))/(8.*p**4*p2*Pi) - (5*Cos(tr))/(32.*p**2*p2*Pi) -
     (5*ab*Cos(tr))/(32.*p**2*p2*Pi) - (2*ab*p2*Cos(tr))/(p**4*Pi) +
     (3*p2*Cos(tr))/(2.*p**2*Pi) + (3*ab*p2*Cos(tr))/(2.*p**2*Pi) -
     (8*p2**3*Cos(tr))/(3.*p**2*Pi) - (8*ab*p2**3*Cos(tr))/(3.*p**2*Pi)+
     (11*ab*Cos(tr))/(960.*p**4*p3**3*Pi) +
     (35*Cos(tr))/(768.*p**2*p3**3*Pi) -
     (7*ab*Cos(tr))/(768.*p**2*p3**3*Pi) -
     (31*ab*Cos(tr))/(20.*p**4*p3*Pi) + (5*Cos(tr))/(16.*p**2*p3*Pi) -
     (ab*Cos(tr))/(16.*p**2*p3*Pi) - (6*ab*p3*Cos(tr))/(p**4*Pi) -
     (3*p3*Cos(tr))/(2.*p**2*Pi) + (7*ab*p3*Cos(tr))/(2.*p**2*Pi) +
     (8*p3**3*Cos(tr))/(3.*p**2*Pi) - (8*ab*p3**3*Cos(tr))/(15.*p**2*Pi) -
     (5*ab*Cos(2*tr))/(256.*p**4*p2**3*Pi) -
     (ab*Cos(2*tr))/(4.*p**4*p2*Pi) + (2*ab*p2*Cos(2*tr))/(p**4*Pi) +
     (ab*Cos(3*tr))/(384.*p**4*p2**3*Pi) +
     (7*Cos(3*tr))/(3072.*p**2*p2**3*Pi) +
     (7*ab*Cos(3*tr))/(3072.*p**2*p2**3*Pi) +
     (ab*Cos(3*tr))/(16.*p**4*p2*Pi) + (5*Cos(3*tr))/(192.*p**2*p2*Pi)+
     (5*ab*Cos(3*tr))/(192.*p**2*p2*Pi) -
     (2*ab*p2*Cos(3*tr))/(3.*p**4*Pi) - (p2*Cos(3*tr))/(6.*p**2*Pi) -
     (ab*p2*Cos(3*tr))/(6.*p**2*Pi) + (ab*Cos(3*tr))/(960.*p**4*p3**3*Pi) -
     (7*Cos(3*tr))/(768.*p**2*p3**3*Pi) +
     (7*ab*Cos(3*tr))/(3840.*p**2*p3**3*Pi) -
     (ab*Cos(3*tr))/(120.*p**4*p3*Pi) - (5*Cos(3*tr))/(96.*p**2*p3*Pi)+
     (ab*Cos(3*tr))/(96.*p**2*p3*Pi) + (2*ab*p3*Cos(3*tr))/(3.*p**4*Pi)+
     (p3*Cos(3*tr))/(6.*p**2*Pi) - (ab*p3*Cos(3*tr))/(30.*p**2*Pi) +
     (ab*Cos(4*tr))/(128.*p**4*p2**3*Pi) +
     (ab*Cos(4*tr))/(16.*p**4*p2*Pi) -
     (3*ab*Cos(5*tr))/(640.*p**4*p2**3*Pi) -
     (7*Cos(5*tr))/(15360.*p**2*p2**3*Pi) -
     (7*ab*Cos(5*tr))/(15360.*p**2*p2**3*Pi) -
     (3*ab*Cos(5*tr))/(80.*p**4*p2*Pi) - Cos(5*tr)/(320.*p**2*p2*Pi) -
     (ab*Cos(5*tr))/(320.*p**2*p2*Pi) +
     (31*ab*Cos(5*tr))/(4800.*p**4*p3**3*Pi) +
     (7*Cos(5*tr))/(3840.*p**2*p3**3*Pi) -
     (7*ab*Cos(5*tr))/(19200.*p**2*p3**3*Pi) +
     (13*ab*Cos(5*tr))/(200.*p**4*p3*Pi) + Cos(5*tr)/(160.*p**2*p3*Pi)-
     (ab*Cos(5*tr))/(800.*p**2*p3*Pi) -
     (ab*Cos(6*tr))/(768.*p**4*p2**3*Pi) +
     (ab*Cos(7*tr))/(896.*p**4*p2**3*Pi) +
     Cos(7*tr)/(21504.*p**2*p2**3*Pi) +
     (ab*Cos(7*tr))/(21504.*p**2*p2**3*Pi) -
     (5*ab*Cos(7*tr))/(1344.*p**4*p3**3*Pi) -
     Cos(7*tr)/(5376.*p**2*p3**3*Pi) +
(ab*Cos(7*tr))/(26880.*p**2*p3**3*Pi)\) + hr**3*((-
957*ab)/(71680.*p**4*p2**3*Pi) - (181*ab)/(960.*p**4*p2*Pi) +
     (23*ab*p2)/(12.*p**4*Pi) - (4*ab*p2**3)/(p**4*Pi) -
     (353*ab)/(1920.*p**4*p3**3*Pi) - (23*ab)/(40.*p**4*p3*Pi) +
     (21*ab*p3)/(5.*p**4*Pi) + (8*ab*p3**3)/(5.*p**4*Pi) +
     (ab*Cos(tp))/(2.*p**4*Pi) - (31*ab*Cos(2*tp))/(120.*p**4*p3**3*Pi)-
     (4*ab*Cos(2*tp))/(5.*p**4*p3*Pi) + (8*ab*p3*Cos(2*tp))/(5.*p**4*Pi) +
     (ab*Cos(3*tp))/(4.*p**4*Pi) - (19*ab*Cos(4*tp))/(240.*p**4*p3**3*Pi) -
     (ab*Cos(4*tp))/(5.*p**4*p3*Pi) + (2*ab*p3*Cos(4*tp))/(5.*p**4*Pi)+
     (ab*Cos(5*tp))/(20.*p**4*Pi) - (ab*Cos(6*tp))/(120.*p**4*p3**3*Pi)-
     (ab*Cos(8*tp))/(960.*p**4*p3**3*Pi) +
     (35*ab*Cos(tr))/(1536.*p**4*p2**3*Pi) +
     (5*ab*Cos(tr))/(16.*p**4*p2*Pi) - (3*ab*p2*Cos(tr))/(p**4*Pi) +
```

```
     (16*ab*p2**3*Cos(tr))/(3.*p**4*Pi) - (16*ab*p3*Cos(tr))/(5.*p**4*Pi) -
     (32*ab*p3**3*Cos(tr))/(15.*p**4*Pi) -
     (7*ab*Cos(2*tr))/(768.*p**4*p2**3*Pi) -
     (15*ab*Cos(2*tr))/(128.*p**4*p2*Pi) + (ab*p2*Cos(2*tr))/(p**4*Pi)-
     (4*ab*p2**3*Cos(2*tr))/(3.*p**4*Pi) -
     (ab*Cos(2*tr))/(480.*p**4*p3**3*Pi) -
     (ab*Cos(2*tr))/(80.*p**4*p3*Pi) +
     (8*ab*p3**3*Cos(2*tr))/(15.*p**4*Pi) -
     (7*ab*Cos(3*tr))/(1536.*p**4*p2**3*Pi) -
     (5*ab*Cos(3*tr))/(96.*p**4*p2*Pi) + (ab*p2*Cos(3*tr))/(3.*p**4*Pi)+
     (7*ab*Cos(4*tr))/(1536.*p**4*p2**3*Pi) +
     (3*ab*Cos(4*tr))/(64.*p**4*p2*Pi) - (ab*p2*Cos(4*tr))/(4.*p**4*Pi)-
     (ab*Cos(4*tr))/(480.*p**4*p3**3*Pi) -
     (ab*Cos(4*tr))/(40.*p**4*p3*Pi) + (ab*p3*Cos(4*tr))/(5.*p**4*Pi) +
     (7*ab*Cos(5*tr))/(7680.*p**4*p2**3*Pi) +
     (ab*Cos(5*tr))/(160.*p**4*p2*Pi) -
     (ab*Cos(6*tr))/(768.*p**4*p2**3*Pi) -
     (ab*Cos(6*tr))/(128.*p**4*p2*Pi) +
     (ab*Cos(6*tr))/(480.*p**4*p3**3*Pi) +
     (ab*Cos(6*tr))/(80.*p**4*p3*Pi) -
     (ab*Cos(7*tr))/(10752.*p**4*p2**3*Pi) +
     (ab*Cos(8*tr))/(6144.*p**4*p2**3*Pi) -
     (ab*Cos(8*tr))/(1920.*p**4*p3**3*Pi)) +
  hr**4*((-8*ab)/(945.*p**4*p2**3*Pi) - (4*ab)/(35.*p**4*p2*Pi) +
     (16*ab*p2)/(15.*p**4*Pi) - (16*ab*p2**3)/(9.*p**4*Pi) -
     (16*ab)/(4725.*p**4*p3**3*Pi) - (16*ab)/(525.*p**4*p3*Pi) +
     (16*ab*p3)/(75.*p**4*Pi) + (32*ab*p3**3)/(45.*p**4*Pi) +
     (11*ab*Cos(tp))/(192.*p**4*p3**3*Pi) + (ab*Cos(tp))/(5.*p**4*p3*Pi) -
     (2*ab*p3*Cos(tp))/(5.*p**4*Pi) +
     (43*ab*Cos(3*tp))/(1440.*p**4*p3**3*Pi) +
     (ab*Cos(3*tp))/(10.*p**4*p3*Pi) - (ab*p3*Cos(3*tp))/(5.*p**4*Pi) +
     (17*ab*Cos(5*tp))/(2400.*p**4*p3**3*Pi) +
     (ab*Cos(5*tp))/(50.*p**4*p3*Pi) - (ab*p3*Cos(5*tp))/(25.*p**4*Pi)+
     (ab*Cos(7*tp))/(1920.*p**4*p3**3*Pi) +
     (ab*Cos(9*tp))/(17280.*p**4*p3**3*Pi) +
     (21*ab*Cos(tr))/(2048.*p**4*p2**3*Pi) +
     (35*ab*Cos(tr))/(256.*p**4*p2*Pi) - (5*ab*p2*Cos(tr))/(4.*p**4*Pi)+
     (2*ab*p2**3*Cos(tr))/(p**4*Pi) + (7*ab*Cos(tr))/(1920.*p**4*p3**3*Pi) +
     (ab*Cos(tr))/(32.*p**4*p3*Pi) - (ab*p3*Cos(tr))/(5.*p**4*Pi) -
     (4*ab*p3**3*Cos(tr))/(5.*p**4*Pi) -
     (7*ab*Cos(3*tr))/(3072.*p**4*p2**3*Pi) -
     (7*ab*Cos(3*tr))/(256.*p**4*p2*Pi) +
     (5*ab*p2*Cos(3*tr))/(24.*p**4*Pi) -
     (2*ab*p2**3*Cos(3*tr))/(9.*p**4*Pi) +
     (ab*Cos(3*tr))/(480.*p**4*p3*Pi) - (ab*p3*Cos(3*tr))/(30.*p**4*Pi)+
     (4*ab*p3**3*Cos(3*tr))/(45.*p**4*Pi) +
     (3*ab*Cos(5*tr))/(5120.*p**4*p2**3*Pi) +
     (7*ab*Cos(5*tr))/(1280.*p**4*p2*Pi) - (ab*p2*Cos(5*tr))/(40.*p**4*Pi) -
     (ab*Cos(5*tr))/(2400.*p**4*p3**3*Pi) -
     (3*ab*Cos(5*tr))/(800.*p**4*p3*Pi) + (ab*p3*Cos(5*tr))/(50.*p**4*Pi) -
     (3*ab*Cos(7*tr))/(28672.*p**4*p2**3*Pi) -
     (ab*Cos(7*tr))/(1792.*p**4*p2*Pi) +
     (ab*Cos(7*tr))/(5376.*p**4*p3**3*Pi) +
     (ab*Cos(7*tr))/(1120.*p**4*p3*Pi) +
     (ab*Cos(9*tr))/(110592.*p**4*p2**3*Pi) -
     (ab*Cos(9*tr))/(34560.*p**4*p3**3*Pi))
```

Similarly, the expressions for $\chi_m^{/}$ and $\chi_m^{//}$ derived from Kim model at medium field region are given as follows.

```
χm/ = -1 - (8*ab)/(3.*p**4) + 2/p**2 + (2*ab)/p**2- 4/(15.*p**2*p2**3*Pi)-
  (4*ab)/(15.*p**2*p2**3*Pi) + (ab*tm)/(8.*p**4*p2**3*Pi) -
  (4*tp)/(p**2*Pi) - (4*ab*tp)/(p**2*Pi) -
  (5*ab*Sin(tm))/(24.*p**4*p2**3*Pi) + (11*Sin(tm))/(32.*p**2*p2**3*Pi)+
  (11*ab*Sin(tm))/(32.*p**2*p2**3*Pi) + (3*Sin(tm))/(4.*p**2*p2*Pi) +
  (3*ab*Sin(tm))/(4.*p**2*p2*Pi) - (3*ab*Sin(tm))/(2.*p**4*p3**3*Pi) -
  (11*Sin(tm))/(8.*p**2*p3**3*Pi) + (15*ab*Sin(tm))/(8.*p**2*p3**3*Pi)+
  (8*ab*Sin(tm))/(5.*p3*Pi) + (2*ab*Sin(tm))/(5.*p**4*p3*Pi) -
  (7*Sin(tm))/(2.*p**2*p3*Pi) - (57*ab*Sin(tm))/(10.*p**2*p3*Pi) +
  (4*p3*Sin(tm))/Pi - (4*ab*p3*Sin(tm))/(5.*Pi) -
  (16*ab*p3*Sin(tm))/(5.*p**2*Pi) + (ab*Sin(2*tm))/(12.*p**4*p2**3*Pi)-
  (5*ab*Sin(3*tm))/(144.*p**4*p2**3*Pi) +
  (3*Sin(3*tm))/(64.*p**2*p2**3*Pi) + (3*ab*Sin(3*tm))/(64.*p**2*p2**3*Pi) +
 Sin(3*tm)/(12.*p**2*p2*Pi) + (ab*Sin(3*tm))/(12.*p**2*p2*Pi) -
  (7*ab*Sin(3*tm))/(180.*p**4*p3**3*Pi) -
  (3*Sin(3*tm))/(16.*p**2*p3**3*Pi) + (3*ab*Sin(3*tm))/(80.*p**2*p3**3*Pi) -
  (2*ab*Sin(3*tm))/(15.*p**4*p3*Pi) - Sin(3*tm)/(6.*p**2*p3*Pi) +
  (ab*Sin(3*tm))/(30.*p**2*p3*Pi) + (ab*Sin(4*tm))/(96.*p**4*p2**3*Pi)-
  (ab*Sin(5*tm))/(240.*p**4*p2**3*Pi) + Sin(5*tm)/(320.*p**2*p2**3*Pi)+
  (ab*Sin(5*tm))/(320.*p**2*p2**3*Pi) +
  (ab*Sin(5*tm))/(300.*p**4*p3**3*Pi) - Sin(5*tm)/(80.*p**2*p3**3*Pi) +
  (ab*Sin(5*tm))/(400.*p**2*p3**3*Pi) - Sin(tp)/(16.*p3**3*Pi) +
  (9*ab*Sin(tp))/(80.*p3**3*Pi) - (2*ab*Sin(tp))/(15.*p**4*p3**3*Pi) +
  (5*Sin(tp))/(4.*p**2*p3**3*Pi) + (2*ab*Sin(tp))/(5.*p**2*p3**3*Pi) -
 Sin(tp)/(2.*p3*Pi) + (13*ab*Sin(tp))/(10.*p3*Pi) +
  (12*ab*Sin(tp))/(5.*p**4*p3*Pi) - (22*ab*Sin(tp))/(5.*p**2*p3*Pi) +
  (4*p3*Sin(tp))/Pi - (4*ab*p3*Sin(tp))/(5.*Pi) -
  (16*ab*p3*Sin(tp))/(5.*p**2*Pi) +
  ((8*ab*p**2*Sin(tm))/(15.*p3**3*Pi) - (2*p**4*Sin(tm))/(3.*p3**3*Pi)+
     (2*ab*p**4*Sin(tm))/(15.*p3**3*Pi) +
     (8*ab*p**2*Sin(tp))/(15.*p3**3*Pi) - (2*p**4*Sin(tp))/(3.*p3**3*Pi) +
     (2*ab*p**4*Sin(tp))/(15.*p3**3*Pi))/hr**4 - (2*Sin(2*tp))/(p**2*Pi) -
  (2*ab*Sin(2*tp))/(p**2*Pi) +
  ((-4*ab)/(5.*p3**3) + p**2/p3**3 + (ab*p**2)/(3.*p3**3) +
     (4*ab*tp)/(5.*p3**3*Pi) - (p**2*tp)/(p3**3*Pi) -
     (ab*p**2*tp)/(3.*p3**3*Pi) - (8*ab*Sin(tm))/(5.*p3**3*Pi) +
     (2*p**2*Sin(tm))/(p3**3*Pi) + (2*ab*p**2*Sin(tm))/(3.*p3**3*Pi) +
     (2*ab*Sin(2*tp))/(5.*p3**3*Pi) - (p**2*Sin(2*tp))/(2.*p3**3*Pi) -
     (ab*p**2*Sin(2*tp))/(6.*p3**3*Pi))/hr**3 + Sin(3*tp)/(32.*p3**3*Pi) -
  (11*ab*Sin(3*tp))/(480.*p3**3*Pi) - (4*ab*Sin(3*tp))/(45.*p**4*p3**3*Pi) +
  (5*Sin(3*tp))/(24.*p**2*p3**3*Pi) + (ab*Sin(3*tp))/(6.*p**2*p3**3*Pi)+
 Sin(3*tp)/(6.*p3*Pi) + (ab*Sin(3*tp))/(10.*p3*Pi) +
  (4*ab*Sin(3*tp))/(15.*p**4*p3*Pi) - (2*ab*Sin(3*tp))/(3.*p**2*p3*Pi)+
  ((-2*Sin(tm))/(p3**3*Pi) - (14*ab*Sin(tm))/(5.*p3**3*Pi) +
     (8*ab*Sin(tm))/(5.*p**2*p3**3*Pi) +
     (8*ab*p**2*Sin(tm))/(15.*p3**3*Pi) + (8*ab*Sin(tm))/(5.*p3*Pi) -
     (2*p**2*Sin(tm))/(p3*Pi) + (2*ab*p**2*Sin(tm))/(5.*p3*Pi) -
     (3*Sin(tp))/(2.*p3**3*Pi) - (19*ab*Sin(tp))/(10.*p3**3*Pi) +
     (6*ab*Sin(tp))/(5.*p**2*p3**3*Pi) - (p**2*Sin(tp))/(4.*p3**3*Pi) +
     (9*ab*p**2*Sin(tp))/(20.*p3**3*Pi) + (8*ab*Sin(tp))/(5.*p3*Pi) -
     (2*p**2*Sin(tp))/(p3*Pi) + (2*ab*p**2*Sin(tp))/(5.*p3*Pi) -
    Sin(3*tp)/(6.*p3**3*Pi) - (3*ab*Sin(3*tp))/(10.*p3**3*Pi) +
     (2*ab*Sin(3*tp))/(15.*p**2*p3**3*Pi) +
     (p**2*Sin(3*tp))/(12.*p3**3*Pi) + (ab*p**2*Sin(3*tp))/(36.*p3**3*Pi))/
```

```
   hr**2 + (1/(4.*p3**3) - (9*ab)/(20.*p3**3) - ab/(5.*p**4*p3**3) +
     1/(4.*p**2*p3**3) + (19*ab)/(20.*p**2*p3**3) + 2/p3 +
     (6*ab)/(5.*p3) - (8*ab)/(5.*p**2*p3) - tm/(16.*p**2*p2**3*Pi) -
     (ab*tm)/(16.*p**2*p2**3*Pi) + (ab*tm)/(5.*p**4*p3**3*Pi) +
     tm/(4.*p**2*p3**3*Pi) - (ab*tm)/(20.*p**2*p3**3*Pi) -
     tp/(4.*p3**3*Pi) + (9*ab*tp)/(20.*p3**3*Pi) - tp/(2.*p**2*p3**3*Pi) -
     (9*ab*tp)/(10.*p**2*p3**3*Pi) - (2*tp)/(p3*Pi) -
     (6*ab*tp)/(5.*p3*Pi) + (8*ab*tp)/(5.*p**2*p3*Pi) -
     (8*ab*Sin(tm))/(5.*p3**3*Pi) - (8*ab*Sin(tm))/(15.*p**4*p3**3*Pi)+
     (2*Sin(tm))/(3.*p**2*p3**3*Pi) +
     (46*ab*Sin(tm))/(15.*p**2*p3**3*Pi) + (4*Sin(tm))/(p3*Pi) +
     (12*ab*Sin(tm))/(5.*p3*Pi) - (16*ab*Sin(tm))/(5.*p**2*p3*Pi) -
     Sin(2*tm)/(24.*p**2*p2**3*Pi) - (ab*Sin(2*tm))/(24.*p**2*p2**3*Pi)+
     (2*ab*Sin(2*tm))/(15.*p**4*p3**3*Pi) + Sin(2*tm)/(6.*p**2*p3**3*Pi) -
     (ab*Sin(2*tm))/(30.*p**2*p3**3*Pi) - Sin(4*tm)/(192.*p**2*p2**3*Pi) -
     (ab*Sin(4*tm))/(192.*p**2*p2**3*Pi) +
     (ab*Sin(4*tm))/(60.*p**4*p3**3*Pi) + Sin(4*tm)/(48.*p**2*p3**3*Pi)-
     (ab*Sin(4*tm))/(240.*p**2*p3**3*Pi) - (4*Sin(tp))/Pi -
     (32*ab*Sin(tp))/(15.*p**4*Pi) + (2*ab*Sin(2*tp))/(5.*p3**3*Pi) -
     Sin(2*tp)/(3.*p**2*p3**3*Pi) -
     (11*ab*Sin(2*tp))/(15.*p**2*p3**3*Pi) - Sin(2*tp)/(p3*Pi) -
     (3*ab*Sin(2*tp))/(5.*p3*Pi) + (4*ab*Sin(2*tp))/(5.*p**2*p3*Pi) +
     Sin(4*tp)/(16.*p3**3*Pi) + (7*ab*Sin(4*tp))/(80.*p3**3*Pi) -
     Sin(4*tp)/(24.*p**2*p3**3*Pi) -
(17*ab*Sin(4*tp))/(120.*p**2*p3**3*Pi)\)/hr - Sin(5*tp)/(160.*p3**3*Pi)-
(7*ab*Sin(5*tp))/(800.*p3**3*Pi) -
  (2*ab*Sin(5*tp))/(75.*p**4*p3**3*Pi) + Sin(5*tp)/(40.*p**2*p3**3*Pi)+
  (3*ab*Sin(5*tp))/(50.*p**2*p3**3*Pi) +
  hr*((-5*ab)/(24.*p**4*p2**3) + 3/(32.*p**2*p2**3) +
     (3*ab)/(32.*p**2*p2**3) + 3/(8.*p**2*p2) + (3*ab)/(8.*p**2*p2) -
     (11*ab)/(120.*p**4*p3**3) + 1/(32.*p**2*p3**3) -
     (9*ab)/(160.*p**2*p3**3) + ab/(p**4*p3) + 1/(4.*p**2*p3) -
     (17*ab)/(20.*p**2*p3) + (8*ab*p3)/(5.*p**4) - (2*p3)/p**2 -
     (14*ab*p3)/(5.*p**2) - (32*ab)/(9.*p**4*Pi) - 8/(3.*p**2*Pi) -
     (8*ab)/(3.*p**2*Pi) + (8*ab)/(15.*p**4*p2**3*Pi) +
     (11*ab*tm)/(24.*p**4*p2**3*Pi) - (25*tm)/(128.*p**2*p2**3*Pi) -
     (25*ab*tm)/(128.*p**2*p2**3*Pi) + (3*ab*tm)/(4.*p**4*p2*Pi) -
     (7*tm)/(8.*p**2*p2*Pi) - (7*ab*tm)/(8.*p**2*p2*Pi) +
     (2*p2*tm)/(p**2*Pi) + (2*ab*p2*tm)/(p**2*Pi) -
     (77*ab*tm)/(120.*p**4*p3**3*Pi) + (25*tm)/(32.*p**2*p3**3*Pi) -
     (5*ab*tm)/(32.*p**2*p3**3*Pi) + (ab*tm)/(5.*p**4*p3*Pi) +
     (7*tm)/(4.*p**2*p3*Pi) - (7*ab*tm)/(20.*p**2*p3*Pi) -
     (8*ab*p3*tm)/(5.*p**4*Pi) - (2*p3*tm)/(p**2*Pi) +
     (2*ab*p3*tm)/(5.*p**2*Pi) + (11*ab*tp)/(15.*p**4*p3**3*Pi) -
     (13*tp)/(16.*p**2*p3**3*Pi) + (17*ab*tp)/(80.*p**2*p3**3*Pi) -
     (6*ab*tp)/(5.*p**4*p3*Pi) - (2*tp)/(p**2*p3*Pi) +
     (6*ab*tp)/(5.*p**2*p3*Pi) + (4*p3*tp)/(p**2*Pi) +
     (12*ab*p3*tp)/(5.*p**2*Pi) - (11*ab*Sin(tm))/(16.*p**4*p2**3*Pi) -
     (3*ab*Sin(tm))/(2.*p**4*p2*Pi) - (8*ab*Sin(tm))/(15.*p**4*p3**3*Pi) +
     (16*ab*Sin(tm))/(5.*p**4*p3*Pi) - (16*ab*Sin(tm))/(5.*p**2*p3*Pi)+
     (16*ab*p3*Sin(tm))/(5.*p**4*Pi) - (4*p3*Sin(tm))/(p**2*Pi) -
     (28*ab*p3*Sin(tm))/(5.*p**2*Pi) +
     (31*ab*Sin(2*tm))/(96.*p**4*p2**3*Pi) -
     (63*Sin(2*tm))/(512.*p**2*p2**3*Pi) -
     (63*ab*Sin(2*tm))/(512.*p**2*p2**3*Pi) +
     (ab*Sin(2*tm))/(2.*p**4*p2*Pi) - Sin(2*tm)/(2.*p**2*p2*Pi) -
     (ab*Sin(2*tm))/(2.*p**2*p2*Pi) + (p2*Sin(2*tm))/(p**2*Pi) +
```

```
     (ab*p2*Sin(2*tm))/(p**2*Pi) - (81*ab*Sin(2*tm))/(160.*p**4*p3**3*Pi) +
     (63*Sin(2*tm))/(128.*p**2*p3**3*Pi) -
     (63*ab*Sin(2*tm))/(640.*p**2*p3**3*Pi) + Sin(2*tm)/(p**2*p3*Pi) -
     (ab*Sin(2*tm))/(5.*p**2*p3*Pi) - (4*ab*p3*Sin(2*tm))/(5.*p**4*Pi)-
     (p3*Sin(2*tm))/(p**2*Pi) + (ab*p3*Sin(2*tm))/(5.*p**2*Pi) -
     (3*ab*Sin(3*tm))/(32.*p**4*p2**3*Pi) -
     (ab*Sin(3*tm))/(6.*p**4*p2*Pi) +
     (5*ab*Sin(4*tm))/(96.*p**4*p2**3*Pi) -
     (7*Sin(4*tm))/(512.*p**2*p2**3*Pi) -
     (7*ab*Sin(4*tm))/(512.*p**2*p2**3*Pi) +
     (ab*Sin(4*tm))/(16.*p**4*p2*Pi) - Sin(4*tm)/(32.*p**2*p2*Pi) -
     (ab*Sin(4*tm))/(32.*p**2*p2*Pi) -
     (17*ab*Sin(4*tm))/(160.*p**4*p3**3*Pi) +
     (7*Sin(4*tm))/(128.*p**2*p3**3*Pi) -
     (7*ab*Sin(4*tm))/(640.*p**2*p3**3*Pi) -
     (ab*Sin(4*tm))/(20.*p**4*p3*Pi) + Sin(4*tm)/(16.*p**2*p3*Pi) -
     (ab*Sin(4*tm))/(80.*p**2*p3*Pi) -
     (ab*Sin(5*tm))/(160.*p**4*p2**3*Pi) +
     (ab*Sin(6*tm))/(288.*p**4*p2**3*Pi) -
     Sin(6*tm)/(1536.*p**2*p2**3*Pi) -
     (ab*Sin(6*tm))/(1536.*p**2*p2**3*Pi) -
     (13*ab*Sin(6*tm))/(1440.*p**4*p3**3*Pi) +
     Sin(6*tm)/(384.*p**2*p3**3*Pi) -
     (ab*Sin(6*tm))/(1920.*p**2*p3**3*Pi) - (12*ab*Sin(tp))/(p**4*Pi) +
     (3*Sin(tp))/(p**2*Pi) + (3*ab*Sin(tp))/(p**2*Pi) +
     (3*ab*Sin(2*tp))/(5.*p**4*p3**3*Pi) -
     (31*Sin(2*tp))/(64.*p**2*p3**3*Pi) +
     (43*ab*Sin(2*tp))/(320.*p**2*p3**3*Pi) -
     (4*ab*Sin(2*tp))/(5.*p**4*p3*Pi) - Sin(2*tp)/(p**2*p3*Pi) +
     (ab*Sin(2*tp))/(p**2*p3*Pi) + (2*p3*Sin(2*tp))/(p**2*Pi) +
     (6*ab*p3*Sin(2*tp))/(5.*p**2*Pi) - (4*ab*Sin(3*tp))/(3.*p**4*Pi) +
     Sin(3*tp)/(3.*p**2*Pi) + (ab*Sin(3*tp))/(3.*p**2*Pi) +
     (3*ab*Sin(4*tp))/(20.*p**4*p3**3*Pi) -
     (3*Sin(4*tp))/(64.*p**2*p3**3*Pi) -
     (ab*Sin(4*tp))/(320.*p**2*p3**3*Pi) -
     (ab*Sin(4*tp))/(10.*p**4*p3*Pi) + (ab*Sin(4*tp))/(5.*p**2*p3*Pi) +
     (ab*Sin(6*tp))/(45.*p**4*p3**3*Pi) - Sin(6*tp)/(192.*p**2*p3**3*Pi) -
     (11*ab*Sin(6*tp))/(960.*p**2*p3**3*Pi)) +
  hr**2*((-7*ab)/p**4 - (3*ab)/(16.*p**4*p2**3) - (3*ab)/(4.*p**4*p2) +
     (16*ab)/(15.*p**4*p2**3*Pi) - 43/(420.*p**2*p2**3*Pi) -
     (43*ab)/(420.*p**2*p2**3*Pi) + (16*ab)/(5.*p**4*p2*Pi) -
     2/(3.*p**2*p2*Pi) - (2*ab)/(3.*p**2*p2*Pi) + (8*p2)/(3.*p**2*Pi) +
     (8*ab*p2)/(3.*p**2*Pi) + (25*ab*tm)/(64.*p**4*p2**3*Pi) +
     (7*ab*tm)/(4.*p**4*p2*Pi) - (4*ab*p2*tm)/(p**4*Pi) +
     (6*ab*tp)/(p**4*Pi) - (163*ab*Sin(tm))/(128.*p**4*p2**3*Pi) +
     (121*Sin(tm))/(1024.*p**2*p2**3*Pi) +
     (121*ab*Sin(tm))/(1024.*p**2*p2**3*Pi) -
     (33*ab*Sin(tm))/(8.*p**4*p2*Pi) + (25*Sin(tm))/(32.*p**2*p2*Pi) +
     (25*ab*Sin(tm))/(32.*p**2*p2*Pi) + (6*ab*p2*Sin(tm))/(p**4*Pi) -
     (7*p2*Sin(tm))/(2.*p**2*Pi) - (7*ab*p2*Sin(tm))/(2.*p**2*Pi) +
     (8*p2**3*Sin(tm))/(3.*p**2*Pi) + (8*ab*p2**3*Sin(tm))/(3.*p**2*Pi)+
     (831*ab*Sin(tm))/(320.*p**4*p3**3*Pi) -
     (121*Sin(tm))/(256.*p**2*p3**3*Pi) +
     (121*ab*Sin(tm))/(1280.*p**2*p3**3*Pi) +
     (23*ab*Sin(tm))/(4.*p**4*p3*Pi) - (25*Sin(tm))/(16.*p**2*p3*Pi) +
     (5*ab*Sin(tm))/(16.*p**2*p3*Pi) + (22*ab*p3*Sin(tm))/(5.*p**4*Pi)+
     (7*p3*Sin(tm))/(2.*p**2*Pi) - (39*ab*p3*Sin(tm))/(10.*p**2*Pi) -
```

```
(8*p3**3*Sin(tm))/(3.*p**2*Pi) + (8*ab*p3**3*Sin(tm))/(15.*p**2*Pi) +
(63*ab*Sin(2*tm))/(256.*p**4*p2**3*Pi) + (ab*Sin(2*tm))/(p**4*p2*Pi) -
(2*ab*p2*Sin(2*tm))/(p**4*Pi) -
(77*ab*Sin(3*tm))/(384.*p**4*p2**3*Pi) +
(43*Sin(3*tm))/(3072.*p**2*p2**3*Pi) +
(43*ab*Sin(3*tm))/(3072.*p**2*p2**3*Pi) -
(9*ab*Sin(3*tm))/(16.*p**4*p2*Pi) + (13*Sin(3*tm))/(192.*p**2*p2*Pi) +
(13*ab*Sin(3*tm))/(192.*p**2*p2*Pi) +
(2*ab*p2*Sin(3*tm))/(3.*p**4*Pi) - (p2*Sin(3*tm))/(6.*p**2*Pi) -
(ab*p2*Sin(3*tm))/(6.*p**2*Pi) +
(143*ab*Sin(3*tm))/(320.*p**4*p3**3*Pi) -
(43*Sin(3*tm))/(768.*p**2*p3**3*Pi) +
(43*ab*Sin(3*tm))/(3840.*p**2*p3**3*Pi) +
(79*ab*Sin(3*tm))/(120.*p**4*p3*Pi) -
(13*Sin(3*tm))/(96.*p**2*p3*Pi) +
(13*ab*Sin(3*tm))/(480.*p**2*p3*Pi) -
(2*ab*p3*Sin(3*tm))/(5.*p**4*Pi) + (p3*Sin(3*tm))/(6.*p**2*Pi) -
(ab*p3*Sin(3*tm))/(30.*p**2*Pi) +
(7*ab*Sin(4*tm))/(256.*p**4*p2**3*Pi) +
(ab*Sin(4*tm))/(16.*p**4*p2*Pi) -
(3*ab*Sin(5*tm))/(128.*p**4*p2**3*Pi) +
(19*Sin(5*tm))/(15360.*p**2*p2**3*Pi) +
(19*ab*Sin(5*tm))/(15360.*p**2*p2**3*Pi) -
(3*ab*Sin(5*tm))/(80.*p**4*p2*Pi) + Sin(5*tm)/(320.*p**2*p2*Pi) +
(ab*Sin(5*tm))/(320.*p**2*p2*Pi) +
(293*ab*Sin(5*tm))/(4800.*p**4*p3**3*Pi) -
(19*Sin(5*tm))/(3840.*p**2*p3**3*Pi) +
(19*ab*Sin(5*tm))/(19200.*p**2*p3**3*Pi) +
(11*ab*Sin(5*tm))/(200.*p**4*p3*Pi) - Sin(5*tm)/(160.*p**2*p3*Pi)+
(ab*Sin(5*tm))/(800.*p**2*p3*Pi) +
(ab*Sin(6*tm))/(768.*p**4*p2**3*Pi) -
(ab*Sin(7*tm))/(896.*p**4*p2**3*Pi) +
Sin(7*tm)/(21504.*p**2*p2**3*Pi) +
(ab*Sin(7*tm))/(21504.*p**2*p2**3*Pi) +
(23*ab*Sin(7*tm))/(6720.*p**4*p3**3*Pi) -
Sin(7*tm)/(5376.*p**2*p3**3*Pi) +
(ab*Sin(7*tm))/(26880.*p**2*p3**3*Pi) -
(77*ab*Sin(tp))/(30.*p**4*p3**3*Pi) +
(179*Sin(tp))/(384.*p**2*p3**3*Pi) -
(143*ab*Sin(tp))/(1920.*p**2*p3**3*Pi) -
(7*ab*Sin(tp))/(2.*p**4*p3*Pi) + (3*Sin(tp))/(2.*p**2*p3*Pi) -
(ab*Sin(tp))/(10.*p**2*p3*Pi) + (32*ab*p3*Sin(tp))/(5.*p**4*Pi) -
(3*p3*Sin(tp))/(p**2*Pi) - (9*ab*p3*Sin(tp))/(5.*p**2*Pi) +
(32*ab*p3**3*Sin(tp))/(15.*p**4*Pi) + (4*ab*Sin(2*tp))/(p**4*Pi) -
(53*ab*Sin(3*tp))/(120.*p**4*p3**3*Pi) +
(23*Sin(3*tp))/(384.*p**2*p3**3*Pi) -
(7*ab*Sin(3*tp))/(384.*p**2*p3**3*Pi) -
(9*ab*Sin(3*tp))/(20.*p**4*p3*Pi) + Sin(3*tp)/(6.*p**2*p3*Pi) -
(ab*Sin(3*tp))/(15.*p**2*p3*Pi) + (16*ab*p3*Sin(3*tp))/(15.*p**4*Pi) -
(p3*Sin(3*tp))/(3.*p**2*Pi) - (ab*p3*Sin(3*tp))/(5.*p**2*Pi) +
(ab*Sin(4*tp))/(2.*p**4*Pi) - (13*ab*Sin(5*tp))/(200.*p**4*p3**3*Pi) +
(7*Sin(5*tp))/(1920.*p**2*p3**3*Pi) -
(19*ab*Sin(5*tp))/(9600.*p**2*p3**3*Pi) +
(ab*Sin(5*tp))/(100.*p**4*p3*Pi) - (ab*Sin(5*tp))/(50.*p**2*p3*Pi)-
(ab*Sin(7*tp))/(140.*p**4*p3**3*Pi) +
Sin(7*tp)/(2688.*p**2*p3**3*Pi) +
(11*ab*Sin(7*tp))/(13440.*p**2*p3**3*Pi)) +
```

```
hr**3*((-179*ab)/(768.*p**4*p2**3) - (9*ab)/(8.*p**4*p2) +
   (3*ab*p2)/p**4 - ab/(240.*p**4*p3**3) - ab/(20.*p**4*p3) +
   (4*ab*p3)/(5.*p**4) + (16*ab*p3**3)/(15.*p**4) -
   (32*ab)/(9.*p**4*Pi) + (43*ab)/(210.*p**4*p2**3*Pi) +
   (4*ab)/(3.*p**4*p2*Pi) - (16*ab*p2)/(3.*p**4*Pi) +
   (121*ab*tm)/(256.*p**4*p2**3*Pi) + (75*ab*tm)/(32.*p**4*p2*Pi) -
   (7*ab*p2*tm)/(p**4*Pi) + (8*ab*p2**3*tm)/(3.*p**4*Pi) -
   (71*ab*tm)/(80.*p**4*p3**3*Pi) - (47*ab*tm)/(20.*p**4*p3*Pi) +
   (4*ab*p3*tm)/(p**4*Pi) - (16*ab*p3**3*tm)/(15.*p**4*Pi) +
   (107*ab*tp)/(120.*p**4*p3**3*Pi) + (12*ab*tp)/(5.*p**4*p3*Pi) -
   (24*ab*p3*tp)/(5.*p**4*Pi) - (121*ab*Sin(tm))/(512.*p**4*p2**3*Pi)-
   (25*ab*Sin(tm))/(16.*p**4*p2*Pi) + (7*ab*p2*Sin(tm))/(p**4*Pi) -
   (16*ab*p2**3*Sin(tm))/(3.*p**4*Pi) + (16*ab*p3*Sin(tm))/(5.*p**4*Pi) +
   (32*ab*p3**3*Sin(tm))/(15.*p**4*Pi) +
   (41*ab*Sin(2*tm))/(128.*p**4*p2**3*Pi) +
   (189*ab*Sin(2*tm))/(128.*p**4*p2*Pi) - (4*ab*p2*Sin(2*tm))/(p**4*Pi) +
   (4*ab*p2**3*Sin(2*tm))/(3.*p**4*Pi) -
   (101*ab*Sin(2*tm))/(160.*p**4*p3**3*Pi) -
   (25*ab*Sin(2*tm))/(16.*p**4*p3*Pi) +
   (12*ab*p3*Sin(2*tm))/(5.*p**4*Pi) -
   (8*ab*p3**3*Sin(2*tm))/(15.*p**4*Pi) -
   (43*ab*Sin(3*tm))/(1536.*p**4*p2**3*Pi) -
   (13*ab*Sin(3*tm))/(96.*p**4*p2*Pi) + (ab*p2*Sin(3*tm))/(3.*p**4*Pi) +
   (37*ab*Sin(4*tm))/(768.*p**4*p2**3*Pi) +
   (21*ab*Sin(4*tm))/(128.*p**4*p2*Pi) - (ab*p2*Sin(4*tm))/(4.*p**4*Pi) -
   (53*ab*Sin(4*tm))/(480.*p**4*p3**3*Pi) -
   (17*ab*Sin(4*tm))/(80.*p**4*p3*Pi) + (ab*p3*Sin(4*tm))/(5.*p**4*Pi) -
   (19*ab*Sin(5*tm))/(7680.*p**4*p2**3*Pi) -
   (ab*Sin(5*tm))/(160.*p**4*p2*Pi) +
   (5*ab*Sin(6*tm))/(1152.*p**4*p2**3*Pi) +
   (ab*Sin(6*tm))/(128.*p**4*p2*Pi) -
   (17*ab*Sin(6*tm))/(1440.*p**4*p3**3*Pi) -
   (ab*Sin(6*tm))/(80.*p**4*p3*Pi) -
   (ab*Sin(7*tm))/(10752.*p**4*p2**3*Pi) +
   (ab*Sin(8*tm))/(6144.*p**4*p2**3*Pi) -
   (ab*Sin(8*tm))/(1920.*p**4*p3**3*Pi) - (5*ab*Sin(tp))/(2.*p**4*Pi)+
   (19*ab*Sin(2*tp))/(30.*p**4*p3**3*Pi) +
   (8*ab*Sin(2*tp))/(5.*p**4*p3*Pi) - (16*ab*p3*Sin(2*tp))/(5.*p**4*Pi) -
   (5*ab*Sin(3*tp))/(12.*p**4*Pi) +
   (13*ab*Sin(4*tp))/(120.*p**4*p3**3*Pi) +
   (ab*Sin(4*tp))/(5.*p**4*p3*Pi) - (2*ab*p3*Sin(4*tp))/(5.*p**4*Pi)-
   (ab*Sin(5*tp))/(20.*p**4*Pi) + (ab*Sin(6*tp))/(90.*p**4*p3**3*Pi)+
   (ab*Sin(8*tp))/(960.*p**4*p3**3*Pi)) +
hr**4*(-ab/(3.*p**4) + (59*ab)/(315.*p**4*p2**3*Pi) +
   (43*ab)/(35.*p**4*p2*Pi) - (16*ab*p2)/(3.*p**4*Pi) +
   (32*ab*p2**3)/(9.*p**4*Pi) - (445*ab*Sin(tm))/(2048.*p**4*p2**3*Pi) -
   (363*ab*Sin(tm))/(256.*p**4*p2*Pi) + (25*ab*p2*Sin(tm))/(4.*p**4*Pi) -
   (14*ab*p2**3*Sin(tm))/(3.*p**4*Pi) +
   (203*ab*Sin(tm))/(640.*p**4*p3**3*Pi) +
   (163*ab*Sin(tm))/(160.*p**4*p3*Pi) - (11*ab*p3*Sin(tm))/(5.*p**4*Pi) +
   (28*ab*p3**3*Sin(tm))/(15.*p**4*Pi) -
   (289*ab*Sin(3*tm))/(9216.*p**4*p2**3*Pi) -
   (43*ab*Sin(3*tm))/(256.*p**4*p2*Pi) +
   (13*ab*p2*Sin(3*tm))/(24.*p**4*Pi) -
   (2*ab*p2**3*Sin(3*tm))/(9.*p**4*Pi) +
   (ab*Sin(3*tm))/(18.*p**4*p3**3*Pi) +
   (77*ab*Sin(3*tm))/(480.*p**4*p3*Pi) -
```

```
     (3*ab*p3*Sin(3*tm))/(10.*p**4*Pi) +
     (4*ab*p3**3*Sin(3*tm))/(45.*p**4*Pi) -
     (61*ab*Sin(5*tm))/(15360.*p**4*p2**3*Pi) -
     (19*ab*Sin(5*tm))/(1280.*p**4*p2*Pi) +
     (ab*p2*Sin(5*tm))/(40.*p**4*Pi) +
     (7*ab*Sin(5*tm))/(800.*p**4*p3**3*Pi) +
     (3*ab*Sin(5*tm))/(160.*p**4*p3*Pi) - (ab*p3*Sin(5*tm))/(50.*p**4*Pi) -
     (25*ab*Sin(7*tm))/(86016.*p**4*p2**3*Pi) -
     (ab*Sin(7*tm))/(1792.*p**4*p2*Pi) +
     (ab*Sin(7*tm))/(1280.*p**4*p3**3*Pi) +
     (ab*Sin(7*tm))/(1120.*p**4*p3*Pi) -
     (ab*Sin(9*tm))/(110592.*p**4*p2**3*Pi) +
     (ab*Sin(9*tm))/(34560.*p**4*p3**3*Pi) -
     (101*ab*Sin(tp))/(320.*p**4*p3**3*Pi) - (ab*Sin(tp))/(p**4*p3*Pi)+
     (2*ab*p3*Sin(tp))/(p**4*Pi) - (9*ab*Sin(3*tp))/(160.*p**4*p3**3*Pi) -
     (ab*Sin(3*tp))/(6.*p**4*p3*Pi) + (ab*p3*Sin(3*tp))/(3.*p**4*Pi) -
     (7*ab*Sin(5*tp))/(800.*p**4*p3**3*Pi) -
     (ab*Sin(5*tp))/(50.*p**4*p3*Pi) + (ab*p3*Sin(5*tp))/(25.*p**4*Pi)-
     (3*ab*Sin(7*tp))/(4480.*p**4*p3**3*Pi) -
     (ab*Sin(9*tp))/(17280.*p**4*p3**3*Pi))
```

and $\chi_m^{//}$= -2/(p**2*Pi) - (2*ab)/(p**2*Pi) - (7*ab)/(480.*p**4*p2**3*Pi) +
1/(30.*p**2*p2**3*Pi) + ab/(30.*p**2*p2**3*Pi) + 1/(3.*p**2*p2*Pi) +
ab/(3.*p**2*p2*Pi) + 4/(15.*p3**3*Pi) - (4*ab)/(25.*p3**3*Pi) -
(24*ab)/(25.*p**4*p3**3*Pi) + 2/(15.*p**2*p3**3*Pi) +
(22*ab)/(15.*p**2*p3**3*Pi) + 4/(3.*p3*Pi) + (4*ab)/(5.*p3*Pi) +
(16*ab)/(15.*p**4*p3*Pi) - 4/(3.*p**2*p3*Pi) - (76*ab)/(15.*p**2*p3*Pi) +
(ab*Cos(tm))/(24.*p**4*p2**3*Pi) - (3*Cos(tm))/(32.*p**2*p2**3*Pi) -
(3*ab*Cos(tm))/(32.*p**2*p2**3*Pi) - Cos(tm)/(4.*p**2*p2*Pi) -
(ab*Cos(tm))/(4.*p**2*p2*Pi) + (37*ab*Cos(tm))/(30.*p**4*p3**3*Pi) +
(3*Cos(tm))/(8.*p**2*p3**3*Pi) - (67*ab*Cos(tm))/(40.*p**2*p3**3*Pi)-
(8*ab*Cos(tm))/(5.*p3*Pi) - (6*ab*Cos(tm))/(5.*p**4*p3*Pi) +
(5*Cos(tm))/(2.*p**2*p3*Pi) + (59*ab*Cos(tm))/(10.*p**2*p3*Pi) -
(4*p3*Cos(tm))/Pi + (4*ab*p3*Cos(tm))/(5.*Pi) +
(16*ab*p3*Cos(tm))/(5.*p**2*Pi) - (ab*Cos(2*tm))/(24.*p**4*p2**3*Pi)+
(ab*Cos(3*tm))/(48.*p**4*p2**3*Pi) - (7*Cos(3*tm))/(192.*p**2*p2**3*Pi) -
(7*ab*Cos(3*tm))/(192.*p**2*p2**3*Pi) - Cos(3*tm)/(12.*p**2*p2*Pi) -
(ab*Cos(3*tm))/(12.*p**2*p2*Pi) + (ab*Cos(3*tm))/(20.*p**4*p3**3*Pi)+
(7*Cos(3*tm))/(48.*p**2*p3**3*Pi) -
(7*ab*Cos(3*tm))/(240.*p**2*p3**3*Pi) +
(2*ab*Cos(3*tm))/(15.*p**4*p3*Pi) + Cos(3*tm)/(6.*p**2*p3*Pi) -
(ab*Cos(3*tm))/(30.*p**2*p3*Pi) - (ab*Cos(4*tm))/(96.*p**4*p2**3*Pi)+
(ab*Cos(5*tm))/(240.*p**4*p2**3*Pi) - Cos(5*tm)/(320.*p**2*p2**3*Pi)-
(ab*Cos(5*tm))/(320.*p**2*p2**3*Pi) -
(ab*Cos(5*tm))/(300.*p**4*p3**3*Pi) + Cos(5*tm)/(80.*p**2*p3**3*Pi) -
(ab*Cos(5*tm))/(400.*p**2*p3**3*Pi) + (5*Cos(tp))/(16.*p3**3*Pi) -
(13*ab*Cos(tp))/(80.*p3**3*Pi) - (2*ab*Cos(tp))/(15.*p**4*p3**3*Pi) -
Cos(tp)/(4.*p**2*p3**3*Pi) + (3*Cos(tp))/(2.*p3*Pi) -
(7*ab*Cos(tp))/(10.*p3*Pi) - (4*ab*Cos(tp))/(5.*p**4*p3*Pi) +
(2*ab*Cos(tp))/(5.*p**2*p3*Pi) - (4*p3*Cos(tp))/Pi +
(4*ab*p3*Cos(tp))/(5.*Pi) + (16*ab*p3*Cos(tp))/(5.*p**2*Pi) +
((-8*ab*p**2*Cos(tm))/(15.*p3**3*Pi) + (2*p**4*Cos(tm))/(3.*p3**3*Pi)-
   (2*ab*p**4*Cos(tm))/(15.*p3**3*Pi) -
   (8*ab*p**2*Cos(tp))/(15.*p3**3*Pi) + (2*p**4*Cos(tp))/(3.*p3**3*Pi) -
   (2*ab*p**4*Cos(tp))/(15.*p3**3*Pi))/hr**4 + (2*Cos(2*tp))/(p**2*Pi) +
(2*ab*Cos(2*tp))/(p**2*Pi) +

```
  ((-6*ab)/(5.*p3**3*Pi) + (3*p**2)/(2.*p3**3*Pi) +
     (ab*p**2)/(2.*p3**3*Pi) + (8*ab*Cos(tm))/(5.*p3**3*Pi) -
     (2*p**2*Cos(tm))/(p3**3*Pi) - (2*ab*p**2*Cos(tm))/(3.*p3**3*Pi) -
     (2*ab*Cos(2*tp))/(5.*p3**3*Pi) + (p**2*Cos(2*tp))/(2.*p3**3*Pi) +
     (ab*p**2*Cos(2*tp))/(6.*p3**3*Pi))/hr**3 -
  (5*Cos(3*tp))/(96.*p3**3*Pi) - (ab*Cos(3*tp))/(160.*p3**3*Pi) -
  Cos(3*tp)/(8.*p**2*p3**3*Pi) + (ab*Cos(3*tp))/(30.*p**2*p3**3*Pi) -
  Cos(3*tp)/(6.*p3*Pi) - (ab*Cos(3*tp))/(10.*p3*Pi) -
  (4*ab*Cos(3*tp))/(15.*p**4*p3*Pi) + (2*ab*Cos(3*tp))/(3.*p**2*p3*Pi)+
  (-4/(3.*p3**3*Pi) - (12*ab)/(5.*p3**3*Pi) +
     (16*ab)/(15.*p**2*p3**3*Pi) + (2*p**2)/(3.*p3**3*Pi) +
     (2*ab*p**2)/(9.*p3**3*Pi) + (2*Cos(tm))/(p3**3*Pi) +
     (14*ab*Cos(tm))/(5.*p3**3*Pi) - (8*ab*Cos(tm))/(5.*p**2*p3**3*Pi)-
     (8*ab*p**2*Cos(tm))/(15.*p3**3*Pi) - (8*ab*Cos(tm))/(5.*p3*Pi) +
     (2*p**2*Cos(tm))/(p3*Pi) - (2*ab*p**2*Cos(tm))/(5.*p3*Pi) +
     Cos(tp)/(2.*p3**3*Pi) + (ab*Cos(tp))/(10.*p3**3*Pi) -
     (2*ab*Cos(tp))/(5.*p**2*p3**3*Pi) + (3*p**2*Cos(tp))/(4.*p3**3*Pi)-
     (17*ab*p**2*Cos(tp))/(60.*p3**3*Pi) - (8*ab*Cos(tp))/(5.*p3*Pi) +
     (2*p**2*Cos(tp))/(p3*Pi) - (2*ab*p**2*Cos(tp))/(5.*p3*Pi) +
     Cos(3*tp)/(6.*p3**3*Pi) + (3*ab*Cos(3*tp))/(10.*p3**3*Pi) -
     (2*ab*Cos(3*tp))/(15.*p**2*p3**3*Pi) -
     (p**2*Cos(3*tp))/(12.*p3**3*Pi) - (ab*p**2*Cos(3*tp))/(36.*p3**3*Pi))/
   hr**2 + (-8/(3.*p**2*Pi) - (8*ab)/(3.*p**2*Pi) -
     5/(192.*p**2*p2**3*Pi) - (5*ab)/(192.*p**2*p2**3*Pi) -
     3/(16.*p3**3*Pi) - (117*ab)/(80.*p3**3*Pi) -
     (9*ab)/(20.*p**4*p3**3*Pi) + 9/(16.*p**2*p3**3*Pi) +
     (219*ab)/(80.*p**2*p3**3*Pi) + 3/(p3*Pi) + (9*ab)/(5.*p3*Pi) -
     (12*ab)/(5.*p**2*p3*Pi) + (8*ab*Cos(tm))/(5.*p3**3*Pi) +
     (8*ab*Cos(tm))/(15.*p**4*p3**3*Pi) - (2*Cos(tm))/(3.*p**2*p3**3*Pi) -
     (46*ab*Cos(tm))/(15.*p**2*p3**3*Pi) - (4*Cos(tm))/(p3*Pi) -
     (12*ab*Cos(tm))/(5.*p3*Pi) + (16*ab*Cos(tm))/(5.*p**2*p3*Pi) +
     Cos(2*tm)/(48.*p**2*p2**3*Pi) + (ab*Cos(2*tm))/(48.*p**2*p2**3*Pi)-
     (ab*Cos(2*tm))/(15.*p**4*p3**3*Pi) - Cos(2*tm)/(12.*p**2*p3**3*Pi)+
     (ab*Cos(2*tm))/(60.*p**2*p3**3*Pi) + Cos(4*tm)/(192.*p**2*p2**3*Pi) +
     (ab*Cos(4*tm))/(192.*p**2*p2**3*Pi) -
     (ab*Cos(4*tm))/(60.*p**4*p3**3*Pi) - Cos(4*tm)/(48.*p**2*p3**3*Pi)+
     (ab*Cos(4*tm))/(240.*p**2*p3**3*Pi) + (4*Cos(tp))/Pi +
     (32*ab*Cos(tp))/(15.*p**4*Pi) + Cos(2*tp)/(4.*p3**3*Pi) -
     (ab*Cos(2*tp))/(20.*p3**3*Pi) + Cos(2*tp)/(6.*p**2*p3**3*Pi) +
     (ab*Cos(2*tp))/(6.*p**2*p3**3*Pi) + Cos(2*tp)/(p3*Pi) +
     (3*ab*Cos(2*tp))/(5.*p3*Pi) - (4*ab*Cos(2*tp))/(5.*p**2*p3*Pi) -
     Cos(4*tp)/(16.*p3**3*Pi) - (7*ab*Cos(4*tp))/(80.*p3**3*Pi) +
     Cos(4*tp)/(24.*p**2*p3**3*Pi) +
     (17*ab*Cos(4*tp))/(120.*p**2*p3**3*Pi)\)/hr +
Cos(5*tp)/(160.*p3**3*Pi) + (7*ab*Cos(5*tp))/(800.*p3**3*Pi) +
  (2*ab*Cos(5*tp))/(75.*p**4*p3**3*Pi) - Cos(5*tp)/(40.*p**2*p3**3*Pi)-
  (3*ab*Cos(5*tp))/(50.*p**2*p3**3*Pi) +
  hr*(-8/(3.*p**2*Pi) - (8*ab)/(3.*p**2*Pi) -
     (13*ab)/(120.*p**4*p2**3*Pi) + 31/(768.*p**2*p2**3*Pi) +
     (31*ab)/(768.*p**2*p2**3*Pi) - (17*ab)/(48.*p**4*p2*Pi) +
     3/(32.*p**2*p2*Pi) + (3*ab)/(32.*p**2*p2*Pi) + p2/(p**2*Pi) +
     (ab*p2)/(p**2*Pi) - (373*ab)/(720.*p**4*p3**3*Pi) -
     5/(192.*p**2*p3**3*Pi) + (29*ab)/(960.*p**2*p3**3*Pi) +
     (57*ab)/(20.*p**4*p3*Pi) - 3/(16.*p**2*p3*Pi) -
     (237*ab)/(80.*p**2*p3*Pi) + (12*ab*p3)/(5.*p**4*Pi) -
     (3*p3)/(p**2*Pi) - (21*ab*p3)/(5.*p**2*Pi) +
     (3*ab*Cos(tm))/(16.*p**4*p2**3*Pi) + (ab*Cos(tm))/(2.*p**4*p2*Pi)+
```

```
     (8*ab*Cos(tm))/(15.*p**4*p3**3*Pi) - (16*ab*Cos(tm))/(5.*p**4*p3*Pi) +
     (16*ab*Cos(tm))/(5.*p**2*p3*Pi) - (16*ab*p3*Cos(tm))/(5.*p**4*Pi)+
     (4*p3*Cos(tm))/(p**2*Pi) + (28*ab*p3*Cos(tm))/(5.*p**2*Pi) -
     (13*ab*Cos(2*tm))/(96.*p**4*p2**3*Pi) +
     (37*Cos(2*tm))/(512.*p**2*p2**3*Pi) +
     (37*ab*Cos(2*tm))/(512.*p**2*p2**3*Pi) -
     (ab*Cos(2*tm))/(4.*p**4*p2*Pi) + (3*Cos(2*tm))/(8.*p**2*p2*Pi) +
     (3*ab*Cos(2*tm))/(8.*p**2*p2*Pi) - (p2*Cos(2*tm))/(p**2*Pi) -
     (ab*p2*Cos(2*tm))/(p**2*Pi) + (13*ab*Cos(2*tm))/(96.*p**4*p3**3*Pi) -
     (37*Cos(2*tm))/(128.*p**2*p3**3*Pi) +
     (37*ab*Cos(2*tm))/(640.*p**2*p3**3*Pi) -
     (ab*Cos(2*tm))/(5.*p**4*p3*Pi) - (3*Cos(2*tm))/(4.*p**2*p3*Pi) +
     (3*ab*Cos(2*tm))/(20.*p**2*p3*Pi) + (4*ab*p3*Cos(2*tm))/(5.*p**4*Pi) +
     (p3*Cos(2*tm))/(p**2*Pi) - (ab*p3*Cos(2*tm))/(5.*p**2*Pi) +
     (7*ab*Cos(3*tm))/(96.*p**4*p2**3*Pi) +
     (ab*Cos(3*tm))/(6.*p**4*p2*Pi) - (ab*Cos(4*tm))/(24.*p**4*p2**3*Pi) +
     (3*Cos(4*tm))/(256.*p**2*p2**3*Pi) +
     (3*ab*Cos(4*tm))/(256.*p**2*p2**3*Pi) -
     (ab*Cos(4*tm))/(16.*p**4*p2*Pi) + Cos(4*tm)/(32.*p**2*p2*Pi) +
     (ab*Cos(4*tm))/(32.*p**2*p2*Pi) +
     (19*ab*Cos(4*tm))/(240.*p**4*p3**3*Pi) -
     (3*Cos(4*tm))/(64.*p**2*p3**3*Pi) +
     (3*ab*Cos(4*tm))/(320.*p**2*p3**3*Pi) +
     (ab*Cos(4*tm))/(20.*p**4*p3*Pi) - Cos(4*tm)/(16.*p**2*p3*Pi) +
     (ab*Cos(4*tm))/(80.*p**2*p3*Pi) +
     (ab*Cos(5*tm))/(160.*p**4*p2**3*Pi) -
     (ab*Cos(6*tm))/(288.*p**4*p2**3*Pi) +
     Cos(6*tm)/(1536.*p**2*p2**3*Pi) +
     (ab*Cos(6*tm))/(1536.*p**2*p2**3*Pi) +
     (13*ab*Cos(6*tm))/(1440.*p**4*p3**3*Pi) -
     Cos(6*tm)/(384.*p**2*p3**3*Pi) +
     (ab*Cos(6*tm))/(1920.*p**2*p3**3*Pi) + (4*ab*Cos(tp))/(p**4*Pi) -
     Cos(tp)/(p**2*Pi) - (ab*Cos(tp))/(p**2*Pi) -
     (2*ab*Cos(2*tp))/(15.*p**4*p3**3*Pi) +
     (21*Cos(2*tp))/(64.*p**2*p3**3*Pi) -
     (5*ab*Cos(2*tp))/(64.*p**2*p3**3*Pi) +
     (2*ab*Cos(2*tp))/(5.*p**4*p3*Pi) + Cos(2*tp)/(p**2*p3*Pi) -
     (ab*Cos(2*tp))/(5.*p**2*p3*Pi) - (2*p3*Cos(2*tp))/(p**2*Pi) -
     (6*ab*p3*Cos(2*tp))/(5.*p**2*Pi) + (4*ab*Cos(3*tp))/(3.*p**4*Pi) -
     Cos(3*tp)/(3.*p**2*Pi) - (ab*Cos(3*tp))/(3.*p**2*Pi) -
     (ab*Cos(4*tp))/(12.*p**4*p3**3*Pi) + Cos(4*tp)/(32.*p**2*p3**3*Pi)-
     (ab*Cos(4*tp))/(32.*p**2*p3**3*Pi) + (ab*Cos(4*tp))/(10.*p**4*p3*Pi) -
     (ab*Cos(4*tp))/(5.*p**2*p3*Pi) - (ab*Cos(6*tp))/(45.*p**4*p3**3*Pi) +
     Cos(6*tp)/(192.*p**2*p3**3*Pi) +
(11*ab*Cos(6*tp))/(960.*p**2*p3**3*Pi)\) + hr**2*((-3*ab)/(2.*p**4*Pi)-
2/(3.*p**2*Pi) - (2*ab)/(3.*p**2*Pi)-
     (1597*ab)/(13440.*p**4*p2**3*Pi) + 1/(105.*p**2*p2**3*Pi) +
     ab/(105.*p**2*p2**3*Pi) - (47*ab)/(80.*p**4*p2*Pi) +
     2/(15.*p**2*p2*Pi) + (2*ab)/(15.*p**2*p2*Pi) +
     (2*ab*p2)/(3.*p**4*Pi) - (4*p2)/(3.*p**2*Pi) -
     (4*ab*p2)/(3.*p**2*Pi) + (8*p2**3)/(3.*p**2*Pi) +
     (8*ab*p2**3)/(3.*p**2*Pi) - (8*ab)/(525.*p**4*p3**3*Pi) +
     4/(105.*p**2*p3**3*Pi) - (4*ab)/(105.*p**2*p3**3*Pi) +
     (112*ab)/(75.*p**4*p3*Pi) + 4/(15.*p**2*p3*Pi) -
     (4*ab)/(15.*p**2*p3*Pi) + (16*ab*p3)/(3.*p**4*Pi) -
     (4*p3)/(3.*p**2*Pi) - (28*ab*p3)/(15.*p**2*Pi) +
     (37*ab*Cos(tm))/(128.*p**4*p2**3*Pi) -
```

```
(47*Cos(tm))/(1024.*p**2*p2**3*Pi) -
(47*ab*Cos(tm))/(1024.*p**2*p2**3*Pi) +
(9*ab*Cos(tm))/(8.*p**4*p2*Pi) - (13*Cos(tm))/(32.*p**2*p2*Pi) -
(13*ab*Cos(tm))/(32.*p**2*p2*Pi) - (2*ab*p2*Cos(tm))/(p**4*Pi) +
(5*p2*Cos(tm))/(2.*p**2*Pi) + (5*ab*p2*Cos(tm))/(2.*p**2*Pi) -
(8*p2**3*Cos(tm))/(3.*p**2*Pi) - (8*ab*p2**3*Cos(tm))/(3.*p**2*Pi)-
(153*ab*Cos(tm))/(320.*p**4*p3**3*Pi) +
(47*Cos(tm))/(256.*p**2*p3**3*Pi) -
(47*ab*Cos(tm))/(1280.*p**2*p3**3*Pi) -
(47*ab*Cos(tm))/(20.*p**4*p3*Pi) + (13*Cos(tm))/(16.*p**2*p3*Pi) -
(13*ab*Cos(tm))/(80.*p**2*p3*Pi) - (34*ab*p3*Cos(tm))/(5.*p**4*Pi)-
(5*p3*Cos(tm))/(2.*p**2*Pi) + (37*ab*p3*Cos(tm))/(10.*p**2*Pi) +
(8*p3**3*Cos(tm))/(3.*p**2*Pi) - (8*ab*p3**3*Cos(tm))/(15.*p**2*Pi) -
(37*ab*Cos(2*tm))/(256.*p**4*p2**3*Pi) -
(3*ab*Cos(2*tm))/(4.*p**4*p2*Pi) + (2*ab*p2*Cos(2*tm))/(p**4*Pi) +
(49*ab*Cos(3*tm))/(384.*p**4*p2**3*Pi) -
(31*Cos(3*tm))/(3072.*p**2*p2**3*Pi) -
(31*ab*Cos(3*tm))/(3072.*p**2*p2**3*Pi) +
(7*ab*Cos(3*tm))/(16.*p**4*p2*Pi) - (11*Cos(3*tm))/(192.*p**2*p2*Pi) -
(11*ab*Cos(3*tm))/(192.*p**2*p2*Pi) -
(2*ab*p2*Cos(3*tm))/(3.*p**4*Pi) + (p2*Cos(3*tm))/(6.*p**2*Pi) +
(ab*p2*Cos(3*tm))/(6.*p**2*Pi) -
(83*ab*Cos(3*tm))/(320.*p**4*p3**3*Pi) +
(31*Cos(3*tm))/(768.*p**2*p3**3*Pi) -
(31*ab*Cos(3*tm))/(3840.*p**2*p3**3*Pi) -
(19*ab*Cos(3*tm))/(40.*p**4*p3*Pi) + (11*Cos(3*tm))/(96.*p**2*p3*Pi) -
(11*ab*Cos(3*tm))/(480.*p**2*p3*Pi) +
(2*ab*p3*Cos(3*tm))/(5.*p**4*Pi) - (p3*Cos(3*tm))/(6.*p**2*Pi) +
(ab*p3*Cos(3*tm))/(30.*p**2*Pi) -
(3*ab*Cos(4*tm))/(128.*p**4*p2**3*Pi) -
(ab*Cos(4*tm))/(16.*p**4*p2*Pi) +
(13*ab*Cos(5*tm))/(640.*p**4*p2**3*Pi) -
(17*Cos(5*tm))/(15360.*p**2*p2**3*Pi) -
(17*ab*Cos(5*tm))/(15360.*p**2*p2**3*Pi) +
(3*ab*Cos(5*tm))/(80.*p**4*p2*Pi) - Cos(5*tm)/(320.*p**2*p2*Pi) -
(ab*Cos(5*tm))/(320.*p**2*p2*Pi) -
(247*ab*Cos(5*tm))/(4800.*p**4*p3**3*Pi) +
(17*Cos(5*tm))/(3840.*p**2*p3**3*Pi) -
(17*ab*Cos(5*tm))/(19200.*p**2*p3**3*Pi) -
(11*ab*Cos(5*tm))/(200.*p**4*p3*Pi) + Cos(5*tm)/(160.*p**2*p3*Pi)-
(ab*Cos(5*tm))/(800.*p**2*p3*Pi) -
(ab*Cos(6*tm))/(768.*p**4*p2**3*Pi) +
(ab*Cos(7*tm))/(896.*p**4*p2**3*Pi) -
Cos(7*tm)/(21504.*p**2*p2**3*Pi) -
(ab*Cos(7*tm))/(21504.*p**2*p2**3*Pi) -
(23*ab*Cos(7*tm))/(6720.*p**4*p3**3*Pi) +
Cos(7*tm)/(5376.*p**2*p3**3*Pi) -
(ab*Cos(7*tm))/(26880.*p**2*p3**3*Pi) +
(7*ab*Cos(tp))/(15.*p**4*p3**3*Pi) -
(53*Cos(tp))/(384.*p**2*p3**3*Pi) -
(7*ab*Cos(tp))/(1920.*p**2*p3**3*Pi) +
(7*ab*Cos(tp))/(10.*p**4*p3*Pi) - Cos(tp)/(2.*p**2*p3*Pi) -
(ab*Cos(tp))/(10.*p**2*p3*Pi) + (p3*Cos(tp))/(p**2*Pi) +
(3*ab*p3*Cos(tp))/(5.*p**2*Pi) - (32*ab*p3**3*Cos(tp))/(15.*p**4*Pi) -
(2*ab*Cos(2*tp))/(p**4*Pi) + (31*ab*Cos(3*tp))/(120.*p**4*p3**3*Pi) -
(19*Cos(3*tp))/(384.*p**2*p3**3*Pi) +
(ab*Cos(3*tp))/(128.*p**2*p3**3*Pi) +
```

```
     (29*ab*Cos(3*tp))/(60.*p**4*p3*Pi) - Cos(3*tp)/(6.*p**2*p3*Pi) -
     (16*ab*p3*Cos(3*tp))/(15.*p**4*Pi) + (p3*Cos(3*tp))/(3.*p**2*Pi) +
     (ab*p3*Cos(3*tp))/(5.*p**2*Pi) - (ab*Cos(4*tp))/(2.*p**4*Pi) +
     (9*ab*Cos(5*tp))/(200.*p**4*p3**3*Pi) -
     Cos(5*tp)/(384.*p**2*p3**3*Pi) +
     (41*ab*Cos(5*tp))/(9600.*p**2*p3**3*Pi) -
     (ab*Cos(5*tp))/(100.*p**4*p3*Pi) + (ab*Cos(5*tp))/(50.*p**2*p3*Pi)+
     (ab*Cos(7*tp))/(140.*p**4*p3**3*Pi) -
     Cos(7*tp)/(2688.*p**2*p3**3*Pi) -
     (11*ab*Cos(7*tp))/(13440.*p**2*p3**3*Pi)) +
  hr**3*((-25481*ab)/(215040.*p**4*p2**3*Pi) - (721*ab)/(960.*p**4*p2*Pi) +
     (41*ab*p2)/(12.*p**4*Pi) - (4*ab*p2**3)/(p**4*Pi) +
     ab/(384.*p**4*p3**3*Pi) + ab/(40.*p**4*p3*Pi) + (3*ab*p3)/(p**4*Pi) +
     (8*ab*p3**3)/(5.*p**4*Pi) + (47*ab*Cos(tm))/(512.*p**4*p2**3*Pi) +
     (13*ab*Cos(tm))/(16.*p**4*p2*Pi) - (5*ab*p2*Cos(tm))/(p**4*Pi) +
     (16*ab*p2**3*Cos(tm))/(3.*p**4*Pi) - (16*ab*p3*Cos(tm))/(5.*p**4*Pi) -
     (32*ab*p3**3*Cos(tm))/(15.*p**4*Pi) -
     (39*ab*Cos(2*tm))/(256.*p**4*p2**3*Pi) -
     (111*ab*Cos(2*tm))/(128.*p**4*p2*Pi) + (3*ab*p2*Cos(2*tm))/(p**4*Pi) -
     (4*ab*p2**3*Cos(2*tm))/(3.*p**4*Pi) +
     (41*ab*Cos(2*tm))/(160.*p**4*p3**3*Pi) +
     (63*ab*Cos(2*tm))/(80.*p**4*p3*Pi) -
     (8*ab*p3*Cos(2*tm))/(5.*p**4*Pi) +
     (8*ab*p3**3*Cos(2*tm))/(15.*p**4*Pi) +
     (31*ab*Cos(3*tm))/(1536.*p**4*p2**3*Pi) +
     (11*ab*Cos(3*tm))/(96.*p**4*p2*Pi) - (ab*p2*Cos(3*tm))/(3.*p**4*Pi) -
     (55*ab*Cos(4*tm))/(1536.*p**4*p2**3*Pi) -
     (9*ab*Cos(4*tm))/(64.*p**4*p2*Pi) + (ab*p2*Cos(4*tm))/(4.*p**4*Pi)+
     (37*ab*Cos(4*tm))/(480.*p**4*p3**3*Pi) +
     (7*ab*Cos(4*tm))/(40.*p**4*p3*Pi) - (ab*p3*Cos(4*tm))/(5.*p**4*Pi)+
     (17*ab*Cos(5*tm))/(7680.*p**4*p2**3*Pi) +
     (ab*Cos(5*tm))/(160.*p**4*p2*Pi) -
     (ab*Cos(6*tm))/(256.*p**4*p2**3*Pi) -
     (ab*Cos(6*tm))/(128.*p**4*p2*Pi) +
     (ab*Cos(6*tm))/(96.*p**4*p3**3*Pi) + (ab*Cos(6*tm))/(80.*p**4*p3*Pi) +
     (ab*Cos(7*tm))/(10752.*p**4*p2**3*Pi) -
     (ab*Cos(8*tm))/(6144.*p**4*p2**3*Pi) +
     (ab*Cos(8*tm))/(1920.*p**4*p3**3*Pi) + (ab*Cos(tp))/(2.*p**4*Pi) -
     (31*ab*Cos(2*tp))/(120.*p**4*p3**3*Pi) -
     (4*ab*Cos(2*tp))/(5.*p**4*p3*Pi) + (8*ab*p3*Cos(2*tp))/(5.*p**4*Pi) +
     (ab*Cos(3*tp))/(4.*p**4*Pi) - (19*ab*Cos(4*tp))/(240.*p**4*p3**3*Pi) -
     (ab*Cos(4*tp))/(5.*p**4*p3*Pi) + (2*ab*p3*Cos(4*tp))/(5.*p**4*Pi)+
     (ab*Cos(5*tp))/(20.*p**4*Pi) - (ab*Cos(6*tp))/(120.*p**4*p3**3*Pi)-
     (ab*Cos(8*tp))/(960.*p**4*p3**3*Pi)) +
  hr**4*((-8*ab)/(945.*p**4*p2**3*Pi) - (4*ab)/(35.*p**4*p2*Pi) +
     (16*ab*p2)/(15.*p**4*Pi) - (16*ab*p2**3)/(9.*p**4*Pi) -
     (16*ab)/(4725.*p**4*p3**3*Pi) - (16*ab)/(525.*p**4*p3*Pi) +
     (16*ab*p3)/(75.*p**4*Pi) + (32*ab*p3**3)/(45.*p**4*Pi) +
     (133*ab*Cos(tm))/(2048.*p**4*p2**3*Pi) +
     (141*ab*Cos(tm))/(256.*p**4*p2*Pi) - (13*ab*p2*Cos(tm))/(4.*p**4*Pi) +
     (10*ab*p2**3*Cos(tm))/(3.*p**4*Pi) -
     (39*ab*Cos(tm))/(640.*p**4*p3**3*Pi) -
     (37*ab*Cos(tm))/(160.*p**4*p3*Pi) + (3*ab*p3*Cos(tm))/(5.*p**4*Pi)-
     (4*ab*p3**3*Cos(tm))/(3.*p**4*Pi) +
     (179*ab*Cos(3*tm))/(9216.*p**4*p2**3*Pi) +
     (31*ab*Cos(3*tm))/(256.*p**4*p2*Pi) -
     (11*ab*p2*Cos(3*tm))/(24.*p**4*Pi) +
```

```
(2*ab*p2**3*Cos(3*tm))/(9.*p**4*Pi) -
(43*ab*Cos(3*tm))/(1440.*p**4*p3**3*Pi) -
(49*ab*Cos(3*tm))/(480.*p**4*p3*Pi) +
(7*ab*p3*Cos(3*tm))/(30.*p**4*Pi) -
(4*ab*p3**3*Cos(3*tm))/(45.*p**4*Pi) +
(49*ab*Cos(5*tm))/(15360.*p**4*p2**3*Pi) +
(17*ab*Cos(5*tm))/(1280.*p**4*p2*Pi) -
(ab*p2*Cos(5*tm))/(40.*p**4*Pi) - (ab*Cos(5*tm))/(150.*p**4*p3**3*Pi) -
(13*ab*Cos(5*tm))/(800.*p**4*p3*Pi) + (ab*p3*Cos(5*tm))/(50.*p**4*Pi) +
(23*ab*Cos(7*tm))/(86016.*p**4*p2**3*Pi) +
(ab*Cos(7*tm))/(1792.*p**4*p2*Pi) -
(19*ab*Cos(7*tm))/(26880.*p**4*p3**3*Pi) -
(ab*Cos(7*tm))/(1120.*p**4*p3*Pi) +
(ab*Cos(9*tm))/(110592.*p**4*p2**3*Pi) -
(ab*Cos(9*tm))/(34560.*p**4*p3**3*Pi) +
(11*ab*Cos(tp))/(192.*p**4*p3**3*Pi) + (ab*Cos(tp))/(5.*p**4*p3*Pi) -
(2*ab*p3*Cos(tp))/(5.*p**4*Pi) +
(43*ab*Cos(3*tp))/(1440.*p**4*p3**3*Pi) +
(ab*Cos(3*tp))/(10.*p**4*p3*Pi) - (ab*p3*Cos(3*tp))/(5.*p**4*Pi) +
(17*ab*Cos(5*tp))/(2400.*p**4*p3**3*Pi) +
(ab*Cos(5*tp))/(50.*p**4*p3*Pi) - (ab*p3*Cos(5*tp))/(25.*p**4*Pi)+
(ab*Cos(7*tp))/(1920.*p**4*p3**3*Pi) +
(ab*Cos(9*tp))/(17280.*p**4*p3**3*Pi))
```

Where hmp = H_m/H_p, p1 = p_1, p2 = p_2, p3 = p_3, Pi = π, ab = a/b

hr = h_r = hmp*p1= $(H_m/H_p)p_1$

tp = $t_p = \cos^{-1}(-1/hmp)$,

tr = $t_r = \cos^{-1}[-1/hr+((1+1/hr)^2-2p^2/hr^2)^{1/2}]$

tm = $t_m = \cos^{-1}[(1/(p_1\ hmp))(1-(2(1+p^2)-(1+p_1\ hmp)^2)^{1/2}]$

----------XXX----------